

DOCTORAL THESIS

Future Power System Out-of-Step Protection Concept Utilizing Synchronized Phasor Measurements

Marko Tealane

TALLINN UNIVERSITY OF TECHNOLOGY
DOCTORAL THESIS
9/2023

Future Power System Out-of-Step Protection Concept Utilizing Synchronized Phasor Measurements

MARKO TEALANE



TALLINN UNIVERSITY OF TECHNOLOGY
School of Engineering
Department of Electrical Power Engineering and Mechatronics

**The dissertation was accepted for the defence of the degree of Doctor of Philosophy on
6th of February 2023**

Supervisor: Professor Jako Kilter,
Department of Electrical Power Engineering and Mechatronics, School of Engineering
Tallinn University of Technology
Tallinn, Estonia

Co-supervisor: Mart Landsberg, PhD
Elering AS, Head of Grid Management Department
Tallinn, Estonia

Opponents: Professor Athula D. Rajapakse,
University of Manitoba
Winnipeg, Manitoba, Canada

Professor Brian K. Johnson,
University of Idaho
Moscow, Idaho, United States of America

Defence of the thesis: 19th of April 2023, Tallinn

Declaration:

Hereby I declare that this doctoral thesis, my original investigation and achievement, submitted for the doctoral degree at Tallinn University of Technology, has not been submitted for any academic degree elsewhere.

Marko Tealane

signature

Financial support was provided by the Estonian Ministry of Education and Research (The Kristjan Jaak Scholarship for study period abroad and Dora Plus mobility scholarship), Elering AS (Future energy system scholarship) and Nederlandse Organisatie voor Wetenschappelijk Onderzoek (NWO Take-Off Project "Power swing detection and prevention in future networks with high penetration of renewable energy") grant no. 19279.



Copyright: Marko Tealane, 2023

ISSN 2585-6898 (publication)

ISBN 978-9949-83-956-8 (publication)

ISSN 2585-6901 (PDF)

ISBN 978-9949-83-957-5 (PDF)

Printed by Koopia Niini & Rauam

TALLINNA TEHNIKAÜLIKOOL
DOKTORITÖÖ
9/2023

Tuleviku elektrisüsteemi faasimõõtmistel põhinev sünkronismikaotuskaitse kontseptsioon

MARKO TEALANE



Contents

List of Publications	7
Author's Contributions to the Publications	8
List of Symbols and Abbreviations	9
Introduction	11
1 Power Swings - Phenomenon, Monitoring and Protection.....	15
1.1 Power System Stability and Power Swing Phenomena	15
1.2 Wide-Area Monitoring Systems	17
1.3 Power Swing Detection and Out-of-Step Protection Methods	21
1.4 Challenges for Existing Out-of-Step Protection	36
1.5 Intermediate Summary	44
2 Out-of-Step Protection Based on Equivalent Impedances	45
2.1 Proposed Out-of-Step Protection Concept	45
2.2 Out-of-Step Protection Concept Evaluation	50
2.3 Algorithm Response to Grid Events	62
2.4 Intermediate Summary	72
3 Out-of-Step Protection Using Discrete Angle Derivatives	73
3.1 Decoupled Out-of-Step Protection Concept	73
3.2 Constraints and Verification of the Decoupled Algorithm.....	76
3.3 Effect of Grid Events on Algorithm Operation	84
3.4 Intermediate Summary	90
4 Case Studies	91
4.1 Test Model Descriptions	91
4.2 Hardware-in-the-Loop Testing Principles	99
4.3 Performance Comparison of Real-Time Testing of Out-of-Step Protection...	106
4.3.1 SMIB Model Results	107
4.3.2 IEEE39 Bus System Results	111
4.3.3 Iceland Power System Case Studies	115
4.4 Intermediate Summary	121
Conclusions and Further Work	125
List of Figures	127
List of Tables	135
References	137
Acknowledgements	143
Abstract.....	145
Kokkuvöte	147

Appendix 1.....	149
Appendix 2	157
Appendix 3	171
Curriculum Vitae	189
Elulookirjeldus.....	193

List of Publications

The present Ph.D. thesis is based on the following publications that are referred to in the text by Roman numbers.

- I M. Tealane, J. Kilter, and K. Pill, "Real-time testing of out-of-step protection devices," in *2021 IEEE PES Innovative Smart Grid Technologies Europe (ISGT Europe)*, pp. 1–5, 2021
- II M. Tealane, J. Kilter, M. Popov, O. Bagleybter, and D. Klaar, "Online detection of out-of-step condition using pmu-determined system impedances," *IEEE Access*, vol. 10, pp. 14807–14818, 2022
- III M. Tealane, J. Kilter, O. Bagleybter, B. Heimisson, and M. Popov, "Out-of-step protection based on discrete angle derivatives," *IEEE Access*, vol. 10, pp. 78290–78305, 2022

Author's Contributions to the Publications

- I In I, Marko Tealane was the main author, wrote the simulation program, developed the test system and carried out the analysis of the results, prepared the figures, wrote the manuscript and presented the work in the IEEE ISGT Europe 2021 conference.
- II In II, Marko Tealane was the main author, developed the proposed algorithm, conducted the simulations and hardware implementation of the algorithm, analyzed the results, prepared the figures, and wrote the manuscript.
- III In III, Marko Tealane was the main author, developed the algorithm, conducted simulation, prepared the hardware implementation of the algorithm and analyzed the mass testing results, as well as wrote the manuscript.

List of Symbols and Abbreviations

δ	Angle difference between two internal voltages of a source, <i>rad</i>
θ	Phase shift with respect to a rotational frame, <i>rad</i>
ϕ	Angle difference, <i>rad</i>
$\Phi(t)$	Rotor initial phase angle, <i>rad</i>
$\phi(t)$	Rotor phase angle at a specific time instant, <i>rad</i>
ω	Rotational speed, s^{-1}
\bar{E}	Equivalent voltage phasor inside a machine, <i>p.u.</i>
f	Frequency, Hz
\bar{I}	Current phasor, <i>p.u.</i>
\bar{V}	Measured voltage phasor, <i>p.u.</i>
\underline{Z}	Complex impedance value, <i>p.u.</i>
LSA	Last stable angle point on the Power-angle curve
DER	Derivatives-based protection algorithm
EAC	Equal-Area Criterion
GPS	Global Positioning System
HW	Hardware
IBR	Inverter-based resource
OOS	Out-of-step
PDC	Phasor Data Concentrator
PMU	Phasor Measurement Unit
RES	Renewable energy source
RTDS	Real-Time Digital Simulator
SIR	Short-circuit Impedance Ratio
SLG	Single-line to ground fault
SW	Software
TPH	Three-phase fault
WAMS	Wide-Area Measurement System

Introduction

This thesis presents the research and development work carried out by the author during PhD studies at Tallinn University of Technology (TalTech). Most of this work was conducted at TalTech. However, very important parts of the work were performed during joint research work in the Netherlands at Delft University of Technology. The work started from the Horizon 2020 project "MIGRATE (Massive InteGRATION of power Electronic devices)", which the author had the pleasure of being a part of.

Motivation and Background

The electric power system is in a constant state of evolution, starting from the commissioning of the first power plants in the 19th century. Across over 100 years the power system has evolved into the modern large interconnected power systems we know today. The evolution, however, is ongoing, and with it comes challenges. The modern interconnected power grid can be considered a reservoir, where all the connected generators deliver their produced energy and any load can tap into that reservoir to receive the amount of energy it needs. It is impossible to know which generator produces the energy a load consumes in the network at any given time. The interconnected nature of the modern electric system enables the transmission of energy from the generators to loads effectively, and allows for the consumers to access the reservoir of energy. As there is currently no effective way to store large amounts of energy, the generated power must be consumed immediately by all loads connected to the grid as well as the various losses in the system itself, otherwise the imbalance between consumption and production will result in changes in frequency in the power network. Thus, a large deficiency or surplus in the power system may lead to a blackout if not reacted to.

The power sector is a large contributor to greenhouse gas emissions [1], and with the push towards more sustainable energy sources, an increasing number of power plants are connected to the power grid, which use renewable energy sources, e.g. wind or solar energy, in order to reduce the emissions of the power sector. These sources [2, 3] are usually intermittent in nature, meaning, that their electrical output is dependent on the specific weather conditions at any given time. The intermittent nature of these energy sources makes using a traditional synchronous machine impractical for producing electric power. Therefore, these power plants are commonly connected to the bulk system by using inverters, which means, that the primary energy source is decoupled from the alternating power grid. This usually means that the renewable energy sources using inverters provide little to no mechanical inertia (which is inherent to synchronously connected units) to the power network. The aforementioned issue, in turn, makes the power system more susceptible to disturbances.

Additionally, due to the intermittent nature of the renewable energy sources, the composition of the generating units in the network becomes unknown. This adds additional stress on the operation of the power systems in terms of balancing load as well as the existing protection systems in the network, which necessitates faster and more accurate measurement techniques to better understand the system state. Driven by the need to ensure a more detailed understanding, there is a rapid increase in the adoption of wide-area measurement systems (WAMS) in power grids [4]. WAMS allow for better situational awareness, which can be used to maximise power grid transfer capacity as well as help mitigate risks of major disturbances through enhanced monitoring.

Thus, the inclusion of asynchronously-connected resources is expected to influence the existing unit and system integrity protections in the power system. The influences of inverter-based resources on unit protections have been thoroughly studied in large-scale

research projects, e.g. in [5]. However, the effects on system protection have not been widely studied in a similar manner or extent thus far as there is a limited amount of research performed. Therefore, it becomes essential to understand the nature of this impact and its consequences to existing system protection systems in order to have confidence in the protection operation in cases of system level events, such as the European transmission system separation in 2021 [6]. This event culminated in the European system not being able to maintain synchronous operation, and the out-of-step (OOS) protection installed in the network successfully splitting the network into two separate areas, avoiding large oscillations in voltages and currents which can cause equipment damage. This system level event resulted in a total of 1.7 GW of load being disconnected from the network in order to continue stable operation.

OOS protection is designed, in principle, to detect loss of synchronism between a single generator and the rest of the system, or between neighbouring generator groups. Loss of synchronism between parts of the system or interconnected system can be caused by major disturbances such as faults on transmission lines. It is preferable to separate these asynchronous parts as soon as possible in order to avoid equipment damage and further outages. During unstable swings, the rotor angle difference will keep increasing because a balance between power generation and consumption cannot be retained, leading to loss of synchronism between generators or parts of the network. Fast separation of desynchronised regions within a system becomes necessary in such a condition to protect equipment from damage, and prevent further system outages. For this, a reliable OOS protection method must be determined, which is robust and able to cope with the changing nature of the power system.

Main Objectives and Tasks of the Thesis

The key research question asked in this thesis is "*How can we reliably detect and act on out-of-step conditions in future electric power systems?*". The answers to this question should form an understanding of how the currently used protection system copes with changing generation mix in the network and develop a protection mechanism that can consistently provide reliable results in identifying out-of-step conditions in the future power system.

To answer the key question formulated for the thesis, several hypotheses were devised:

- Changing composition of generators in the power grid results in changes in source impedances, which has an adverse effect on currently existing out-of-step protections.
- It is possible to determine the source impedance behind the observed transmission lines from real-time wide-area measurements.
- It is possible to realise an improved out-of-step condition detection using determined source impedances.
- It is possible to create an algorithm for out-of-step condition detection, which does not make use of any pre-calculated values.

Based on the hypotheses listed above, the following tasks were formulated:

- Assess the effects of changing source impedance, due to the changes in generator composition, on commercially available out-of-step protection devices.

- Develop a scalable test model for real-time testing in order to assess the performance of existing out-of-step protection devices with changing generation mix in the power network.
- Develop a method for out-of-step protection, that utilises the computed impedances seen from the terminals of the observed transmission line in real-time.
- Develop an algorithm for out-of-step protection which negates the necessity of computing the source impedance values at the observed transmission line terminals.
- Analyse and compare the performances of existing and developed out-of-step protection algorithms.

Contribution of the Thesis and Dissemination

Theoretical contribution:

- Issues related to the changes of the generation mix in the power grid regarding the ability to detect out-of-step conditions by using commercially available protections have been described.
- A method for computation of system impedance at the ends of transmission lines has been developed and the accuracy of the method verified.
- A novel algorithm for out-of-step protection has been developed utilising the determined power system impedances.
- An advanced algorithm decoupled from the power network parameters has been developed.

Practical contribution of the dissertation:

- Three types of existing out-of-step protection devices have been extensively tested and performance concerns are detailed.
- Developed protection algorithms are confirmed to outperform the existing commercially available impedance-based out-of-step protection.
- The novel algorithms has been tested using real-time simulations and event recordings.
- A developed protection algorithm has been implemented by Landsnet in the Iceland power system.

Dissemination of the Research Work

The first part of the research and development work for this dissertation has been presented at the scientific conference of IEEE (publication [I]). Two master's theses [7, 8] were defended on the related topic. The work on the computation of system impedances as well as utilising the computed impedances for out-of-step protection has been published in a peer-reviewed journal paper [II] as well as in the RTDS Technologies' User Spotlight 2.0 webinar [9] and Power System Protection Center's Communication Based Protection seminar [10]. In addition, the work on the developed discrete angle derivative algorithm and the implementation of the aforementioned algorithm in the Iceland transmission network has been published in a journal paper [III].

Outline of the Thesis

The thesis is divided into four main chapters to form a complete picture from the power system transient stability, out-of-step phenomenon, the existing protection devices as well as the developed two protection algorithms and the performance of difference out-of-step devices. Chapter 1 focuses on the phenomenon of transient stability, the power swing phenomenon, monitoring and reacting to power swings by using commercially available devices and the challenges that the current methods face in future power systems. Chapter 2 develops a new out-of-step protection algorithm based on determined network impedances using a wide-area measurement system. Chapter 3 develops an out-of-step protection concept, that is decoupled from network parameters and relies on discrete derivatives of measured angle difference. Chapter 4 presents several case studies proving concerns in the capability of out-of-step condition detection by the existing protection devices and displaying the effectiveness of the novel developed protection approaches. The thesis ends with conclusions and recommendations for further work.

1 Power Swings - Phenomenon, Monitoring and Protection

This chapter first explains the phenomenon of power system transient stability using a simplified power system. Following the simple system example is the explanation of wide-area measurement systems, which allow for more detailed observations and monitoring of the power system in real-time. The structure and devices used in a wide-area measurement system are discussed. Using a wide-area measurement system opens the way for creating different system-level protection applications, including out-of-step protection functions. Existing proven and commercially available methods for detecting power swings and out-of-step conditions are also discussed. Furthermore, the challenges related to existing out-of-step protection systems in the context of changing power grids are also analysed.

The objective of this chapter is to explain the mechanism of stable and unstable power swings in the network, highlight the wide-area monitoring system and its structure as well as introduce commercially available out-of-step protection methods and the vulnerability of existing methods to changing power system production or grid scenarios.

1.1 Power System Stability and Power Swing Phenomena

An electric power system is considered to be a backbone for the modern society. It is critical that the power system remains operational at all times. In normal conditions, the power system is operated very close to its nominal frequency of 50 Hz (or 60 Hz) with very small deviations in magnitudes of several tens of mHz for larger electric power systems [11]. In these nominal conditions the system power generation and consumption are balanced at any given moment and electric power is being transmitted across transmission lines. A simple system, shown in Fig. 1 below can be used to illustrate the power transmission as well as the transient stability phenomenon in the power system.

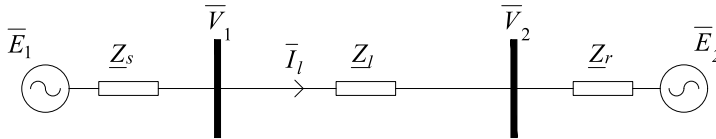


Figure 1 - Simple system equivalent scheme.

According to the physical properties of alternating power [12], the active electrical power transmitted between the two busbars in the system depends on angle difference between the receiving system voltage phasor and the power source internal voltage phasor, the magnitudes of voltage phasors and the total system impedance between the two power sources. Therefore, the first power source's electrical output power of the simple system scheme can be represented by the equation (1),

$$P_e(\delta) = \frac{|E_1||E_2|}{|Z_t|} \sin \delta \quad (1)$$

where

$|E_1|, |E_2|$ - are the equivalent internal voltage magnitudes of the machines;
 $|Z_t|$ - is total reactance between the two sources which is equal to sum of element reactances as $|Z_t| = |Z_s + Z_l + Z_r|$, and
 δ - is angle by which E_1 leads E_2 phasor.

The power-angle characteristic, shown in Fig. 2a, graphically describes the relationship between the power transmission across a transmission line and the angle difference between the two sources. Based on the characteristic the power transfer increases while the angular difference is increasing from 0 to 90° , and thereafter with the further increase in angular difference, the power transfer is decreasing. Power systems are normally operated well below the maximum power transfer point indicated by δ_m .

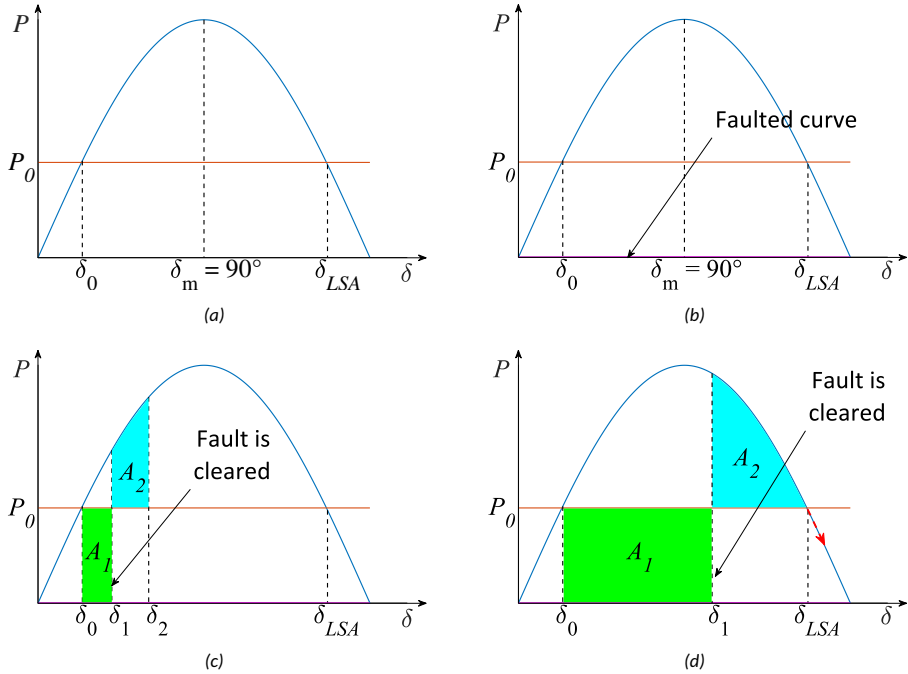


Figure 2 - Power-angle curves for the two-machine system, δ_{LSA} denotes the Last Stable Angle point. (a) - Curve displaying the steady state operation, (b) - Curve showing the faulted state in the network (c) - Power-angle curve with a case of short fault clearing time δ_1 and δ_2 denote the angle values after fault clearance and the maximum angle after deceleration, respectively (d) - Power-angle curve with a case of long fault clearing time δ_1 denotes the angle value after fault clearance.

By using the power-angle characteristic, the transient stability of this simple system can be studied. The stability is directly linked to the internal angle differences of the two equivalent sources. On the power-angle characteristic, two operating points can be fixed using the mechanical input power of the machine, marked as P_0 , and the electrical power characteristic as shown in Fig. 2a. The operating point located in the first half of the characteristic is a stable operating point, shown as δ_0 . The second operating point denotes the maximum angle difference between the sources for a recoverable power swing according to the Equal-Area Criterion (EAC) [13] and is marked as δ_{LSA} . Further increase of the angle beyond δ_{LSA} point results in an unstable generator operation.

When a large disturbance, such as a fault on the generator E_1 busbar, occurs in the network, the power transmitted is suddenly reduced, according to Equation (1) due to the voltage values being reduced and the transmission impedance increasing in the network. This is represented by the lowered curve in Fig. 2b, which drops to 0 for the case of a fault on the busbar. During the fault the electrical output of the source E_1 decreases to a faulted value, whereas the mechanical input power P_0 remains equivalent to the mechanical torque applied before the disturbance. This imbalance causes the rotor angle

to start accelerating, and consequently, the angle δ , to increase.

In this context, the machine dynamics can be represented by the swing equation (2):

$$\frac{M}{\omega_s} \frac{d^2 \delta}{dt^2} = P_m - P_e(\delta) \quad (2)$$

where

M - inertia constant of the equivalent machine;

ω_s - rotor speed of the generator;

δ - internal voltage angle of the generator;

P_m - mechanical input power of the generator;

P_e - electrical output power of the generator.

It has to be noted that this approach is simplified and does not take into account the operation of turbine governors that can influence the mechanical input, and generator automatic voltage regulators (AVR) that control the excitation and can therefore effect the machine voltage magnitudes.

When a fault is cleared from the network after some time, the electrical angle has increased to a value of δ_1 . At this point, the electrical power is now greater than the mechanical input power P_0 and the machine will start to decelerate. Due to inertia, the machine rotor angle will continue to increase, reaching a maximum value of δ_2 , where the energy used for acceleration during the fault, marked as A_1 , will be equal to the decelerating energy represented by A_2 , as shown in Fig. 2c.

If the fault is cleared from the network quickly, the deceleration area A_2 can become equal to the acceleration area A_1 before the angular difference can exceed the limiting last stable angle value δ_{LSA} , and upon reaching a maximum angle value, the rotor angle will start decreasing. After some oscillations the generator will eventually settle in a steady state operation point located at δ_0 . This is referred to as the equal-area criterion in power system transient stability, and the previously described process is also known as a stable power swing in the network.

Contrastingly, when the fault clearance in the network is slow, the angle δ_1 will advance too far during the fault. Subsequently, the area A_1 becomes large enough so that the remaining area A_2 cannot become equal to the acceleration area before the last stable angle δ_{LSA} is reached, as shown in Fig. 2d. Beyond the δ_{LSA} point the electrical power becomes lower than the mechanical input power, which in turn means that the rotor will be accelerated once again. Thereupon the synchronising torque between the two machines is lost and the angular difference will continue to increase beyond 180° and what is known as a pole slip will occur. This means that synchronous operation between the two machines is no longer possible and the machines will continue to rotate at different speeds. The described situation is considered as an unstable power swing or an out-of-step condition.

1.2 Wide-Area Monitoring Systems

Situational awareness of the state of the power system is necessary to operate the power system effectively and reliably. For this monitoring systems are used, the most common of which is the supervisory control and data acquisition (SCADA) system. However, these SCADA systems usually come with a limit in respect to the speed of monitoring. In recent years the need for faster monitoring for more effective decision making as well as more prompt reaction to events in the network has emerged. Due to this the usage of wide-area measurement systems has become more prevalent in the electric power grid.

Wide-area measurement systems (WAMS) are measurement systems that are based on the transmission of analogue and/or digital information through telecommunication systems and utilising synchronisation techniques (time stamping) of the measured data using a common time reference [14]. Measuring devices, referred to as phasor measurement units (PMUs), used by WAMS have their own clocks synchronised with a common time reference using synchronization devices, e.g. GPS clocks. This concept is not new, and has been used for many years [15]. The opportunity of measuring synchronised voltage and current phasors in an electric power system creates several new control possibilities:

- Monitoring the operation of a large system from the point of view of voltage angles and magnitudes, and frequency. This is referred to as *wide-area monitoring* (WAM).
- Application of special power system protection based on measurement of phasor quantities in parts of a power system. Such protection is referred to as *wide-area protection* (WAP).
- Application of control systems based on measuring phasors in large parts of a power system. Such control is referred to as *wide-area control* (WAC).

WAMS integrated with these applications and monitoring techniques are referred to as *wide-area measurement, protection and control* (WAMPAC). The wide-area measurement system makes use of phasor quantities, where the definition of a phasor is closely connected to the concept of representing a periodic waveform as a rotating vector.

A rotating vector \vec{V}_m is rotating with an angular velocity ω with respect to a stationary reference axis. Its position at any instant of time can be represented as

$$\vec{V}_m(t) = V_m e^{j(\omega t + \theta)} \quad (3)$$

where

V_m - amplitude of the periodic signal;

θ - phase shift with respect to the reference frame Re;

The reference frame together with an orthogonal axis Im constitutes the rotating complex plane Re-Im. This is illustrated in Fig 3.

The projection of the vector \vec{V}_m on the horizontal axis is periodically time-varying (Fig. 3b), and is expressed as $v(t) = V_m \cos(\omega t + \theta)$. The frequency at which the periodic change happens is related to the angular velocity by $\omega = 2\pi f = 2\pi/T$, where the T represents the period of the rotation. The RMS value of the sinusoidal waveform is given by $V = V_m/\sqrt{2}$, therefore Equation 3 can be transformed as follows:

$$\vec{V}_m(t) = V_m e^{j(\omega t + \theta)} = \sqrt{2} V e^{j\theta} e^{j\omega t} = \sqrt{2} \bar{V} e^{j\omega t} \quad (4)$$

The vector $\bar{V} = V e^{j\theta}$ is referred to as a phasor. The length of the vector (magnitude) is V and it is equal to the effective value of the periodic waveform $v(t)$. The angle θ is defined by the location of the rotating vector with respect to the axis Re.

The definition shown above assumes that the reference frame Re and the complex plane rotate at the same velocity ω as the vector \vec{V}_m . However, those two velocities may be different, i.e. the vector \vec{V}_m may rotate with velocity ω , while the reference frame may rotate with a velocity $\omega_{ref} \neq \omega$. In this case the phase shift θ is not constant but changes with a velocity that is equal to the difference between the two rotational speeds $d\theta/dt = \Delta\omega$, where $\Delta\omega = \omega - \omega_{ref}$. A special case is when ω oscillates around ω_{ref} , the movement of the phasor on the complex plane is referred to as swinging.

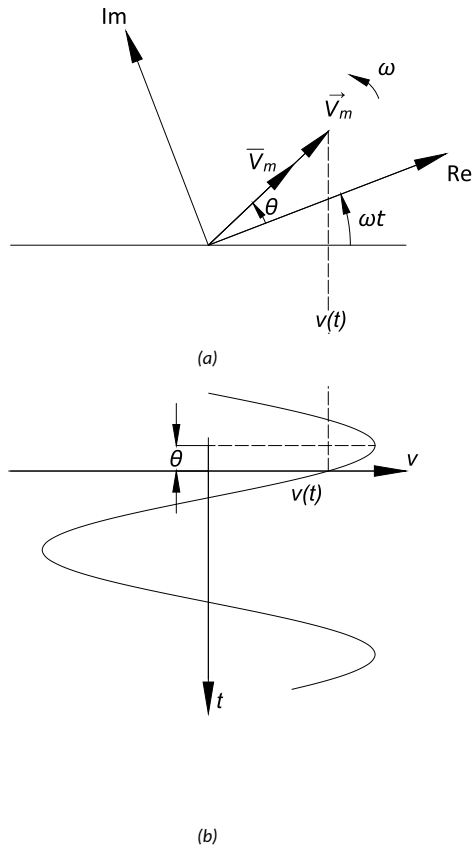


Figure 3 – Graphical representation of phasor formation. (a) a rotating vector, (b) - a corresponding time-domain signal.

A power network generally has a multitude of nodes. The phasors of all the nodal voltages can be placed in common complex coordinates. A state of the network is determined by the voltage magnitudes and the differences between the voltage angles, which means that the common coordinates used can be changed by rotating them by an angle value, since adding the same value to all phase angles does not equal the differences between the phasors. The freedom to choose any common coordinates is important for the methodology of phasor measurements using a WAMS system. The common coordinates for the whole WAMS are obtained by synchronising the measurements using a time signal, which is usually obtained from the GPS system.

Phasor measurement units

A measurement system allowing measurement of the phasors of voltages and currents in an electric power system is referred to as a phasor measurement unit (PMU) and the block diagram of its components is shown schematically in Fig. 4. Voltages and cur-

rents are measured as analogue input values, for which the phasors need to be determined, getting the signals from voltage and current transformers installed in the power network. Each analogue signal passes through an anti-aliasing filter and thereafter the measurement signal is sent to an analogue to digital converter. In the conversion, the signal is sampled and converted in to digital format. The sampler impulses are generated by a phase-locked oscillator, which together with the GPS time synchronisation provides a phase-locked loop system. Consequent data samples and the time stamps are sent to a processing unit containing a microprocessor, which then constructs a phasor quantity from the measurements.

The components of the phasors are usually calculated at every sampling time step and the calculated values assigned to a time corresponding to the centre of the measurement window. This means that theoretically the phasor available at any given moment on the PMU output is delayed by the time resulting from half of the measurement window and by the time consumed by the phasor calculation algorithm. The processor then reports the data using a communication interface to other WAMS devices using a PMU-specific data protocol (C37.118 [16]). The reporting time interval for PMU devices can vary, typically being in the range of 20 - 100 ms for a 50 Hz system.

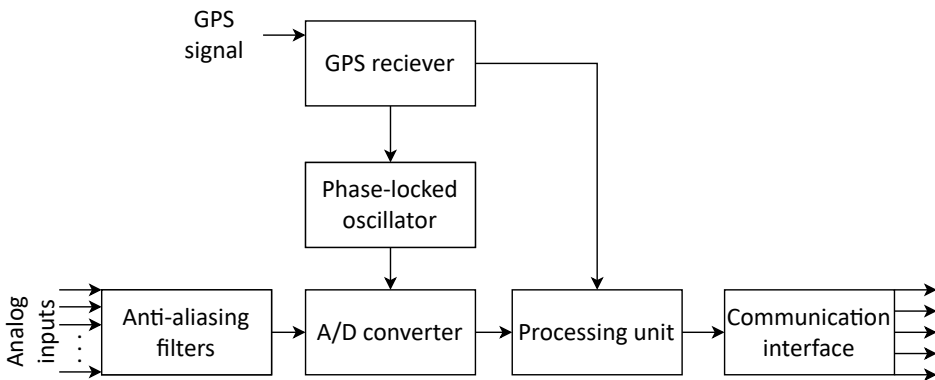


Figure 4 - Functional diagram of PMU device.

The IEC60255-118-1 [16] standard defines two classes of PMUs: P-class, which is dedicated to protection systems and M-class, provided for other needs related to measurements in the power system . The P-class is characterised by a shorter reaction time to changes and as an example the P-class reference model filtering has a step response that is monotonic (free of over-and undershoot) and fully settled within one cycle. The M-class is characterized by smaller errors than P-class; however, this comes with the drawback of slower responses to a change in the measured signal. Due to this the P-class PMU is more suitable for use in wide-area protection systems.

Structure of WAMS systems

The basic elements of a WAMS system are: the time source for timestamping (GPS clock), PMUs, phasor data concentrators (PDCs), data transmission networks and information systems for processing the measurement data for control, state estimation, protection, etc. An example of a structure of a wide-area measurement system is shown in Fig. 5. A WAMS system may have a different structure depending on the telecommunications used. Utilising point-to-point connections, the structure may be multi-layered where measure-

ment data from PMUs is sent to local PDCs. One local concentrator may service a number of PMUs, depending on the capability of the concentrator (20-40 PMUs). Thereafter, the data from data concentrators are sent to computers executing SCADA/EMS or WAMS monitoring, control or protection functions based on phasor data.

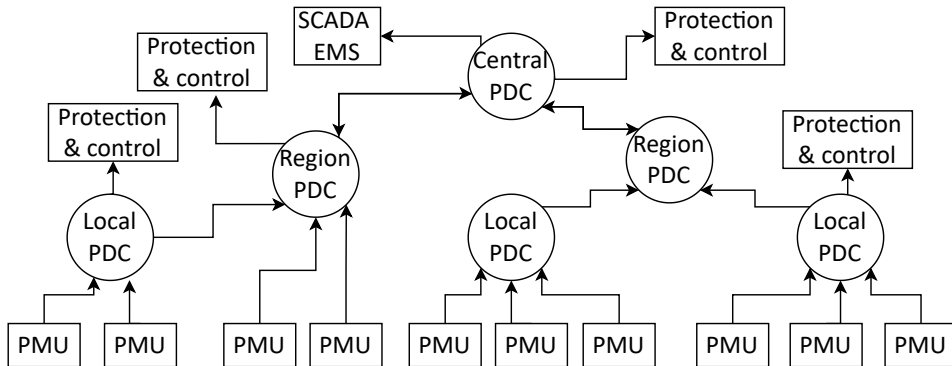


Figure 5 – An example of a layered structure of WAMS system including protection and control. PMU - Phasor Measurement Unit; PDC - Phasor Data Concentrator.

It has to be noted that in each stage of data transmission delays are incurred. Concentrators in the local layer, closest to the PMUs, may not only supply data for monitoring purposes, but also for protection and control functions, due to the lowest delays in the data transmission. The regional-level PDCs are usually used to combine data from individual areas of an electric power system. The data there can be used for some protection or control functions. The central PDC receives data from regional PDCs and usually has data from all over the monitored power system. Since at this stage the delays are longest, the central PDC may mainly be used for monitoring and SCADA/EMS and protection functions that are not very time critical in nature. Some examples of time delays introduced by various elements of the WAMS are analogue input filtering, sampling and calculation algorithms, data processing by the PMU and PDC, and data transfer using the telecommunication link. Delays of 100 - 150 ms [17] related to measurement and data transmission are considered acceptable for most wide-area protection and control applications [18, 19].

1.3 Power Swing Detection and Out-of-Step Protection Methods

Disturbances in power systems can cause oscillations in machine rotor angles, which can result in unstable power swings. These in turn cause large current and voltage oscillations leading to excess heat generation and extra mechanical stress in power system components [20, 21]. Therefore, it is important to detect these types of swings as fast as possible. Detection of unstable swings and out-of-step conditions is commonly realised by special relays. Out-of-step relays are usually installed on transmission lines and generators. The algorithms for detecting out-of-step conditions on transmission lines and generators are presently based on the same principle, while the settings for the algorithms are determined by specific grid conditions at the installed relay location. The relay manufacturers often provide guidelines, and, together with the network parameters, the utility can compute the specific settings needed for the protection operation.

Most of the out of step algorithms in use in today's power systems have been developed considering the availability of synchronous generation. For the future it is seen that more power electronic (PE) based renewable generation is integrated into the system [22] and it is currently unknown how these types of protection will behave in the future. From

the literature [23, 24, 25] it is seen that the out-of-step algorithms are usually tested and proven in numerical simulations. There have also been tests performed using real devices and real-time simulations, e.g. in [26]. These results however have not clarified the performance of the algorithms in situations where the synchronously connected units are substituted by PE-based (power electronics based) solutions. Therefore, it is not technically clear how the existing algorithms would perform, while the composition of the power generation is changing to include significant levels of inverter-based resources (IBR).

There are multiple approaches to detect out-of-step conditions in power systems. The advantages and disadvantages of the main methods commercially available for out-of-step detection used in power systems are summarised in Table 1.

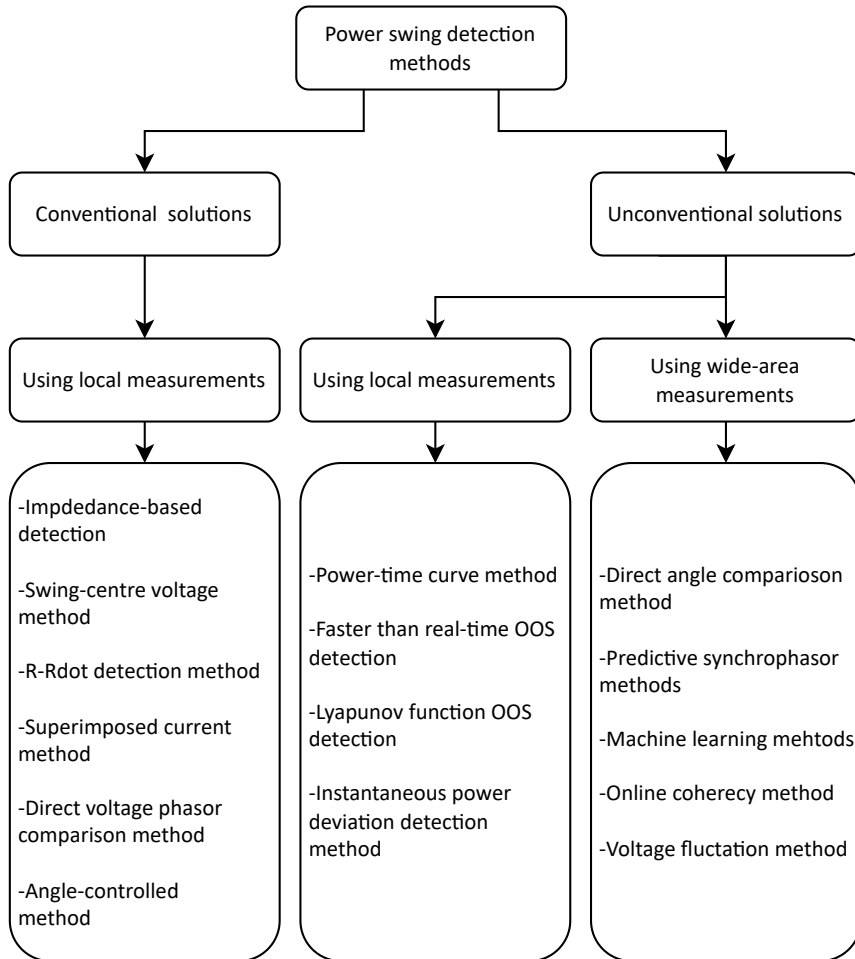


Figure 6 – General classification of OOS detection methods.

In the context of this dissertation the most common conventional solutions are considered, and in the following part an overview of the methods' workings is given.

Impedance based out-of-step detection

Impedance based out-of-step detection is realised in distance protection IEDs in the power system and it can be implemented in multiple different approaches. To understand how an impedance relay can be used for out-of-step detection and operation, it is essential to

Table 1 – Comparison of commercially used power swing and out-of-step detection methods.

Method	Advantages	Disadvantages
Impedance-based detection	Depending on implementation the ability to differentiate stable and unstable swings.	Difficulties detecting very fast swings. Rigorous analysis is required for setting the blinders.
R-Rdot detection method	Faster detection than impedance based algorithms	Dynamic stability studies needed to provide functional settings.
Superimposed current detection	Very quick power swing identification. Ability to detect faster oscillations.	Difficulties with detection of slower power oscillations. Inability to differentiate between stable and unstable power swings.
Swing-centre voltage detection	Easy to set up. Known for its reliability.	Longer time to detect out-of-step conditions.
Direct voltage phasor comparison detection	Quick identification of out-of-step condition. Detects unstable swings at the swinging centre of the system.	Requires direct communication link between two ends of transmission line.
Angle-controlled method	Provides more reliable and faster detection than impedance-based detection.	Requires power system studies to determine equivalent impedance settings.

show how the relay measurement is affected during power swings in the network [27]. Fig. 7 shows the simple power system scheme together with an impedance relay installed on the transmission line at the Bus 1 side. The voltages and currents are measured by the protective relay can be calculated by the following equations:

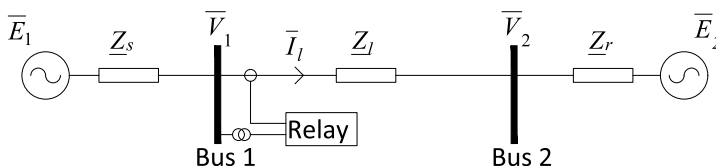


Figure 7 – Simple system equivalent scheme with impedance relay installed at Bus 1 side on the transmission line.

$$\bar{I}_l = \frac{\bar{E}_1 - \bar{E}_2}{\underline{Z}_s + \underline{Z}_l + \underline{Z}_r} \quad (5)$$

$$\bar{V}_1 = \bar{E}_1 - \bar{I}_l \cdot \underline{Z}_s \quad (6)$$

where

\bar{I}_l is the current flowing through the transmission line;

\bar{E}_1 and \bar{E}_2 - are the equivalent electromotive force values inside the two machines;

\underline{Z}_s , \underline{Z}_l and \underline{Z}_r - are the impedances of machine 1, transmission line and machine 2;

Based on the voltage and current, the impedance seen by an impedance relay at the relay location at Bus 1 is calculated as:

$$\underline{Z}_{relay} = \frac{\bar{V}_1}{\bar{I}_l} \quad (7)$$

where

\bar{V}_1 is the voltage measured by the relay at Bus 1;

\bar{I}_l is the current measured by the relay in the transmission line;

During power swings the frequencies of the two sources, f_1 and f_2 , become different, and the instantaneous values of the voltages and currents have to be calculated utilising the time-varying rotor phase angles of both machines. The rotor angles of both of the machines at any point in time can be represented as:

$$\phi_{E_1}(t) = \Phi_{E_1} + 2\pi f_1 t \quad (8)$$

$$\phi_{E_2}(t) = \Phi_{E_2} + 2\pi f_2 t \quad (9)$$

where

Φ_{E_1} is the initial rotor angle of machine 1;

Φ_{E_2} is the initial rotor angle of machine 2;

f_1 is the frequency of machine 1;

f_2 is the frequency of machine 2;

Using the variations of machine frequencies, the currents and voltages at Bus 1 and Bus 2 can be computed as follows:

$$|V_1|e^{j\phi_{V_1}(t)} = |E_1|e^{j\phi_{E_1}(t)} - |I_l|e^{j\phi_{I_l}(t)} \cdot |Z_s|e^{j\Phi_{Z_s}} \quad (10)$$

$$|V_2|e^{j\phi_{V_2}(t)} = |E_2|e^{j\phi_{E_2}(t)} + |I_l|e^{j\phi_{I_l}(t)} \cdot |Z_r|e^{j\Phi_{Z_r}} \quad (11)$$

$$|I_l|e^{j\phi_{I_l}(t)} = \frac{|E_1|e^{j\phi_{E_1}(t)} - |E_2|e^{j\phi_{E_2}(t)}}{|Z_t|e^{j\Phi_{Z_t}}} \quad (12)$$

The time-varying quantities computed by Eq. 10, Eq. 11 and Eq. 12 above represent single-phase quantities. A power swing in the network is generally a three-phase phenomenon. The phase B and phase C quantities can be also computed by shifting the initial angles by $\pm 120^\circ$. For illustration, Fig. 8 shows a plot of three phase voltages and currents during an out-of-step condition.

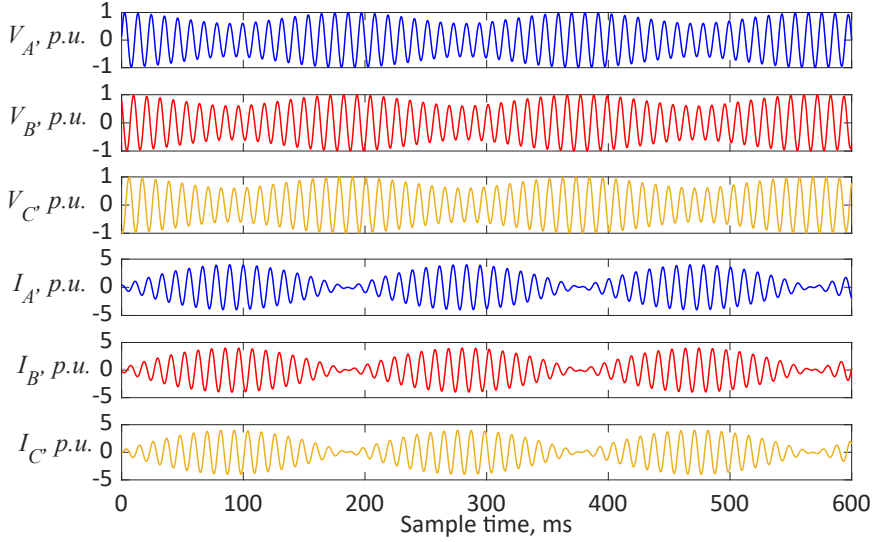


Figure 8 - Variations in currents and voltages during out-of-step conditions.

The positive sequence impedance seen by the relay at Bus 1 in Fig. 7 in the direction of the line at any point in time can be calculated by the equation:

$$Z_{relay}(t) = \frac{|\bar{V}_1|}{|\bar{I}_1|} e^{j(\phi_{V_1}(t) - \phi_{I_1}(t))} \quad (13)$$

Assuming the sources have equal impedance amplitudes, the positive sequence impedance related to a particular phase angle δ is represented by the following equation:

$$Z_{relay}(\delta) = Z_t \frac{\bar{E}_1 \angle \delta}{\bar{E}_1 \angle \delta - \bar{E}_2} - Z_s \quad (14)$$

In Fig. 9 the impedance locus seen by a distance relay at Bus 1 in Fig. 7 is shown. The trajectory during a power swing depends on the ratio of the source voltage amplitudes (E_1 and E_2) at either side of the transmission line, as well as where the electrical centre of the system is located.

The electrical centre is the midpoint of the total system impedance Z_t . As seen in Fig. 9, when both power source internal voltages are equal, the resulting swing locus is a straight line, which is perpendicular to the total system impedance, and the locus is passing through the electrical centre, at which the angular difference δ of the two machines is equal to 180° . A point labelled "M" is also shown in Fig. 9, where the $\delta = 90^\circ$, and the resulting measured phasor of the impedance relay on Bus 1 during that particular situation.

When the electromotive force located behind the impedance relay (E_1) is greater than the electromotive force at the opposing end of the transmission line (E_2) the impedance trajectory follows a large circle that passes the total impedance above the electrical centre. When E_1 is lower than E_2 the trajectory is a circle passing below the electrical centre. If the frequency of the power source on Bus 1 (f_1) is greater of the Bus 2 power source frequency (f_2) the impedance locus follows the trajectory from right to left, as indicated in Fig. 9, whereas, the impedance locus will move from left to right if f_1 is smaller than f_2 .

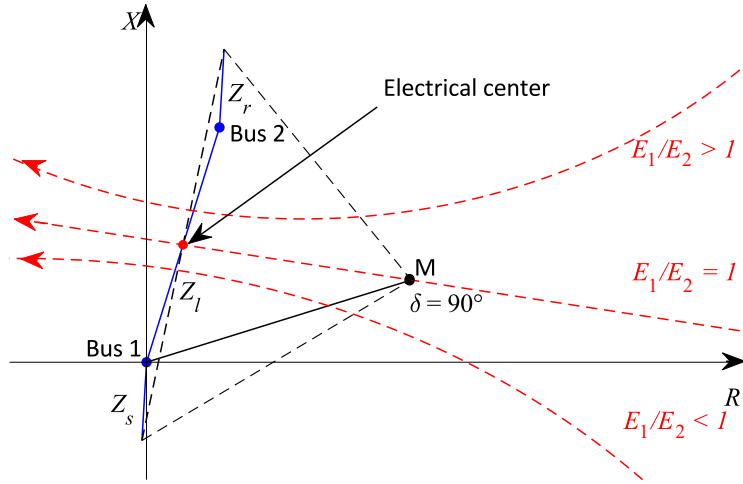


Figure 9 - Impedance trajectories seen by a distance relay at Bus 1 depending on the angle difference δ between the two machines. Top trajectory shows the seen impedance locus in the case of $E_1/E_2 > 1$, middle trajectory in the case of $E_1/E_2 = 1$ and bottom trajectory indicates impedance trajectory in the case of $E_1/E_2 < 1$.

In a real power system, the machines are not ideal power sources as have been considered in the equivalent two-machine system example. Furthermore, the voltages of the machines are controlled by the existing automatic voltage regulation. Therefore, during power swings, the ratio of the two power source voltage magnitudes is not a constant value. This means that the resulting locus of the measured impedance will move smoothly from one circle to another, depending on the instantaneous magnitude ratio of the two equivalent sources [28]. Fig. 10 shows a family of impedance trajectories for different ratios of $|E_1/E_2|$ to show the effects of voltage magnitude ratios for impedance measurement. As the ratio of $|E_1/E_2|$ increases, the impedance locus becomes a circular trajectory that moves away from the measurement location, whilst in the case of a decrease in the ratio of $|E_1/E_2|$, the impedance trajectory moves closer to the measurement location.

Based on the explanation above, it is clear that the power swings present themselves in the impedance plane. Conventionally, the power swing detection methods measure positive-sequence impedance seen by the relay and the rate-of-change of measured impedance. Several characteristics can be implemented for detecting stable and unstable power swings, e.g. blinder schemes, concentric impedance characteristics and continuous measurement of impedance.

During normal operation the impedance measured by the relay represents the load current, and is normally situated on the far right or left, near the active impedance axis on the impedance plane. When a fault occurs in the network, the measured impedance by the relay jumps immediately from the load impedance to a point on the impedance plane representing a fault. However, when a power swing takes place, the measured impedance moves slowly at a certain speed that represents the slip frequency between the parts of the network, and following some trajectory in the impedance plane. The three situations are depicted in Fig. 11. The difference in the impedance change speed and continuity of movement is used to differentiate between faults and power swings.

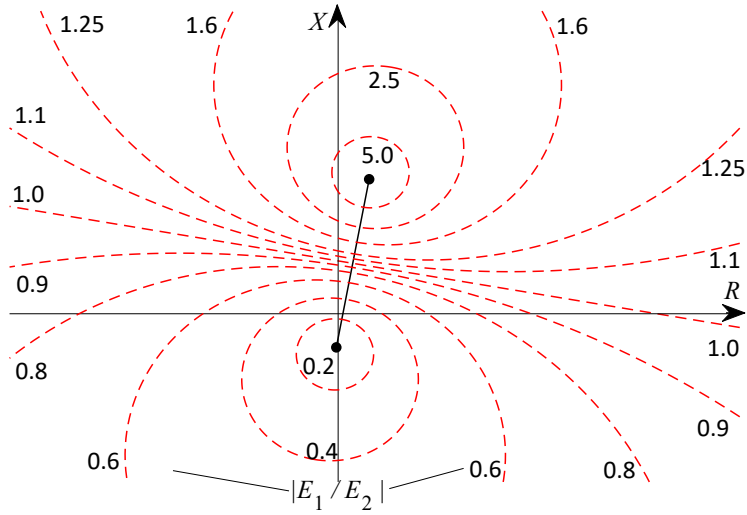


Figure 10 - Impedance trajectories for various ratios of $|E_1/E_2|$. While the ratio of the voltages increases the impedance trajectory moves further away from the measurement location, and as the ratio decreases the impedance trajectory moves closer to the measurement location.

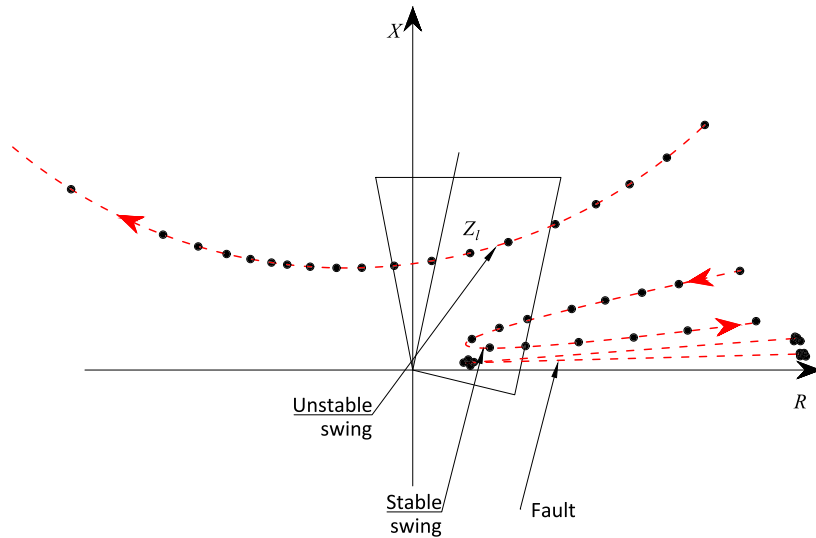


Figure 11 - Impedance trajectories in the case of unstable swing, stable swing and faulted conditions in the network.

This method of differentiation is usually implemented by using two impedance characteristics, which are separated by a known impedance value ΔZ and a timer with a known value Δt . This may be realised by a double blinder or a concentric characteristic scheme, which are shown in Fig. 12 and Fig. 13, respectively. The timer is started when the measured impedance crosses the outer blinder (labelled "A" in Fig. 12). For a fault condition the measured impedance moves immediately to the fault point and crosses the inner

blinder stopping the timer before it expires. In the case of a power swing, the impedance, shown in Fig. 12 as impedance trajectory, moves more slowly from the load area towards the distance protection characteristic. The timer Δt will expire before the swing locus crosses the inner blinder in point B in Fig. 12, in which case a power swing is declared. If the swing continues its trajectory and crosses the inner blinder on the other side of the impedance plane the power swing is unstable, and an out-of-step condition is declared (point "C" in Fig. 12). This is referred to as "trip on the way out (TOWO)" or "delayed tripping".

Another approach is to trip immediately when the inner blinder is crossed and a power swing has been declared. This is referred to as "trip on the way in (TOWI)", "predictive tripping" or "early tripping". The drawback of this approach is that the power swing may be a stable swing, however, if the relay is set to trip early, it may worsen the situation for the network in general.

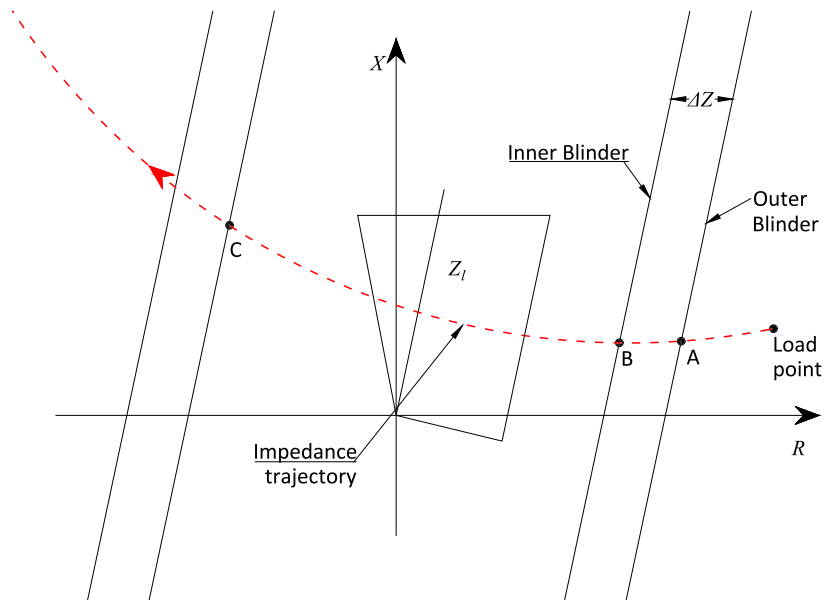


Figure 12 – Double blinder scheme. Point "A" represents the starting of a timer value for power swing detection, point B is where the timer value is stopped and a power swing is declared. Point "C" is where an OOS condition is declared.

The concentric characteristics scheme (Fig. 13) for power swing detection uses the same principle as the double blinder scheme, but the impedance characteristics are used for the impedance movement speed measurement are placed concentric to each other. The inner impedance zone can be an existing distance protection zone, or it may be an additional impedance element specifically for the purpose of detecting power swings. The outer zone is usually an additional element only used for the detection of power swings. Additionally, a counter can be set to operate the out-of-step protection after a set number of pole slips in the network, instead of operation on the first pole slip. Concentric out-of-step protection schemes include a range of characteristics with varying levels of complexity, flexibility, security and dependability [29]. Fig. 14 shows some of these concentric characteristic types. the Mho-type concentric characteristic is used for transmission lines and generators, the lens-type characteristic is most commonly found for generator protection and the polygonal characteristic is commonly found for transmission lines [21, 27, 29].

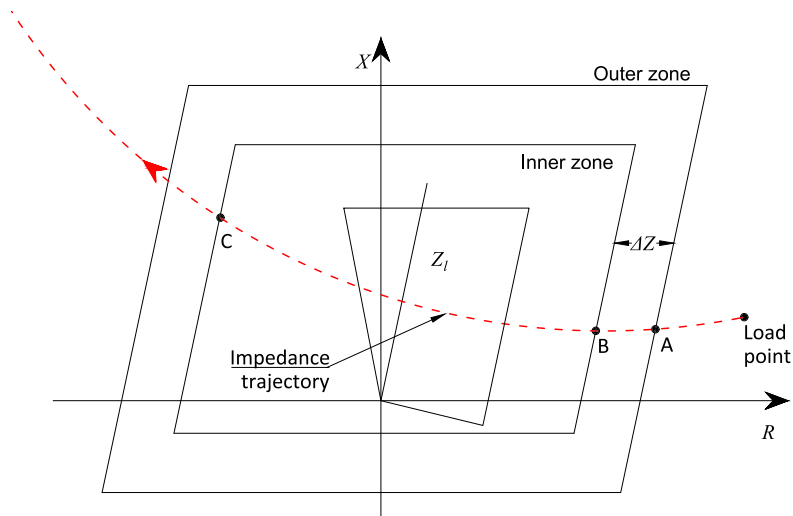


Figure 13 – Concentric characteristic scheme. Point "A" represents the starting of a timer value for power swing detection, point B is where the timer value is stopped and a power swing is declared. Point "C" is where an OOS condition is declared.

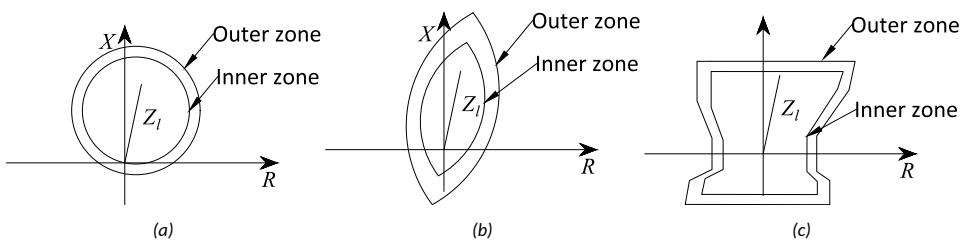


Figure 14 – Examples of concentric characteristic types. (a) - rho characteristic, (b) - lens characteristic, (c) - polygonal characteristic.

The concentric characteristic scheme allows for more control over the limits of detection and reaction to power swings by the relay compared to the double blinder scheme. This is desirable. Because of the impedance relay being installed in a certain network location, limiting that particular relay's ability to react to power swings too far in the network is essential for the prevention of maloperation of the relay. Due to this, the concentric characteristic scheme is used in most of the commercially available impedance protection relays.

The single-blinder scheme shown in Fig. 15 can be used for detecting unstable power swings or out-of-step conditions. It uses a single set of blinder characteristics. The single-blinder cannot distinguish between a fault and an out-of-step condition - due to this limitation this scheme is unsuitable for blocking distance protection during power swings. The scheme is secure against false out-of-step trips because a command is only given after the swing has already passed both blinders, and there has been a pole slipped during an unstable swing.

Some versions of the single blinder scheme require additional logic in order to determine the direction from where the swing entered and where it left. When the impedance

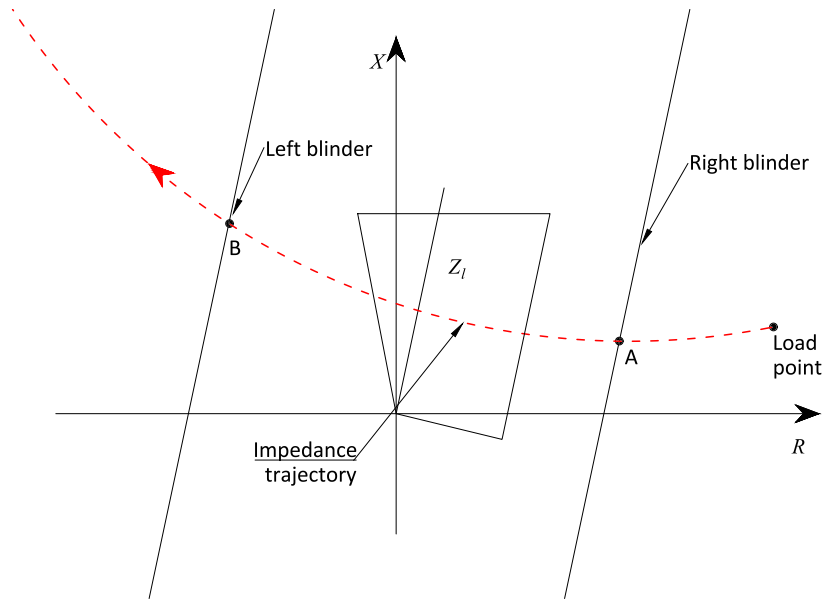


Figure 15 – Single blinder scheme. Point "A" is when the OOS detection element is started and an out-of-step condition is declared when the impedance crosses the second blinder at point "B".

locus during a power swing crosses one blinder, indicated by point "A" in Fig. 15, from one side a timer is started. An out-of-step condition is declared, when the measured impedance stays between the two blinders until the timer expires and the locus later crosses the other blinder going the opposite direction from where it entered (indicated by point "B").

This makes the scheme more sensitive to the system swing rate in order to assess the stability of the power swing. Additionally, if the impedance does not exit the blinder characteristic following the fault clearance, this scheme will not operate until the second pole slip. Similarly to the double blinder of concentric characteristic scheme, a counter can be implemented to provide tripping after several pole slips have occurred.

The continuous impedance calculation and its rate of change scheme are shown in Fig. 16. This method consists of monitoring the progression of the impedance locus in the complex plane according to three criteria [30]. For this the positive sequence impedance is usually computed every 1/4 cycle. The criteria used for power swing detection are:

- Trajectory monotony - During a power swing, the measured impedance has a directional course of movement.
- Trajectory continuity - During a power swing, the distance between two subsequent measurement values shows a clear change in resistive or inductive impedance.
- Trajectory uniformity - During a power swing, the ratio between the two subsequent changes of resistive or inductive impedance will not exceed a threshold value.

The criteria for monotony verify that the trajectory does not change direction by checking the successive ΔR and ΔX have the same signs. Continuity criteria ensures that the impedance trajectory is not motionless and requires the successive ΔR and ΔX to exceed a certain threshold. Finally, the uniformity criterion verifies that there are no sudden changes in the impedance measurement by looking at the ratios of ΔR and ΔX , which must remain

under a threshold. A power swing is declared when three criteria have been fulfilled for some consecutive measurements.

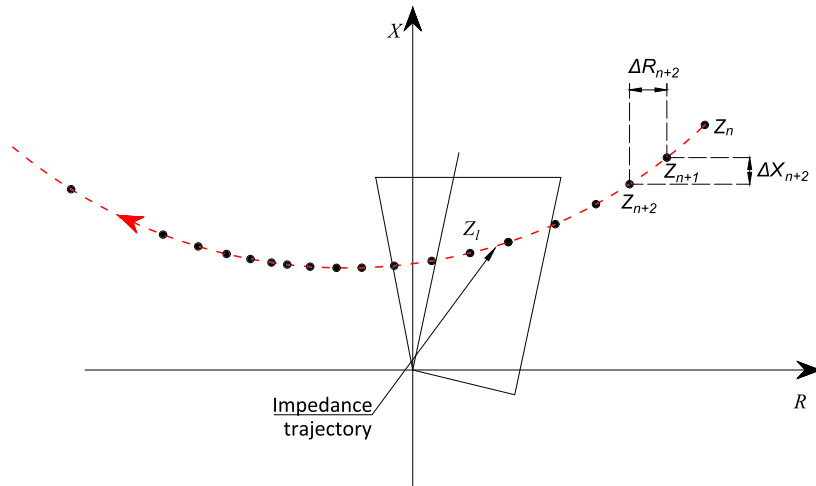


Figure 16 – Continuous impedance measuring scheme. The impedance locus movement is constantly tracked and the ΔR and ΔX values computed in order to verify the trajectory monotony, continuity and uniformity.

The continuous impedance calculation scheme is supplemented by a concentric characteristic to detect very slow swings. An advantage of this method is that it does not require setting calculations, and is able to detect very fast power swings. However, without the addition of a concentric characteristic, this method is unable to differentiate between stable and unstable power swings.

R-Rdot detection method

The rate of change of apparent resistance method for detecting out of step conditions was first proposed in [31]. This scheme was applied to the US Pacific AC Intertie [32]. The method utilises resistance measurement and computed rate of change of resistance. In the R-Rdot characteristic the x-axis is used to display the resistance value measured at the relay, whereas the reactance value is replaced by the rate of change of the measured resistance. The principle of R-Rdot method creates an additional impedance-based control law for OOS detection by defining the following function:

$$U_1 = (R_m - R_1) + T_1 \frac{\delta R}{\delta t} \quad (15)$$

where:

U_1 - control variable;

R_m - is the resistance value measured by the relay;

R_1, T_1 - are setting values derived from system studies.

The advantage of the R-Rdot method compared to conventional impedance-based power swing detection methods is that the relay becomes less sensitive to the location of the swing centre, and therefore could have superior performance because of the inclusion of the rate of change of resistance as an additional input [11, 31, 32].

Fig. 17 shows an example of R-Rdot relay characteristic, where the switching line U_1 is defined by the parameters R_1 , and a slope of T_1 in the R-Rdot plane. Operation is initiated

when the output of the control variable U_1 becomes negative. In the actual implementation the relay uses a linear characteristic consisting of two line segments rather than a straight line shown in Fig. 17.

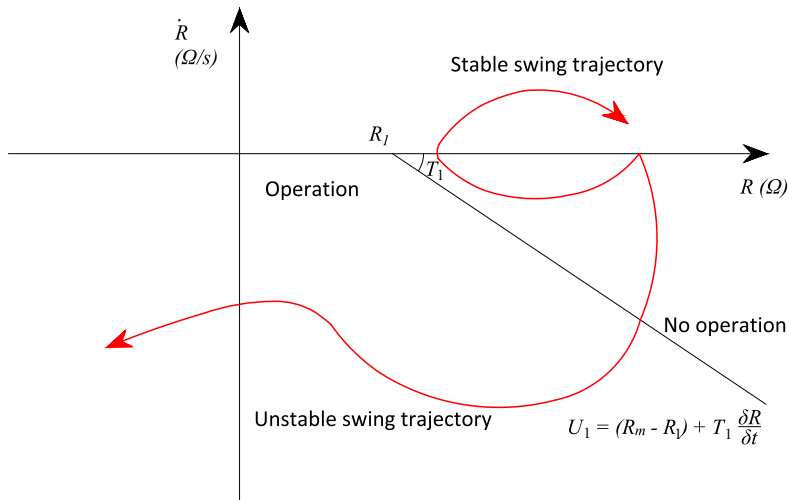


Figure 17 – R-Rdot OOS characteristic in the phase plane [11].

The main drawback of the R-Rdot method is the need for conducting dynamic stability studies in order to determine the functional values of R_1 and T_1 . This requirement is the same with impedance-based out-of-step protection, and due to impedance relays being common in the transmission network, the R-Rdot protection has not seen widespread adoption in existing power systems.

Superimposed current detection

During a power swing the phase current measured at locations between asynchronous areas undergoes magnitude variations. A power swing detection method [25] is developed based on this characteristic current magnitude variation during power swings. Fig. 18 shows a typical current waveform during a power swing. It is seen that the magnitude of the measured current increases with each period during the swing process. The superimposed current method compares the present values of currents with a buffer that is taken two cycles earlier. A delta current ΔI is detected if the difference between the current amplitudes is more than 5%.

The main advantage of this method is that it can detect very fast power swings, particularly for heavy load conditions. The main drawback, however, is that this method has trouble detecting very slow power swings with frequencies in the range of 0.1 Hz, because the current amplitude change cycle per cycle may be lower, than the required threshold for swing detection [11, 25, 33]. Additionally, this method can identify the power swing, but cannot determine, if the power swing is unstable or stable, therefore it needs to be complemented by other methods to provide out-of-step protection.

Swing-centre voltage based detection

In a two-machine equivalent system the electrical centre is the electrical midpoint of the total impedance of the line and two sources [34]. When a power swing occurs the voltage magnitude at the electrical centre reaches zero when the angle difference between the

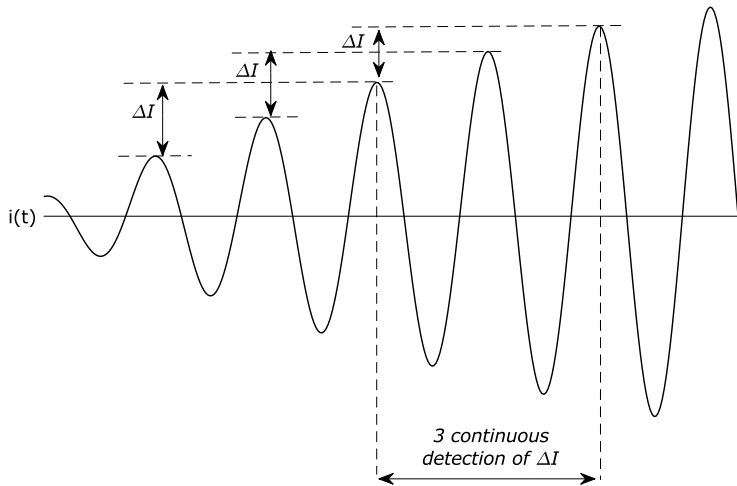


Figure 18 - The incremental increase in measured current values during a power swing.

two machines are 180° apart. The voltage at the electrical centre of the system is referred to as the swing-centre voltage (SCV). Fig. 19 illustrates the voltage phasor diagram of a general two-machine system, with the swing-centre voltage as the phasor from the origin of the point 'o'.

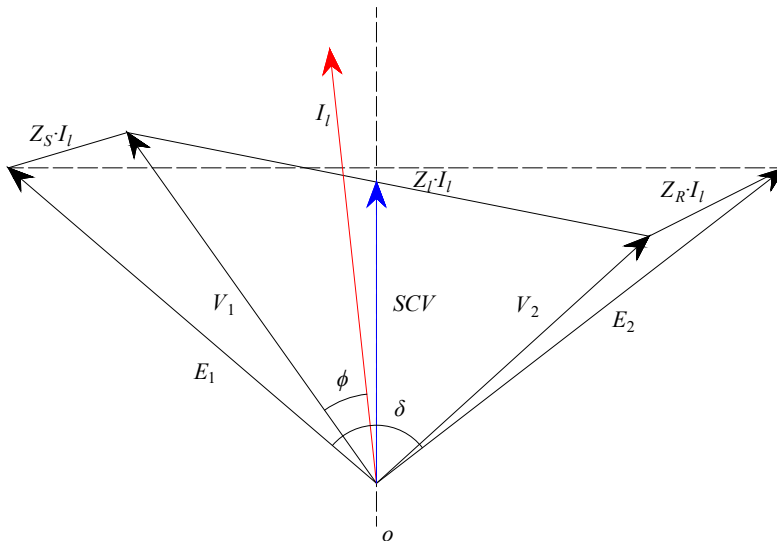


Figure 19 - Voltage phasor diagram of a two-machine system. The swing-centre voltage used by this method is shown by the blue phasor, the locally measured voltage is shown as V_1 and the measured current I_l in red [34].

When a two-machine system loses stability the angle difference of the two sources (δ) increases as a function of time. The magnitude of the swing-centre voltage changes between 0 and 1 per unit of system nominal voltage, and is directly linked to the angular

difference between the two equivalent sources. Under normal conditions the magnitude stays constant.

One approximation [11] of the SCV is obtained by locally available quantities according to Eq. 16 [35].

$$SCV \approx V_I \cdot \cos(\phi) \quad (16)$$

where:

$|V_I|$ - magnitude of the locally measured voltage;

ϕ - the angle difference between locally measured voltage and current phasors.

Using this method, it is possible to successfully approximate the swing-centre voltage magnitude based on local quantities, when the system impedance angles are close to 90 degrees. For the purpose of power-swing detection, it is the rate of change of the SCV that provides the main information of system swings, therefore some differences in magnitude between the real and approximated SCV value have little effect in detecting power swings.

It has to be noted, however, that when there is no load flowing in the transmission line, the current measured from the line terminal is the line charging current, which leads the voltage by about 90 degrees. In this case the local estimate of SCV is close to zero and does not represent the true value of SCV. Additionally, the local estimate of the SCV introduces a sign change in its value when the angle difference δ of the two equivalent sources goes through zero degrees [35].

Direct voltage comparison based detection

The direct voltage comparison algorithm is using two IED's for directly comparing the voltage vectors in each end of the transmission line, using telecommunication between the two devices. The principle scheme of the protection is shown in Fig. 20a. Voltage U_A is acquired by IED A, and corresponding voltage U_B is acquired by IED B. Using a telecommunication channel between the relays, the voltage data at both terminals are provided to the respective opposite terminals. Voltage phasor obtained from IED A is used as a reference and is fixed on the x-axis of the protection characteristic. In the case of unstable swings compared to the reference voltage U_A , the second voltage phasor U_B will appear in second or third quadrant (α -zone or β -zone) of the protection zone that is shown in Fig. 20b. In order for the protection to issue a tripping command the voltage vector U_B needs to be stable in each quadrant for at least 1.5 cycles to avoid tripping from transient situations [36].

The drawback of the direct voltage phasor comparison out-of-step tripping is that for the algorithm to function, the electrical center of the swing needs to be located on the protected line.

Angle-controlled out-of-step protection

The angle control-based method relies on the detection of the angle difference between two equivalent voltage phasors, measured at critical network locations. The protection algorithm operates when the angle difference between two modelled voltage phasors exceeds the maximum allowed value. For the algorithm operation measurement of local voltage and current values is needed, as well as setting values of the equivalent network impedance [38]. The two modelled voltage phasors \bar{U}_1 and \bar{U}_2 are used to monitor the angle difference ϕ between the equivalent generation sources and the rate-of-change of the angular difference. The voltage phasors are modelled as follows:

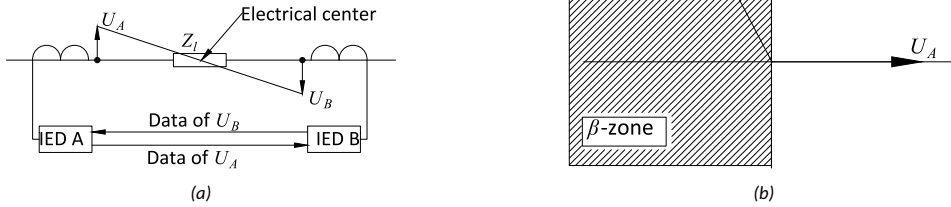


Figure 20 – Principle scheme of voltage comparison algorithm: a) – measurement principle; b) direct voltage comparison based algorithm tripping characteristic. U_A – voltage phasor measured by IED A, U_B – voltage phasor measured by IED B. Adapted from [37].

$$\bar{U}_1 = \bar{U}_m + \bar{I} \cdot \bar{Z}_1 \quad (17)$$

$$\bar{U}_2 = \bar{U}_m - \bar{I} \cdot \bar{Z}_2 \quad (18)$$

$$\phi = \text{atan}\left(\frac{\bar{U}_1}{\bar{U}_2}\right) \quad (19)$$

where:

\bar{I} - measured phase current;

\bar{U}_1, \bar{U}_2 - simulated voltage vectors;

ϕ - angle difference between simulated vectors;

\bar{U}_m - measured phase voltage;

\bar{Z}_1, \bar{Z}_2 - compensating grid impedance settings depending on the power system parameters.

From the two simulated vectors, the protection device fixes vector \bar{U}_1 onto 0 degrees and moves vector \bar{U}_2 in relation to that. An out-of-step condition is detected when the angle between the two simulated voltage vectors exceeds the limit value of 55 degrees or 80 degrees [38]. The main drawback of the protection is its dependency on the compensating grid impedance settings, which need to be calculated with care, as compromised setting values may deteriorate the performance of the protection.

This algorithm has been complemented by adding communication links between multiple terminals to enhance the capability of this approach [39]. Additionally, a variation of the method asks for terminals to be installed directly at generator terminals, to mitigate the algorithm's requirement for protection settings. However, this requires high observability in the network in order to be truly effective [40] [41].

Unconventional out-of-step protection

Additionally to the conventional methods of power swing detection used in power systems, which have been described in the previous part of this thesis, there are numerous unconventional approaches for detecting power swings presented in literature. These methods include solutions based on local and wide-area measurements and this section will provide an overview of some of the presented methods. The most notable methods using localised measurements, and their main advantages and disadvantages over the conventionally used methods, are given in Table 2.

Table 2 – Comparison of unconventional out-of-step detection methods based on local measurements.

Method	Advantages	Disadvantages
Power-time ($P-t$) curve based detection [42] [43]	Instability is directly detected from measurements.	Can only be applied directly at generator terminals. No predictive properties.
Faster than real-time OOS detection [44]	Provides extremely fast OOS detection; predicts if a swing will become unstable.	Requires detailed knowledge about generator parameters; can only be applied directly at generator terminals.
Lyapunov function based OOS detection [45]	The method shows excellent results in OOS detection.	Highly dependent on the estimation of swing-center voltage value.
OOS protection based on instantaneous power deviation [46]	The method presents fast and reliable OOS detection.	Only applicable at generator terminals, requires input from generator rotor speed; no predictive properties.

In addition to the OOS detection methods based on local measurements, a number of unconventional techniques utilising wide-area information have been developed. An adaptive OOS relay design and application based on wide-area measurements utilising equal-area criterion was already proposed more than 20 years ago [47]. The proposed approach relies on checking the measurement data against pre-stored network, generation and load data as well as breaker and line data. There also exist adaptive OOS protection solutions making use of tripping indices [48] as well as new coordinate systems [49]. However, these methods have not seen adoption in the actual power networks.

Additional OOS protection algorithms using wide-area information from the literature together with their advantages and disadvantages are shown in Table 3. The methods include direct voltage angle comparison [50], that makes use of comparing the measured angles directly to declare OOS conditions, as well as predictive [51] and machine learning solutions [52, 53, 54]. Some developed methods found in the literature are based on online coherency detection [55] and as well as observing voltage fluctuations across the transmission network [56].

All of the unconventional solutions shown in Tables 2 and 3 are not commercially available, and have been showcased in laboratory environments or simulations thus far.

1.4 Challenges for Existing Out-of-Step Protection

The electric power system is evolving as the push towards more renewable and sustainable energy system continues. This means that more renewable energy sources are being integrated into the network with the objective of reaching close to 100 % renewable-based

Table 3 – Comparison of unconventional out-of-step detection methods based on wide-area measurements.

Method	Advantages	Disadvantages
Direct angle comparison based OOS protection [50]	The method does not require any computation of protection settings.	Requires monitoring of all the generator buses in the network; operates after several out-of-step cycles.
Predictive OOS based on synchrophasors [51]	Enhances existing OOS protection, provides more secure and reliable operation for oscillatory OOS compared to existing methods; has predictive properties.	OOS detection speed is not known; not effective in detecting non-oscillatory unstable swings.
Clarke transform based method [57]	Provides settingless OOS protection, has been prototyped.	OOS detection speed is not elaborated; no predictive properties.
Machine learning approaches [52, 53, 54]	Methods offer fast and accurate OOS condition detection, can predict OOS conditions.	The correct performance of the methods requires extensive training using detailed models.
OOS detection based on PMU-determined impedances [58]	The method is more secure and provides faster OOS detection than conventional solutions.	Requires a step change in the network to determine network impedances for OOS detection; no predictive properties.
Fast online coherency OOS detection [55]	The method shows more reliable OOS detection than conventional solutions.	OOS detection speed is not elaborated; only applicable at generator terminals, requires a threshold setting; no predictive properties.
Voltage fluctuations based OOS detection [56]	The method shows fast detection of instability.	Requires a high level of observability in the network; no predictive properties.

energy system [22]. The renewable energy sources, and also energy storage devices, often use inverters to connect to the existing alternating power grid. The inverter-based resources (IBRs) have characteristics that fundamentally differ from those of synchronous

machines. IBRs are usually limited in their current output due to the limitations in the semiconductor switches used in them, which means that with more of these types of energy source integration the source impedances of the electric power system will change, as well as the inertia level in the system.

This will not only affect the unit protections as the short-circuit current levels and characteristics of the current are changing, but will also affect the whole system dynamic behaviour. In order to reflect the situation change with added inverter-based sources an IBR plant is added at Bus 2 to the simple system first introduced in Fig. 1. The resulting test system is shown in Fig. 21.

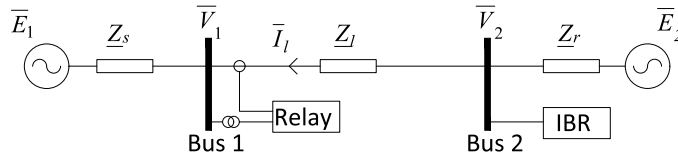


Figure 21 – Simple system equivalent scheme with added IBR source.

Considering the system loading to be a constant value, the IBR renewable sources will start replacing the power produced by the synchronous machines. This means that the total synchronous machine equivalent at Bus 2 will start decreasing. The IBRs have a limited output capacity dictated by the current limit of the converter, therefore the system equivalent on Bus 2 side will also start to change when connecting IBRs to the same bus. This change in equivalent impedance, as well as change in inertia, in turn has an effect on the existing out-of-step protection. The theoretical impact of changing system equivalent source impedance on three of the most common OOS protection algorithms is observed.

Effect of changing grid conditions on impedance-based out-of-step protection

Impedance-based out-of-step protection utilises the impedance locus movement to detect instability during power swings, as has been explained in more detail in Section 1.3. When looking at the simple network shown on Figure 21, Eq. 1 still dictates the power transfer across the transmission line connecting the two parts of the network. From this we can also compute the impedance seen during swings by the impedance protection installed at the relay location on the network using Eq. 14. However, when replacing the synchronous generation with an IBR, the network impedance value becomes of question.

Neglecting the effect of IBR, the source impedance at Bus 2 starts to increase in accordance to the RES penetration level. For example, if the synchronous generation level is 50 % lower, i.e. half of the synchronous machines connected to the bus are switched off, than the initial base case, the source impedance would be twice as high. Assuming equal electromotive force magnitudes at each source, it is possible to compute the apparent impedance trajectory with the changed source impedance, seen by the relay installed in the network using Eq. 14. The apparent impedance trajectories with the base case and the changed source impedance are shown in Fig. 22.

The impedance protection characteristic is also added to the impedance trajectories, to see how the operation of protection can be affected by the source impedance changes. In Fig. 22 the computed OOS protection polygon for a concentric characteristic, computed according to [59] and the trajectories of impedances, are shown.

Often, together with the increase of the source impedance, the electromotive force of the smaller generator appears lower from the system point of view, which affects the

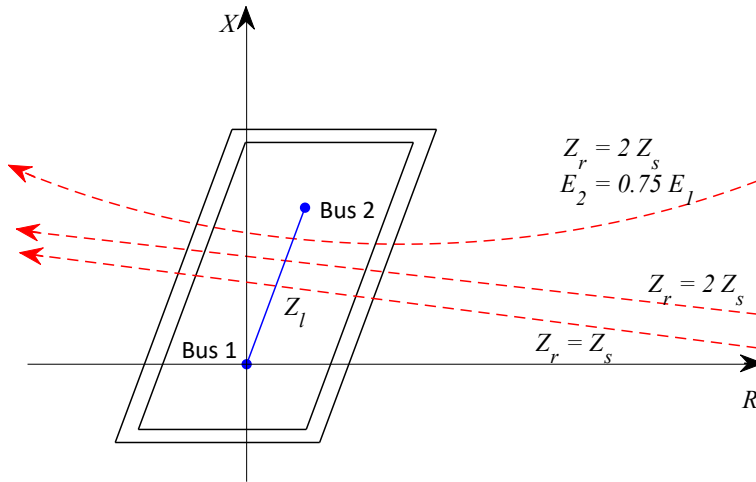


Figure 22 - OOS protection characteristic and impedance trajectories seen by a distance relay at Bus 1 when source impedance changes in the case of an electrically long line (SIR = 0.33).

impedance during swinging even more, as is shown by the trajectory, where $E_2 = 0.75E_1$, shown in Fig. 22.

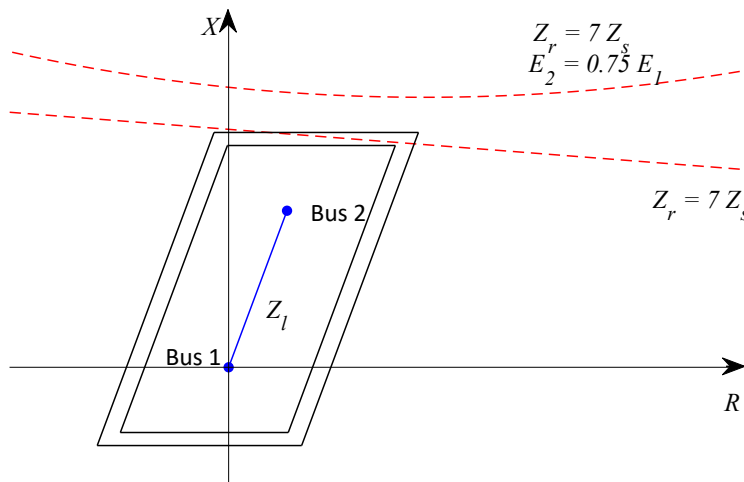


Figure 23 - OOS protection characteristic and impedance trajectories seen by a distance relay at Bus 1 with further increase in source impedance in the case of an electrically long line (SIR = 0.33).

The measured impedance locus moves higher on the OOS protection characteristic due to both the source impedance change as well as the electromotive force change. If the synchronous generation share continues to decrease on Bus 2, the impedance locus

during swings moves further up the Y-axis, and will not enter the OOS protection characteristic (Fig. 23). This means that the impedance relay will not be able to detect the out-of-step condition, because the impedance locus will not enter the detection characteristic. One possible solution is to increase the OOS detection zone, however, it has to be noted that this makes the protection more sensitive, which can cause problems of its own, e.g. maloperation of the protection during stable swings. Overly sensitive protection can make the impedance relay detect OOS conditions too far inside the power network, which may lead to maloperation. Furthermore, when a fault occurs farther in the network and a power swing follows, the impedance locus can jump inside the OOS detection characteristic and thereafter start moving, causing the OOS detection element to fail or delay its operation.

The described set of circumstances illustrate the situation of what is known as an electrically long ($SIR < 0.5$) transmission line [60]. When considering an electrically short transmission line ($SIR > 4$), the change in source impedance has a greater impact on the protection system. The impact of source impedance change in the case of an electrically short transmission line is shown in Fig. 24, where the source impedance values have been kept the same, however the transmission line impedance has been reduced. It can be seen that in this case the impedance locus does not enter the OOS detection characteristic any longer with a ratio of 4 between the two source impedances compared to 7 of a long transmission line. Therefore, it can be concluded that the source impedance changes affect the OOS protection and the extent of the effect depends on the source impedance ratios as well as the transmission line length where the protection is implemented. Real-time testing of a commercially available impedance protection is performed in more detail in [37]. All of the examples provided in this section use fixed values for the electromotive forces, whereas in an actual power system these values are not constant during an OOS condition. This fact also changes the measured impedance trajectory, making the locus follow a circular course, as has been described in Section 1.3.

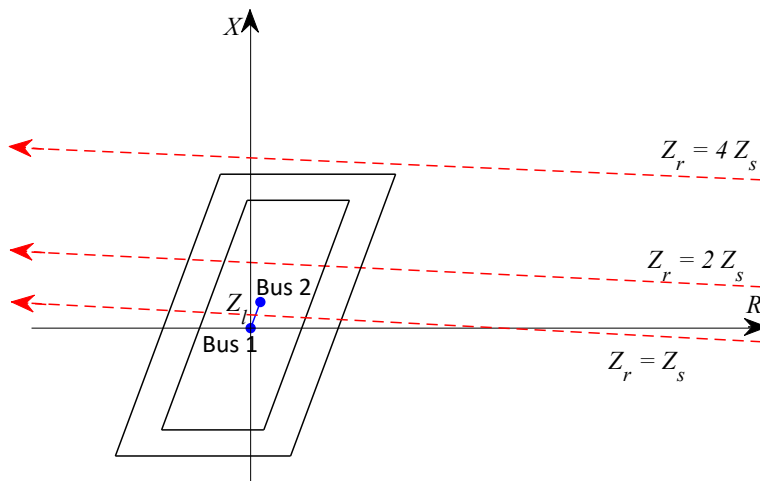


Figure 24 – OOS protection characteristic and impedance trajectories seen by a distance relay at Bus 1 in the case of an electrically short line ($SIR = 4.0$).

Effect of changing grid conditions on OOS protection using direct angle comparison

The influence of changing equivalent impedance on OOS protection using direct angle comparison can be illustrated by plotting the measured angle difference of the protection algorithm compared to the angular difference of the two equivalent sources at the remote ends of the transmission line. By adding the thresholds of α -zone and β -zone to the plot it is possible to assess the theoretical operation of the OOS protection algorithm and how different source impedance values influence the protection algorithm. Fig. 25 shows the measured voltage angle difference as well as the threshold values for the protection in the case of an electrically long transmission line.

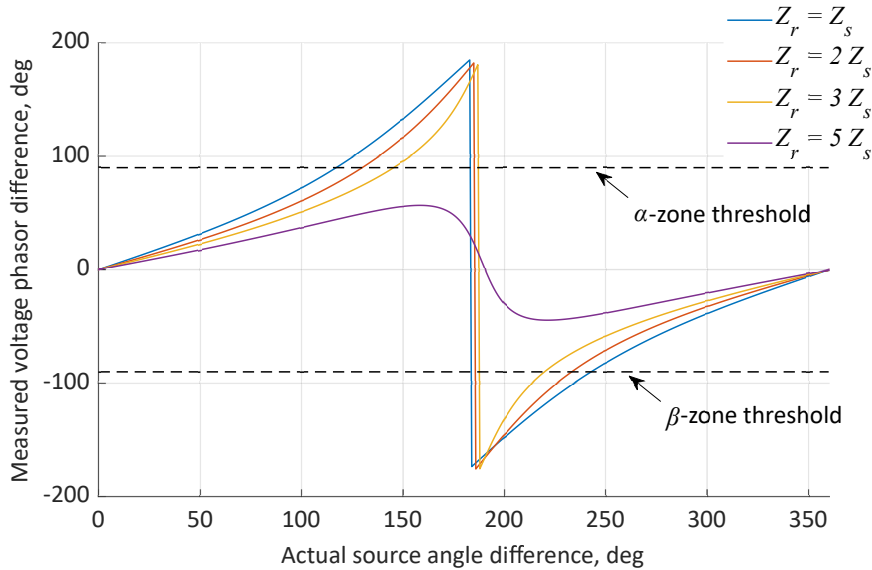


Figure 25 – Measured voltage angle difference in relation to source angle difference with different Z_r/Z_s ratios in the case of an electrically long line ($SIR = 0.33$).

Fig. 25 shows, based on the characteristics of the protection given in Section 1.3, that the direct voltage comparison algorithm fails to operate for an OOS condition with the Z_s/Z_r ratio of 5, due to the measured voltage angle difference not exceeding either operation threshold value. This makes the direct voltage comparison algorithm more sensitive to source impedance changes than the angle-controlled OOS protection.

When observing the case of an electrically short transmission line, the direct angle comparison algorithm becomes further constrained. The measured voltage angle difference and protection threshold values are shown in Fig. 26. In this case the protection is only able to operate up to Z_s/Z_r a ratio of 1.25. This means that the direct angle comparison algorithm is extremely sensitive to changing source impedance, and its ability to detect OOS condition also greatly depends on the electrical length of the transmission line the algorithm is used on. Similarly to the two observed protection algorithms, the electromotive force in the equivalent sources has been considered as constant in the examples given. In an actual OOS condition this varies and further increases the protection algorithm's ability to detect unstable power swings in the network.

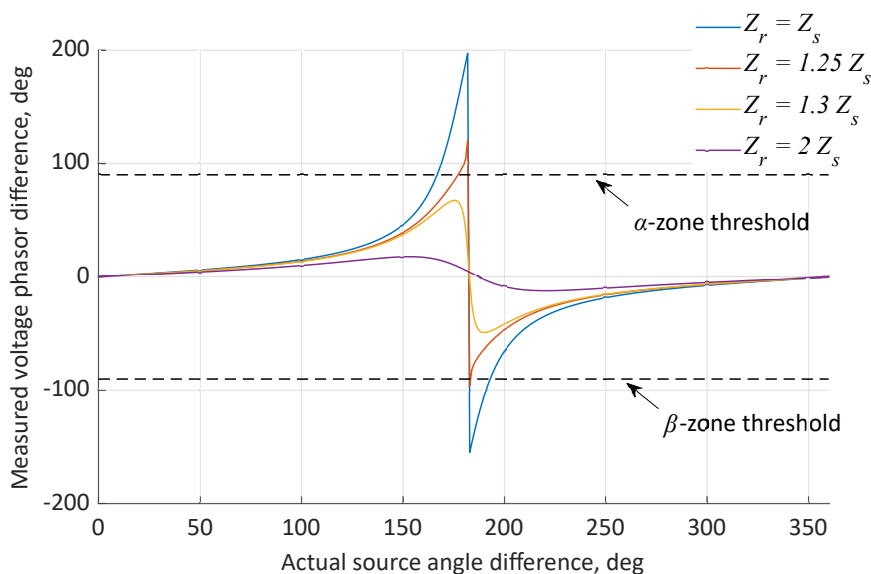


Figure 26 – Measured voltage angle difference in relation to source angle difference with different Z_r/Z_s ratios in the case of an electrically short line ($SIR = 4.0$).

Effect of changing grid conditions on angle-controlled OOS protection

The changes in source impedance affect the operation of the angle-controlled OOS algorithm. Considering the simple system example, shown in Fig. 21, initially with an electrically long transmission line ($SIR = 0.33$), and using Eq. 17, Eq. 18 and Eq. 19 it is possible to plot the phasor angle difference modelled by the algorithm and the actual angular difference between the two equivalent sources. Setting the compensating impedance values as the values according to the fully synchronous scenario with equal Z_S and Z_r values allows for theoretical assessment of OOS detection using this algorithm. Keeping the compensating impedance settings and equivalent voltage magnitudes constant, and changing the source impedance at Bus 2 to simulate the effects of changing grid conditions, the modelled angular difference, and therefore the behaviour of the protection, can be assessed. This is illustrated in Fig. 27.

From Fig. 27 it is observed, that with the increase of the impedance on Bus 2 the angle-controlled protection operation is delayed. This is indicated by the modelled angle difference values shown as the blue, red and orange curves exceeding the operation threshold at higher actual source angle difference values. It is also seen that, with a larger Z_s/Z_r ratio the modelled angle difference by the algorithm will not exceed the operation threshold of the protection as is shown by the purple line. This means that the protection will fail to operate in the case of an OOS condition in the network.

Furthermore, when considering an electrically short transmission line, the effects of source impedance change have a greater influence on this protection algorithm, similarly to impedance-based OOS protection. The modelled and actual angle differences are shown in Fig. 28 for the short line case. From the figure it can be observed that in the case of an electrically short transmission line, the protection algorithm will fail to operate at the ratio of $Z_r = 4Z_s$ compared to the long line case of $Z_r = 8Z_s$ represented by the purple line on both figures. A commercially available OOS protection utilising this algorithm has been tested in various grid conditions using real-time hardware-in-the-loop testing in

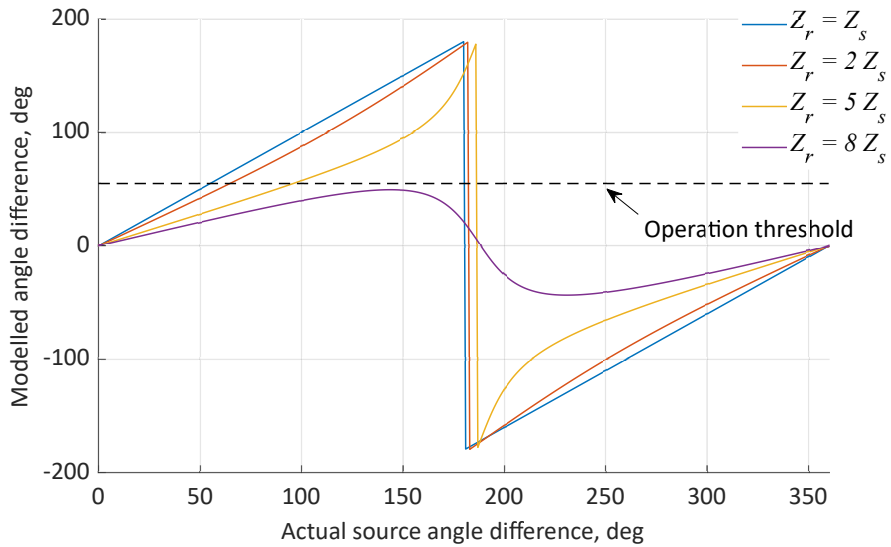


Figure 27 – Modelled angular difference in relation to source angle difference with different Z_r/Z_s ratios in the case of an electrically long line ($SIR = 0.33$).

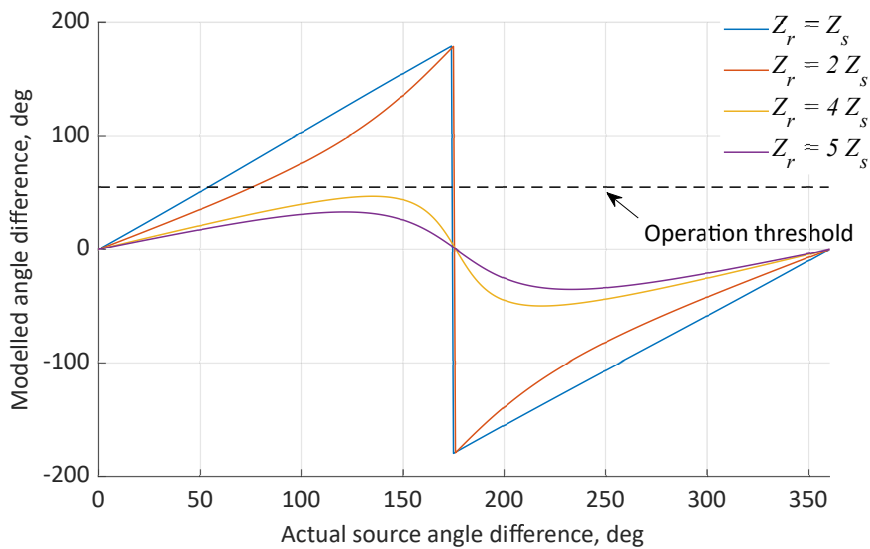


Figure 28 – Modelled angular difference in relation to source angle difference with different Z_r/Z_s ratios in the case of an electrically short line ($SIR = 4.0$).

[37], and the results from the testing are also shown in Section 4.3. The examples shown consider the electromotive forces in the equivalent sources to be constant, however, in a real OOS situation the EMF also changes, further influencing the protection behaviour.

1.5 Intermediate Summary

Power system stability, wide-area monitoring, power swing detection and challenges associated to existing OOS protection functions were described in this chapter. Power swings in the network may be stable or unstable in nature. The stable power swings are a normal phenomenon in the network, whilst unstable power swings cause abnormal stress to installed equipment in the network. This means that the unstable power swings need to be detected and something needs to react in order to stop the unstable condition in the network.

For a detailed overview of the network wide-area monitoring can be utilised, which provides measurements over the network in real-time. Inputs from WAMS can be used for protection functionality, including out-of-step protection functions, as well as monitoring the network.

Several methods exist commercially and in the literature for out-of-step protection. Most commonly an impedance-based out-of-step protection algorithm is used in power networks today. This can be realised as a single or double blinder scheme, concentric characteristic scheme or a continuous impedance monitoring scheme. The other commercially available methods include swing-centre voltage algorithm, R-Rdot detection method, superimposed current method, direct voltage comparison algorithm and angle-controlled algorithm.

As the power networks are evolving, and more IBRs are added to the grid, the existing OOS protections face challenges, which may lead to the algorithms not operating in the case of unstable power swings in the network. One major challenge posed by the changing grid conditions is the changes in the source impedance due to the synchronous generation share changing in the network. At a theoretical level the effect of changing source impedance was considered on three commercially used protection algorithms, and the analysis shows that all three algorithms pose risks for maloperation in the changing grid conditions.

2 Out-of-Step Protection Based on Equivalent Impedances

Considering the challenge of changing source impedance values for commercially available out-of-step protection algorithms in this chapter, a novel OOS protection algorithm is presented. The developed algorithm is based on equivalent impedances determined by utilising WAMS data.

Using a simple system model, the protection concept is verified and the operation of the protection algorithm is demonstrated. Then, the developed OOS protection is implemented on a hardware solution and the response of the developed algorithm to various grid events evaluated and compared to software implementation by making use of real-time hardware-in-the-loop testing. The developed concept and results presented in this chapter have been published in [II].

2.1 Proposed Out-of-Step Protection Concept

From the explanation given in Section 1.4, it is clear that the changing network source impedance has an effect on the existing OOS protection. The proposed OOS protection algorithm, developed and verified in the following subsections of this chapter, aims to counter the effects of changing source impedance by continuous computation of equivalent network impedances and applying an equal-area criterion [13] to detect an out-of-step condition. According to the equal-area criterion, a theoretical Last Stable Angle value (*LSA*) can be fixed in the constructed power-angle curve, using computed equivalent impedances and the measured quantities. After a disturbance takes place, the angle and the angle change between two equivalent sources is computed and compared to the *LSA* value. The proposed algorithm is verified by using a real-time digital simulator (RTDS). Furthermore, the algorithm is implemented in a programmable controller and tested by streaming PMU data from the test system to the external device.

Equivalent system impedance computation

The concept driving the developed algorithm is that the bulk system can be represented by two inertia centres around a tie-line and simplified into a two-machine equivalent system [61]. Thereafter, the representative two-machine system constructed around the observed tie-line can be considered as a single machine infinite bus (SMIB) network, with the parameters used in Eq. 1 and Eq. 2 in order to represent the power flow as well as the transient behaviour of the network. For the SMIB equivalent, a power-angle curve can thereafter be constructed and the angle difference between the two inertia centres computed, together with the last stable angle point, which defines the protection operation threshold. Therefore, the *LSA* point is critical for the developed algorithm, to distinguish between a stable and an unstable swing. In order to compute the *LSA* point, the impedances of the equivalent sources must be known. Fig. 29a illustrates the change of the *LSA* point with in the case of different system equivalent impedance values.

The determination of the system's actual strength or the Thevenin impedance of a power network based on local measurements and small disturbances (such as load changes) was described in [62]. The approach shows the computation of short circuit impedance for a particular node in a power system. The Thevenin equivalent impedance of the system (Z_{eq}), which is seen from the measured location is calculated from the recorded voltage and current measurements. The scheme of impedance computation is illustrated in Fig. 29b, where the measured voltage and current values at the bus are denoted by \bar{V} and \bar{I} .

In order to find the upstream system impedance from the locally measured quantities, two assumptions should be taken into account:

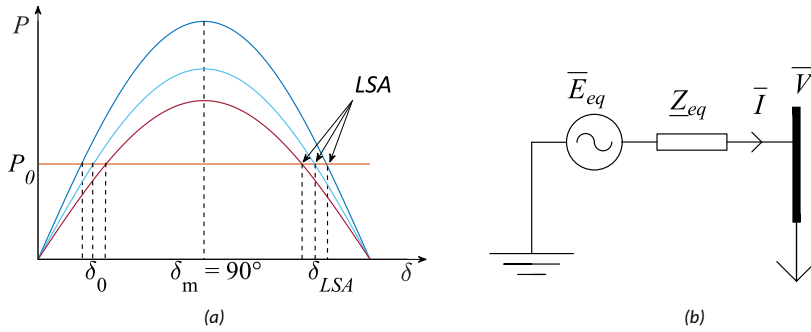


Figure 29 – Power-angle curve with Last Stable Angle point and equivalent impedance scheme. (a) - Power-angle curve constructed from calculated values, with Last Stable Angle point denoted as LSA, (b) - equivalent impedance computation scheme illustration.

- The downstream load is volatile, i.e. switching or step changes are expected in the network;
- During this variation in the load, the rest of the system remains constant.

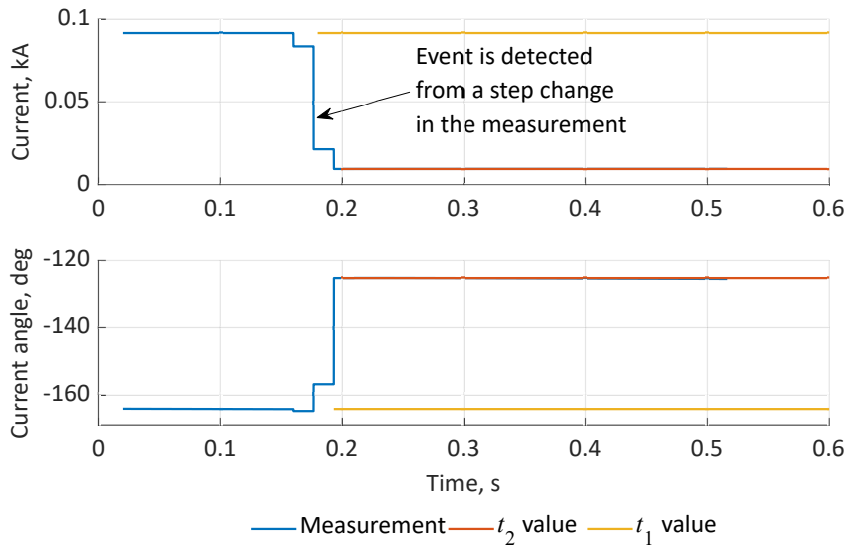
For the system impedance computation, voltage $\bar{V}(t)$ and current $\bar{I}(t)$ are measured and sampled at different time instants t_1 and t_2 . The time instants correspond to the pre- and post-disturbance values in the measured signals. Hence, the equivalent system impedance \underline{Z}_{eq} can be found by using the following equation [62]:

$$\underline{Z}_{eq} = -\frac{\bar{V}(t_2) - \bar{V}(t_1)}{\bar{I}(t_2) - \bar{I}(t_1)} = -\frac{\Delta\bar{V}}{\Delta\bar{I}} \quad (20)$$

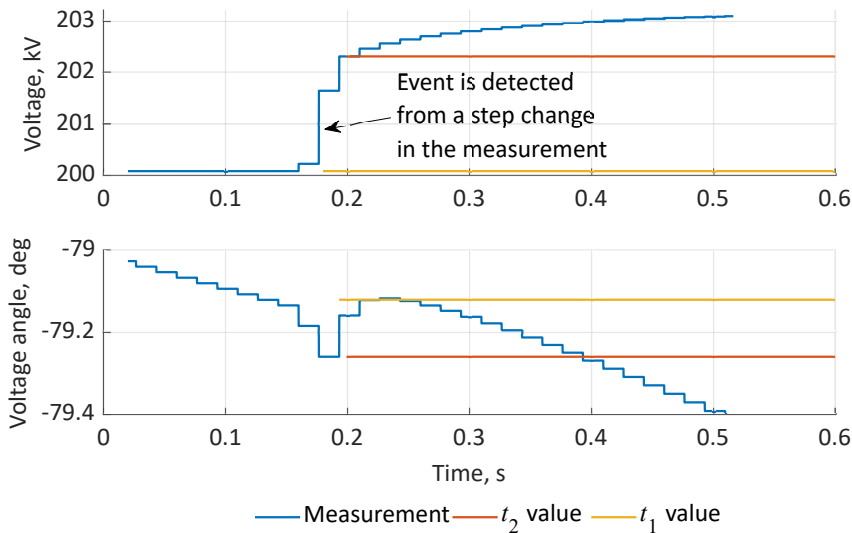
The threshold value for the disturbance detection to compute the system impedance can be set empirically [62] or, in order to improve the accuracy and the noise reduction of the measurements, an adaptive threshold can be implemented [63]. In this dissertation, the threshold values for detecting a disturbance are set empirically to 1% of the primary measurement quantity. This threshold has been based on measurements of load currents and voltages in the Estonian transmission system, from which it is observed that the normal instantaneous fluctuations in the load are within the 1% threshold [64]. Therefore, an actual step change is identified when the measurement exceeds the threshold value. Additionally, the impedance computation is vulnerable to phasor drift due to off-nominal system frequency. In this case angle shift in the time between the pre- and post-disturbance quantity sampling takes place. This problem, however, can be overcome by compensating the phasor drift [65]. The sampling of voltage and current components is shown in Fig. 30a and Fig. 30b respectively.

After an event is detected from a step change in voltage or current, the measurement values are sampled and stored. In order to record the time instant t_1 values, some memory is allocated for a rolling buffer. In this a few measurement samples are stored and continuously updated. As the event is detected, the values of instants t_2 are fixed, and at the same time, the values for t_1 are retrieved from the rolling memory buffer. The sampling of the values is shown in Fig. 30.

In a meshed transmission network all of the connected sources contribute to the current and voltage changes in the case of a step change in the network. Therefore, the approach for impedance computation can only be directly applied in the case of a radial



(a)



(b)

Figure 30 - Current and voltage measurements and sampling of quantities in the case of an event in the grid. (a) - sampling of current magnitude and angle, (b) - sampling of voltage magnitude and angle.

network. This means that the whole system impedance cannot be computed using only one measurement location, since the contribution of all the sources cannot be observed. The same concept, however, can be used to determine the system equivalent impedance behind a tie-line by making use of the superposition criterion, and utilising two measurement points. The modified method proposed for the system impedance computation of

meshed networks requires measurement at two locations in the same substation. An illustration for the measurement points is shown in Fig. 31, where one PMU measures bus voltage (\bar{V}_1), the currents of the tie-line (\bar{I}_{tl}) and additionally a load feeder (\bar{I}_{r1}), in which a step change in load may occur. Another PMU measures the same parameters at the receiving end of the tie-line.

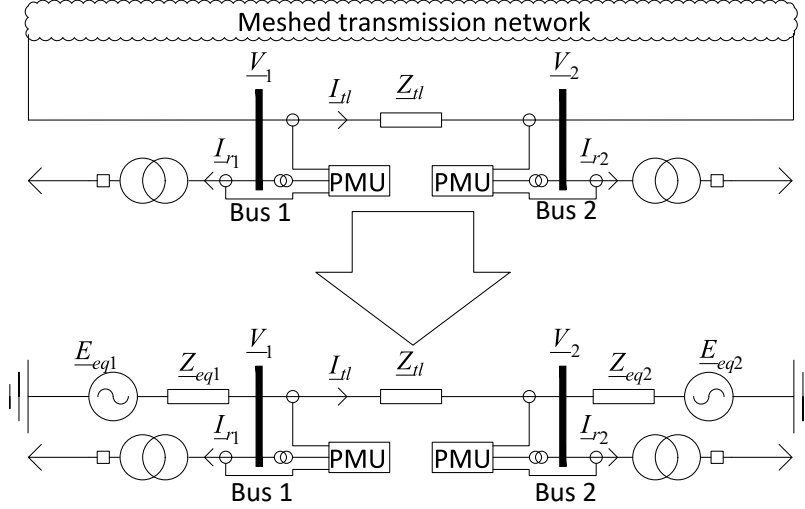


Figure 31 – Principle scheme for system impedance computation on meshed networks.

Whenever a step change in the measured current or voltage occurs, e.g. due to switching of the load feeder, the whole system impedance seen from that bus is determined according to Eq. 20. Thereafter, by applying the superposition criterion, the system equivalent impedance \underline{Z}_{eq1} behind Bus 1 in Fig. 31 can be calculated using the proportional change of current in the measured load feeder and the change of the tie-line current as follows:

$$\underline{Z}_{eq1} = \underline{Z}_{r1} \frac{\bar{I}_{r1}(t_2) - \bar{I}_{r1}(t_1)}{(\bar{I}_{r1}(t_2) - \bar{I}_{r1}(t_1)) - (\bar{I}_{tl}(t_2) - \bar{I}_{tl}(t_1))} = \underline{Z}_{r1} \frac{\Delta I_{r1}}{\Delta I_{r1} - \Delta I_{tl}} \quad (21)$$

where

\bar{I}_{r1} is the current measured in the load feeder,

\bar{I}_{tl} is the current measured in the observed tie-line,

\underline{Z}_{r1} is the value of computed impedance according to Eq. 20.

For the computation result to be valid, the impedance phasor must be in the first quadrant of the impedance plane, hence the angle of the computed \underline{Z}_{eq1} impedance is checked. This means that the angle value needs to be between 0° and 90° . Incorrect angle value means that the step change took place somewhere else in the transmission network, not in the load feeder, and therefore the computation of system impedance is discarded. The approach proposed in Eq. 21 is used to compute the system impedance behind the tie-line, which is needed to determine the power-angle curve. Protection operation and out-of-step condition identification are based on the generated power-angle characteristic.

Out-of-step protection concept

The out-of-step protection concept utilises the change of two equivalent calculated voltage vectors of the two inertia centres located behind the computed impedances at the remote ends of the observed tie-lines. The required equivalent system voltage phasor is computed at both ends of the tie-line according to Eq. 22:

$$\begin{aligned}\bar{E}_{eq1} &= \underline{Z}_{eq1} \cdot \bar{I}_{tl} - \bar{V}_1 \\ \bar{E}_{eq2} &= \underline{Z}_{eq2} \cdot \bar{I}_{tl} + \bar{V}_2\end{aligned}\quad (22)$$

The angle difference between the two calculated equivalent phasors, representing the two centres of inertia, is observed. This is illustrated in Fig. 32 where the vector diagram of the equivalent system depicted in Fig. 31 is shown.

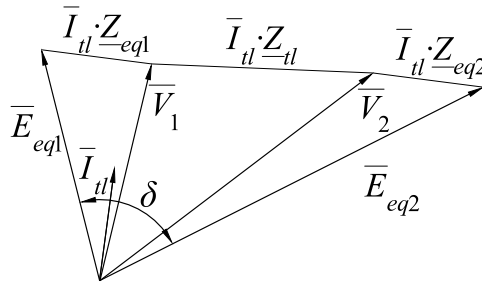


Figure 32 – Equivalent phasor diagram constructed from computed equivalent system impedances and measured quantities.

Using the calculated equivalent centre of inertia voltage phasors, the angle difference between the phasors and the measured transmitted power in the observed tie-line, a power-angle curve is constructed. On the power-angle curve the last stable angle (noted as δ_{LSA} in Fig. 29a) point is fixed. The LSA point is found by using the angle difference of the equivalent vectors as $\pi - \delta_0$ and is recalculated continuously by using the measurement values and the computed equivalent impedances. The value of LSA is sampled and used for OOS protection when a disturbance or a fault condition is identified by the protection.

During an out-of-step condition the angle difference between the two equivalent source voltages increases, moving beyond the LSA point. The protection will declare an out-of-step condition when the following conditions are met:

$$\left\{ \begin{array}{ll} \delta > \delta_{LSA} & \text{for two consecutive measurements} \\ \frac{d\delta}{dt} > 0 & \text{for two consecutive measurements} \\ V_1 > 0.5 p.u. & \\ V_2 > 0.5 p.u. & \\ \frac{d\delta}{dt} < 20\pi \frac{rad}{s} & \text{for two consecutive measurements} \end{array} \right.$$

The first two criteria are indications, that the angle difference between the two inertia centres on either end of the transmission line has exceeded the LSA, and is continuing to increase, meaning, that there is an out-of-step condition occurring in the network. The last three criteria are used as a safety feature in order to block the protection from operating in the case of short-circuit fault occurring in the network.

The voltage threshold values of 0.5 p.u. have been chosen to verify that the busbars on either side of the transmission line are in energised state, as well as to confirm non-faulted

operation. The $\frac{d\delta}{dt}$ threshold is used as an additional mechanism for fault-detection. Additionally, the angle derivative threshold limits the protection from operating when there are high-frequency oscillations in the network. During a fault occurrence a step change will appear in the computed angular difference value, which can exceed the *LSA* value for the duration of the fault, however the protection must not operate during the fault. When any of the blocking criteria of the protection are fulfilled, the out-of-step algorithm will be blocked for 200 ms. If thereafter any of the criteria are still fulfilled, the blocking will be applied until the criterion is no longer satisfied.

The *LSA* point is limited by a minimum of 90 degrees, in order to prevent the developed protection algorithm from maloperating in the stable operation region at the first half of the power-angle characteristic. At the same time, the *LSA* point is limited to a maximum of 130 degrees. This is important, because the protection should still be operational during low or no load current in the observed tie-line before the *LSA* value is sampled.

2.2 Out-of-Step Protection Concept Evaluation

The developed OOS protection algorithm has been developed and tested using a real-time simulation environment (RTDS). The algorithm has been tested as software-in-the-loop with the algorithm running directly using data from the simulation environment, as well as in a hardware-in-the-loop (HIL) configuration. For HIL testing the algorithm has been implemented on an industrial programmable logic controller [66], and the input data was fed from the real-time simulations into the controller. The structure of the developed OOS protection is shown in Fig. 33, where it can be seen that the algorithm is divided into four main branches.

First, in order for any measurement data to proceed into data processing, the validity of the PMU measurement signals is checked. The data validity check includes verifying the synchronisation state and the timestamps of the incoming data, as well as the calibration rates, numbers of included phasors and analogue and digital signal mapping in the configuration frame. If the incoming data fails the validity check, e.g. the data is not time synchronised or is missing, the protection algorithm is blocked from operation. When the validity check is passed then the algorithm proceeds with processing the measurement data. From the measured values, the voltage values are checked and compared to the threshold values set to detect short-circuit faults. If any measurement point has a lower value than the specified threshold, the protection is blocked for the predetermined time, or until the measured voltage returns above the threshold value. This is done in order to avoid protection maloperation during faults occurring in the network, when the PMU measurements are affected by faulted conditions in the network and do not represent the electromechanical behaviour of the grid.

Simultaneously, the data processing provides input data to the event detection part of the algorithm, which is responsible for the equivalent network impedance computation. Upon detecting a step change in the measured quantities, the event detection block buffers the measured values, which are thereafter used to compute the equivalent impedance for the centre of inertia on either end of the observed transmission line. When the event detection computes a new value, it is then fed into the equivalent machine vector construction block. When no event is detected from the measurement values, the event detection block will output the previously computed equivalent impedance value.

Making use of the measured voltage and current phasors and the previously computed equivalent impedances, the equivalent machine voltage phasors of the centres of inertia are computed according to Eq. 22. Thereafter the equivalent phasors provide input to the δ value computation as well as the *LSA* value determination. The *LSA* values is com-

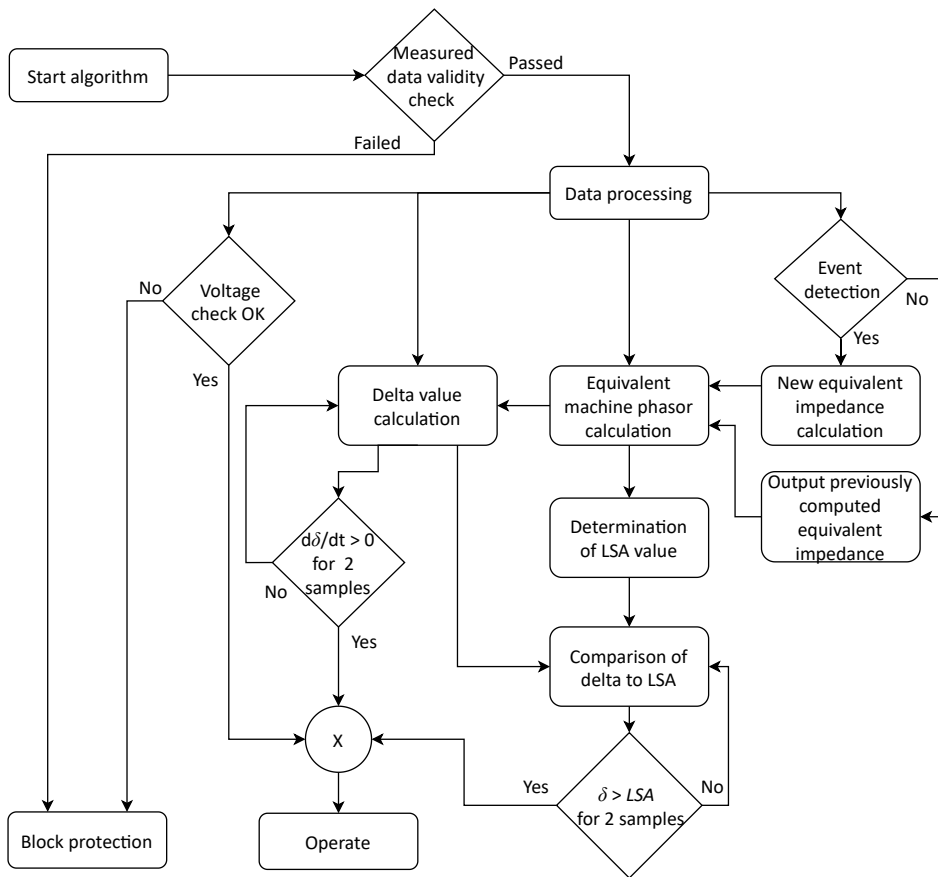


Figure 33 – Principle diagram of the developed algorithm in the hardware controller [58].

puted using the difference in angular value of the two equivalent phasors according to the power-angle characteristic as $\pi - \delta$. In parallel, the current δ value is continuously computed and compared against the determined LSA threshold value, and the derivative value of δ is being monitored. When the δ value exceeds the LSA value for two consecutive samples, and the derivative value of the angle difference has been positive for the past two samples, the protection issues an operation command.

Impedance computation verification

The equivalent impedance computation has a key role in the developed algorithm's operation. In order to test and verify the impedance computation part of the algorithm a simple system shown in Fig. 34 is used. The system consists of two ideal voltage sources, three transmission lines and three loads with a nominal voltage level of 345 kV. The ideal sources have a variable source impedance. The algorithm's measurements are taken from two locations, marked with red and blue in Fig. 34. The location chosen at the source bus, marked in red, represents a generator bus. The second location, marked in blue, is situated in the middle of the test network to represent an arbitrary node in the power system. The source voltage values as well as the frequencies of the sources are kept at a constant value of 1.0 p.u. Their source impedance value is varied between 5 and 100 Ohm on either

side of the transmission line in order to see the effects on the accuracy of the impedance computation of the developed algorithm. The system consists of three identical transmission lines with impedance of $Z_{tl} = 0.91 + j18.81\Omega$

The results of the impedance computation are shown in Fig. 35. The figure shows heatmaps of the impedance computation error for magnitude and angle for the developed algorithm.

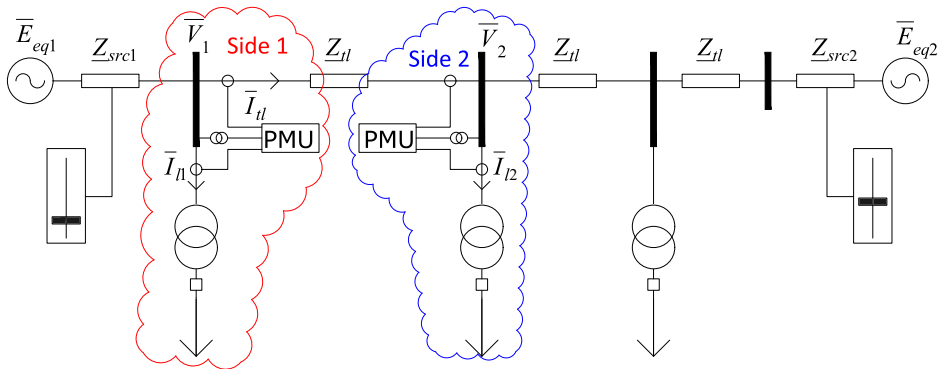


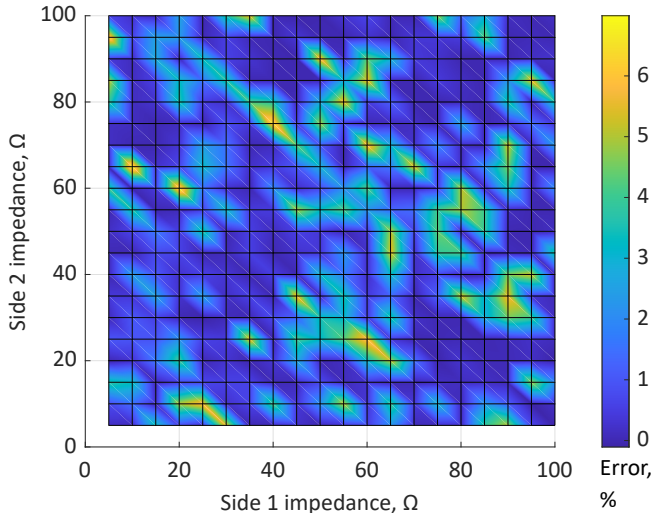
Figure 34 - Test network for testing impedance computation of the developed algorithm.

Fig. 35a shows the error of impedance computation of the algorithm for Side 1, that is circled in red in Fig. 34. The average absolute impedance computation error is 1.36 % with a standard deviation of 0.55 Ω . Therefore, this impedance computation is considered reliable for the purpose of the out-of-step protection.

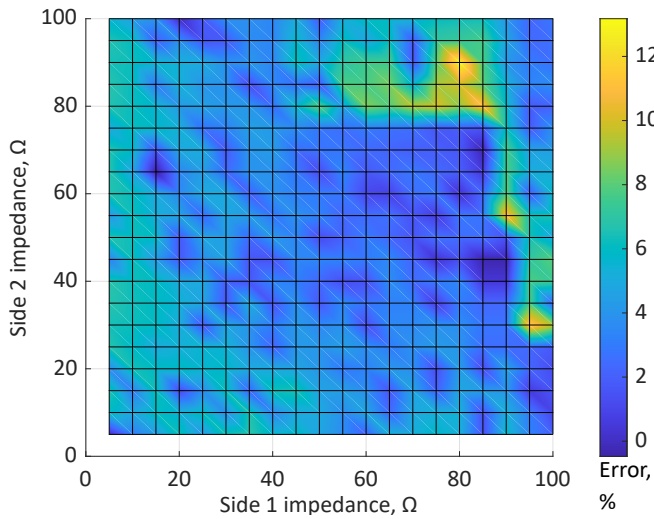
Fig. 35b displays the error of impedance computation for the node located within the system that is marked as Side 2 in blue in Fig. 34. The average absolute impedance computation error is 3.6 % with a standard deviation of 2.05 Ω . From the figure, it can be seen that the error of the impedance computation increases when the system impedance is increased, and the impedance as seen behind the measurement point on Side 2 has a greater influence on the system impedance computation. The maximum error of the impedance computation for Side 2 is observed to be 13.2 %, and for Side 1 the maximum absolute error is observed to be 7.0 %.

The impedance computation has been verified in a meshed network using IEEE 39 bus power network model [67], the detailed description of the modified power system model is shown in Section 4.1. The generator impedance is not constant during transient processes, and therefore it is difficult to evaluate the accuracy of the impedance computation part of the algorithm in a real system as machine impedance can vary from subtransient to transient to synchronous impedance depending on the event that is taking place in the network.

For OOS events usually the transient impedance of the generators is considered [68]. In order to illustrate the change of the perceived network impedance in the test system, a fault is created on line 14-15 at Bus 15 terminals, and the perceived network impedance during the fault is computed using the measured 3 phase RMS fault current and pre-fault network voltage. The perceived impedance together with the computed impedance by the protection algorithm and corresponding fault currents are shown in Fig. 36. From the fault currents (Fig. 36a) it can be seen that they lower, as the fault time increases, which is caused by the DC component decay as well as the impedance change of the generating units.



(a)



(b)

Figure 35 - Errors of impedance computation of the algorithm. (a) - Error heatmap for impedance computation on Side 1, (b) - Error heatmap for impedance computation on Side 2.

Fig. 36b shows the perceived network impedance during the fault in blue and the the computed impedance value in red. It can be seen that the perceived impedance lowers to a minimum value at the fault inception at 0.0 seconds and thereafter begins to slowly increase. From the figure, it can be observed, that the computed and perceived impedance intercept at 240 ms after fault inception. Thus, it can be said that the computed network impedance corresponds to the transient impedance of the network and is suitable to be used for OOS protection purposes.

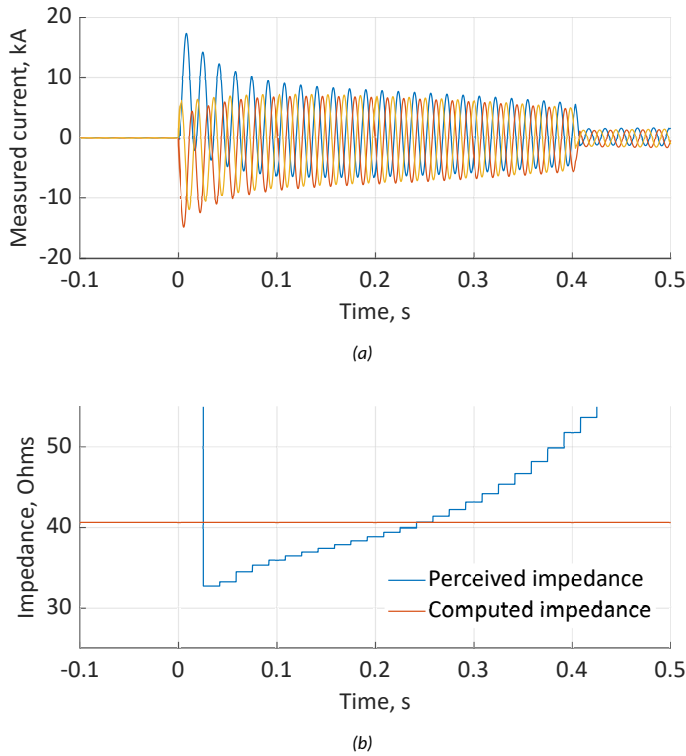


Figure 36 – Fault currents and the perceived impedance together with impedance computed by the OOS algorithm. (a) - Fault currents for the example, (b) - Perceived impedance with computed impedance by the OOS algorithm.

OOS algorithm verification

The developed algorithm concept has been tested in the test network that has been previously created for impedance testing setup, shown in Fig. 34. The controlled source Z_{src2} in the impedance computation network model has been replaced with a synchronous machine, and a fault is created inside the network in order to see the response of the algorithm to stable and unstable swings in the network. Side 1 source impedance is kept at the minimum level of 5Ω . The test setup is shown in Fig. 37.

The unsaturated parameters for the used synchronous machine on 1000 MVA base are as given in Table 4. The generator is connected to the network through a step-up transformer with a reactance of 0.1 per unit on 1000 MVA base, both the generator and transformer have a nominal capacity of 1000 MVA. Additionally, the generator used is equipped with an IEEE Type 1 type exciter and a TGOV1 type turbine governor. The parameters of the exciter and governor are shown in Table 5 and Table 6 respectively.

Table 4 – Used data for the synchronous generator for OOS verification test system in per unit on 1000 MVA base.

$X_d = 2.106$	$X_q = 2.05$	$X'_d = 0.57$	$X'_q = 0.587$
$X''_d = 0.45$	$X''_q = 0.45$	$R_a = 0.00125$	$T'_{d0} = 4.79 \text{ s}$
$T_{q0} = 1.96 \text{ s}$	$T''_{d0} = 0.050 \text{ s}$	$T''_{q0} = 0.045 \text{ s}$	$H = 3.45$

Table 5 – Used data for the synchronous generator IEEE Type 1 type exciter for OOS verification test system.

$T_r = 0.00s$	$T_e = 1.4 s$	$K_f = 0.03$	$T_f = 1.0 s$
$K_a = 40$	$T_a = 0.02 s$	$V_{mx} = 10.5$	$V_{mn} = -10.5$
$K_e = 1.0$			

Table 6 – Used data for the synchronous generator TGOV1 turbine governor for OOS verification test system in per unit on 1000 MVA base.

$R = 0.05$	$T_1 = 0.5 s$	$V_{max} = 1.0$	$V_{min} = 0.0$
$T_2 = 2.1 s$	$T_3 = 7.0 s$	$D_1 t = 0.0$	

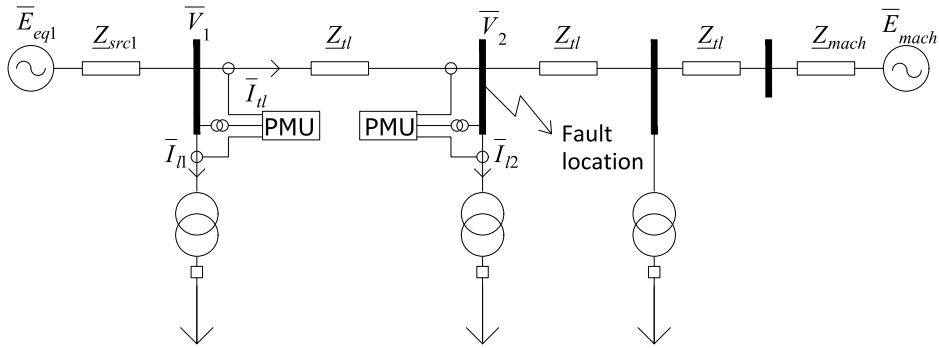


Figure 37 – Test network for OOS algorithm verification.

A fault is created on Bus 2, indicated by fault location in the network, after which the system experiences power swings. A three-phase fault is introduced at 0.5 seconds in the simulation for the duration of five cycles and subsequently cleared without any changes in the network topology. After the fault clearance the system experiences a stable power swing. The response of the generator angle, computed angle value of the OOS algorithm, and the algorithm operation and blocking signals are shown in Fig. 38.

From the measured generator rotor angle, depicted in Fig. 38a, it is seen that the event produces a stable power swing with the generator rotor angle value nearly stabilising by five seconds at the end of the plot. Fig. 38b shows the computed angle difference value by the developed algorithm in blue, as well as the LSA threshold value for the protection operation in red. It is seen that during the faulted condition, the computed angle difference exceeds the operation threshold value and thereafter closely follows the measured generator rotor angle value in the swing process. Despite the computed angle difference exceeding the threshold value, the protection does not operate, as can be seen in Fig. 38c, where the blocking and operation signals of the protection are shown. During the faulted condition, the blocking signal becomes active, which inhibits the OOS protection from issuing an operation command, due to a fault. After fault clearance, the blocking criterion drops off and during the following power swing the computed angle value stabilises and the operation signal does not activate.

Fig. 39 shows the measured generator rotor angle, computed angle value and the protection signals for the case of an unstable power swing in the system. The power swing is initiated by a six cycle long three-phase fault on the fault location (Bus 2) indicated on the scheme in Fig. 37.

The measured generator rotor angle is shown in Fig. 39a, where it can be seen that, af-

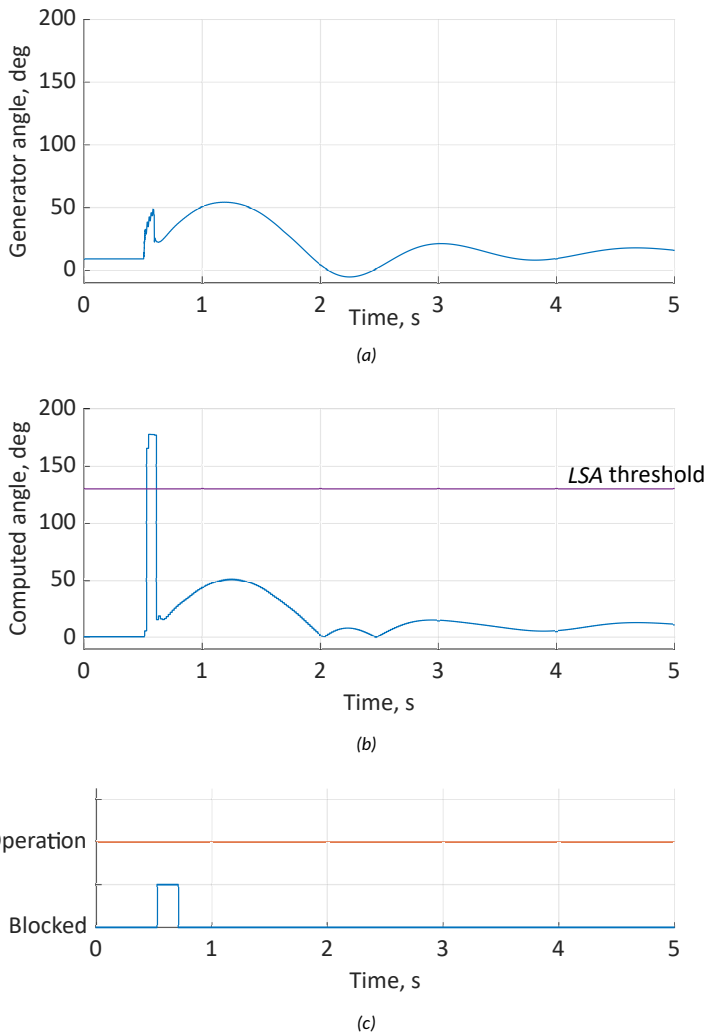
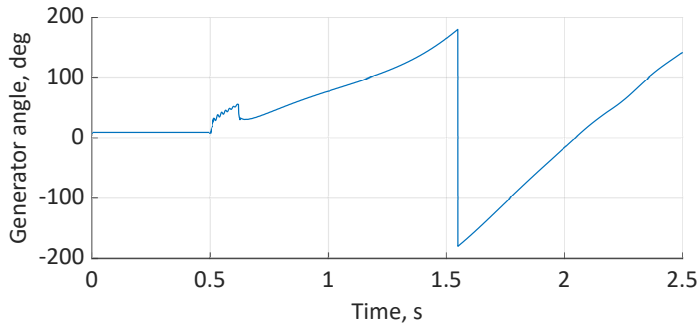
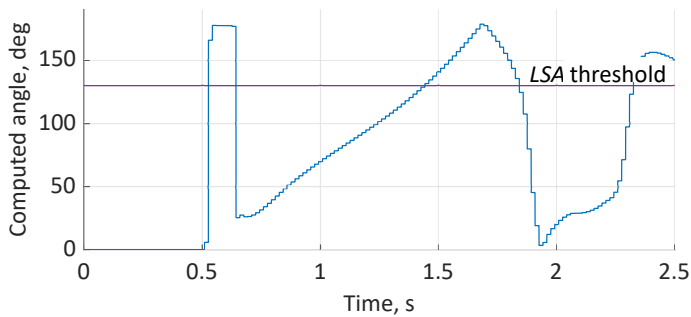


Figure 38 – Measured generator (E_{mach}) angle in respect to equivalent source E_{eq1} , computed angle value and algorithm signals. (a) - generator measured angle value, (b) - computed angle value by the algorithm and LSA value, (c) - algorithm operation and blocking signals in time.

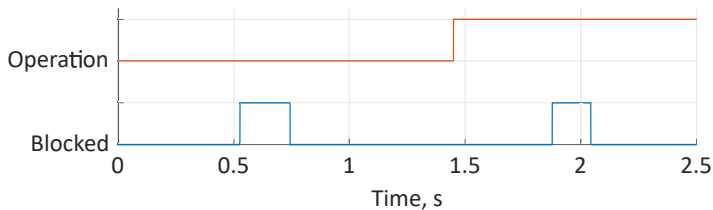
ter the fault, the generator rotor angle continues to increase, passing 180° at 1.6 seconds, where a pole slip occurs. In Fig. 39b the computed angle difference and the LSA threshold value is shown. After fault clearance, the computed angle value is increasing, as the system is heading into instability. The computed angle difference passes the LSA threshold value at 1.45 seconds. From the protection signals, shown in Fig. 39c, it is seen that, during the fault occurrence, the protection is blocked from operation and the protection does not output an operation command regardless of the computed angle difference being higher than the LSA threshold value. As the system moves towards instability and the computed angle value exceeds the LSA threshold, however, it is seen that the protection does not immediately operate, due to requiring two consecutive measurement values to fulfil the operation criteria. Hence the protection operation signal becomes active after the criterion has been fulfilled and the command is issued at 1.46 seconds.



(a)



(b)

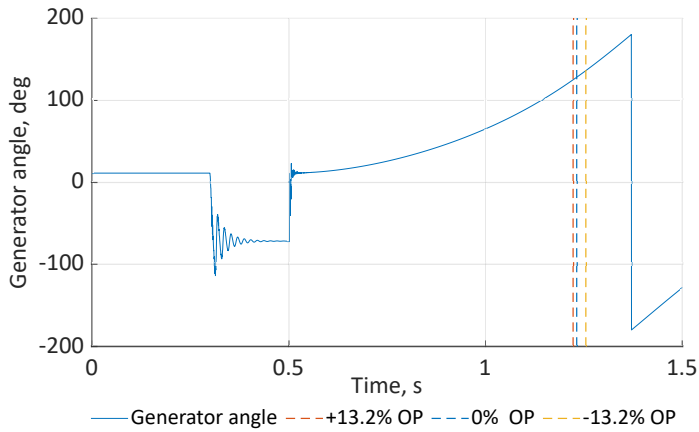


(c)

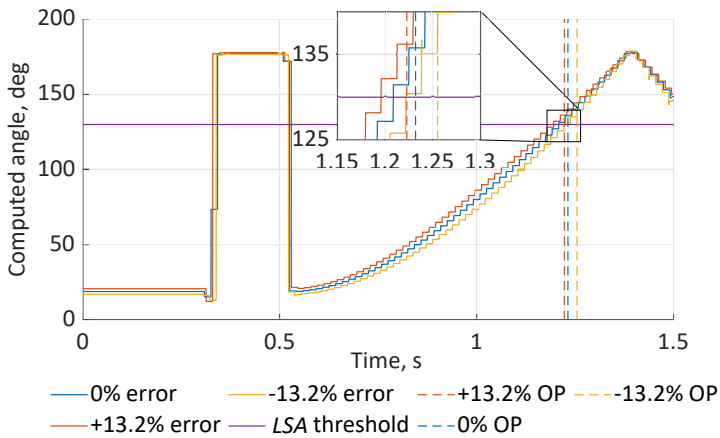
Figure 39 – Measured generator (E_{mach}) angle in respect to equivalent source E_{eq1} , computed angle value and algorithm signals. (a) - generator measured angle value, (b) - computed angle value by the algorithm and LSA value, (c) - algorithm operation and blocking signals in time.

Considering that the impedance computation part of the algorithm has a maximum observed error of 13.2 %, the effect of error in impedance computation on the protection algorithm function has been tested. Fig 40 shows the measured generator angle value in the case of an out-of-step condition in the network, the computed angle by the algorithm with no error in the impedance computation and with both, negative and positive maximum observed error in the impedance computation, as well as the instants, when the protection issues an operation command.

In Fig. 40a it can be seen that the operation points with no error and both of the negative and positive error are located close together. Fig. 40b shows the computed angle values for the three considered cases. The blue line shows the computed angle value with no error in the impedance computation and the dashed blue line indicates the operation in the case of no error. The red and orange lines indicate the cases of positive



(a)



(b)

Figure 40 – Measured generator (E_{mach}) angle in respect to equivalent source E_{eq1} , operation instants in the case of different error values in impedance computation and the associated computed angle values by the algorithm. (a) - measured generator angle and operation time instants in time, (b) - computed angle value, operation threshold and operation instants in time.

and negative error respectively. From the figure, it can be seen that all of the cases behave similarly, and the reaction of the protection algorithm is marginally affected by the errors in impedance computation. The magnification shows the time between 1.15 and 1.3 s and computed angle between 125 and 140°. From the magnification, it can be observed, that the case with a positive error value in the impedance computation outputs an operation command one sample before the base case with no error, whereas the negative error case outputs the operation command two samples after the base case. This, considering a 50 Hz system, means that the protection algorithm's operation time can vary within a 60 ms window depending on the impedance computation error.

From this it can be concluded that the developed protection algorithm expresses stable behaviour in the case of stable power swings, and is able to distinguish between unstable and stable conditions. The protection is marginally affected by the errors in the impedance computation part of the algorithm, that may cause a slight delay in the protection algorithm operation.

Hardware implementation verification

The developed protection algorithm is adapted into a hardware Programmable Logic Controller platform [66] (GE PhasorController), that can be used for executing wide-area schemes using measurement data from PMUs. The principle diagram for laboratory setup for verifying the hardware implementation of the developed algorithm is shown in Fig. 41. The hardware implementation consists of the controller running the logic for the developed algorithm, the connecting LAN, a GPS time source and real-time simulator RTDS. An external GPS clock is used to provide time synchronisation for the measurements using a 1PPS signal in the case of the RTDS and an NTP time signal to the controller. The RTDS runs the network simulation in real-time and provides the external PhasorController with C37.118 data from the two PMUs installed in the network. The PMUs are modelled using RTDS standard library components [69]. The PhasorController processes the measured data and provides feedback to the RTDS simulator using IEC 61850 GOOSE [70] messages. In parallel to the algorithm running on the PhasorController, it is also being processed by the RTDS in order to compare the reactions of the software and hardware implementations of the algorithm.

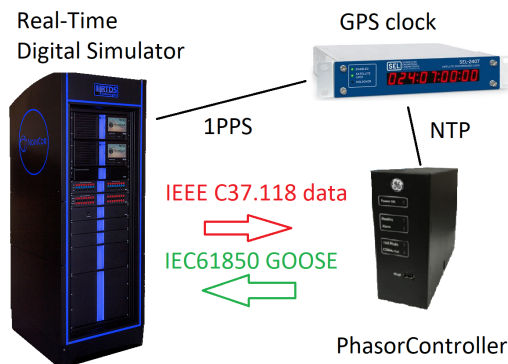


Figure 41 – Principle diagram for the verification of the hardware implementation of the developed algorithm.

The laboratory environment network latency from the RTDS to the PhasorController was measured to be under 1 ms. However, in order to represent a more realistic scenario, a PDC Wait Time setting of 100 ms was implemented in the controller, which is representative of real-world PMU applications [71]. Normally, the PDC Wait Time setting means that in order to align the measurement data from different PMUs in the network, the controller will wait for some time for the measurements to arrive. Thereafter, the processing of measurements will begin in the logic built inside the device. Fig. 42 shows the protection algorithm implementation in the external controller.

The logic in the controller is split into three types of submodules: event detection, angle computation and threshold and operation. There are two event detection modules used for the whole protection algorithm, one for each measurement location. The event detection modules use the line current, load feeder current and the voltages as input values, and are responsible for detecting the step changes in the load current and computing the equivalent impedance value at that particular transmission line terminal. The angle computation module is used to compute the δ value between the two equivalent inertia centres. Lastly, the threshold and operation module continuously computes

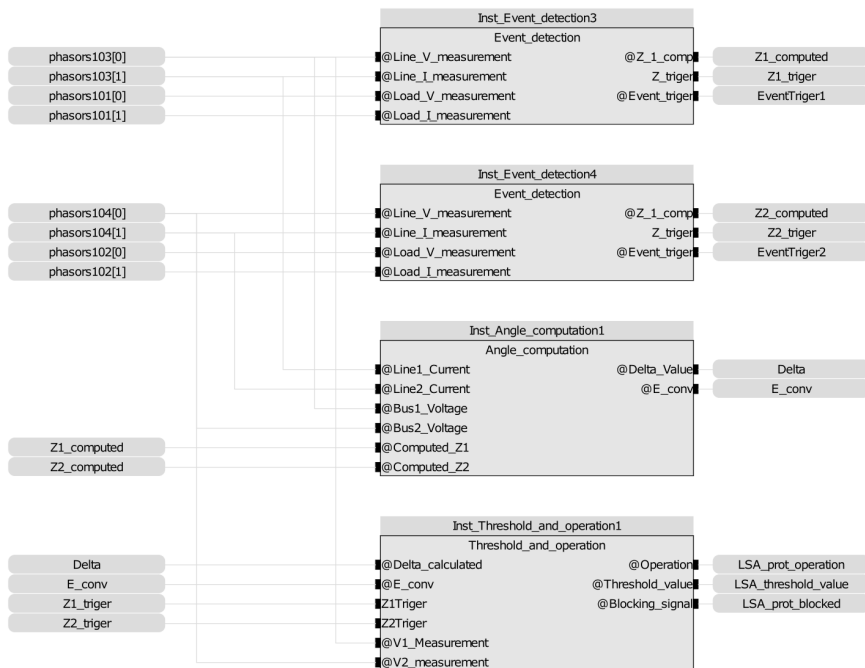


Figure 42 – Diagram of the developed OOS protection algorithm in the hardware implementation from the controller software showing the event detection, angle computation and the threshold and operation submodules.

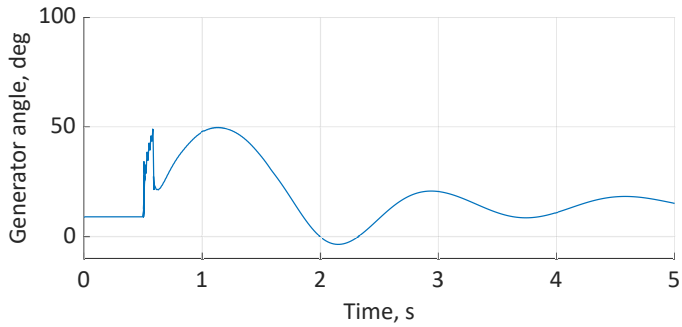
the LSA threshold value and provides the blocking and operating signals of the protection algorithm.

In order to assess the hardware implementation of the developed algorithm, the δ value computed by the algorithm in both software and hardware implementation and generator reaction for a stable power swing is shown in Fig. 43. The test is conducted in the same manner and using the same system as shown in Fig. 37.

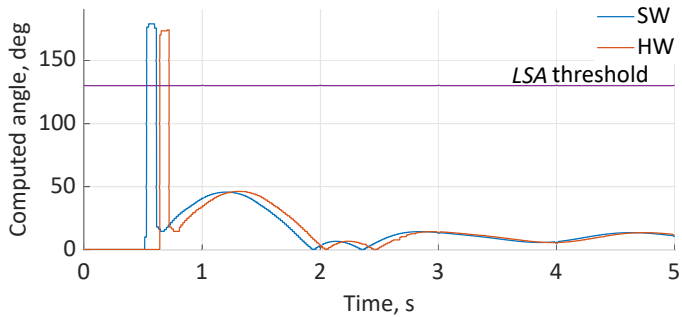
The Fig. 43a shows the generator angle, where it can be seen that the fault produces a stable swing in the generator angle value, which is stabilising by the end of the plot at 5 seconds. Fig. 43b displays the calculated δ values of the software and hardware implementations, marked as SW and HW respectively. It is observed that the value computed in the PhasorController is lagging behind the software application for around 110 ms. This is due to the previously mentioned PDC Wait Time setting of 100 ms and delay related to the processing of the controller logic itself. Fig. 43c presents the operation and blocking signals for both of the hardware and software implementations. The time difference in the two implementations is also seen from the activation of the algorithm blocking signal activation.

Fig. 44 shows the reaction of the algorithm in software and in hardware implementation for a six-cycle fault, which causes an unstable power swing in the network. Fig. 44a displays the generator rotor angle reaction, where the generator rotor angle continues to increase after the fault clearing passing 180° at 1.9 seconds, where a pole slip occurs.

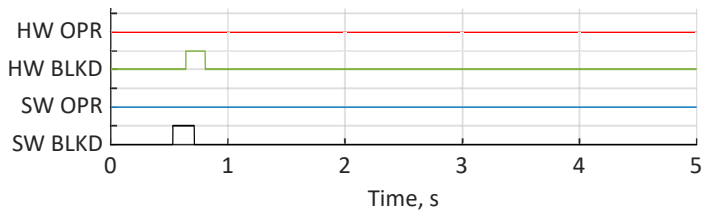
The computed δ values are shown for both software and hardware implementation in Fig. 44b. It can be observed that during the faulted state the computed angle value exceeds the LSA threshold value, and the protection should be blocked for this event.



(a)



(b)

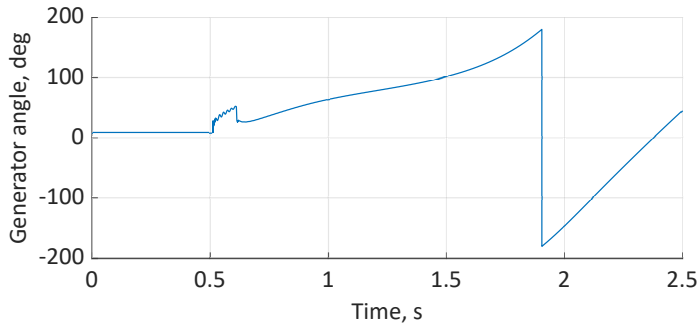


(c)

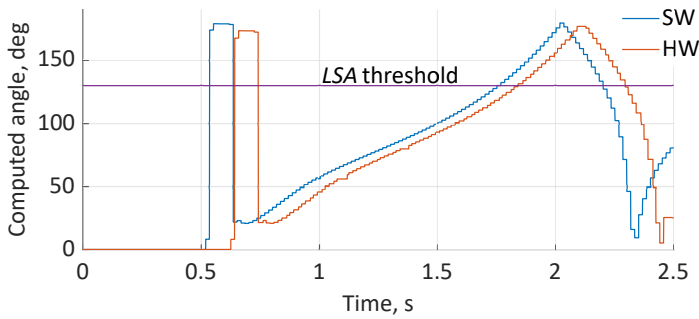
Figure 43 – Measured generator (E_{mach}) angle in respect to equivalent source E_{eq1} , computed angle value and algorithm signals. (a) - generator measured angle value, (b) - computed angle value by the algorithm and LSA value, (c) - algorithm operation and blocking signals in time.

Thereafter, due to the unstable swing in the network, the computed δ value exceeds the algorithm's predetermined LSA threshold once more and keeps increasing. This should produce a trip command from the developed algorithm. The behaviour of the algorithm can be confirmed by observing the operation signals that are displayed in Fig. 44c. The operation signals show that during the initial faulted conditions, both the software and hardware algorithm become blocked, and deblocked after the faulted is cleared. After the computed angle value surpasses the threshold value, the operation signal activates, indicating protection operation. Comparatively to the stable case (Fig. 43), it can also be noted in the unstable case that the time shift of δ computation and the signal activation between the software and hardware implementation of the algorithm is 110 ms.

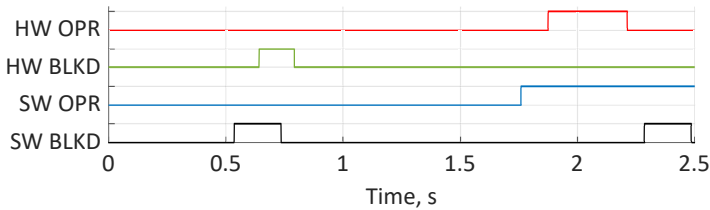
Based on the reaction of the hardware and software implementation for stable and



(a)



(b)



(c)

Figure 44 – Measured generator (E_{mach}) angle in respect to equivalent source E_{eq1} , computed angle value and algorithm signals. (a) - generator measured angle value, (b) - computed angle value by the algorithm and LSA value, (c) - algorithm operation and blocking signals in time.

unstable power swing it can be seen that the two implementations of the algorithm exhibit the same general reaction, apart from the hardware implementation introducing a delay. This is, however, expected, because of the PDC wait time needed to collect measurement data from the PMUs that are located in the field in the real world. Therefore, it can be said that the hardware implementation of the algorithm performs successfully, taking into account the limitations introduced by a real-world installation scenario.

2.3 Algorithm Response to Grid Events

The proposed algorithm needs to act only in the case of unstable power swings in the power network. Therefore, the algorithm's reaction to various normal system events, e.g. faults and different switching operations, needs to be assessed. In the previous subsection the OOS protection algorithm was developed, and the operation of the algorithm verified.

For the purpose of checking the algorithm's security during different grid events the test network is augmented through adding a parallel transmission line, that can be switched off, in order to check the algorithm's response, as well as the measurement points of the algorithm have been moved.

Response to faults outside of the observed transmission line

First, the response to faults in the unobserved network is assessed. The small test network used first for algorithm verification, is altered by adding additional lines with the same parameters to the system, as well as loads in order to create more scenarios for testing. Faults are created in locations shown in Fig. 45 as F1 and F2. In both locations two types of faults (single-phase and three-phase), are created and the algorithm's response to the fault and subsequent power swing is shown. In all of the tested scenarios auto-reclose function is used to switch the faulted line on after the fault occurs and all faults are considered to be temporary faults. The tested contingencies produce a stable power swing in the network. In the case of single-phase fault a single-pole open condition is also created during the dead-time of the auto-reclose cycle, so that the algorithm's behaviour during a pole open condition can also be seen. The response of the algorithm is shown from the external controller, where there is a delay in the protection signals and the computed angle value. The delay for the response signals and the computed angle value is between 110 and 130 ms.

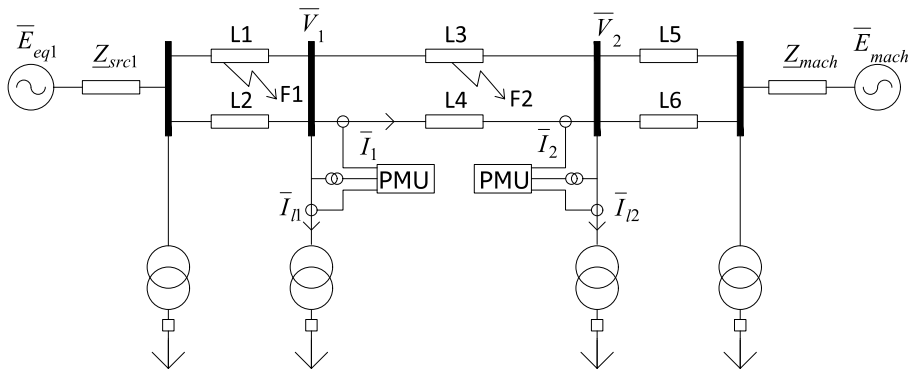
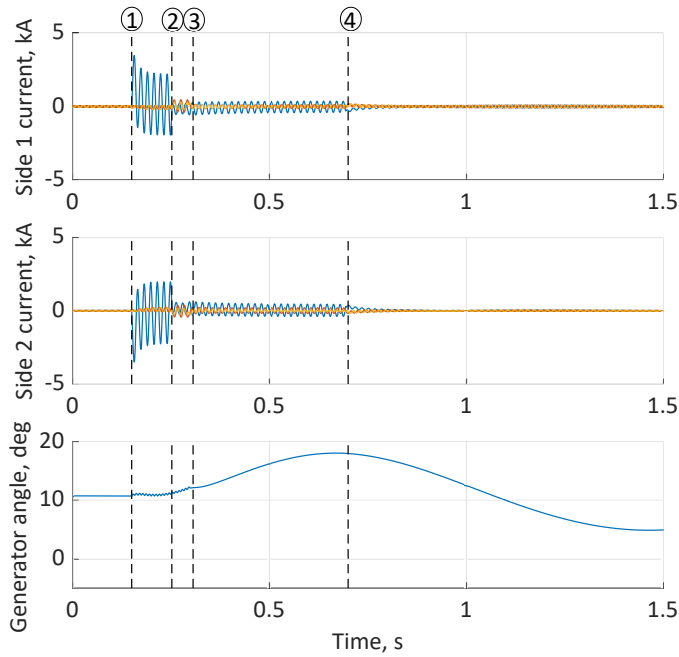


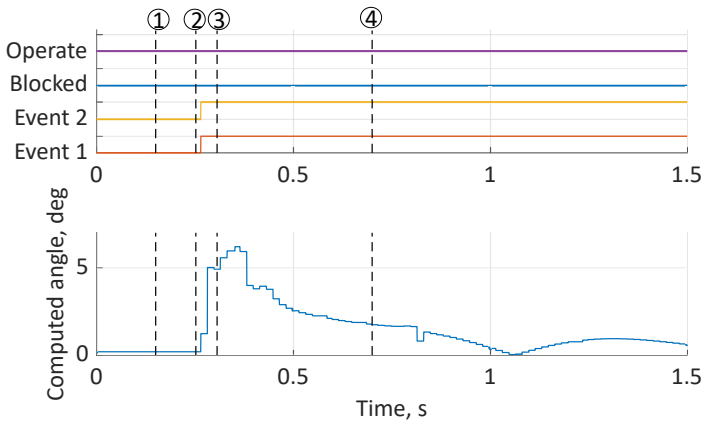
Figure 45 – Fault locations for testing algorithm's security for faults outside of the observed transmission line.

Fig. 46 displays the instantaneous current values from both measured line ends and the generator rotor angle value as well as the algorithm's signals and computed angle difference value for a single-phase (SLG) fault at location F1. Fault is created at 0.15 s which is indicated by ①. Thereafter, one side breaker opens a single pole at ②, followed by the second breaker opening at ③. The system operates with one pole open until ④, when auto-reclose of the breakers energises the open pole.

The SLG fault can be viewed on the instantaneous currents shown in Fig. 46a as from both of the measured locations one phase current value increases. The fault is a through fault from the measured location, as the current values have an opposite direction to each other from Side 1 and Side 2. The following single-pole open condition can also be examined after the fault clearance, where the faulted phase current remains higher than the two healthy phases until the pole is reclosed. From the generator rotor angle it can be seen that the fault has no major effect on the stability of the generator. The rotor angle slightly increases after the fault clearance, and thereafter stabilises. This means that the



(a)



(b)

Figure 46 – Reaction to an SLG fault at location F1. (a) shows the instantaneous current values at both measurement locations and the generator rotor angle (E_{mach}) in respect to source angle (E_{eq1}). (b) shows the protection algorithm signals for operation, blocking and event detection and the computed angle value by the algorithm. ① - fault inception, ② - first breaker opening, ③ - second breaker opening and fault clearance, ④ - reclosure of the faulted line.

system experiences a minor power swing for this event, and the developed protection should not operate, as the system is stable.

From the protection signals, indicated in Fig. 46b, it can be observed, that both measurement locations detect an event, which is shown by the Event 1 and Event 2 signals activation. The operation and blocking signals do not activate. The computed angle by

the protection does not exceed 7° . Furthermore, during the following single-pole open condition the protection shows stable operation, which can be observed from the computed angle value, which is decreasing. Based on this it can be said that the protection is showing stable behaviour for a SLG fault elsewhere in the power network.

Fig. 47 presents the instantaneous current values from the measurement locations, the generator angle, protection signals and computed angle for a three-phase fault (TPH) at location F1. The fault is created at 0.15 s, illustrated by ①, followed by first breaker opening at ② and fault clearing at ③. The faulted line is reclosed at ④. This process is seen in the instantaneous current values shown at both measurement locations in Fig. 47a. For this fault the generator experiences a stable swing, that is more severe than the SLG case in the same location as can be seen from the generator rotor angle reaction. The generator rotor angle reaches a maximum of 57° , and starts decreasing then the faulted line is reclosed.

Observing the protection algorithm signals for the same process, shown in Fig. 47b, it can be seen that, similarly to the SLG fault in location F1, the algorithm detects an event at both measurement locations, indicated by the Event 1 and Event 2 signal activation. From the computed angle value can be seen that for this event there is a significant jump in the value. This jump is registered as a fault, and the protection algorithm is blocked, as can be seen by the blocking signal activation. After fault clearance, the angle value decreases, and the blocking signal deactivates. Following the subsequent power swing, it can be seen that the computed angle value has minor oscillations, and the protection outputs no operation command, as the power swing is stable in the network. Therefore, based on the reaction, it can be concluded that the protection algorithm is stable for TPH fault elsewhere in the power network.

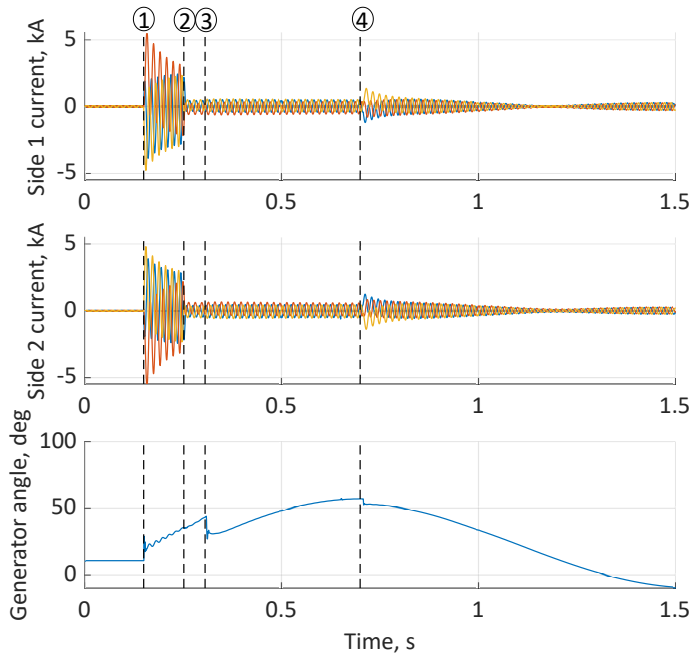
The measured quantities and protection algorithm reaction to a SLG fault at location F2 on the parallel transmission line are shown in Fig. 48. The fault is created at 0.15 s indicated by ①. The first breaker opening is shown by ② and the clearing of the fault by the second breaker opening is marked by ③. Therefore, the system is operating in a single-pole open condition until ④, when auto-reclosure of the breaker energises the open pole.

Fig. 48a displays the measured currents from both measurement locations as well as the measured generator rotor angle. From the measured current values the first and second breaker opening and the subsequent reclosure can be seen. The generator rotor angle shows, that the fault produces a minor power swing, similarly to the SLG fault at location F1. Therefore, the protection algorithm should not operate during the process.

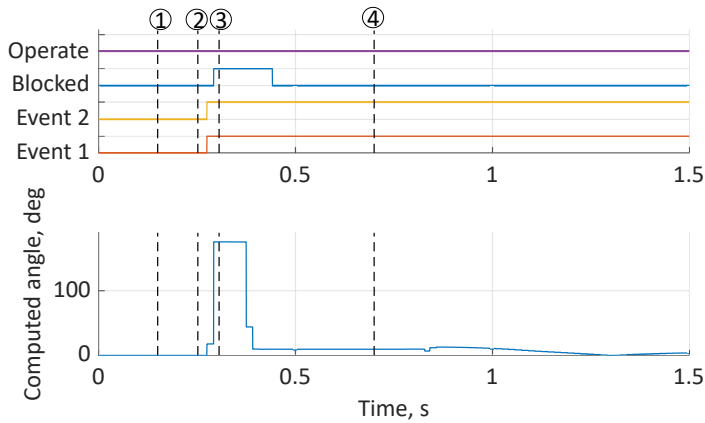
Protection operation signals, shown in Fig. 48b, confirm that the protection remains stable throughout the faulted state and the following power swing in the network. The protection algorithm event detection signals on both ends activate; however, when looking at the computed angle value, it is seen that the angle difference is minor. The algorithm does not output an operation command for the fault and for oscillation following the fault. Hence, it can be said that the algorithm exhibits stable behaviour for a SLG fault on a parallel transmission line to the installation location.

The measured quantities and protection reaction for a TPH fault on a parallel transmission line in location F2 is shown in Fig. 49. The start of the faulted condition is indicated with ① at 0.15 s, followed by the first breaker opening at ② and thereafter fault clearing at ③ when the second line breaker opens. Thereafter, the system is operating with the parallel transmission line switched off until ④, then the parallel transmission line is switched on by auto-reclosure.

The instantaneous current values and the measured generator rotor angle value are



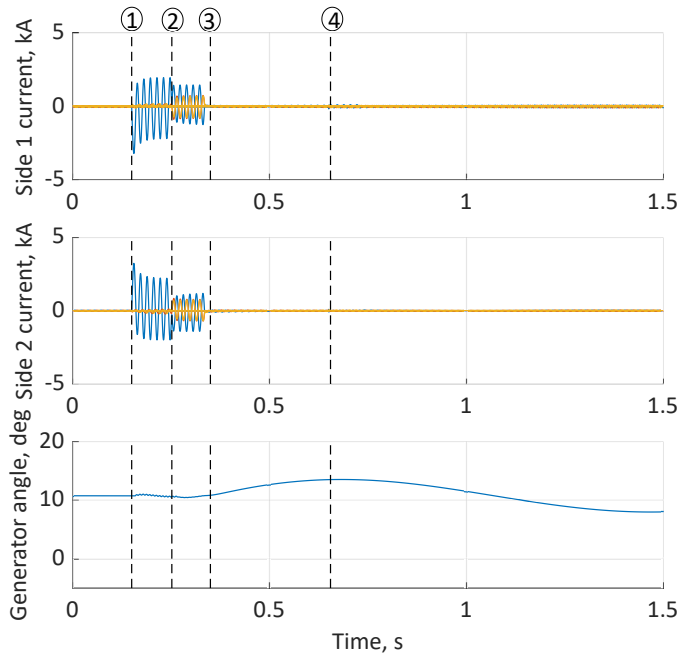
(a)



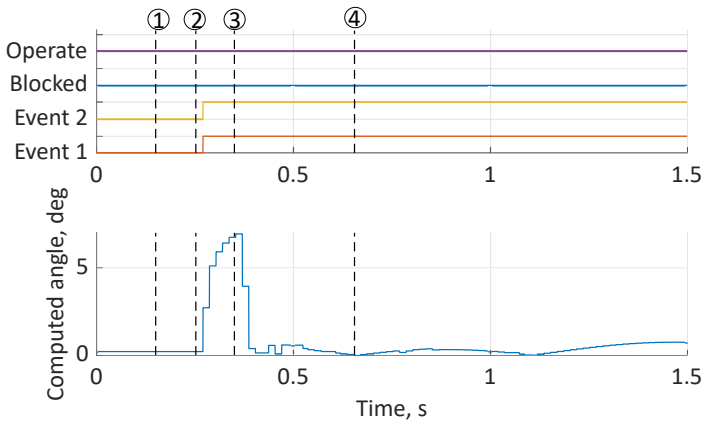
(b)

Figure 47 - Reaction to an TPH fault at location F1. (a) shows the instantaneous current values at both measurement locations and the generator rotor angle (E_{mach}) in respect to source angle (E_{eq1}). (b) shows the protection algorithm signals for operation, blocking and event detection and the computed angle value by the algorithm. ① - fault inception, ② - first breaker opening, ③ - second breaker opening and fault clearance, ④ - reclosure of the faulted line.

shown in Fig. 49a. The measured currents display that the observed transmission line experiences a stable power swing when the parallel line is switched off. This is also confirmed by the generator rotor angle value, which increases to a maximum of 40° , and thereafter starts decreasing right before the parallel line is reclosed. During this process the protection algorithm needs to remain stable and not operate.



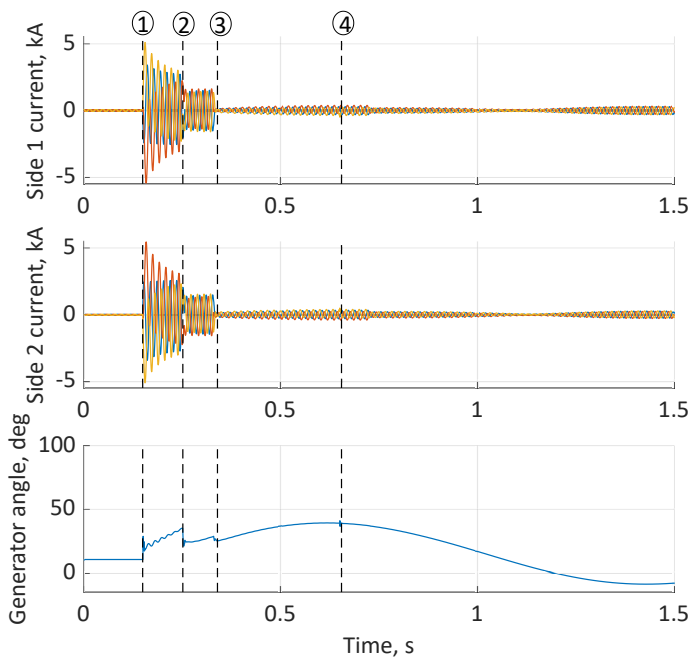
(a)



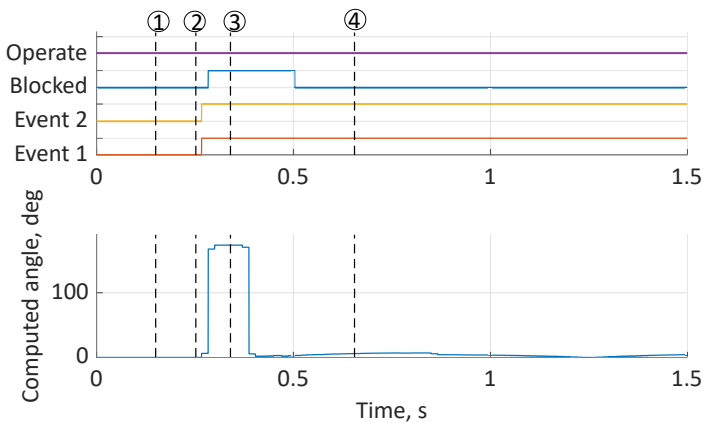
(b)

Figure 48 - Reaction to an SLG fault at location F2. (a) shows the instantaneous current values at both measurement locations and the generator rotor angle (E_{mach}) in respect to source angle (E_{eq1}). (b) shows the protection algorithm signals for operation, blocking and event detection and the computed angle value by the algorithm. ① - fault inception, ② - first breaker opening, ③ - second breaker opening and fault clearance, ④ - reclosure of the faulted line.

The protection algorithm signals and computed rotor angle are shown in Fig. 49b. From the signals it can be seen that the protection registers an event on both of the measurement locations, and thereafter the algorithm blocking signal becomes active. The blocking signal activation is necessary due to the computed angle value's sharp increase during the faulted state, when it can exceed the LSA limit value, and therefore cause pro-



(a)



(b)

Figure 49 – Reaction to an TPH fault at location F2. (a) shows the instantaneous current values at both measurement locations and the generator rotor angle (E_{mach}) in respect to source angle (E_{eq1}). (b) shows the protection algorithm signals for operation, blocking and event detection and the computed angle value by the algorithm. ① - fault inception, ② - first breaker opening, ③ - second breaker opening and fault clearance, ④ - reclosure of the faulted line.

tection operation during faulted state. After fault clearing, the blocking signal drops off. The computed angle value is showing minor oscillations and the protection remains stable during the following power swing in the network. Based on this, it can be concluded that the protection algorithm is stable in the case of a TPH fault on a parallel transmission line.

From the conducted tests shown, it can be summarised that the protection algorithm

remains stable in the case of different types of faults outside of the observed transmission line.

Response to faults on the observed transmission line

In order to assess the algorithm's behaviour for internal faults on the observed transmission line, the system shown in Fig. 50 is used and the faults are created in the location shown as F3. The test system is the same as the one used for fault response testing elsewhere in the network, and the parameters of the system are described in Section 2.3. SLG and TPH faults are created on the observed transmission line and in the case of SLG fault, the system is also operated in a single-pole open condition during the dead time of the auto-reclose cycle.

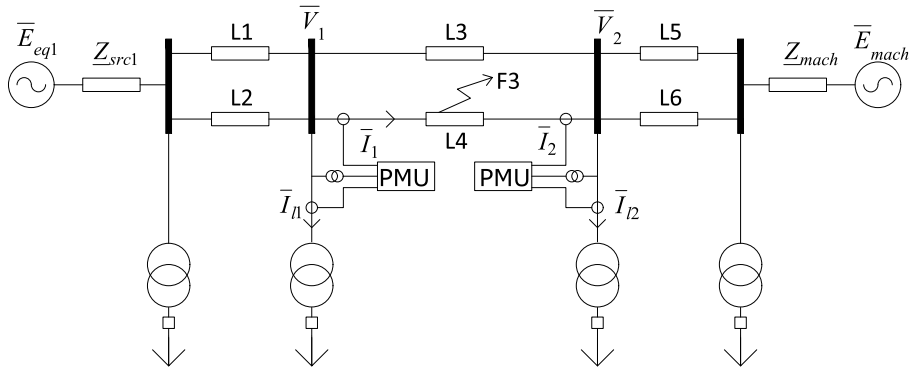


Figure 50 - Fault location for testing algorithm's security for faults on the observed transmission line.

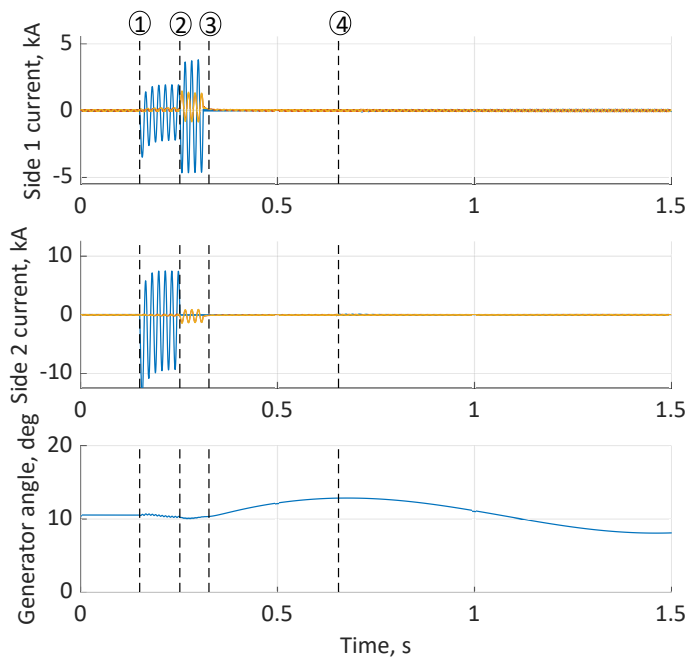
Fig. 51 shows the measured currents, rotor angle and the protection algorithm signals as well as the computed angle value for a SLG fault at location F3. The ① denotes the fault inception at 0.15 s. Thereafter, ② marks one pole opening of the first circuit breaker and ③ the fault clearance due to the second breaker pole opening. Until ④ the line is operating in a single-pole open condition, when reclosure of the open pole occurs.

Observing the measured quantities, shown in Fig. 51a, the circuit breaker operations for this event are displayed. The generator rotor angle reaction shows that the event causes a minor power swing, where the generator rotor angle oscillates within $\pm 3^\circ$.

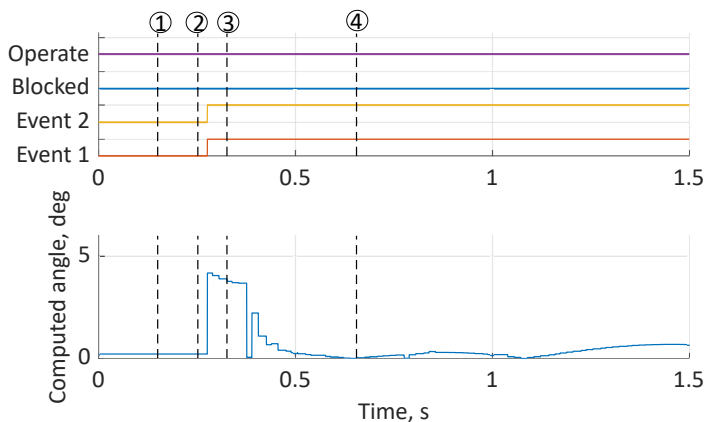
The protection signals, shown in Fig. 51b, indicate that at both measurement locations an event in the system has been registered, due to the Event 1 and Event 2 signals activating. The computed angle difference in this event does not exceed 5° , as can also be noted from the figure. Following the clearing of the fault a small oscillation in the computed angle value can be observed, and it can also be noted that the algorithm does not issue an operation command. Therefore, the algorithm exhibits stable behaviour for a SLG fault at location F3, as well as the following single-pole open condition.

The current values, the generator angle, protection signals and computed angle value for a TPH fault in location F3 are shown in Fig. 52. The fault is introduced at 0.15 s, marked by ①. The first breaker opening is signified by ②, and the second breaker opening clears the fault from the network at ③. After fault clearing the observed line is in switched off state until ④, when auto-reclose re-energises the line.

The measured quantities for the TPH fault in location F3, shown in Fig. 52a, indicate that after the fault the power system experiences a stable power swing for most of the dead-time of the observed transmission line. When the observed line is switched on at



(a)

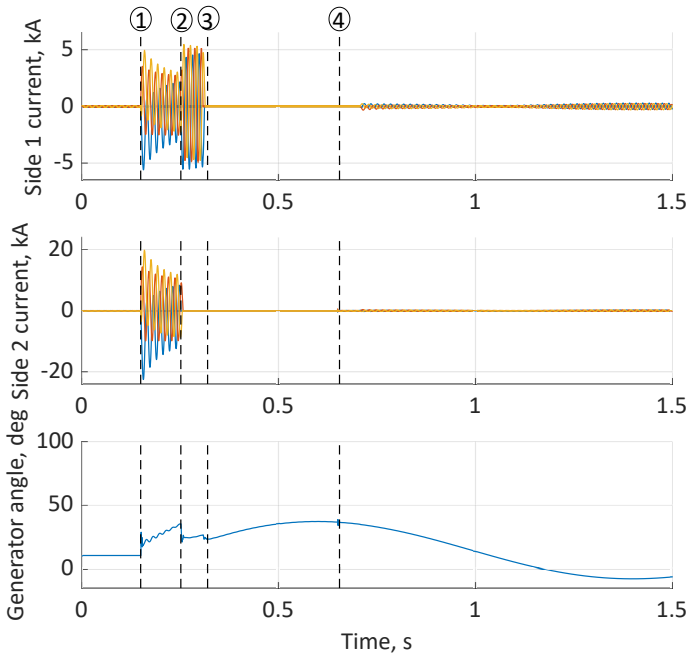


(b)

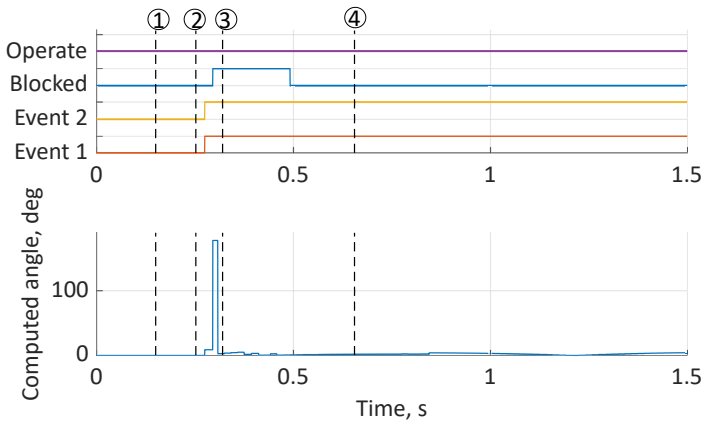
Figure 51 – Reaction to a SLG fault at location F3. (a) shows the instantaneous current values at both measurement locations and the generator rotor angle (E_{mach}) in respect to source angle (E_{eq1}). (b) shows the protection algorithm signals for operation, blocking and event detection and the computed angle value by the algorithm. ① - fault inception, ② - first breaker opening, ③ - second breaker opening and fault clearance, ④ - reclosure of the faulted line.

④ the system is already in the stabilising phase of the power swing. This means that the protection algorithm should not operate, because the system is proceeding towards stable operation.

The protection algorithm signals are shown in Fig. 52b for the TPH fault case at location F3. The signals indicate that the protection registers events at both measurement locations and, similarly to faults elsewhere in the network, the blocking signal activates.



(a)



(b)

Figure 52 – Reaction to a TPH fault at location F3. (a) shows the instantaneous current values at both measurement locations and the generator rotor angle (E_{mach}) in respect to source angle (E_{eq1}). (b) shows the protection algorithm signals for operation, blocking and event detection and the computed angle value by the algorithm. ① - fault inception, ② - first breaker opening, ③ - second breaker opening and fault clearance, ④ - reclosure of the faulted line.

This occurs due to the computed angle value jumping during the fault, and triggering the fault detection logic, which blocks the protection operation. After the line is switched off the computed angle value is at 0° , and after energisation a minor oscillation can be seen in the computed angle value. The protection operation signal does not activate. Therefore, it can be concluded, that the protection algorithm shows stable behavior in the case of faults on the observed transmission line.

2.4 Intermediate Summary

An out-of-step protection algorithm was proposed in this chapter based on computing equivalent impedance of the power network using wide-area measurement data. The accuracy of the impedance computation based on PMU measurements has been tested, and it is shown that the computation error is smaller when the measurement location is closer to a generator unit. The maximum observed error in the impedance computation is observed to be 13.2 %.

The proposed algorithm has been developed in a software implementation and the algorithm's performance for unstable power swings has been verified. Thereafter, the algorithm has been installed on a hardware platform, and the hardware implementation has been successfully confirmed against the software implementation. The algorithm has been tested for security for different types of faults in the power network. The assessed cases were:

- Single-phase fault outside of the observed transmission line.
- Three-phase fault outside of the observed transmission line.
- Single-phase fault on a parallel transmission line.
- Three-phase fault on a parallel transmission line.
- Single-phase fault on the observed transmission line.
- Three-phase fault on the observed transmission line.

For all the tested cases the algorithm has shown stable operation without any maloperation, therefore it can be concluded that the algorithm is secure. This means that the algorithm shall not operate in the case of any faults on the observed transmission line of elsewhere in the network. The protection shall only operate in the presence of unstable power swings in the network.

3 Out-of-Step Protection Using Discrete Angle Derivatives

The out-of-step protection concept developed in Section 2 requires equivalent impedances to be computed in order for the algorithm to function properly. This requires the load to be volatile in such a way where step changes in the observed load occur. However, this may not always be the case, therefore this property may be a drawback for utilising that particular algorithm in actual networks. In order to overcome this limitation, a novel algorithm is developed, that is decoupled from the network parameters, and focuses on instability detection based purely on measured quantities and the derivative values of those quantities.

In this chapter a new settingless out-of-step protection algorithm decoupled from network parameters using wide-area information is presented. The protection algorithm is developed as a software solution, and thereafter implemented to an external hardware platform. The developed solution is tested using real-time simulation in both hardware and software implementations using software-in-the-loop and hardware-in-the-loop testing, where the hardware testing takes into account delays associated with collecting wide-area measurements. The concept and the results shown in this chapter have been published in [III].

3.1 Decoupled Out-of-Step Protection Concept

The power-angle characteristic, described in Section 1.1, can also be applied to the power transfer across a single transmission line in a meshed transmission network. A multi-machine system can be separated into two groups of machines, that represent the inertia centres at either end of a transmission line [61]. Note that the equation (1) is also applicable for power flow through an arbitrary transmission line, when the equivalent internal voltage phasors are replaced with the voltage values at the ends of the transmission line in question. Hence, by using the power-angle curve, the dynamic stability around a tie-line can be assessed.

In the case of the classical representation [72] the resistances of machines and transmission lines are neglected. The mechanical input power of the generators is assumed to be constant, as well as the generators themselves are represented as constant voltage sources behind an impedance. This neglects the effects of automatic voltage regulation and a damping effect in power swings. In this way, the worst-case scenario is considered for the power-angle relationship in the network. It has to be noted that, due to the simplifications listed here, the real-world power-angle curve may deviate from the idealistic curve used here for illustration of the decoupled out-of-step protection algorithm.

In order to explain the theory behind the developed decoupled protection algorithm a simple system can be considered (Fig. 53). The system consists of two sources and two transmission lines connecting the two equivalent machines. A fault is created on one of the transmission lines, and subsequently the line is switched off to clear the fault from the network. The fault causes a power swing in the network that can be stable or unstable in nature.

For this simple system three power-angle curves can be constructed to represent the three different stages in the power swing process in the network. This is shown in Fig. 54a, where the initial pre-faulted curve, faulted curve and the post-fault curve are shown for the simple system. In addition, the initial power transfer has been noted as P_0 , and, using this, two operating points can be fixed on the power-angle curves. The operating point located in the left half of the characteristic is a stable operating point, denoted by δ_0 . According to the Equal Area Criterion (EAC) [72], the maximum angle difference of

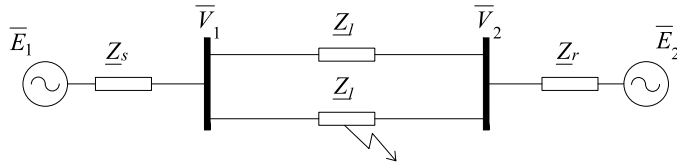


Figure 53 – Simple system equivalent for decoupled out-of-step protection explanation.

a recoverable swing cannot exceed the second operating point (called Last Stable Angle - noted as LSA), though it may be smaller. The further increase of the angle difference beyond the LSA point will definitely result in an unstable generator operation. Thus, the LSA point is critical to distinguish between a stable and an unstable swing. The LSA point is located on the postfault curve, which is situated lower than the prefault curve due to the transmission impedance increasing upon switching off the faulty element.

Examining the dynamic behaviour of a power system, it can be noted that during a fault, the electrical active power is lowered due to the reduced voltage magnitudes. However, the mechanical energy given to the generators by the prime movers remains rather constant [14]. Due to this difference in received and transmitted energy the angular difference between the equivalent voltages begins to increase. After the fault clearing, the angle has increased to a specific value, which is indicated as δ_1 in Fig. 54b. The surplus of energy obtained during the faulted condition is marked by the green area labelled as A_1 .

After the fault is switched off the electrical output power is higher than the mechanical input power, and due to this the rate of change in the angular difference is lowering. Due to inertia, the angular difference and the transmitted electrical power keep increasing, until the surplus of energy obtained during faulted condition is transmitted into the network. This means that, during this process, three criteria are fulfilled based on the power-angle curve:

- The first derivative of the angle value will have a positive value, since the increase in angular difference is ongoing.
- The second derivative of the angle value will be negative, because the rate of which the angle is increasing is lowering.
- The first derivative of output power will be positive, due to the power increasing.

These criteria will be true until the angular difference reaches a maximum value, which is denoted by δ_2 . At this point, equality between the obtained and the dissipated energy is reached. As the electrical power at this point is larger than the mechanical input power, the angular difference between the two sources will start decreasing and the system will start progressing towards a new stable operation point. During this process, the angle change speed and the change in active power will be negative, thus the derivative values are negative. The process is illustrated in Fig. 54c. It has to be noted that during a stable power swing the operating point may pass beyond the maximum power point at 90° , however, it will not cross δ_{LSA} .

The process of an unstable swing is illustrated in Fig. 55, that is caused by a longer fault clearing time in the system. The starting process is similar to the stable case explained before, and this is illustrated in Fig. 55a, where the pre-fault, post-fault and faulted curves are shown as well as the areas indicating the excess and dissipated energy during the power swing. Fig. 55b displays the situation in the network after fault clearing. During

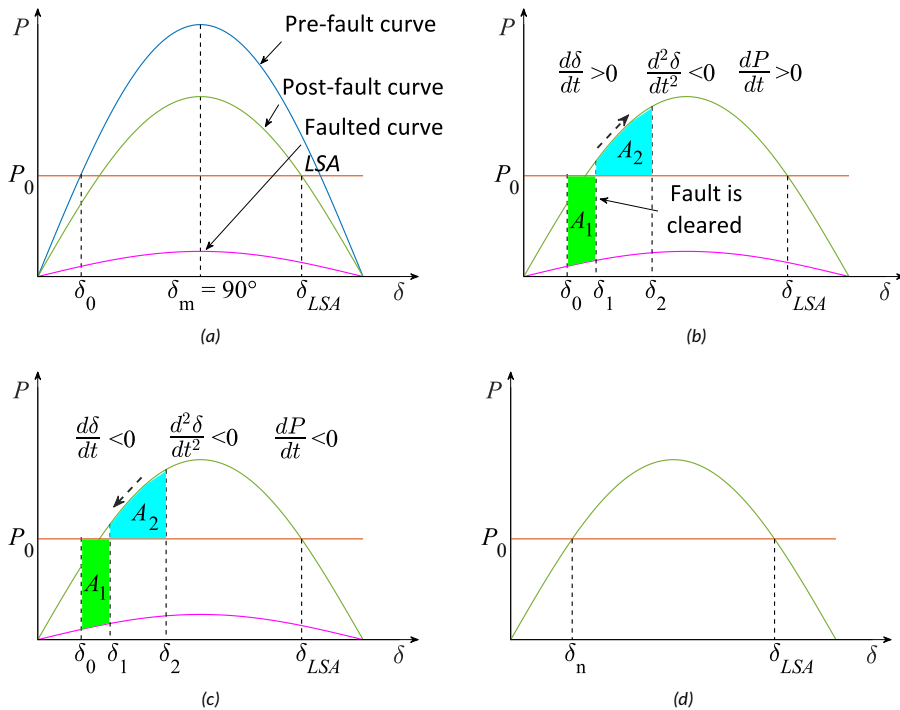


Figure 54 – Power-angle curves for the two-machine system and the demonstration of a stable power swing process on a power-angle curve. (a) Power-angle curves for pre-fault, faulted state and post-fault state, with the LSA point denoted as δ_{LSA} . (b) Power system operation after a disturbance; during this operation the angle difference is decelerating until reaching the maximum angular difference of δ_2 , where all the surplus of energy has been dissipated. (c) Power system operation after the surplus of energy after the disturbance has been dissipated and the angular difference is decreasing while system is settling at a stable operation point. (c) system operation in a new equilibrium point noted as δ_n .

this period the angular difference is increasing, the first and second derivative values of the angle change and the derivative of electrical power have the same sign as those with the stable swing in the network. However, in this case, the angle keeps increasing, and passes the point noted as δ_m , which denotes the maximum electrical power transfer on the power-angle curve. Thereafter, with the further increase in the angular difference, the electrical power output begins to lower, thus, the derivative value of electrical power will become negative, as shown in Fig. 55c. This situation is not yet an indication of an unstable power swing, as the LSA value has not been passed. The excess energy acquired during the faulted condition has not been dissipated and therefore, the angle difference will keep increasing. With the further increase in angular difference, the LSA point (denoted by δ_{LSA}) will be passed. When the system has passed this point, the angular difference will start accelerating. This means that the stable operation of the power system is no longer possible and the system will experience an OOS condition. This condition is indicated by the second derivative of the angle value becoming positive, with the first derivative value remaining positive. Simultaneously, the first derivative value of the active power is negative. This situation is illustrated in Fig. 55d.

It has been shown that the use of the power-angle characteristic and EAC concept

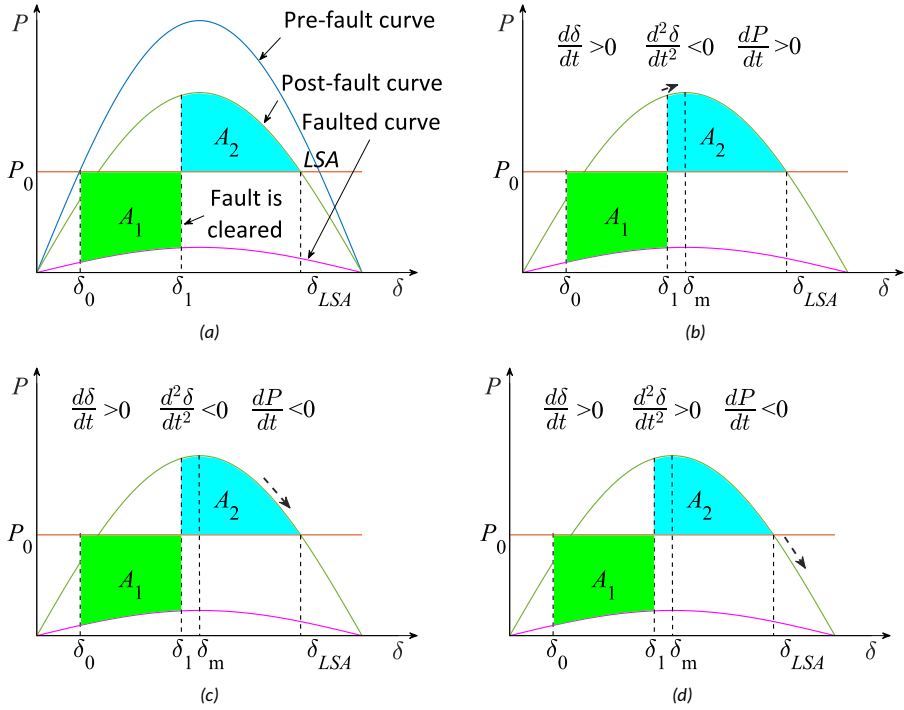


Figure 55 – Demonstration of an unstable power swing process on a power-angle curve from observing derivative values (a) Power-angle curve illustrating the pre-, faulted- and postfault operations, with the LSA point denoted as δ_{LSA} . (b) Power system operation after a disturbance, during this operation the rate of change in the angle difference is negative, and power derivative remains positive until reaching the maximum active power value at δ_m . (c) Power system operation after passing the maximum power value, during this operation the power derivative is negative and the rate of change in the angle difference is negative. (d) System operation becomes unstable after passing the LSA point, the rate of change of the angle difference becomes positive.

applies for assessing complex stability phenomena in large multi-machine systems, in addition to a two-machine equivalent network [73]. In summary, the growing angle difference and dropping active power together point to the right half of the power-angle curve, while the change of sign of the angle difference acceleration (second derivative of the angle value becoming positive) indicates the crossing of the LSA point. These three criteria unambiguously identify that the power swing becomes non-recoverable and therefore can be used as a basis for the proposed OOS protection algorithm.

3.2 Constraints and Verification of the Decoupled Algorithm

The developed protection algorithm uses the measurements provided by the PMUs on both ends of the observed transmission line. This allows for measuring the angle difference between the monitored buses, and the computation of angular difference derivative values. Additionally, the voltage, current and power values are measured from either end of the observed transmission line.

It has to be highlighted that, due to the discrete nature of PMU measurements, the continuous derivatives mentioned in Section 3.1 should be substituted with finite differences, i.e. $\frac{d\delta}{dt}$ should be replaced with $\frac{\Delta\delta}{\Delta t}$. For the purpose of clarity, however, in the fol-

lowing explanations, this thesis will continue to use the same terminology as above, bearing in mind that all the derivatives will be estimated using sampled discrete measurements and finite differences.

According to the explanation given above for a stable and unstable power swing, shown in Figs. 54 and 55, the criteria for the decoupled protection operation can be stated:

$$\begin{cases} \frac{d\delta}{dt} > 0 & \text{for two consecutive measurements} \\ \frac{d^2\delta}{dt^2} > 0 & \text{for three consecutive measurements} \end{cases}$$

These conditions might be also fulfilled during normal power system operation, while the operating point is situated in the stable operation area of the power-angle curve. In order to stop the OOS protection algorithm from operation during normal conditions, blocking and restraining criteria have been defined. The criteria for *blocking* the protection function during normal grid conditions are as follows:

$$\begin{cases} \text{Measured voltage above 0.89 p.u.} \\ \text{Measured voltage below 0.2 p.u.} \end{cases}$$

The first criterion is used to ensure protection is blocked when the network operates in nominal condition, as 0.89 p.u. is often the voltage threshold defined, where emergency operation of a power system begins [74, 75, 76]. The second criterion is used to check if there is a fault present on the protected line and if the protected line is energised, as 0.2 p.u. is considered to be the voltage threshold, from which the line can be considered as energised [77]. The values proposed above should be considered as indicative, the exact thresholds may be adjusted based on the local deployment conditions and depending on the transmission system operator requirements. If either of those conditions is fulfilled, the protection will not operate.

In order to *restrain* the protection from operation while the system is experiencing a stable power swing, the following criteria are used:

$$\begin{cases} \frac{dP}{dt} > 0 & \text{for two consecutive measurements} \\ \frac{dV}{dt} > 0 & \text{for two consecutive measurements} \end{cases}$$

The first criterion restrains the protection from operating whilst the operation point is located in the first half of the power-angle curve, where, during the angular difference increase, the active power transfer also increases. The second criterion restrains the protection algorithm from operation when the system is in the process of leaving the swinging condition, and the voltages increase.

Additionally, a fault detection element has been implemented into the protection algorithm. This element monitors the voltage, and detects a fault if there is a sharp change in the measured voltages. After fault detection, the protection algorithm is blocked, until the fault detection element resets. The fault detection element is reset when an opposite-signed jump in the measured voltage value is observed.

The algorithm is divided into three main segments and its structure is shown in Fig. 56. The first segment, circled in red in Fig. 56, is responsible for checking the data validity and blocking the protection based on voltage measurements as well as blocking the protection algorithm operation during faulted conditions in the network. The second segment, circled in green, computes and assesses the active power and voltage derivative values and restrains the protection operation if necessary. After the restraining and blocking segments a protection allow signal is created, that leads to the third segment of the algorithm. This third segment, denoted in blue, computes the first and second derivatives of the angle difference, and is responsible for the instability detection and issuing a protection operation command.

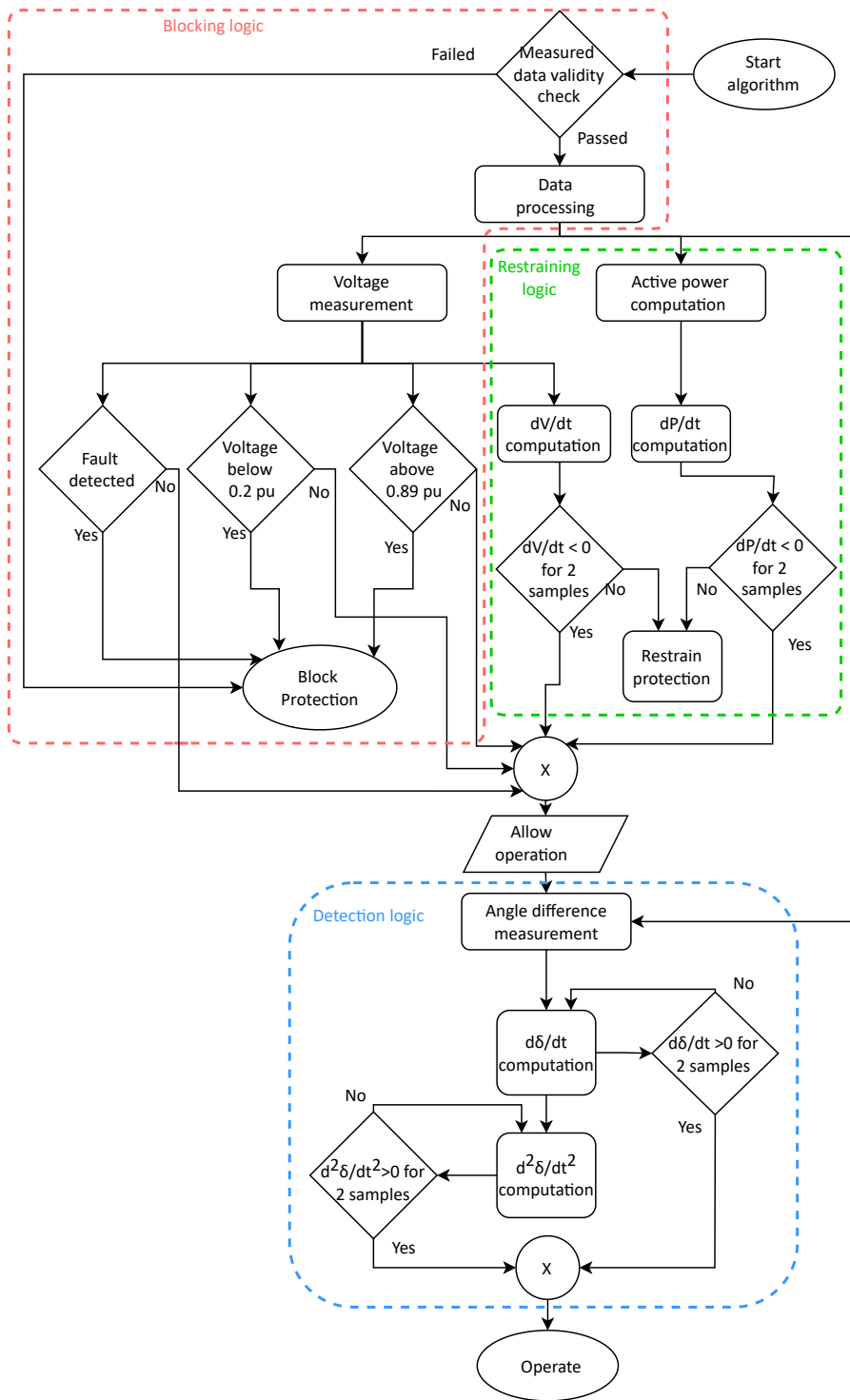


Figure 56 – Principle diagram of the developed discrete angle derivative OOS protection algorithm.

Algorithm signals and variables during a stable swing in the network

The described algorithm has been conceptually tested using a test system shown in Fig. 57. Power swings are initiated in the network by conducting a fault on the parallel line to the one observed, and switching the line off, after which a power swing will take place on the transmission line monitored by PMU 1 and PMU 2. The testing is first conducted with the algorithm running in a software-in-the-loop manner, acquiring measurement data directly from the simulation, with the test network being simulated in real-time using the RTDS simulator.

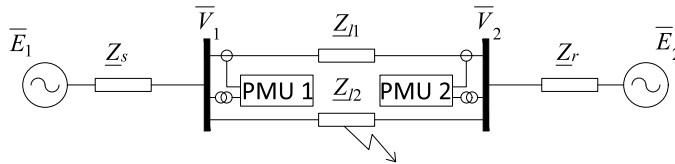


Figure 57 – Simple system for testing the decoupled out-of-step protection algorithm.

First, a stable power swing is observed in the network and the algorithm's response is shown. Fig. 58 shows the measured voltage values, power flow in the transmission line as well as the measured angle difference and the signal states related to the protection algorithm during a stable power swing in the network.

The power swing is initiated by a three-phase fault on the parallel transmission line at 0.5 s (indicated by ①). The protection algorithm's signals, shown in Fig.58b, show that after the short-circuit condition is cleared, the blocking criterion of the protection becomes inactive. This is specified by the BLK signal dropping at ②. However, the restraining criterion is active, as indicated by the RES signal remaining at high state. This is due to the active power transfer increasing in the transmission line, as is shown by the measured quantities displayed in Fig. 58a; therefore, the derivative value of active power is positive. Afterwards, the active power transfer starts decreasing and thus the derivative becomes negative. At the same time, the voltage values start to increase, hence the voltage derivative values become positive. Therefore, the restraint criterion is kept at the activated state. During this power swing process the protection is not allowed to operate (the ALW signal does not become active), since either blocking or restraint criterion is in an activated state during the whole process. After some time the system stabilises as the voltage values return to nominal levels and the power oscillations are damped. Once the voltage levels return to above the threshold of 0.89 p.u. the blocking criterion for the protection is activated, as indicated by ③.

Based on the explanation above, the developed algorithm did not provide an operation command in the case of a stable power swing. In summary, it is concluded, that the developed algorithm shows secure behaviour during stable power swings.

Algorithm signals and variables during an unstable swing in the network

The reaction of the algorithm as well as measured quantities for the case of an unstable power swing are shown in Fig. 59, where Fig. 59a displays the measured voltages and transmitted power, whilst Fig. 59b presents the measured angle difference and the protection algorithm signals. The unstable power swing is initiated by applying a fault on the parallel transmission line at 0.5 s, as shown by ①. The fault clearing time is delayed compared to the stable power swing case. After the fault has been cleared from the network

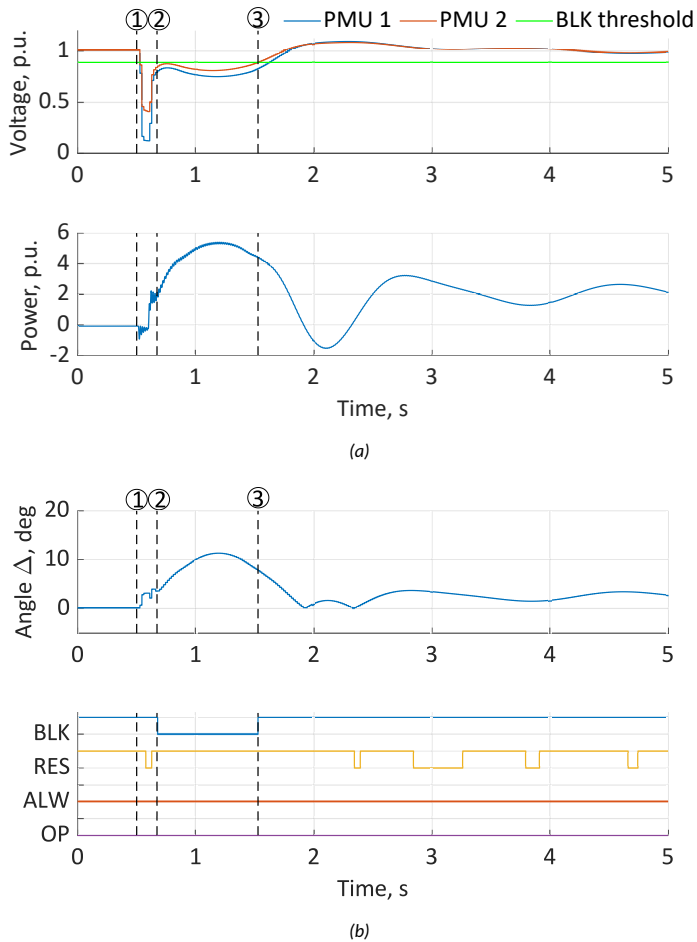


Figure 58 – The decoupled algorithm reaction to a stable power swing in the network. (a) - the measured voltage and active power values, (b) - measured angle difference value between the sources and the signal states of the protection algorithm. BLK - protection blocked, RES - protection restrained, ALW - protection allowed to operate, OP - protection operation. ① - fault inception, ② - Blocking criterion is disabled, ③ - Blocking criterion of the protection reactivates as the voltage returns above the threshold value of 0.89 p.u.

the blocking criterion (BLK signal) of the algorithm is deactivated, which is indicated by ②, because the voltage does not exceed the threshold value after the fault clearing. The restraint criterion (RES signal) in Fig. 59b, however, remains active, since the measured active power through the transmission line is increasing. At the same time, the measured voltage values are decreasing, shown in Fig. 59a, accordingly, the derivative values of the voltages are negative.

After the active power value starts decreasing in the observed transmission line, the restraining criterion deactivates. This means that at this point both the restraining and blocking criteria are deactivated, and the protection is allowed to operate, as shown by the activation of the ALW criterion. Therefore, according to the protection description given before, the algorithm will issue an operation command as soon as the first and second derivative values of the angular difference become positive and stay positive for two and

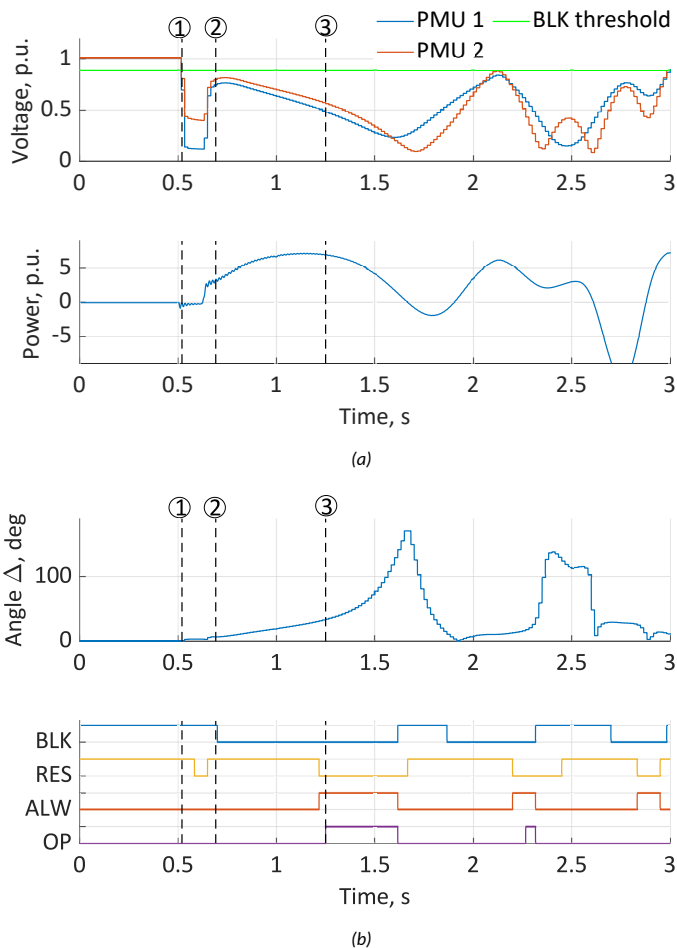


Figure 59 – The decoupled algorithm reaction to a unstable power swing in the network. (a) - the measured voltage values and measured active power values, (b) - measured angle difference value between the sources and the signal states of the protection algorithm. BLK - protection blocked, RES - protection restrained, ALW - protection allowed to operate, OP - protection operation. ① - fault inception, ② - Blocking criterion is disabled, ③ - protection operation command.

three consecutive cycles respectively. The unstable condition is detected at ③, when the operation command (indicated by the OP signal) becomes active. Hence, it can be concluded that the protection algorithm is able to differentiate between a stable and an unstable power swing in the power network, and is able to provide operation commands when there is an unstable swing developing on the observed transmission line.

Hardware implementation of the algorithm

After the software implementation the decoupled out-of-step protection algorithm is re-designed to run on a hardware setup. For the test platform the same Programmable Logic Controller is used as has been described in Section 2.2, as well as the same laboratory test setup consisting of GPS clock, RTDS simulator and the logic controller. The measurements are provided to the controller via IEEE C37.118 data and the feedback from the

implemented algorithm is given back to the real-time simulation using IEC61850 GOOSE messages. Parallel to the hardware-in-the-loop testing using the external controller, the algorithm is also being executed in software-in-the-loop in order to verify and compare the hardware implementation.

Fig. 60 displays the algorithm logic implemented in the external controller. To execute the protection algorithm two submodules have been created - the first submodule is used to provide the blocking, restraining and allow signals, whereas the second submodule is implemented to provide the protection operation command. The blocking and restraining module uses currents and voltages from both measurement locations as input and contains the parts circled in green and red in the protection algorithm logic, whereas the protection operation submodule contains the logic circled with blue in the protection algorithm diagram. The protection operation submodule uses voltages from both measurement locations and blocking, restraining and allowing signals as input values.

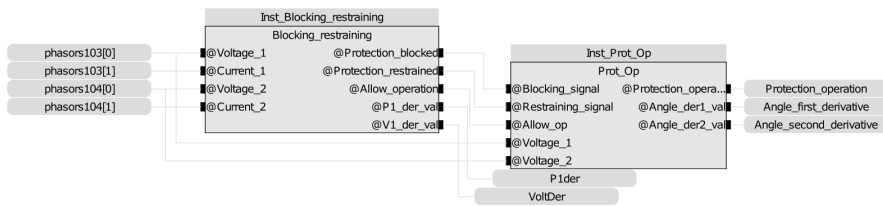


Figure 60 – Principle diagram of the developed OOS protection algorithm in the hardware controller software.

For the purpose of evaluating the development of the hardware implementation of the algorithm, the signals as well as the derivative values of angles are compared with the software implementation of the algorithm for both stable and unstable power swing case in the network. The comparison between the software and hardware implementation of the algorithm in the cases of a stable power swing in the network is displayed in Fig. 61. The first section of the figure shows the measured voltage values and the measured angle difference by the PMUs on either end of the observed transmission line, whilst the second part of the figure shows the first and second derivative values computed by both the software and hardware implementation, as well as the signals associated with the protection algorithm.

The stable power swing is initiated by a fault on the parallel transmission line in the network at 0.5 s, marked by ①, as the measured voltage values drop in Fig. 61a. After the fault is cleared the voltage jumps up, indicated by ②. However, the voltage levels remain under the 0.89 p.u. threshold value for the protection blocking. Thereafter, the system experiences a stable power swing, as shown by the angle difference value reaching a peak 11°, and thereafter starting to lower, and the voltages that stabilise near 1 p.u. value.

Fig. 61b shows the first and second derivative values and signal states of both software and hardware implementations of the protection algorithm. The hardware implementation displays nearly homogeneous derivative values with the software implementation of the algorithm, with the difference being that the values in the hardware implementation have a delay associated with the PDC Wait Time as well as the processing time of the logic in the external controller. During the faulted condition the first and second derivative values display very sporadic behaviour, due to the abrupt changes in the measurement values, for both hardware and software implementation. The protection algorithm remains blocked during this time from the fault detection element, and does not operate. After the fault is cleared in the network, the first derivative value stabilises at a positive

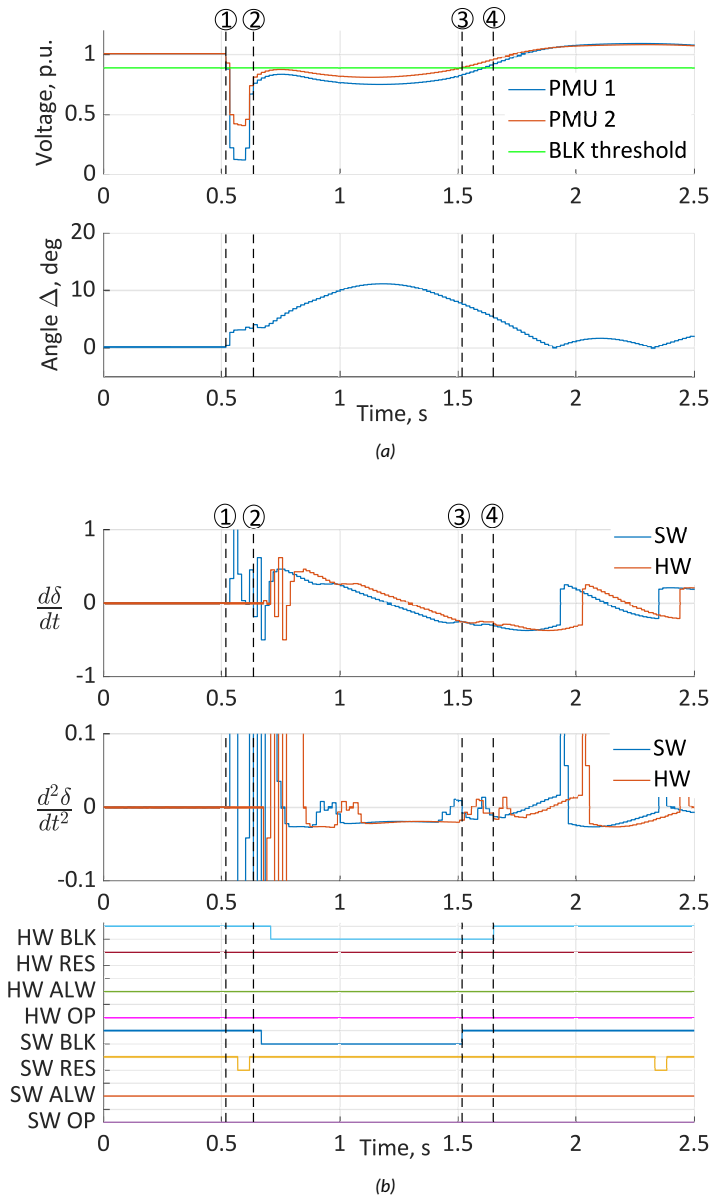


Figure 61 – The decoupled algorithm reaction to a stable power swing in the network. (a) - the measured voltage values and measured angle difference between the sources, (b) - computed first and second derivative values as well as the protection signals for the software and hardware implementation of the protection algorithm. SW - software implementation, HW - hardware implementation, BLK - protection blocked, RES - protection restrained, ALW - protection allowed to operate, OP - protection operation. ① - fault inception, ② - fault clearing in the network, ③ - software implementation reblocking, ④ - hardware implementation reblocking.

value, but is declining in nature, because the rate at which angular difference is increasing is lowering. The first derivative value steadily declines and, after the maximum value of the angle difference during the power swing is reached, turns negative.

The second derivative stabilises after the fault at a negative value, and briefly changes

positive as the first derivative value levels for several samples. The hardware implementation value of the second derivative closely follows the software implementation, however, it is delayed. This is expected, as the hardware implementation takes into account delays in the transmission of measurement values and additionally, there is a small delay in the processing of the logic inside the controller. Based on the first and second derivative values being negative for the stable power swing, the protection is not expected to operate. This is confirmed by the signals of both of the implementations.

During the faulted condition the protection algorithm remains blocked as indicated by the blocking signal (SW BLK and HW BLK signals) being activated. After the faulted condition, the blocking signal is deactivated, as the voltages are above the set threshold of 0.89 p.u. The restraining criterion for both implementations (SW RES and HW RES signals) remains activated throughout the power swing. When the system is stabilising, the blocking criteria are reactivated, as the voltage level is restored. This is indicated by ③ for the software implementation and ④ for the hardware implementation.

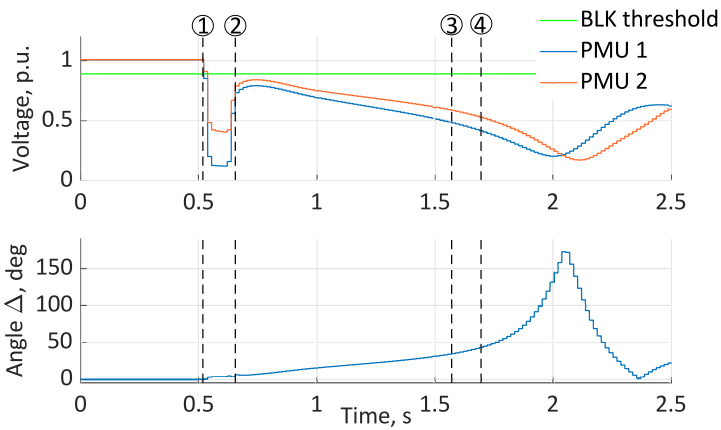
The reaction of software and hardware implementation to an unstable power swing is shown in Fig. 62. The first part of the figure displays the measured voltage values and the angular difference at the ends of the monitored transmission line. The unstable power swing is initiated by a fault on the parallel line and the disconnection as the faulted line. The fault duration is prolonged, and this results in an unstable power swing taking place on the observed transmission line. The fault inception occurs at 0.5 s, marked by ①. The fault clearing is indicated by ②, and after the fault the voltages are restored, however, the voltages remain below the 0.89 p.u. threshold value. Afterwards, due to the power swing process, the voltages continue to decline as the angle difference is increasing as shown in Fig. 62a, until the system experiences a pole slip.

Fig. 62b displays the derivative values and the signals of the protection algorithm for both implementations. Similarly to the stable power swing case, both derivative values are sporadic during the fault event due to the abrupt changes in the measurement values, however the protection in both implementations does not operate due to blocking being active. After the fault clearing, the protection algorithm implementations become deblocked (shown by the HW BLK and SW BLK signals deactivating), however, they remain restrained. The first derivative value stabilises as a positive value while the second derivative remains negative at the start. Thereafter, as the system is heading into an unstable power swing, the second derivative value becomes positive. After the last stable angle has been passed, the protection is allowed to operate, which is indicated by the ALW signal activation. Then, since the first and second derivative values are positive and the protection is allowed to operate, it identifies an unstable power swing in the network and operates. This is shown by ③ and ④ for the software and hardware implementation respectively.

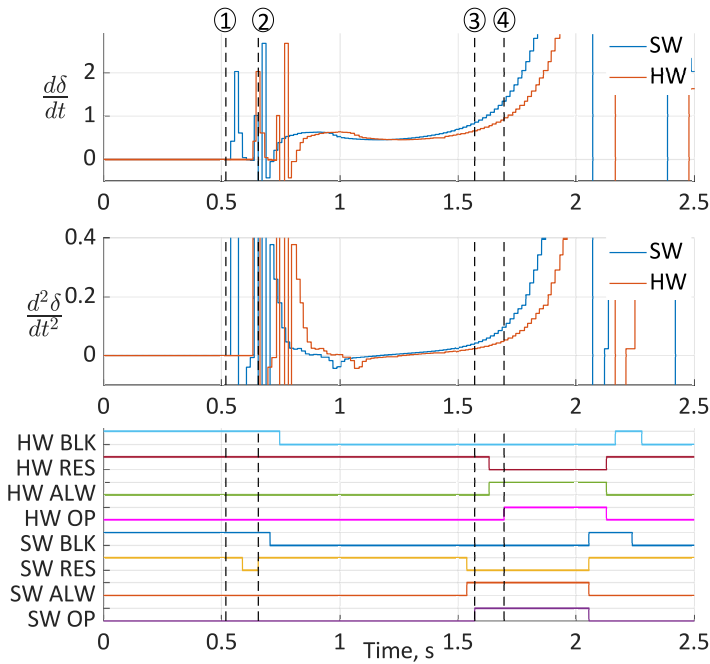
The derivative values computed by the algorithm's hardware and software implementation are closely following each other, where the hardware implementation is experiencing a delay. The same holds true for the associated protection signals. This is, however, expected behaviour. Therefore it is concluded that the hardware implementation of the algorithm is successful, considering the constraints introduced by the delays associated with a real-world network installation scenario.

3.3 Effect of Grid Events on Algorithm Operation

To check the stability and security of the algorithm it has been subjected to different events taking place in the power network. First, the algorithm's response to faults outside of the observed transmission line is investigated, and thereafter the effect of line



(a)



(b)

Figure 62 - The decoupled algorithm reaction to a unstable power swing in the network. (a) - the measured voltage values and measured angle difference between the sources, (b) - computed first and second derivative values as well as the protection signals for the software and hardware implementation of the protection algorithm. SW - software implementation, HW - hardware implementation, BLK - protection blocked, RES - protection restrained, ALW - protection allowed to operate, OP - protection operation. ① - fault inception, ② - fault clearing in the network, ③ - software implementation issues an operation command, ④ - hardware implementation issues and operation command.

disconnection is observed.

Fig. 63 shows the test system to check the algorithm's response to faults outside of the observed transmission line. The test system is the extended system used in the testing of

OOS protection using equivalent impedances in Section 2.3. A fault location is chosen, and is marked as F1 on the figure. At that location single-phase (SLG) and three-phase (TPH) faults are considered, both with a temporary nature. Auto-reclosure function is also used and the faulty line (L1) is reclosed 1 second after being switched off. The fault event creates a stable power swing in the network and the decoupled algorithm's response to the event as well as the following power swing is presented in Fig. 64.

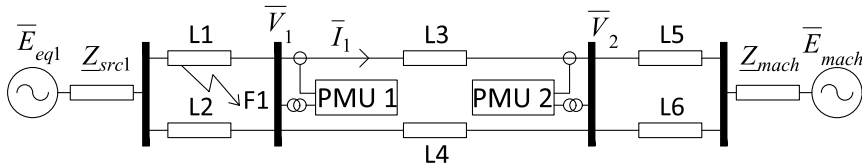


Figure 63 – Fault location for testing the algorithm's security for faults outside of the observed transmission line.

Fig. 64 shows the voltage measurements, angle difference and protection algorithm signals from the external controller for a SLG fault at location F1. The fault is introduced in the network at 0.5 s, indicated by ①, and subsequently cleared at 0.7 s by disconnecting the transmission line from the network, shown by ②. The faulted line is reclosed at ④

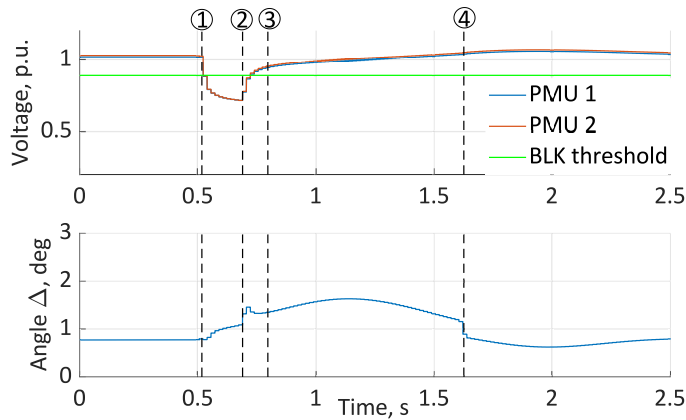
The RMS voltage values, blocking threshold for the voltage as well as the measured angle difference for the SLG fault at location F1 are shown in Fig. 64a. The voltage values drop below the blocking threshold during the faulted condition in the network, and thereafter, they are restored above the threshold value. The fault causes a minor power swing to propagate through the network, and the protection should not operate, as it is a stable situation.

Fig. 64b shows the derivative values and the protection signals during the SLG fault case. During the faulted state of the power system both computed derivative signals show sporadic behaviour due to the abrupt changes in the network. After the fault clearing, the protection is deblocked briefly, indicated by ③, as the voltage value is below the blocking threshold for some time. Thereafter, the protection becomes blocked, as the voltage is restored. During the power swing in the network after the fault the first derivative of the angle value is positive, until the angular difference start to decrease, whereupon it changes sign and becomes negative. The second derivative value of the angle remains negative until the auto-reclosure of the faulted line. The protection does not operate for this fault condition.

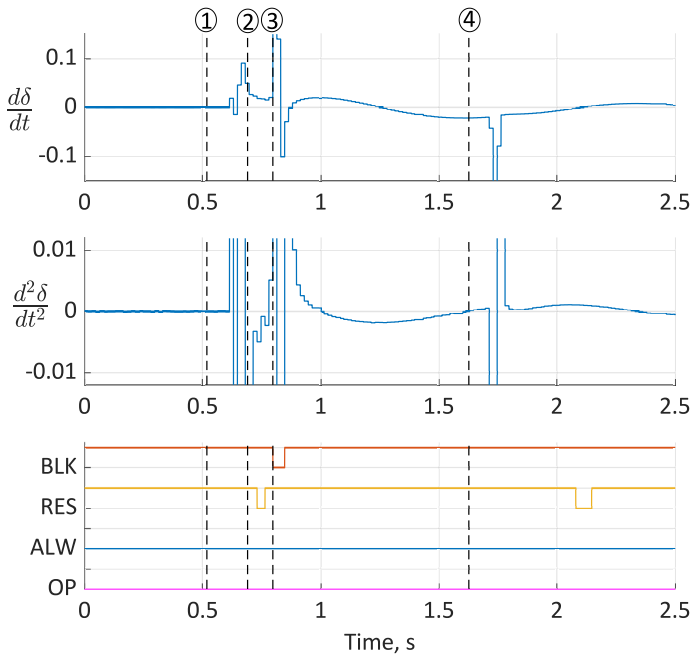
The case of a three-phase fault (TPH) on the transmission line at location F1 is displayed in Fig. 65. For this event, similarly to the SLG fault, the measured voltage values drop below the blocking threshold value at the fault inception, that is indicated by ①. After the fault is cleared by switching off the faulted line at ② a stable power swing takes place in the network. Thereafter, the faulted line is reclosed, indicated by ④.

Fig. 65a shows the measured RMS voltage values, blocking threshold and the measured angle difference for the case of an TPH fault at location F1. The measured voltage values decrease at the fault inception, indicated by ①, and the fault is cleared at ②, the voltages restore to a lower level than the protection blocking threshold. Thereafter, the system experiences a power swing, during which, the measured voltages remain under the blocking threshold for some time, until the system starts stabilising.

Due to the voltage remaining lower than the blocking threshold, the protection algorithm is deblocked after the fault clearing in the network. This is indicated by the BLK



(a)



(b)

Figure 64 – The decoupled algorithm reaction for an SLG fault at location F1. (a) - the measured RMS voltages, voltage threshold for blocking and measured angle difference between E_{mach} and E_{eq1} , (b) - computed first and second derivative values as well as the protection signals for the hardware implementation of the protection algorithm. BLK - protection blocked, RES - protection restrained, ALW - protection allowed to operate, OP - protection operation. ① - fault inception, ② - fault clearing in the network, ③ - protection deblocking, ④ - auto-reclosure of the faulted line.

signal dropping in Fig. 65b at ③. The protection algorithm remains deblocked until the voltage value is restored above the threshold, however, during the whole power swing process, the restraint signal (RES) remains activated.

The first derivative stabilises at a positive value after the fault clearing, and starts lowering, eventually changing sign and turning into a negative value after the angle difference

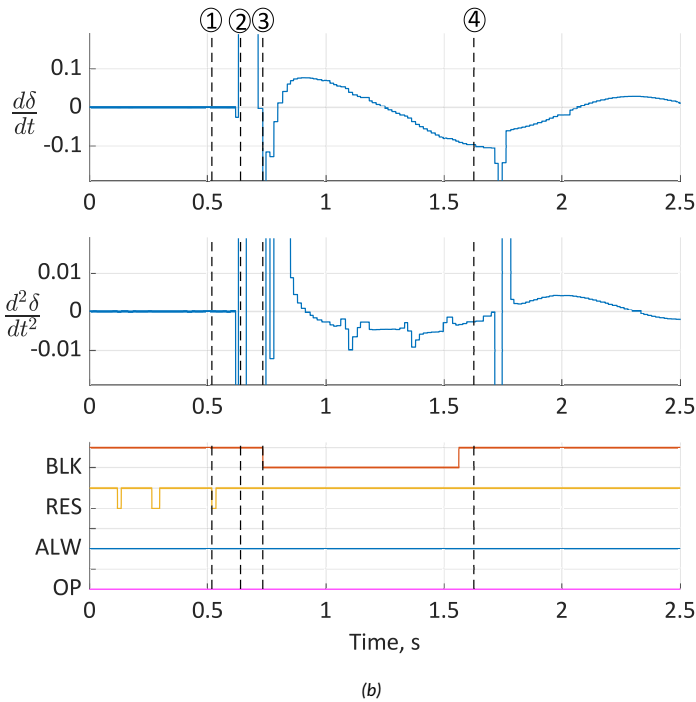
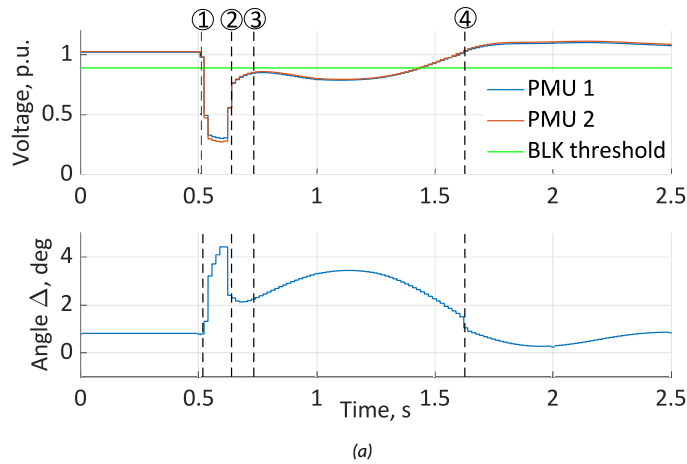


Figure 65 – The decoupled algorithm reaction for a TPH fault at location F1. (a) - the measured RMS voltages, voltage threshold for blocking and measured angle difference between E_{mach} and E_{eq1} , (b) - computed first and second derivative values as well as the protection signals for the hardware implementation of the protection algorithm. BLK - protection blocked, RES - protection restrained, ALW - protection allowed to operate, OP - protection operation. ① - fault inception, ② - fault clearing in the network, ③ - protection deblocking, ④ - auto-reclosure of the faulted line.

value has passed its peak and starts to lower. The second derivative value remains negative after stabilising after the fault, until the faulty line is re-energised at ④. Therefore, the protection does not issue an operation command, and displays stable behaviour for this fault case.

The case of observed transmission line disconnection is shown in Fig. 66. In this case the observed transmission line by the protection algorithm is disconnected, which results in one of the measurement points voltage dropping. The line disconnection occurs at 0.5 s, and is marked by ①.

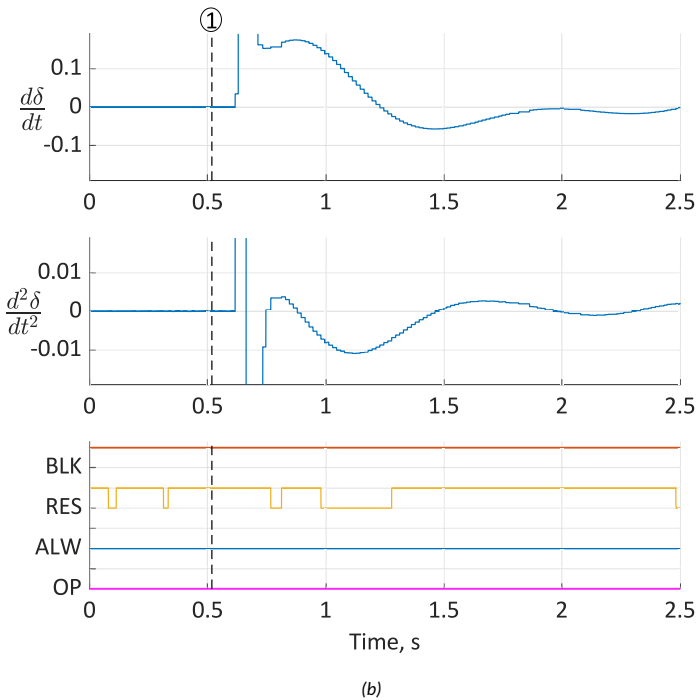
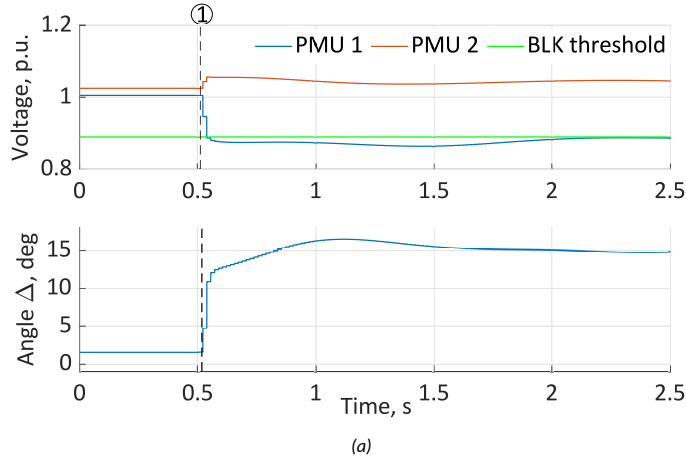


Figure 66 - The decoupled algorithm reaction for disconnection of the observed transmission line. (a) - the measured RMS voltages, voltage threshold for blocking and measured angle difference between E_{mach} and E_{eq1} , (b) - computed first and second derivative values as well as the protection signals for the hardware implementation of the protection algorithm. BLK - protection blocked, RES - protection restrained, ALW - protection allowed to operate, OP - protection operation. ① - line disconnection.

Fig. 66a shows the measured voltage values as well as the measured angle difference between the measurement locations. After the line is disconnected, the voltage at the measurement location of PMU1 drastically drops, and stabilises below the protection blocking threshold. The angle difference also greatly increases, due to the power transmission only being possible through one line.

The computed derivative values and the protection algorithm signals are shown in Fig. 66b for the case of the transmission line disconnection. The derivative values display some oscillation, and stabilise as the angular difference is stabilising after the line disconnection. The protection signals show that, during this event, as one of the voltage values is lower than the deblocking threshold, whilst the second remains higher, the protection is in a blocked state throughout this event in the network. This is correct behaviour, as the power swing following the disconnection of the line is minor, and the system is able to continue operating.

From the cases shown it can be concluded, that the developed protection algorithm shows secure behaviour in the case of stable power swings in the network, as well as when there are faults elsewhere in the network. Additionally, the protection shows reliable operation in the case of an unstable power swing in the network, as the algorithm relies on detecting the condition when the system has passed the critical last stability point.

3.4 Intermediate Summary

A novel settingless out-of-step protection algorithm, that makes use of discrete angle derivatives and therefore is decoupled from network parameters. The algorithm utilises wide-area measurement information, as presented in this chapter. Blocking and restraining criteria have been developed for the algorithm in order to avoid maloperation during stable power swings and normal system operation. The presented algorithm has been validated in a software as well as in a hardware implementation.

The algorithm was subjected to a stable and unstable power swing and the behaviour of the algorithm has been investigated. For the stable power swing case the algorithm behaves securely, providing no operation commands, and for the unstable power swing case the algorithm successfully operates. The hardware implementation of the algorithm displays homogeneous behaviour to the software implementation, though, with a delay in the response. The delay is expected, however, due to the implemented wait time for real-world wide-area information collection. Therefore the hardware implementation of the algorithm is considered successful.

The algorithm has also been verified to be stable for faults outside of the observed transmission line, as well as line disconnection, where the algorithm behaves securely and does not operate.

4 Case Studies

In the previous chapters of this thesis existing out-of-step protection algorithms have been described, and the concerns regarding the protection operation in systems with renewable energy penetration have been brought out. Two novel out-of-step protection algorithms using wide-area information have been developed to overcome the limitations regarding protection settings and the source impedance changing. The concept of the two protection algorithms was verified by conducting stable and unstable power swings together with different grid events in a simple test network.

The aim of this chapter is to assess out-of-step protection behaviour in different network configurations with the inclusion of different levels of IBRs in the power network. For this purpose several case studies are performed. Initially, a case study is conducted to evaluate the performance of commercially available protection in different grid condition and RES% scenarios. Thereafter, a second case study utilises a larger power network together with two commercially available devices and the two protection algorithms developed in this dissertation. Finally, a case study is conducted using the Iceland power system, where the discrete angle derivative (DER) algorithm is tested and implemented in the field.

The beginning of this chapter outlines the power system models used for the case studies, and the different scenarios considered for the case studies. Thereafter, the HiL testing methodology is explained and the protection settings needed for the commercially available devices are computed. Following the testing methodology the results of the tests and a comparison are presented. The results shown, the test models used and the methodology as well have been published in [I], [II] and [III].

4.1 Test Model Descriptions

This subsection contains the power system models' descriptions, which have been used for the conducted case studies. The single-machine infinite-bus model (SMIB) is described first. This is followed by the modified IEEE 39 Bus power system model, and ,finally, the Iceland power system model used for the protection algorithm field implementation verification, is described.

SMIB Model

The test model for testing out-of-step protection devices is shown in Fig. 67. The model has been developed in an RTDS simulator. It consists of a variable network grid equivalent, which is represented by a constant voltage source behind an impedance, two transmission lines that connect the grid equivalent to a generator bus, a generator, and a Type 4 wind power plant with grid following controls. The bus where the generator and wind power plant are connected is noted as Area 1 and the bus where the constant voltage source is connected is named Area 2.

The power system model is based on [72], however it has been modified and changed to a 50 Hz system with a nominal voltage level of 330 kV. The Type 4 wind power plant is modelled with structure and control algorithms taken from the RTDS standard library [78], and the output of the IBR is scaled according to the generation scenario being tested. Different generation scenarios are created by additionally scaling down the synchronous machine apparent power while the IBR output scale is increased. This approach is chosen to change both the apparent power at Area 1 as well as the inertia in that area. Different grid equivalent values in Area 2 as well as different transmission line lengths are combined to test the out-of-step protection performance. This allows the possibility to test the protection devices in situations with different electrical transmission line lengths according

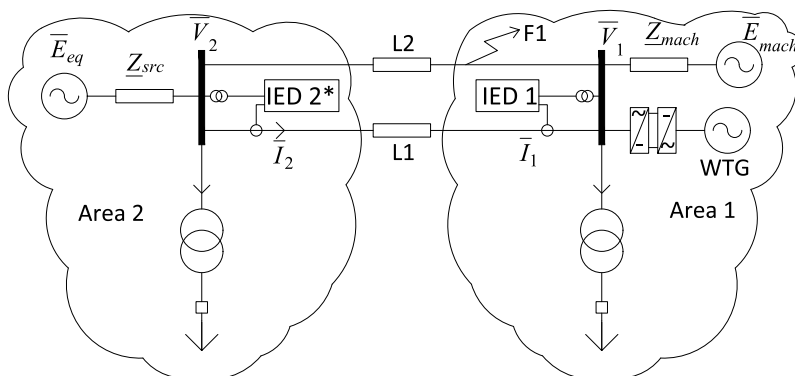


Figure 67 - Diagram of the developed two-area model for testing out-of-step protections. Area 1 is represented by a synchronous generator and a Type 4 wind power plant and Area 2 is modelled as a static source. IED 2 is marked with an asterisk, because the IED in that position was only used by algorithm 3, since it needs two IEDs to function.

to source to impedance rating (SIR rating [60]). The simulation cases are defined by the transmission line lengths used in the testing as follows:

- Case S - represents short transmission lines between the two areas with the value of $Z_l = 0.0017 + j0.0288$ pu
- Case M - represents medium transmission lines between the two areas with the value of $Z_l = 0.0165 + j0.2883$ pu
- Case L - represents long transmission lines between the two areas with the value of $Z_l = 0.0331 + j0.5767$ pu

Table 7 depicts the different aspects of the SMIB test model. For different test scenarios all of the parameter combinations were considered. This results in a total number of 180 different grid scenarios.

The impedances of the transmission lines used are given in per unit on 1000 MVA base. The nominal capacities of the generator, IBR and transformers are 1000 MVA. Additionally, for each test case three different equivalent system strength levels are considered - infinite, medium and weak. The used system impedance values in per unit are as follows:

- Infinite system strength impedance $Z_{src} = 0.0001 + j0.0001$ pu
- Medium system strength impedance $Z_{src} = 0.01 + j0.0955$ pu
- Weak system strength impedance $Z_{src} = 0.1 + j0.955$ pu

The unsaturated parameters for the used synchronous machine on 1000 MVA base are as given in Table 8. The generator is connected to the network through a step-up transformer with a reactance of 0.1 per unit on 1000 MVA base. Additionally, the generator used is equipped with an IEEE ST1 type exciter and a IEEE G1 type turbine governor. The parameters of the exciter and governor are shown in Table 9 and Table 10 respectively.

The used wind turbine uses a permanent magnet synchronous machine as a generator with a nominal power value of 2.0 MVA and nominal voltage of 4.0 kV. The machine parameters are given in Table 11.

Table 7 – System aspects which are varied for protection testing in the SMIB test model.

Aspect	Scenarios
Line length	<p>Three different transmission line lengths are considered:</p> <ul style="list-style-type: none"> • Case S - short transmission line, • Case M - medium transmission line, • Case L - long transmission line.
System strength	<p>Three system strengths are considered:</p> <ul style="list-style-type: none"> • Strong system, • Medium system, • Weak system.
IBR production level	<p>The IBR output (RES%) is varied between 0% and 95% in 5% steps.</p>

Table 8 – Used data for the synchronous generator for SMIB test cases in per unit on 1000 MVA base.

$X_d = 1.7134$	$X_q = 1.6424$	$X'_d = 0.4245$	$X'_q = 0.6168$
$X''_d = 0.3253$	$X''_q = 0.3253$	$R_a = 0.002$	$T'_{d0} = 6.174 \text{ s}$
$T_{q0} = 0.388 \text{ s}$	$T''_{d0} = 0.032 \text{ s}$	$T''_{q0} = 0.047 \text{ s}$	$H = 4.7$

Table 9 – Used data for the synchronous generator IEEE ST1 type exciter for SMIB test cases.

$T_r = 0.00\text{s}$	$T_c = 1.0 \text{ s}$	$T_b = 20.0 \text{ s}$	$T_f = 1.0 \text{ s}$
$K_a = 200$	$T_a = 0.02 \text{ s}$	$E_{Fmax} = 5.7$	$E_{Fmin} = -4.9$
$K_c = 0.175$			

Table 10 – Used data for the synchronous generator IEEE G1 turbine governor for SMIB test cases in per unit on 1000 MVA base.

$K = 20.0$	$T_1 = 1.0 \text{ s}$	$T_2 = 1.0 \text{ s}$	$T_3 = 0.25 \text{ s}$
$U_0 = 0.1$	$U_c = -0.2$	$T_4 = 0.2 \text{ s}$	$K_1 = 0.3$
$K_2 = 0.0$	$T_5 = 5.0 \text{ s}$	$K_3 = 0.7$	$K_4 = 0.0$

Table 11 – Used data for the PMSM generator for SMIB test cases in per unit on 2 MVA base.

$X_{ls} = 0.1$	$X_{md} = 0.65$	$X_{lD} = 2.5$	$X_{mq} = 1.0$
$X_{lQ} = 2.5$	$R_s = 0.01$	$R_D = 2.0$	$R_Q = 2.0$
$\Psi_m = 1.3$			

The grid-side converter of the wind power plant is current regulated and utilises PI control. The structure of the grid-side controller is shown in Fig. 68, and the parameter values are displayed in Table 12, respectively.

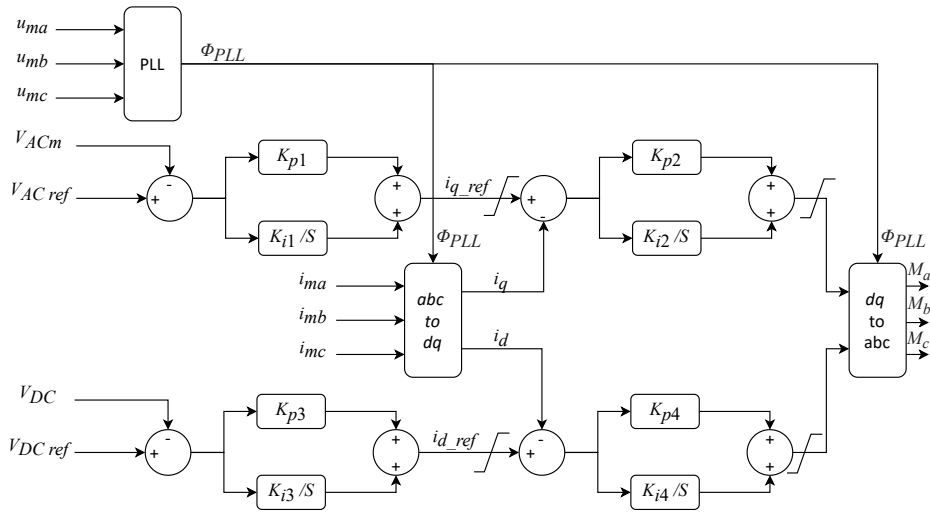


Figure 68 – Schematic diagram of the control of the used Type 4 wind turbine.

Table 12 – Parameters of the Type 4 wind power plant grid-side converter.

$K_{p1} = 5.0$	$K_{i1} = 0.05$	$K_{p2} = 0.5$	$K_{i2} = 0.03$
$K_{p3} = 5.0$	$K_{i3} = 0.05$	$K_{p4} = 0.5$	$K_{i4} = 0.03$

To create a power swing in the network a 3-phase permanent fault is introduced on L2 terminals at Area 1, after which L2 is disconnected from the network. This causes a power swing to occur on L1. The fault created is prolonged, so that the resulting power swing will result in an out-of-step condition.

IEEE 39 Bus System Model

In order to test the out-of-step protection algorithms in a larger network than the two-area scenario, the IEEE 39 bus network model is used. The model is modified from the original by adding generic grid-following wind farms at some buses, whose control structure and parameters are the same as the ones used for the two-area power system Type 4 wind power plant. This allows us to create variable generation scenarios to test the OOS protection devices in different grid conditions. The modified test network is shown in Fig. 69.

Additionally, two different test locations are chosen to test the protection devices' performance when considering different installation locations. The first test location is circled in red and shown as Case A, and the other denoted in blue is Case B. The location marked in red is representative for the swings between two areas and the location marked in blue represents a single machine connected to an infinite bus system.

For both locations, two tie-lines are included in the testing, one of which represents a shorter tie-line and the other a longer transmission line. For Case A, the protection devices were tested on the transmission lines between buses 14-15 and 16-17. To create an OOS condition between the two areas of the network, a three-phase short circuit is introduced on bus 16. The fault is cleared by disconnecting one of the transmission lines emanating from bus 16, and thereafter oscillations take place on the remaining tie-line between the two parts of the network. For Case B, the transmission lines under observation are between buses 26-29 and 28-29. Power swings are created by a three-phase

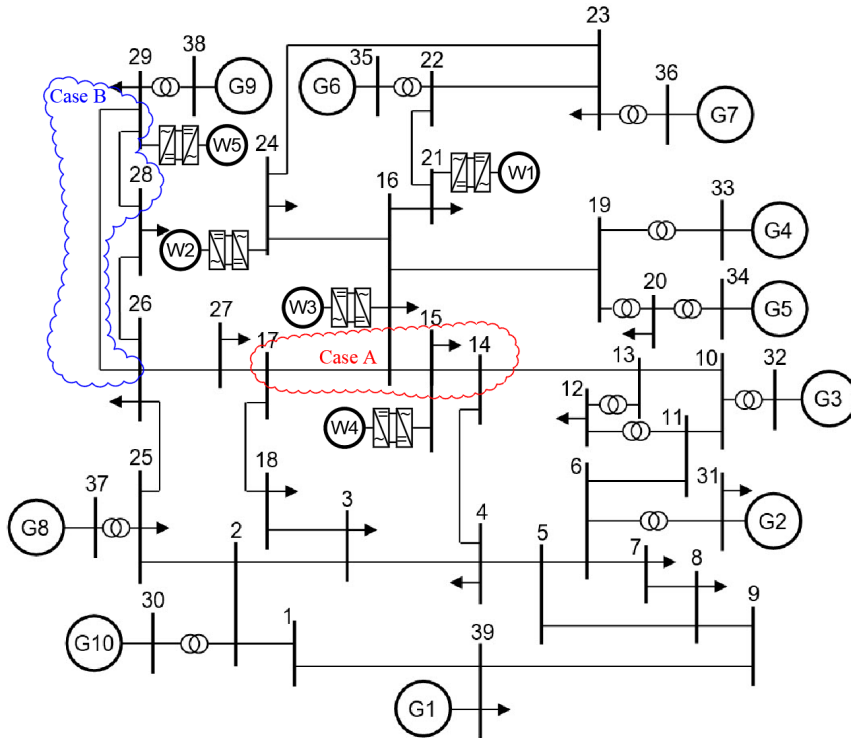


Figure 69 – Modified IEEE 39 bus network with added type 4 wind farms. Red marks Case A testing location and blue Case B testing location, wind farms are added to buses 21, 15, 25, 16 and 29 [79, 80].

short circuit applied on bus 29. The fault is cleared by disconnecting one of the two tie-lines connected to this bus. This contingency causes power swings along the remaining transmission lines. The protection relays are situated on lines 16-17, 15-14, and at the line remote ends near bus 29 for cases A and B respectively, while the PMU measurements are provided to the external controller from both ends of the transmission lines.

For testing protections for various grid conditions, the output power of the windfarms is scaled up while simultaneously decreasing the synchronous generation capacity. This means that, for Case A, to create a specific renewable penetration scenario (RES %), the four windfarms denoted as W1 - W4 in Fig. 69 together with G4, G5, G6 and G7 are scaled. The scaling is realised by decreasing the apparent power of the synchronous machines from the initial value of 1000 MVA by a percentage value corresponding to the specific RES %, while increasing the windfarms output by the same margin. This is done in order to not just decrease the output of the generation, but also to decrease the total inertia of the generators. For Case B, this means changes to one generator (G9) and one windfarm (W5). A total of 70 different scenarios are simulated in the IEEE39 Bus System. Besides this, each test case is repeated five times to verify that the algorithm detects OOS conditions.

Iceland Model

To display the developed algorithm's robustness for the application in an arbitrary power system, the Iceland power system has been used for additional tests. To perform real-time simulations to test the OOS protection, the Iceland power system was modelled in RTDS environment. Fig. 70 shows the power system, which has two centres of inertia, situated

in the southwest and in the eastern part of the island. These two inertia centres are connected with links, known as the northern ring connection (north corridor), circled with red, and the southern ring connection (south corridor), circled with green. The southern ring connection utilises a capacitor for series compensation, that can be switched on or off. On these two ring connections power swings are expected, and the developed protection algorithm is tested.

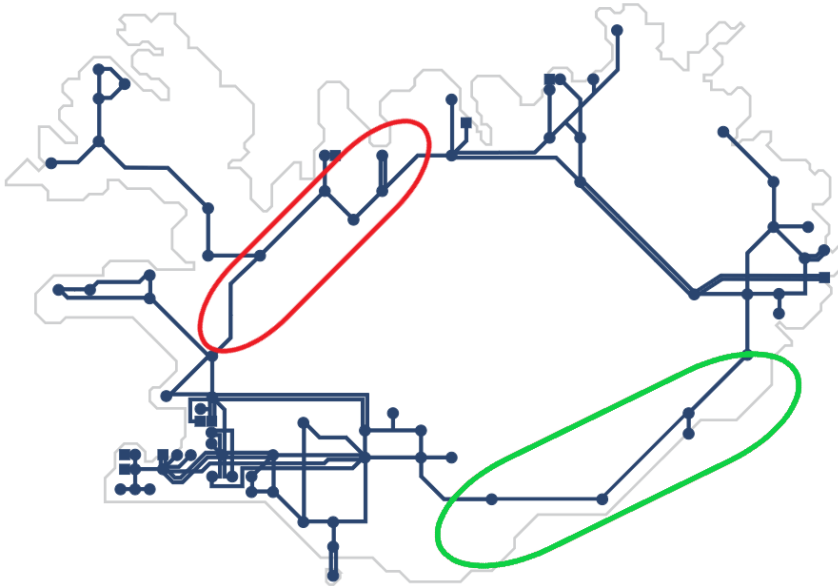


Figure 70 – Iceland power system, the corresponding corridors of lines connecting two parts of the network are outlined in red and green for the northern and southern ring connections respectively [81].

The Iceland grid uses a wide-area monitoring system with a number of PMUs installed in the network. The wide-area monitoring system has recorded several system-level events including OOS conditions, which are used to compare the developed network model behaviour to the actual system behaviour. The network model in RTDS environment was developed based on the PSS/E[®] network model provided by Landsnet.

Two recorded OOS events were used to validate the created model in RTDS. The first OOS event was initiated by a busbar flashover in one of the substations located in the northern ring connection. This event led to the loss of the substation and disconnection of the northern transmission corridor, resulting in an OOS condition in the southern ring. The second event was initiated by a sudden loss of load in the south-western inertia centre. This contingency caused system split, where some generators in the south west system were connected to the rest of eastern network only through the southern ring connection, and led to an OOS condition in the southern corridor of the network.

A comparison of the measured values and the simulated results for the first OOS event is shown in Fig. 71. The frequencies of the south-western inertia centre and the northern inertia centre are shown in Fig. 71a and Fig. 71b, whereas the active power flow in the southern corridor during the event is shown in Fig. 71c. The specific events of interest are marked throughout the figures, where ① marks the start of the sequence of events with a flashover at the substation in the northern corridor, at 10.2 seconds. After 300 ms (marked

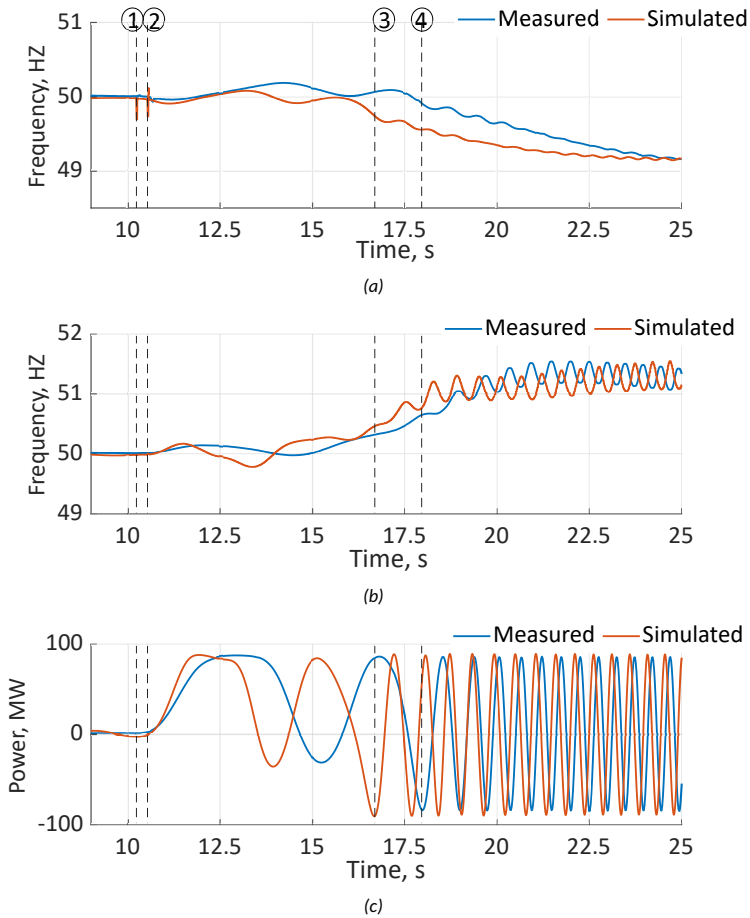


Figure 71 – OOS event 1 measured and simulation values. (a) the frequency in the south-west centre of inertia, (b) the frequency of the east centre of inertia and (c) the active power flow in the southern ring connection, where the OOS event takes place. ① - the start of the event with the fault in the north corridor substation, ② - fault clearance, ③ - first pole slip in simulated values, ④ - first pole slip in measured values.

as ②), the fault is cleared by tripping the remote ends of the lines from the faulted busbar, leading to the disconnection of the northern transmission corridor. Thereafter, the active power is transferred through the southern corridor, and the system goes through a stable swing, after which it fails to maintain stability. The northern and southern parts of the network experience the first pole slip at ③ and ④ for the measured and simulated results respectively.

The simulated and measured values show a slight deviation, however, the general behaviour of the simulated network and the measurement data is similar. For both cases, after the initial event occurs, the system goes through a stable swing. The simulated results show greater swing frequency than the measured one. This is likely to be caused by a difference in generator dispatch during the event, as well as by the effects of the user-defined governor models, which have been replaced with standard generator models.

Fig. 72 shows a comparison of the measured values and simulated results for the sec-

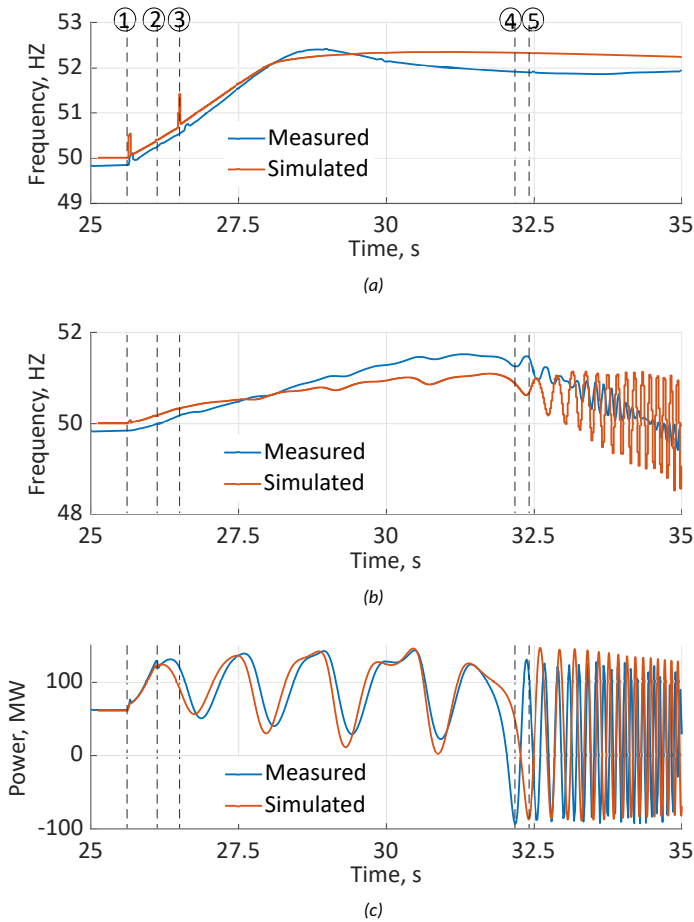


Figure 72 – OOS event 2 measured and simulation values. (a) the frequency in the south-west centre of inertia, (b) the frequency of the east centre of inertia and (c) the active power flow in the southern corridor, where the OOS event takes place. ① - the start of the event with the loss of load, ② - inter-trip on the 220 kV substation at the southern corridor, ③ - north corridor disconnection from overload, ④ - first pole slip in measured values, ⑤ - first pole slip in simulation.

ond OOS event. The frequencies of the south-western inertia centre and the northern inertia centre are shown in Fig. 72a and Fig. 72b, respectively, whereas the active power flow in the southern corridor during the event is shown in Fig. 72c. The specific events of interest are marked throughout the figures, where ① denotes the start of the sequence of events with a large loss of load in the network at 25.6 seconds. The loss of load is followed by an inter-trip from the overload protection of the southern corridor marked as ②. Due to disconnection in the 220 kV substation nearest to the southern link, only two generators remain connected to the network through the southern corridor. At ③, the northern corridor link is disconnected by the overload protection, effectively separating the two inertia centres of the network. As a result, the two generators left on the southern corridor pass through three stable power swings, which are increasing in magnitude, and experience a pole slip at ④ and ⑤ for the measured values and simulation results, respectively.

The results of the model simulation are well aligned with the actual measured values for this event. The frequency in the south-western inertia centre closely follows the measured values, and in the northern part there is a slight difference in the gradient of the frequency increase, which may be caused by a difference in production units during the actual event and the simulation, together with the effect of non-standard governors used in the Iceland power system. As for the power flow in the southern corridor, the simulated values closely match the measured values. Based on these comparisons, it is concluded that the model follows the real-life characteristics of the Iceland power system and can be used to investigate OOS protection algorithm performance.

4.2 Hardware-in-the-Loop Testing Principles

The commercially available protection devices as well as the developed solutions are tested using Hardware-in-the-loop (HiL) testing methodology. Fig. 73 depicts the diagram for the HiL testing. The commercially available relays are provided with current and voltage sig-

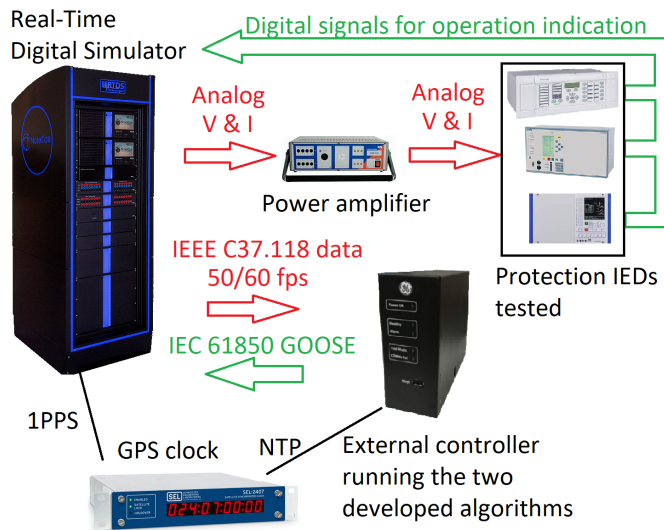


Figure 73 – Experimental setup for OOS protection testing using physical hardware.

nals from the real-time simulation via amplifiers, and they provide feedback to the simulation using digital I/O. Both developed OOS protection algorithms are installed on the external controller and receive data using IEEE C37.118 synchrophasors. The data streaming rate for PMU data is 50 and 60 fps (frames per second) for the 50 Hz and 60 Hz test systems respectively. The external controller provides feedback to the simulation using IEC 61850 GOOSE messages.

The real-time simulator and the external controller require time synchronisation, so that the synchrophasor data used would have the correct timestamps. For this a GPS clock is used, that provides time synchronisation to the RTDS by 1PPS signal and time synchronisation to the external controller using NTP.

Synchrophasor data is related to WAMS, which means, usually, that information is collected from several geographical locations. Time delay, i.e. latency, is one of the most stringent requirements for WAMS systems. Time delays are caused by communication disturbances or data alignment. In general, the permissible time from PMUs to PDCs is 20

ms, if the PDC also needs to transfer data to a central location an extra 40 ms is permitted from PMUs to the central location [82]. The WAMS requires a short time delay to support the local and wide-area real-time response of control and protection [83]. However, the time delay requirements are subject to the actual application type. Some typical time delay requirements for synchrophasor applications are listed in Table 13 [84].

Table 13 – Communication time delay requirement for synchrophasor applications [82, 85, 86].

Synchrophasor application	Communication delay (ms)
Controlled islanding	50
Generator synchronization	50
Intelligent scheduling	50
Oscillation control	200
State estimation	100
System protection	50 - 200

The delay in communication directly affects any application that uses wide-area measurements. This is true for the case of the developed two out-of-step protection algorithms; therefore, different delays or "wait time" settings to align the measurement data from different parts of the power grid are observed. Three delays are considered: 50, 100 and 200 ms, as the system protection functions can be used between a delay of 50 - 200 ms. The comparison of the different delays for the OOS protection based on equivalent impedances [79] is shown in Fig. 74 for a stable power swing in the network and Fig. 75 for an unstable power swing. The network used for the power swings is the shown SMIB power network described in Section 4.1 in fully synchronous generation scenario.

The different time delays have a direct impact on the protection algorithm, where the computed angle value as well as the protection signals are shifted as the time delay increases. This is true for both the stable and unstable case, due to the time delay affecting the input signal processing by the protection algorithm, e.g. for the unstable case the protection operation signal activation occurs at 1.56, 1.61 and 1.7 s in the simulation for 50, 100 and 200 ms delay respectively. This reflects, directly, that the protection operation is delayed depending on the time delay value used.

The response of the OOS protection based on discrete angle derivatives with different time delays in PMU measurements to a stable and unstable power swing in the power network is shown in Fig. 76 and Fig. 77 respectively. Comparably to the OOS protection using equivalent impedances, the wait times in the PMU streams have a direct impact on the protection algorithm's behaviour, e.g. the protection operation signal for the unstable case activates at 1.34, 1.37 and 1.48 s in the simulation for the delay of 50, 100 and 200 ms respectively.

Both of the developed protection algorithms are intended to operate on a local PDC level. Therefore, based on [82] the time delay setting of 50 ms should be sufficient to utilise the protection function. However, in order to account for more usage scenarios, a more relaxed time delay of 100 ms has been used in all of the testing performed in the case studies in this thesis.

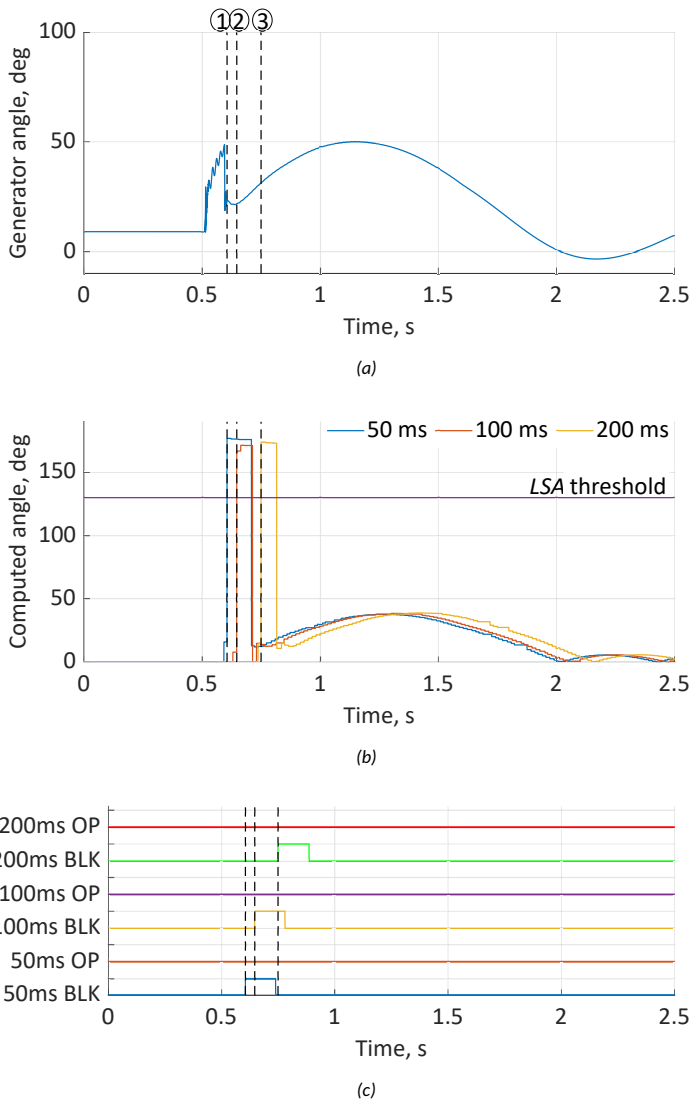
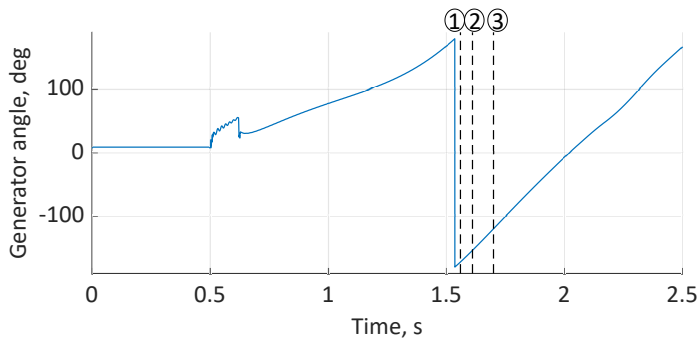
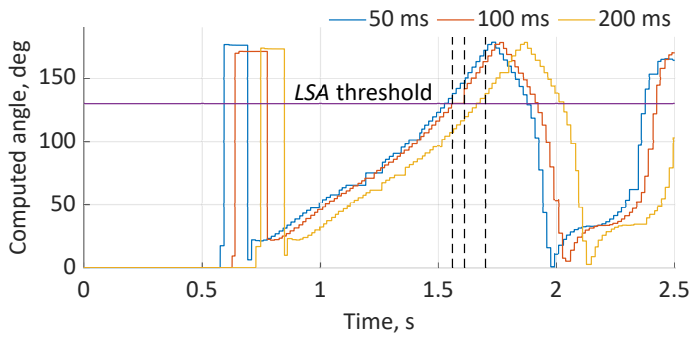


Figure 74 – Measured generator angle in respect to E_{eq} , computed angle value and algorithm signals for different delay settings. (a) - generator measured angle value, (b) - computed angle value by the algorithm and LSA value, (c) - algorithm operation and blocking signals in time. ① - algorithm blocking in the case of 50 ms delay, ② - algorithm blocking in the case of 100 ms delay, ③ - algorithm blocking in the case of 200 ms delay.

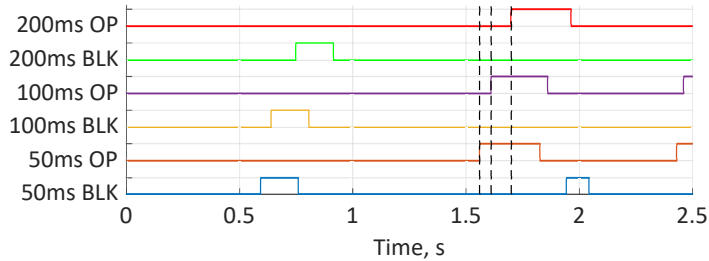
Additionally, two of the other tested protection algorithms require specific settings in order to work. For angle-controlled protection algorithm compensating impedance values that are dependent on the grid, as explained in Section 1.1, are needed. Since the testing is performed with variable grid conditions, a total of nine sets of compensating impedance settings are calculated for the SMIB case study - three for each of the test cases according to the Area 1 grid strength. The settings are calculated as per manufacturer's suggestion shown in the user manual of the device [87]. For calculation of settings the base case of fully synchronous production in Area 1 was considered.



(a)



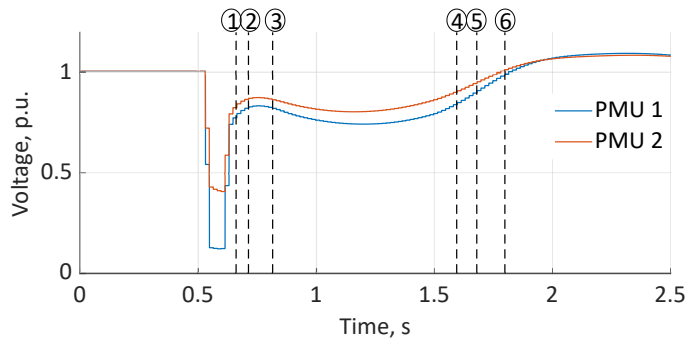
(b)



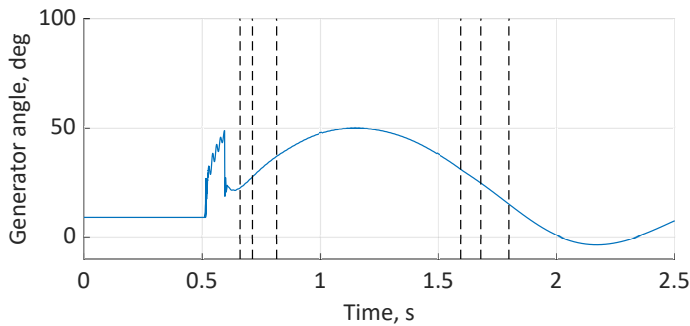
(c)

Figure 75 – Measured generator angle in respect to E_{eq} , computed angle value and algorithm signals for different delay settings. (a) - generator measured angle value, (b) - computed angle value by the algorithm and LSA value, (c) - algorithm operation and blocking signals in time. ① - algorithm operation in the case of 50 ms delay, ② - algorithm operation in the case of 100 ms delay, ③ - algorithm operation in the case of 200 ms delay.

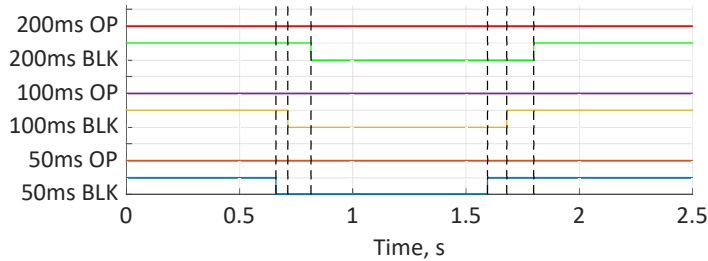
The impedance-based OOS protection settings are computed based on the user manufacturer manual of the device. For the SMIB case study three sets of settings are considered - one set of settings for each of the considered transmission line lengths. The computation of settings and the used setting values are shown in the following section. All of the commercially available devices that were used in the HiL testing included in this thesis are shown in Table 14.



(a)



(b)



(c)

Figure 76 - Measured voltage values, measured generator angle in respect to E_{eq} and algorithm signals for different delay settings for stable power swing case. (a) - measured voltage values, (b) - generator measured angle value, (c) - algorithm operation and blocking signals in time. ① - algorithm unblocking in the case of 50 ms delay, ② - algorithm unblocking in the case of 100 ms delay, ③ - algorithm unblocking in the case of 200 ms delay, ④ - algorithm reblocking in the case of 50 ms delay, ⑤ - algorithm reblocking in the case of 100 ms delay, ⑥ - algorithm reblocking in the case of 200 ms delay.

Settings for Angle-Controlled Protection Algorithm

The tested angle-controlled OOS protection device requires compensating impedance settings. The settings should be computed based on the impedances of the network, however, when the network conditions are changing in terms of generation mix, some compromise should be made. Using this, the settings are computed for the base case scenario, meaning that fully synchronous generation is considered in Area 1 of the test network.

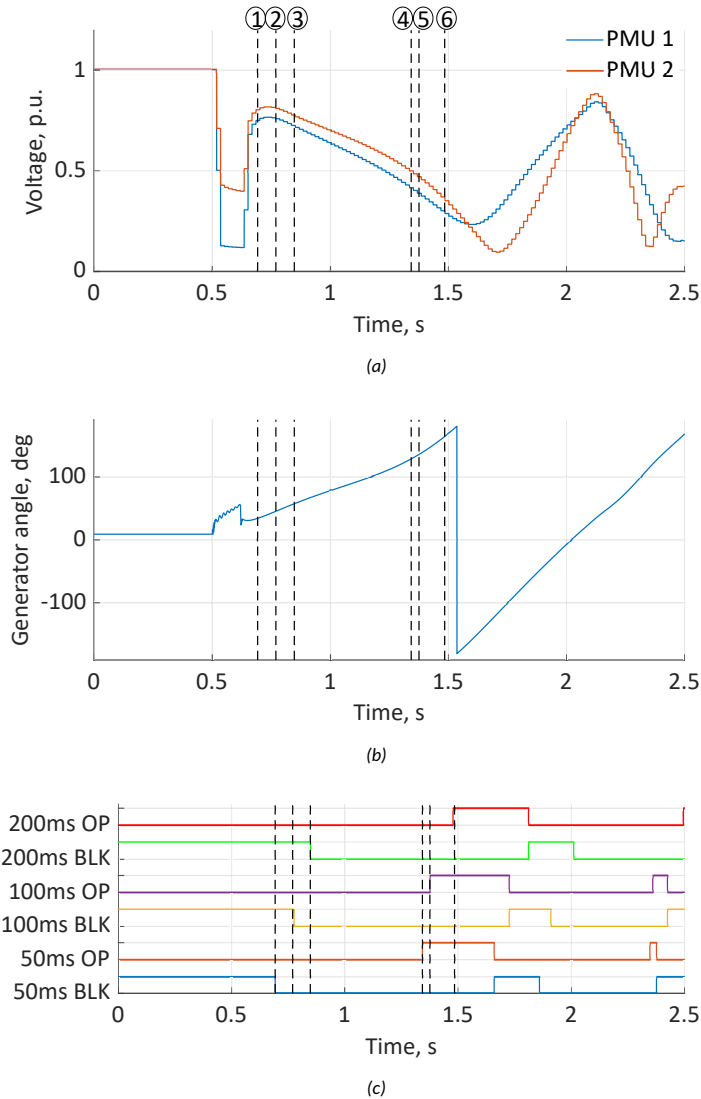


Figure 77 - Measured voltage values, measured generator angle in respect to E_{eq} and algorithm signals for different delay settings for unstable power swing case. (a) - measured voltage values, (b) - generator measured angle value, (c) - algorithm operation and blocking signals in time. ① - algorithm unblocking in the case of 50 ms delay, ② - algorithm unblocking in the case of 100 ms delay, ③ - algorithm unblocking in the case of 200 ms delay, ④ - algorithm operation in the case of 50 ms delay, ⑤ - algorithm operation in the case of 100 ms delay, ⑥ - algorithm operation in the case of 200 ms delay.

The protection is considered to be installed on the location marked as IED 1 (shown in Fig. 67), therefore the \underline{Z}_{k1} impedance is considered to be in the forward direction, and \underline{Z}_{k2} is considered to be in the backward direction from the relay.

For all tests the compensating impedance setting of $\underline{Z}_{k2} = 0 + j46.3 \Omega$ that corresponds to the impedance of the base case of 1000 MVA synchronous machine. The setting comes together from the impedance of 0.1 per unit of the step-up transformer and the machine

Table 14 – Devices used for HiL testing.

Device	Manufacturer	OOS protection algorithm
Device 1	Manufacturer 1	Angle-controlled out-of-step protection [87]
Device 2	Manufacturer 2	Impedance-based out-of-step protection [88]
Device 3	Manufacturer 3	Direct voltage comparison out-of-step protection [36]
Device 4	Manufacturer 4	Impedance-based out-of-step protection [89]

subtransient impedance of 0.3253 per unit.

$$\underline{Z}_{k2} = \underline{Z}_l[p.u.] + \underline{Z}_m[p.u.] \cdot \frac{U_b^2}{S_b} = (j0.1 + j0.3253) \cdot \frac{330^2}{1000} \approx 0 + j46.315\Omega \quad (23)$$

The compensating impedance setting of \underline{Z}_{k1} has been calculated for each line case as well as each system strength. As an example, the computation of the impedance setting for Case M and medium system strength the impedance results as follows:

$$\begin{aligned} \underline{Z}_{k1} &= \underline{Z}_l[p.u.] + \underline{Z}_{sys}[p.u.] \cdot \frac{U_b^2}{S_b} = (0.01 + j0.0955 + 0.0165 + j0.2883) \cdot \frac{330^2}{1000} \approx \\ &\approx 2.886 + j41.796\Omega \quad (24) \end{aligned}$$

The settings for all other cases are computed the same way and are shown in Table 15.

Table 15 – Settings for the angle-controller out-of-step protection algorithm.

Case	Infinite bus	Medium grid	Weak grid
Case S	0.196 + j3.147	1.274 + j13.536	11.075 + j107.136
Case M	1.808 + j31.407	2.886 + j41.796	12.687 + j135.395
Case L	3.615 + j 62.814	4.694 + j73.203	14.495 + j166.802

Settings for Impedance-Based Protection Algorithm

The impedance-based OOS algorithm requires OOS detection characteristic settings to detect unstable power swings. The relay is set to operate on the way in (TOWI) and on the way out (TOWO) of the configured impedance characteristic. The settings of the impedance protection device are computed according to the manufacturer's guidelines as explained in the user manuals of the relay and the settings are calculated using a base case of fully synchronous generation in Area 1 of the test network [88][89].

For the testing in SMIB network three sets of settings have been used - one for each transmission line case. The settings are computed based on the medium grid strength case in Area 2. In larger systems a system study needs to be conducted to determine the

average system impedance to be used in the settings calculation, however, in this case, the medium impedance of the equivalent system is already predetermined, therefore this value is directly used for setting calculation [21]. For the tests, a quadrilateral OOS protection characteristic is used in the protection device. This means that for the computation of the impedance polygon the example of Case M, the following parameters are considered:

- Impedance of the network in Area 1 $Z_s = 0.4253$ per unit (generator and step up transformer impedance).
- Impedance of the network in Area 2 $Z_r = \sqrt{0.01^2 + 0.0955^2} \approx 0.09502$ per unit.
- Transmission line impedance $Z_l = \sqrt{0.0165^2 + 0.2883^2} \approx 0.2888$ per unit.
- Maximum load transfer Z_{load} 1.0 per unit with an angle of 34° .
- Maximum stable power transfer angle $\delta = 120^\circ$.

Using these values the inner and outer polygon active and reactive boundaries are calculated as follows:

$$Z_T = Z_s + Z_r + Z_l \approx 0.81 p.u. \quad (25)$$

$$R_{min} = \frac{\frac{Z_T}{2}}{\tan \frac{\delta}{2}} = \frac{\frac{0.81}{2}}{\tan \frac{120}{2}} \approx 0.23 p.u. \quad (26)$$

$$R_{max} = Z_{load} \cdot \cos(34) = 1.0 \cdot \cos(34) \approx 0.83 p.u. \quad (27)$$

$$X_{min} = Z_T = 0.81 p.u. \quad (28)$$

$$X_{max} = 1.1 \cdot X_{min} \approx 0.891 p.u. \quad (29)$$

The settings apply for both the negative and positive direction of the impedance characteristic. The OOS protection impedance characteristic is tilted by angle α , which corresponds to the transmission line angle. The resulting impedance characteristic is shown in Fig. 78 and the three sets of impedances used for the three test cases for SMIB system are shown in Table 16. The impedances shown in the table are real-ohm values, that have been obtained from base values of 330 kV and 1000 MVA

Device 1 [88] restricts user access to the timer setting for the OOS protection, therefore the timer setting for this device cannot be altered. For the second impedance-based OOS protection (Device 4 [89]) the user is allowed to control the timer setting. For all the conducted simulations the minimum setting for the timer value of 30 ms has been used for the impedance trajectory monitoring in order to have maximum sensitivity for OOS event detection.

4.3 Performance Comparison of Real-Time Testing of Out-of-Step Protection

This subsection discusses the results from real-time testing for the out-of-step protection devices. Generally, OOS protection speed and security can be evaluated with two criteria: a) the amount of time needed to declare OOS condition after a fault is cleared, b) the percentage of correct OOS condition detection [90].

To evaluate the developed protection algorithms' performance, comparison of these two metrics between the software and hardware application across all of the tests done are shown in Fig. 79a and in Fig. 79b, respectively.

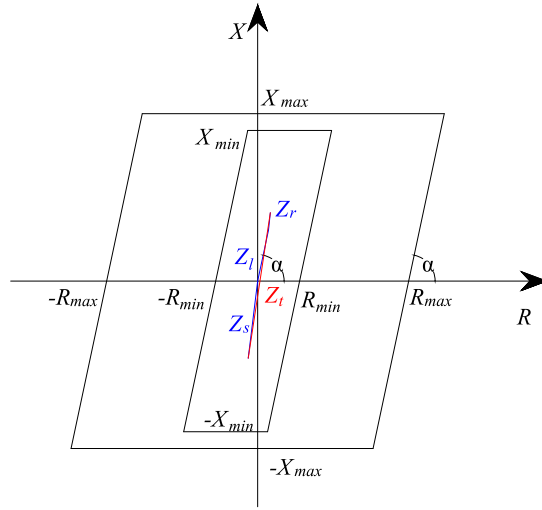


Figure 78 – OOS protection characteristic with the setting values for the computed example case.

Table 16 – Settings for the impedance-based out-of-step protection.

Parameter	Case S	Case M	Case L
R_{min}, Ω	17.30	25.47	34.55
R_{max}, Ω	90.28	90.28	90.28
X_{min}, Ω	59.91	88.22	119.68
X_{max}, Ω	65.91	97.04	131.65

When looking at the average operation time in Fig. 79a, it can be seen that the hardware implementation shows higher operation times than the RTDS implementation of the proposed algorithm. This is expected behaviour due to the delays implemented in the external controller as well as the processing the logic of the developed algorithm. For the PMU determined impedances algorithm, marked as LSA, on average the hardware implementation has an increase of 170 ms in operating time. For the discrete derivative OOS protection algorithm the hardware implementation shows an increase of 110 ms in operating time. In Fig. 79b, the detection rates of all of the OOS conditions for the performed tests of the algorithm are shown. It can be seen that there is no significant difference in the detection rates of software and hardware implementation of the two developed algorithms.

4.3.1 SMIB Model Results

This part includes the results of HiL testing of three out-of-step protection devices using the SMIB test network that has been described in Section 4.1. The results are presented according to short (Case S), medium (Case M) and long line (Case L) test cases. The test cases have been described in Section 4.1. In order to evaluate and compare the performance of the tested protection devices the operation time and the count of operations

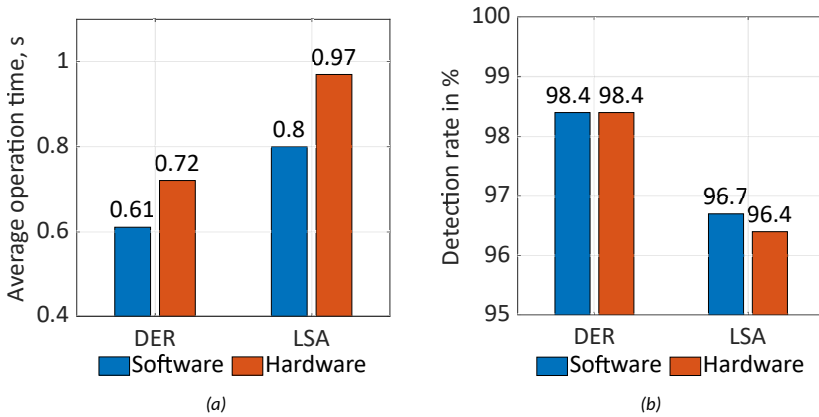


Figure 79 – Comparisons of proposed algorithm performances: (a) Comparison of percentage of OOS conditions detected, (b) Comparison of average operation times. DER - algorithm based on discrete angle derivatives, LSA - algorithm based on PMU-determined impedances.

of the tested devices were recorded. The operation times of the protection are measured starting from after the removal of the faulted line from the network. When the protection operates, then lower operation times are preferred in order to minimise the risk of damaging equipment and further splitting in the network after system separation. The overall results of all the simulations for missed trips are shown in Fig. 80a and the average operation times of the protection devices are shown in Fig. 80b.

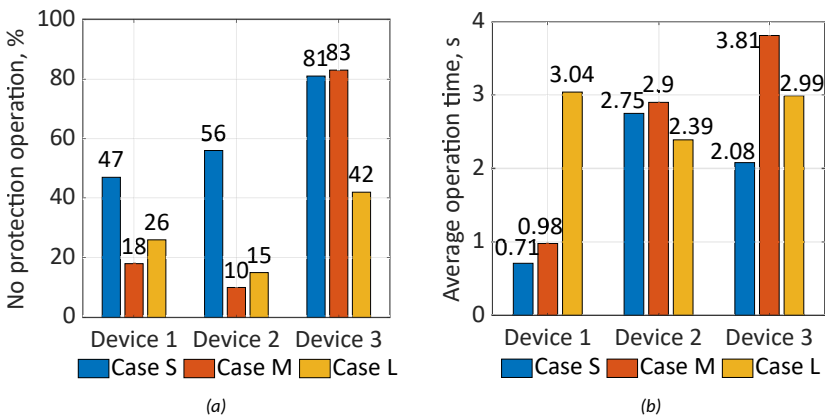


Figure 80 – Overall results from all testing scenarios. (a) shows overall missed operation percentages and (b) shows average operating times of the test scenarios. Blue column represents simulation Case S, red Case M and orange Case L. Device 1 - Angle-controlled OOS protection, Device 2 - Impedance-based OOS protection and Device 3 - OOS algorithm based on direct voltage comparison.

The testing conducted with the SMIB test system indicates that the existing OOS protection devices may experience issues in detecting instability when IBRs are introduced into the power network. Generally, based on the three different test cases, the impedance-based protection is the least influenced, followed by the angle-controlled protection and

the direct voltage comparison protection is the most affected by the changing grid conditions. The lowest operation time is displayed by the angle-controlled protection, followed by impedance-based protection and the direct angle comparison protection shows the slowest operation of the tested devices. As the impedance-based protection generally shows the best results, it is used for further comparison with the two developed protection algorithms, described in detail in Chapter 3 and Chapter 4, using a larger system model to better represent a real-world power network.

Results for Case S

Total missed operation percentages of protection algorithms and the corresponding operation times for simulation case S are shown in Fig. 81a and Fig. 81b, respectively. Regarding detection rates of device 1 for simulation Case S the protection does not detect the out-of-step condition with infinitely strong grid equivalent. However, for the weaker Area 2 grid equivalent device 1 shows best results in terms of detection and speed of detection. Overall for this simulation case, following the two evaluation criteria, device 1 is most suitable for shorter transmission lines, because this algorithm shows the best detection rates as well as fastest detection times.

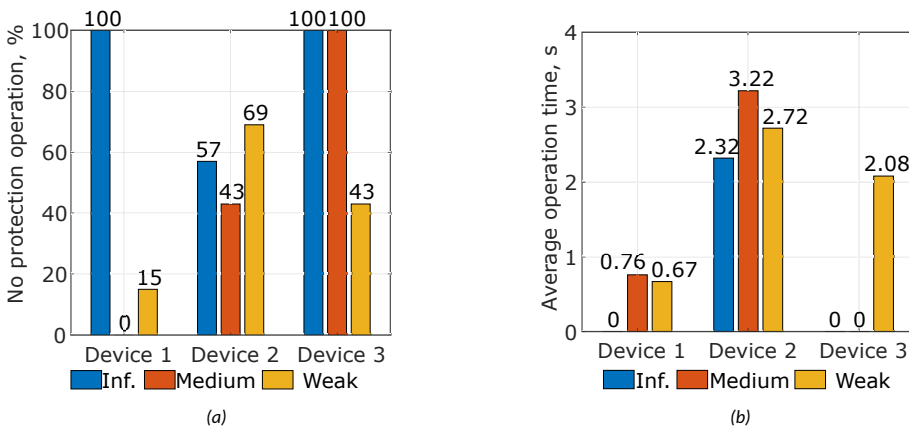


Figure 81 - Total missed operations in percent and average operating times for Case S. Blue, red and yellow columns represent a grid equivalent with infinite, medium and weak network equivalent respectively. (a) - missed operations, (b) - average operation time.

The protection device 2 displays difficulties detecting an out-of-step condition in all receiving system short-circuit capacity levels as shown in Fig. 81a. Overall this algorithm did not operate for 56% of the tests in simulation Case S (Fig. 80a). The best performance for this device is in the case of medium short circuit power in the receiving system, where the protection did not operate during 43% of the simulations. Regarding operation time of this device it poses the slowest operation time values for simulation Case S as is shown in Fig. 81b.

Protection device 3 shows significant shortcomings in detecting an out-of-step condition with simulation Case S. For the infinite and medium grid equivalent the protection did not detect out-of-step conditions in any of the conducted simulations. In the case of weak system equivalent the third device fails to operate in 81% of the simulation cases (Fig. 81a).

Results for Case M

Simulation results for Case M, shown in Fig. 82a and in Fig. 82b, indicate that first device's detection performance is improved compared to Case S, however the operation times have increased. The no operation rate is lower compared to Case S (47% for Case S and to 18% for Case M, shown in Fig. 80a).

The second device is displaying the best detection performance for simulation Case M, providing no operation command in only 10% of the simulations. At the same time this algorithm shows the significantly slower operation times compared to device 1.

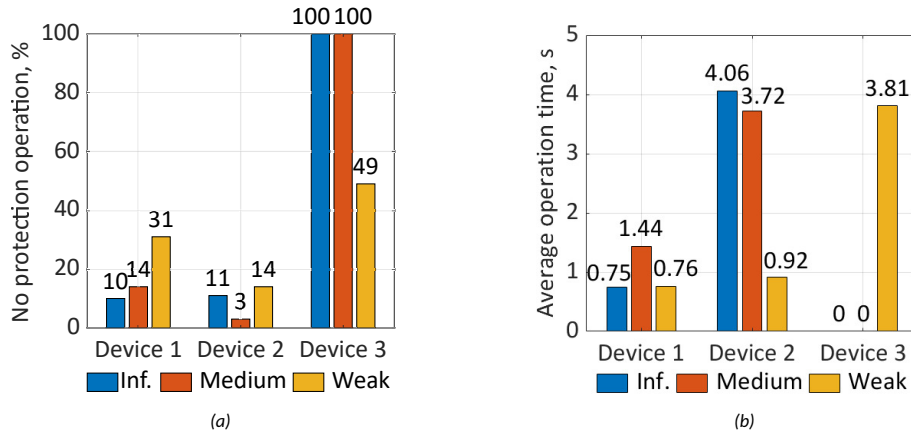


Figure 82 – Total missed operations in percent and average operating times for Case M. Blue, red and yellow columns represent a grid equivalent with infinite, medium and weak network equivalent respectively. (a) - missed operations, (b) - average operation time.

The third device in simulation Case M shows an inferior detection rate compared to the other two algorithms. As with simulation Case S, this device fails to determine out-of-step conditions for instances with infinite and medium strength system equivalents. For the weakest system equivalent used the protection device does not detect an out-of-step condition in 49 % of the test cases. In addition, for this simulation case the third protection device displays the slowest operating times from all the test cases conducted, when the device operates with the weak system equivalent (as shown in Fig. 82b orange column).

Results for Case L

The results for simulation Case L are shown in Fig. 83a and in Fig. 83b. In this case none of the tested devices had a 100% failure rate to detect and out-of-step condition. Regarding operation speed all tested devices show similar results for this simulation case. The first tested device displays inferior performance compared to Case M in both detection rates and operation speed.

The performance of the second device is increased, both regarding detection rate and operation time, when comparing against simulation Case M. For Case L the second device has best overall detection rates with a total missed operation rate of 15% (Shown in Fig. 80a).

For simulation case L, the third tested device presents the best performance metrics when compared to the algorithm's performance with other cases. This indicates that device 3 is more suitable for detecting out-of-step conditions in weaker systems with longer

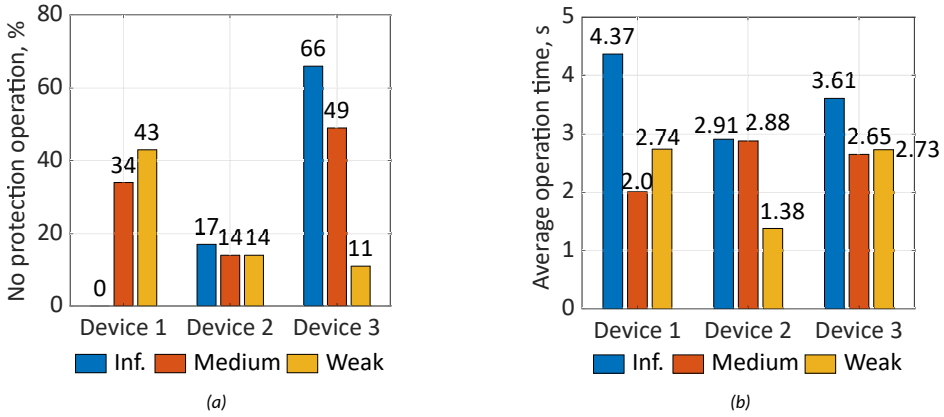


Figure 83 – Total missed operations in percent and average operating times for Case L. Blue, red and yellow columns represent a grid equivalent with infinite, medium and weak network equivalent respectively. (a) - missed operations, (b) - average operation time.

transmission lines. This is confirmed by this device displaying the highest operation rates for the weakest system equivalent used in this simulation case. However, regarding operation time for this scenario, the device falls behind the time shown by impedance-based protection device.

4.3.2 IEEE39 Bus System Results

In this segment the testing results from using the modified IEEE 39 Bus System are shown. For the comparison in these simulation scenarios the two developed algorithms are running in the external controller. Additionally, two impedance-based protection devices are used - device 2 from the tests in SMIB model and device 4, which is an impedance-based protection device from a different manufacturer than device 2. The settings for the impedance-based protection devices are computed using the same principles as described in Section 4.2 for each line case and are shown in Table 17. At any given RES % scenario (defined in Section 4.1) the simulation has been repeated five times and the behaviour of the tested protections recorded.

Table 17 – Settings for the impedance-based out-of-step protection for test cases in IEEE39 Bus System.

Parameter	Line 14-15	Line 16-17	Line 26-29	Line 28-29
R_{min}, Ω	25.37	20.78	50.86	50.86
R_{max}, Ω	49.34	49.34	59.51	59.51
X_{min}, Ω	87.9	72.0	176.2	175.97
X_{max}, Ω	96.69	79.2	193.8	193.57

The overall OOS detection rates for the two impedance-based protection devices and the two developed protection algorithms are shown in Fig. 84. It can be concluded that

both of the developed algorithms in this thesis provide significantly higher detection rates than the tested impedance-based protection algorithms. For Case A, depicted in red, the discrete derivative algorithm provides the highest detection rate (99.3 %), followed by the algorithm based on equivalent impedances (96.4 %). The two impedance-based algorithms are close to the developed algorithms in terms of detection rates for Case A.

In Case B, shown in blue, the detection rates are lower compared to Case A for the developed algorithms as well as the impedance-based protection. However, the developed algorithms provide more than 20 % higher detection rates compared to the impedance-based protection. The comparison of operating times of the two developed solutions and the two impedance-based protection devices for the two test cases is shown in the following segments.

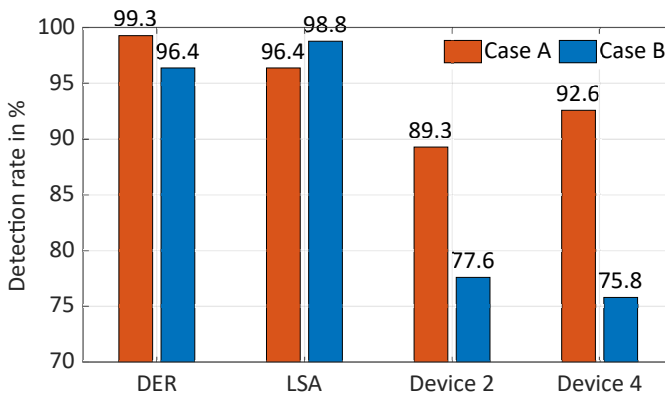


Figure 84 – OOS detection rates for tested cases in the IEEE 39 Bus System. Red displays the detection rate for Case A and blue for Case B. DER - algorithm based on discrete angle derivatives, LSA - algorithm based on PMU-determined impedances, Device 2 and Device 4 - impedance-based OOS protections.

Results for Case A

The test results of protection operation times for Case A (indicated in Fig. 69) are shown in Fig. 85a and in Fig. 85b. The operation times shown in these figures are the times the protection needs to provide a trip command starting from the removal of the fault. The operation time of "0" means that the protection did not provide an OOS tripping command for the duration of five seconds after fault initiation; hence, the simulation was terminated without protection trip for all of the five conducted tests at that RES % scenario.

Fig. 85a shows the operation times for the case of the transmission line between buses 14 and 15. This transmission line represents a longer tie-line between the two parts of the network. The results indicate that when the RES penetration is increased in one of the areas, the difference between the protection operations is narrowing. However, for all situations the OOS protection based on discrete angle derivatives, marked as DER, offers the fastest operation times, followed by the protection based on PMU determined impedances (marked by LSA). Across all the testing scenarios the DER algorithm provides an operation command 340 ms faster than the LSA algorithm. The impedance-based OOS protection relays offer similar operation times when comparing to each other in this case (the difference in operating time being 115 ms). Comparing the two developed algorithms

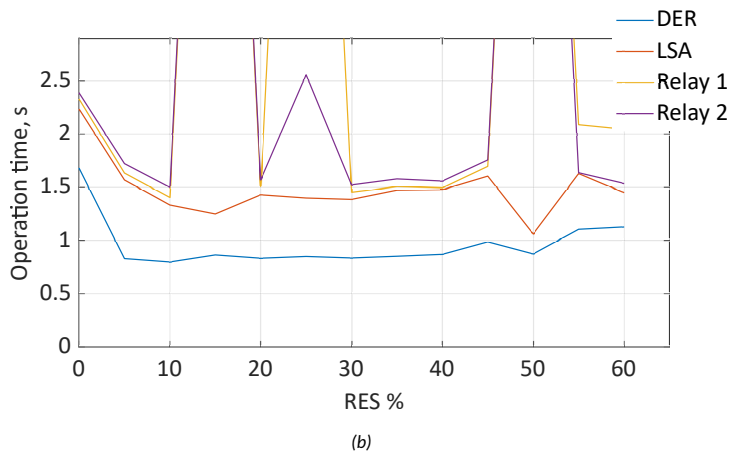
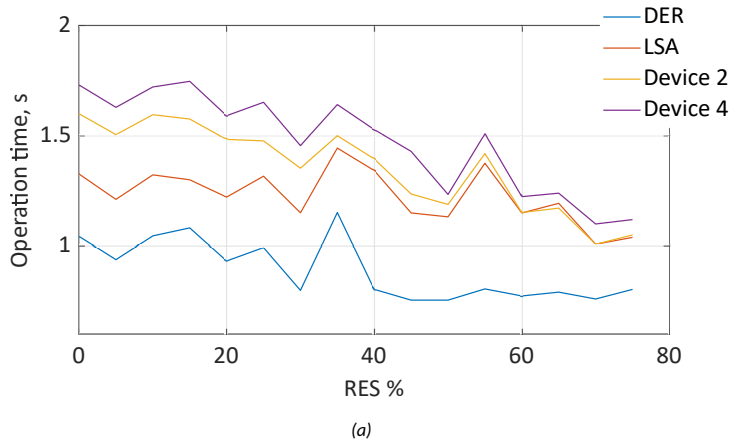


Figure 85 – OOS tripping times of protection devices for Case A. (a) represents the case study with a longer line between two systems and (b) represents a short line between two systems. DER - algorithm based on discrete angle derivatives, LSA - algorithm based on PMU-determined impedances, Device 2 and Device 4 - impedance-based OOS protections.

to the impedance-based OOS protection relays, the DER algorithm is, on average, 470 and 585 ms faster than Device 2 and Device 4, respectively. Meanwhile, the LSA algorithm offers on average 125 and 240 ms faster operation than Device 2 and Device 4.

The shorter line testing results for Case A (Fig. 85b) indicate that the DER algorithm provides the fastest OOS detection times in this scenario. The DER algorithm operating times are followed by the LSA algorithm, which is, on average, 520 ms slower than DER algorithm. The two impedance-based protection relays show very similar behaviour, except the 25 % RES scenario, where Device 2 fails to operate, while Device 4 operating time is delayed and the relay operates during second pole slip. Both of the impedance-based protection relays fail to operate at 15 and 50 % RES scenarios, while the developed DER and LSA algorithms successfully operate. Compared to the impedance-based relays the DER algorithm provides operation command 755 and 795 ms quicker than Device 2 and Device 4 respectively, while the LSA algorithm is faster by 230 and 270 ms, respectively.

Results for Case B

The combined protection operations for both tested lines for Case B (Fig. 69), that is representative of a single machine - infinite bus type scenario, are shown in Fig. 86a and in Fig. 86b. Fig. 86a shows the results of the protection operating times versus the renewable energy penetration level when an OOS condition was created on the longer tie-line.

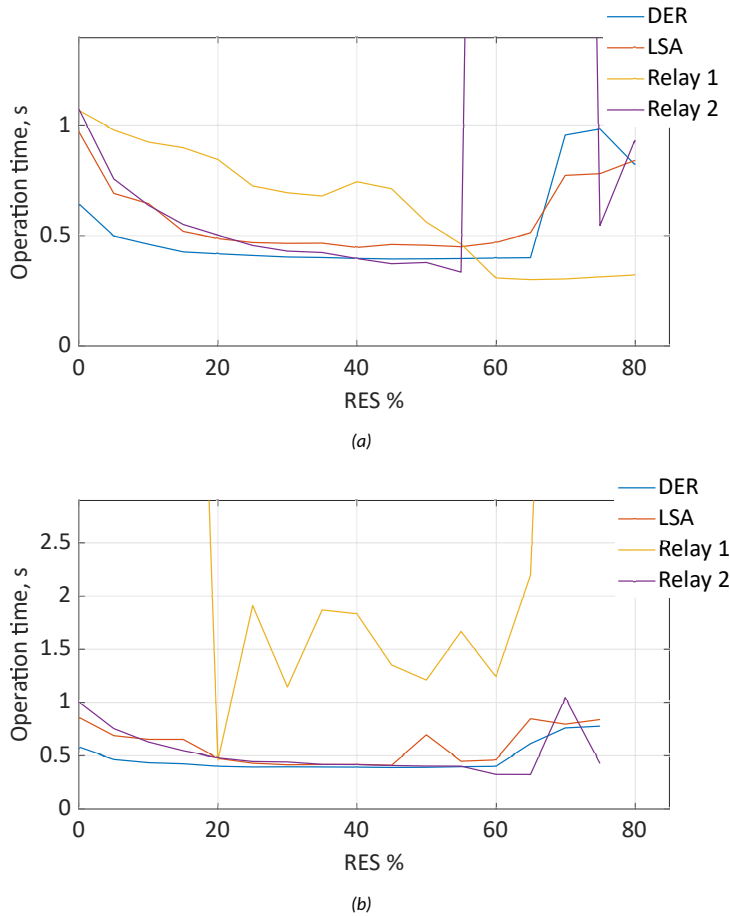


Figure 86 – OOS tripping times of protection devices for Case B. (a) represents a long line between the machine and the system, (b) represents a short line between the machine and the system. DER - algorithm based on discrete angle derivatives, LSA - algorithm based on PMU-determined impedances, Device 2 and Device 4 - impedance-based OOS protections.

In this scenario, the DER protection algorithm provides the fastest operating times up to the 40 % RES scenario, after which Device 4 offers the best operating time until 55 % RES penetration. Thereafter, Device 2 offers the fastest operation times, however, it has to be noted that, starting from the 60 % RES scenario, Device 2 issues a tripping command not from OOS protection, but from the distance protection element, which results in the short operation time. This is an obvious case of maloperation of the distance protection element due to no fault being present in the power system. This is caused by the Power Swing Blocking element not recognising the power swing correctly and blocking the distance protection element. Device 4 fails to operate for the scenarios between 60 % and 70 %

RES penetration, after which it operates correctly.

On average, the DER algorithm in this scenario issues an operation command 65 ms faster than the LSA algorithm and compared to the relays the DER algorithm is 120 and 35 ms faster than Device 2 and Device 4, respectively. The LSA algorithm delivers an operation command 55 ms slower than Device 4 and 25 ms quicker than Device 2, hence, Device 4 is on average 80 ms faster than Device 2 in this simulation scenario.

Fig. 86b shows the protection operation times versus RES % penetration for the case of OOS condition on the shorter tie-line. The DER algorithm provides the fastest operation times until the 55 % RES penetration scenario in this case. Thereafter, for RES penetration scenarios of 60, 65 and 75 % Device 4 provides the quickest operation times, followed by the developed DER algorithm. On average, comparing the two developed algorithms, the DER algorithm operates 120 ms quicker than the LSA algorithm. Comparing the DER algorithm to the two impedance-based protection relays, the DER algorithm issues an operation command 1015 and 55 ms faster than Device 2 and Device 4, respectively. The LSA algorithm shows 65 ms higher operation time than Device 4 and 895 ms quicker operation time than Device 2.

The two impedance-based relays behave very different in this simulation scenario. Device 2 (shown in orange) scores the worst detection rate of the OOS condition, as the device only operated consistently between 20 - 65 % RES penetration, whereas Device 4 did not experience similar difficulties in detecting an OOS condition. It should be noted that Device 2 also does not provide any operation during the first pole slip in this case and that results in a delayed operation, as indicated by the longer operating times. Comparing the two impedance-based protection relays, Device 4 operates on average 960 ms faster than Device 2 in this simulation scenario.

Based on the IEEE 39 Bus System case studies it can be seen that the DER algorithm provides, on average, the fastest operation times, as well as offers the highest out-of-step condition detection rates from all the solutions tested. Therefore, the DER algorithm has been chosen to be implemented in the Iceland power system, and is tested using scenarios in that particular power network in the following subsection of this thesis.

4.3.3 Iceland Power System Case Studies

Using the previously verified Iceland power system model for real-time simulation, which was developed in Section 4.1, multiple scenarios have been conducted. The simulations were performed using Event 1 and Event 4 pre-fault conditions as the base case. Different grid conditions were used to test the developed protection algorithm. This was done by switching the series capacitor on the southern link in and out of operation, as well as disconnecting lines in the system. The simulations consisted of symmetrical and asymmetrical faults performed on different transmission lines in the network including single-pole reclose. The grid situations, events and resulting behaviour is shown in Table 18.

Based on the simulation results, it can be concluded that:

- The algorithm is stable when the power system experiences damped oscillations.
- The algorithm does not operate during the single pole tripping and reclosing process.
- The algorithm provides operation for cases when an OOS event occurs for both the southern ring connection and the northern ring connection.

Table 18 – Conducted real-time simulations using Iceland’s power system model and the simulation results.

Grid situation	Event	Results
Series capacitor in the southern link switched ON.	Line fault in the northern corridor with successful auto-reclose.	Stable power swing in the network, the developed OOS protection does not operate.
	Line fault in the northern corridor with unsuccessful auto-reclose.	OOS condition in the southern corridor, developed protection operates.
	Line fault in the southern corridor with successful auto-reclose.	Stable power swing in the network, the developed OOS protection does not operate.
	Line fault in the southern corridor with unsuccessful auto-reclose.	OOS condition in the northern corridor, developed protection operates.
Series capacitor in the southern link switched OFF.	Line fault in the northern corridor with successful auto-reclose.	Stable power swing in the network, the developed OOS protection does not operate.
	Line fault in the northern corridor with unsuccessful auto-reclose.	OOS condition in the southern corridor, developed protection operates.
	Line fault in the southern corridor with successful auto-reclose.	Overload protection operation in the northern corridor, developed protection does not operate.
	Line fault in the southern corridor with unsuccessful auto-reclose.	Overload protection operation in the northern corridor, developed protection does not operate.

Developed Algorithm Response to Event Recordings

The OOS protection algorithm using discrete angle derivatives has been tested using event recordings from the Iceland power system (Fig. 70). To test the algorithm, the recorded historical PMU data have been streamed from a personal computer (PC) using a C37.118 emulator. The data were streamed to the external controller, where the developed algorithm is installed. The experimental setup for this case is shown in Fig. 87.

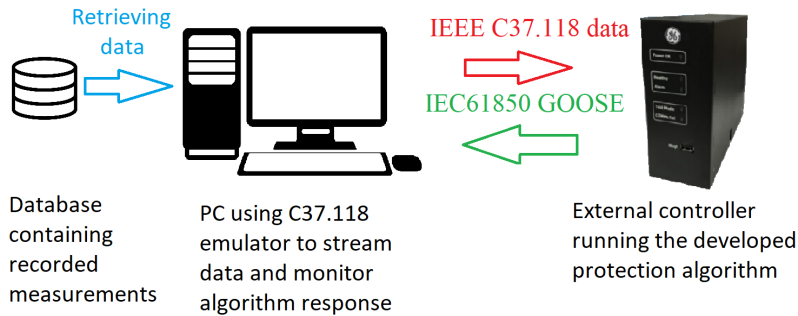


Figure 87 – Developed protection algorithm testing setup with measured data streaming.

The response of the algorithm has been recorded for a total of four OOS events that have been studied. The developed solution showed good results, providing successful operation for all of the recorded OOS events. The OOS event recordings used for the algorithm testing are described as follows:

- Event 1 and event 2 are nearly identical; both events were initiated by a flashover at a substation in the northern corridor of the power system, followed by its disconnection; the increased power flow through the southern corridor triggered an OOS event in the power system.
- Event 3 was initiated by an energisation of a transmission line in the eastern part of the system, which caused undamped oscillations between the two centres of inertia, however, the OOS condition did not occur on the protected line.
- Event 4 was initiated by a large loss of load in the south-western part of the network. After this contingency, overload protection operated on the northern part of the ring connection, and an inter-trip separated the two generators in the southern corridor, which, after a few oscillations, resulted in an OOS condition on the southern ring connection.

Fig. 88 and Fig. 89 show the voltage variation at the two measurement locations in the southern corridor, measured power and the developed OOS protection algorithm response for Event 1 and Event 2, respectively. For both events the power system first goes through a stable swing and afterwards becomes unstable, resulting in an OOS situation.

The dashed line denoted by ① shows the start of the event. The protection signals, shown in Fig. 88c and Fig. 89c for Event 1 and Event 2 respectively, indicate that, during the first stable swing the protection algorithm performs correctly. During this process the algorithm gets deblocked at ②, due to the voltage level lowering in the system, and subsequently the restraint criteria are also lifted. The protection, however, does not give a trip signal, because the swing is stable. The second power swing becomes unstable for

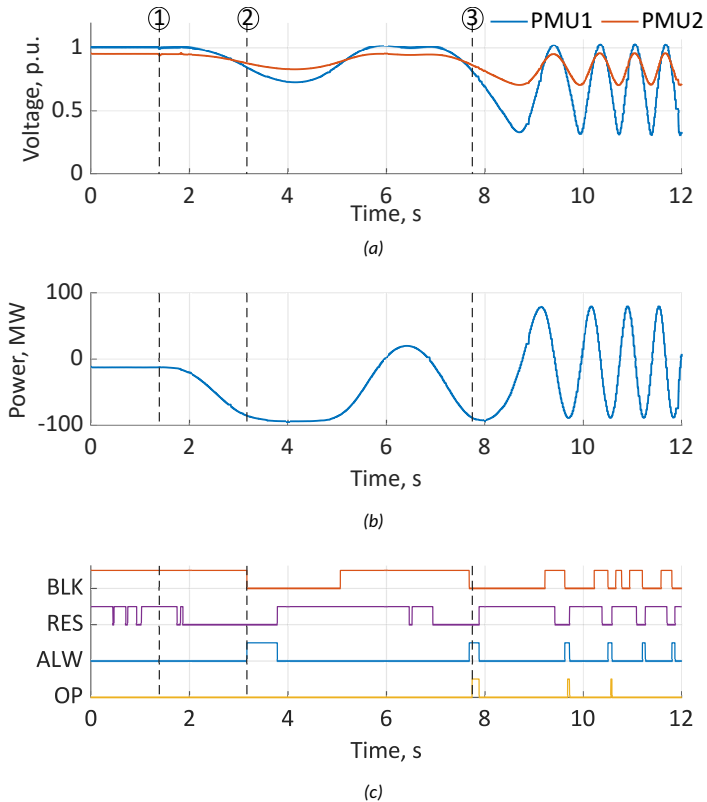


Figure 88 – Protection algorithm response to Event 1 data. The dashed line marked as ① shows the start of the OOS event at 1.3 seconds. (a) the voltage at the two measurement locations in the southern corridor and (b) the measured power in the southern corridor during the event, (c) the protection algorithm signals from the controller. BLK - algorithm blocked, RES - algorithm restrained, ALW - algorithm allowed to operate, OP - algorithm operation signal.

both events, which is seen as large oscillations in the measured voltages and power. For the unstable swings, the protection algorithm operates correctly, which is clearly shown by the activation of the operation signal at ③. Since there is no specific OOS protection currently active in the Iceland system, the recorded event continues to evolve into OOS oscillations with increasing frequency, until a distance protection operates somewhere in the network. As shown in Figs. 88 and Fig. 89, these large oscillations in the power network could have been resolved more rapidly using the developed OOS protection solution, because the developed solution operates at ③.

Fig. 90 shows the measured voltages at the two ends of the southern corridor, the corridor power and the protection algorithm signals corresponding to Event 3. During this event a line energising at 0.5 seconds and marked by ① triggers oscillations in the power system. The oscillations are undamped and increasing in magnitude for both voltages and measured power, as shown in Figs. 90a and Fig. 90b. The protection signal response, depicted in Fig. 90c, indicates that the protection algorithm is deblocked during the power swings, the first of which is denoted by ②. As the OOS condition does not appear on the protected line, the protection is stable and does not provide any operation command. The oscillations are cleared by a distance protection operation elsewhere in the network at 34 seconds (③). Therefore, the developed protection algorithm displays stable behaviour

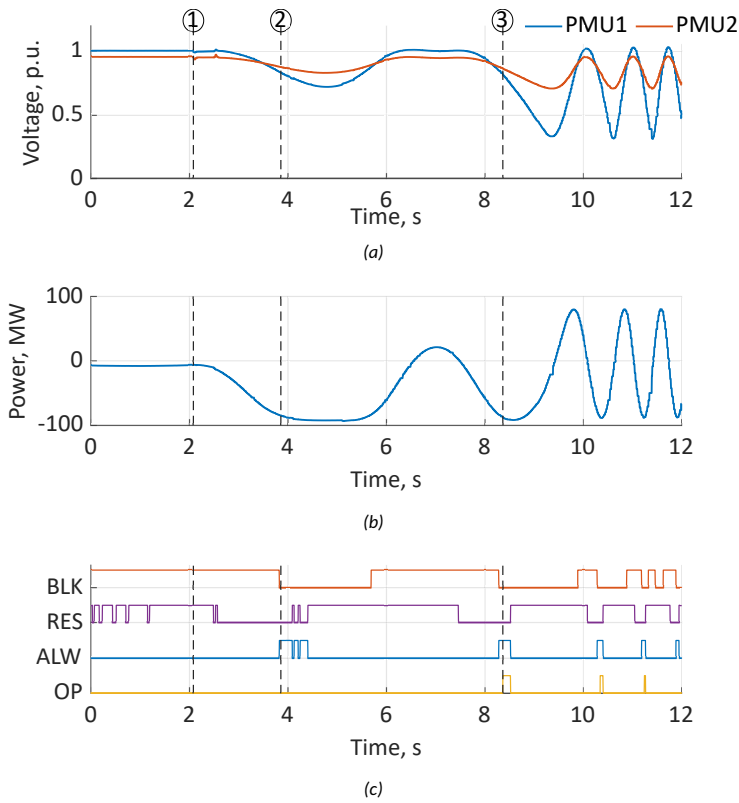


Figure 89 – Protection algorithm response to Event 2 data. The dashed line marked as ① shows the start of the OOS event at 2.1 seconds. (a) the voltage at the two measurement locations in the southern corridor and (b) the measured power in the southern corridor during the event, (c) the protection algorithm signals from the controller. BLK - algorithm blocked, RES - algorithm restrained, ALW - algorithm allowed to operate, OP - algorithm operation signal.

when the OOS condition is not localised to the observed transmission line.

Fig. 91 shows the measured voltages at the two locations in the southern link, the power flow in the southern corridor and the protection algorithm signals for Event 4. The dashed line marked in the figure shows the start of the event with the loss of load at 1.3 seconds, indicated by ①. Following the initial loss of load the power transfer through the corridor, shown in Fig. 91b, starts increasing. At the same time, the voltages, shown in Fig. 91a, decrease. At the time of 1.8 seconds a jump in power transfer occurs, marked by ②. This signifies the northern corridor disconnection due to overload. Thereafter, the southern ring connection experiences four stable swings, with progressively increasing magnitude, during which the protection does not operate. During the third power swing the protection becomes deblocked, as is shown in Fig. 91c. After the fourth swing, the system runs into instability, and the protection operates (marked as ③) due to the OOS conditions being fulfilled.

Real-Time Simulation Case with Protection Operation

The comparison with the developed protection algorithm operation and no operation for Event 1 using the Iceland power system model is shown in Fig. 92. The red line on the plots shows the value when no protection is utilised in the grid, whereas the blue line signifies

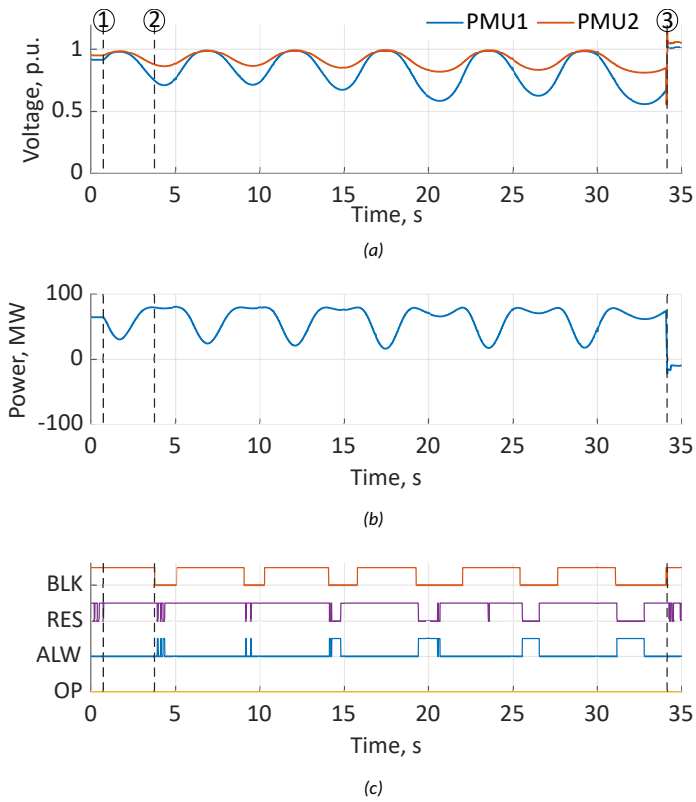


Figure 90 – Protection algorithm response to Event 3 data. The dashed line marked as ① shows the start of the OOS event at 0.5 seconds. (a) the voltage at the two measurement locations in the southern corridor and (b) the measured power in the southern corridor during the event, (c) the protection algorithm signals from the controller. BLK - algorithm blocked, RES - algorithm restrained, ALW - algorithm allowed to operate, OP - algorithm operation signal.

values when the developed DER protection algorithm is put to use in the simulation. Fig. 92a shows the frequency values of the east and west parts of the network for this simulation. After the event takes place, the frequency of the east part of network increases, while the western part of the network sees a decrease in frequency value. Due to the lack of synchronising torque between the two parts of the network an out-of-step condition occurs, which is signified by the continued oscillations in the frequencies shown in red. The developed protection reacts to the unstable condition and operates, which is shown by the dashed line on the plots. For this case, the frequencies are shown in blue, and compared to the situation with no protection, there are no oscillations in the frequency values. Additionally, the frequency in the western part of the system has a lower nadir value compared to no protection case.

The voltages measured from either end of the southern transmission corridor are shown in Fig. 92b. Correspondingly to the frequency plots, the red line signifies the case with no protection in the network, while the blue signifies the network response with the developed protection algorithm installed in the network. With no protection operation large oscillations in the measured voltages are seen, which is indicative of an unstable situation in the network. For the case with the developed protection installed in the network, no oscillations are seen in the voltage values. This means that, with the inclusion

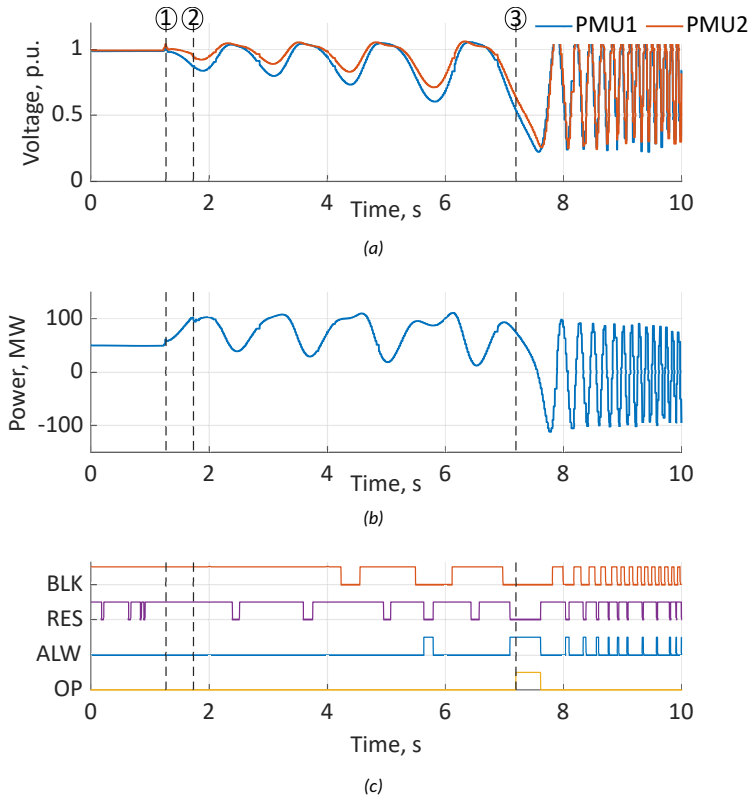


Figure 91 – Protection algorithm response to Event 4 data. The dashed line marked as ① shows the start of the OOS event at 1.3 seconds. (a) the voltage at the two measurement locations in the southern corridor and (b) the measured power in the southern corridor during the event, (c) the protection algorithm signals from the controller. BLK - algorithm blocked, RES - algorithm restrained, ALW - algorithm allowed to operate, OP - algorithm operation signal.

of the developed algorithm in the network the two parts of the system would continue to operate in a stable manner, whereas without the protection, large oscillations in voltages are seen, that are not desirable in the network.

4.4 Intermediate Summary

Case studies and the results to assess the performance of different OOS protections were shown in this chapter. Initially for analysing the existing OOS protection performance, a SMIB system was used, in which the share of PE-based generation, system strength and line lengths was varied. Using the model, the performance of three commercially available out-of-step protection devices was assessed in different grid conditions. The testing results show that:

- All of the tested protection devices experience difficulties detecting out-of-step conditions.
- The tested angle-controlled out-of-step device has better performance compared to others for shorter transmission lines.

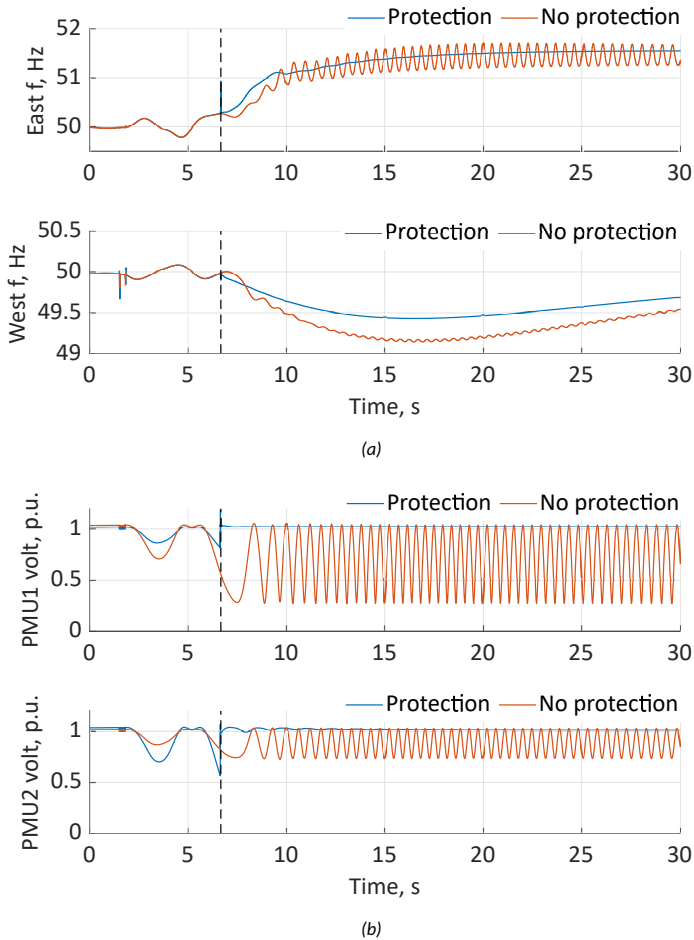


Figure 92 – Frequencies and voltages in the east and west parts of the Iceland power system in the case of developed protection and no protection. The dashed line represents the time of developed protection operation. (a) - frequencies of east and west parts of the network, (b) - voltages of PMU1 and PMU2.

- The impedance-based out-of-step protection device shows better performance for medium and longer transmission lines.
- Direct voltage phasor comparison algorithm is more suitable for longer transmission lines with weaker system configurations.
- The overall best performance is shown by the impedance-based out-of-step protection.

Based on the conducted case studies, it is concluded that some algorithms are more affected by changes in the grid conditions than others. All of the protection devices are influenced the most by the transmission line length. Besides the transmission line length the angle-controlled and impedance-based protections were more affected by the share of renewable penetration in the grid and the receiving end system strength had least influence on the performance of the relays'. For the device utilising the direct voltage comparison

the receiving system strength had a more significant influence on protection performance than the PE penetration levels.

As the impedance-based protection displayed the best performance from the protection devices tested, it was also included in case studies utilising a larger power network together with the two developed protection algorithms. In the case studies performed using the IEEE 39 Bus System the OOS algorithm based on discrete angle derivatives showed the highest detection rates of OOS conditions as well as in general lowest operation times. The algorithm based on PMU-determined impedances displayed superior performance compared to the two impedance-based relays tested.

The developed protection algorithm using discrete angle derivatives has also been tested using recordings from the Iceland power system as well as the developed power system model for that system. Case studies using the recording playback indicate that, by using the developed protection solution the OOS conditions in the power network would have been resolved significantly earlier compared to the real situation. In some cases, a partial blackout of the network could have been avoided. This is confirmed by HiL real-time simulations with the network model, where the developed OOS protection is included. The simulation results show, that the developed protection operates, and as a result, the power system stabilises and continues operation.

Conclusions and Further Work

The thesis presents two different complete methods for out-of-step protection in the power system by using wide-area measurement information. All the hypotheses of this thesis have been confirmed and proved to be possible. The proposed methods provide substantially better performance in regard to out-of-step condition identification as well as operating time compared to impedance-based, angle-controlled and direct voltage comparison protection algorithms. The proposed methodologies overcome the main issues related to the currently used protections, mainly the need for setting values for the algorithm to operate correctly. The main drawbacks related to the present-day protection solutions are eliminated by making the new methodologies setting-less and adaptive to changing conditions in the power system. For this the methods rely on continuously computing the impedance of the network seen at each terminal of the observed transmission line, and the methods rely on the changes in the electrical quantities during unstable power swings.

Scalable models for real-time testing of out-of-step protection devices were developed, which were used to prove, that the currently used protection devices experience problems in detecting unstable power swings with the inclusion of IBRs in the power network. It has been shown, that the type of the protection algorithm used matters, and the performance of the algorithm is dependent on the topology of the power network as well as the particular IBR level in the network. It is also confirmed that the same type of algorithm in different manufacturer's implementation has a different type of reaction to changing grid conditions. Therefore, it becomes necessary to examine the workings of the protection behaviour by conducting real-time hardware-in-the-loop simulations.

The two adaptive protection algorithms developed in this thesis have been implemented on a hardware platform that shows almost an identical detection rate to the software application. The detection speed difference between the hardware and software implementations originate from the delays associated with the delays in the data collection using wide-area information as well as the processing of the protection logic in the external device. The difference in detection speed compared to the two implementations is within the expected values. The developed protection algorithms provide a superior detection rate for unstable power swings, which is up to 20 % higher than the existing protection solutions. Both developed methods' hardware applications allow for quicker operation than the currently existing solutions, where the LSA algorithm is on average 16 % and the DER algorithm 38 % faster compared to the existing impedance-based protection algorithm.

Practical Implementations

For the practical implementation it is essential that the power grid uses an existing wide-area monitoring system, from which the developed methods can receive data. The developed protection algorithms have already been implemented on a hardware platform and tested in a laboratory environment using hardware-in-the-loop tests, thus they can be taken as a plug-and-play type of system.

The developed protection algorithms, described in Chapter 3 and Chapter 4, do not require large amounts of computational power, therefore they are easily adaptable to already existing hardware devices that have been set up in the power network. Additionally, the developed DER out-of-step protection algorithm has been implemented and put into commission in the Iceland power system.

Further Work

The effects of different types of control strategies for IBRs to the existing as well as the developed out-of-step protection should be investigated. The tests conducted in this thesis have involved one type of grid following control, whereas in reality different manufacturers can utilise many different types of control strategies. Providing grid support may also have an influence on the existing protection performance.

The most critical part of the developed methodologies in a field implementation is the obtaining of measurement values and transmission of the protection response signal to actual circuit breakers. In this, the communication network plays a key role. Therefore, the effects of different types of communication-related effects can be an object of study and investigation in further works.

The proposed methodologies for out-of-step protection in this thesis rely on only two measurement points in the network. This makes them adaptable to systems where the data acquisition is highly limited. However, with the rapid developments in adoption of wide-area monitoring system the number of measurement points can be greatly extended. From this a new layer can be built for the proposed protection methodology to include measurements from more locations across the power system and allow for more criteria to be taken into account when there is unstable power swings detected in the network.

List of Figures

1	Simple system equivalent scheme.	15
2	Power-angle curves for the two-machine system, δ_{LSA} denotes the Last Stable Angle point. (a) - Curve displaying the steady state operation, (b) - Curve showing the faulted state in the network (c) - Power-angle curve with a case of short fault clearing time δ_1 and δ_2 denote the angle values after fault clearance and the maximum angle after deceleration, respectively (d) - Power-angle curve with a case of long fault clearing time δ_1 denotes the angle value after fault clearance.....	16
3	Graphical representation of phasor formation. (a) a rotating vector, (b) - a corresponding time-domain signal.	19
4	Functional diagram of PMU device.	20
5	An example of a layered structure of WAMS system including protection and control. PMU - Phasor Measurement Unit; PDC - Phasor Data Concentrator.	21
6	General classification of OOS detection methods.	22
7	Simple system equivalent scheme with impedance relay installed at Bus 1 side on the transmission line.	23
8	Variations in currents and voltages during out-of-step conditions.	25
9	Impedance trajectories seen by a distance relay at Bus 1 depending on the angle difference δ between the two machines. Top trajectory shows the seen impedance locus in the case of $E_1/E_2 > 1$, middle trajectory in the case of $E_1/E_2 = 1$ and bottom trajectory indicates impedance trajectory in the case of $E_1/E_2 < 1$	26
10	Impedance trajectories for various ratios of $ E_1/E_2 $. While the ratio of the voltages increases the impedance trajectory moves further away from the measurement location, and as the ratio decreases the impedance trajectory moves closer to the measurement location.	27
11	Impedance trajectories in the case of unstable swing, stable swing and faulted conditions in the network.	27
12	Double blinder scheme. Point "A" represents the starting of a timer value for power swing detection, point B is where the timer value is stopped and a power swing is declared. Point "C" is where an OOS condition is declared.	28
13	Concentric characteristic scheme. Point "A" represents the starting of a timer value for power swing detection, point B is where the timer value is stopped and a power swing is declared. Point "C" is where an OOS condition is declared.	29
14	Examples of concentric characteristic types. (a) - mho characteristic, (b) - lens characteristic, (c) - polygonal characteristic.	29
15	Single blinder scheme. Point "A" is when the OOS detection element is started and an out-of-step condition is declared when the impedance crosses the second blinder at point "B".	30
16	Continuous impedance measuring scheme. The impedance locus movement is constantly tracked and the ΔR and ΔX values computed in order to verify the trajectory monotony, continuity and uniformity.	31
17	R-Rdot OOS characteristic in the phase plane [11].	32
18	The incremental increase in measured current values during a power swing. .	33

19	Voltage phasor diagram of a two-machine system. The swing-centre voltage used by this method is shown by the blue phasor, the locally measured voltage is shown as V_1 and the measured current I_l in red [34].	33
20	Principle scheme of voltage comparison algorithm: a) – measurement principle; b) direct voltage comparison based algorithm tripping characteristic. U_A – voltage phasor measured by IED A, U_B – voltage phasor measured by IED B. Adapted from [37].	35
21	Simple system equivalent scheme with added IBR source.	38
22	OOS protection characteristic and impedance trajectories seen by a distance relay at Bus 1 when source impedance changes in the case of an electrically long line (SIR = 0.33).	39
23	OOS protection characteristic and impedance trajectories seen by a distance relay at Bus 1 with further increase in source impedance in the case of an electrically long line (SIR = 0.33).	39
24	OOS protection characteristic and impedance trajectories seen by a distance relay at Bus 1 in the case of an electrically short line (SIR = 4.0).	40
25	Measured voltage angle difference in relation to source angle difference with different Z_r/Z_s ratios in the case of an electrically long line (SIR = 0.33).	41
26	Measured voltage angle difference in relation to source angle difference with different Z_r/Z_s ratios in the case of an electrically short line (SIR = 4.0).	42
27	Modelled angular difference in relation to source angle difference with different Z_r/Z_s ratios in the case of an electrically long line (SIR = 0.33).	43
28	Modelled angular difference in relation to source angle difference with different Z_r/Z_s ratios in the case of an electrically short line (SIR = 4.0).	43
29	Power-angle curve with Last Stable Angle point and equivalent impedance scheme. (a) - Power-angle curve constructed from calculated values, with Last Stable Angle point denoted as <i>LSA</i> , (b) - equivalent impedance computation scheme illustration.	46
30	Current and voltage measurements and sampling of quantities in the case of an event in the grid. (a) - sampling of current magnitude and angle, (b) - sampling of voltage magnitude and angle.	47
31	Principle scheme for system impedance computation on meshed networks.	48
32	Equivalent phasor diagram constructed from computed equivalent system impedances and measured quantities.	49
33	Principle diagram of the developed algorithm in the hardware controller [58].	51
34	Test network for testing impedance computation of the developed algorithm.	52
35	Errors of impedance computation of the algorithm. (a) - Error heatmap for impedance computation on Side 1, (b) - Error heatmap for impedance computation on Side 2.	53
36	Fault currents and the perceived impedance together with impedance computed by the OOS algorithm. (a) - Fault currents for the example, (b) - Perceived impedance with computed impedance by the OOS algorithm.	54
37	Test network for OOS algorithm verification.	55
38	Measured generator (E_{mach}) angle in respect to equivalent source E_{eq1} , computed angle value and algorithm signals. (a) - generator measured angle value, (b) - computed angle value by the algorithm and <i>LSA</i> value, (c) - algorithm operation and blocking signals in time.	56

39	Measured generator (E_{mach}) angle in respect to equivalent source E_{eq1} , computed angle value and algorithm signals. (a) - generator measured angle value, (b) - computed angle value by the algorithm and LSA value, (c) - algorithm operation and blocking signals in time.	57
40	Measured generator (E_{mach}) angle in respect to equivalent source E_{eq1} , operation time instants in the case of different error values in impedance computation and the associated computed angle values by the algorithm. (a) - measured generator angle and operation time instants in time, (b) - computed angle value, operation threshold and operation instants in time.	58
41	Principle diagram for the verification of the hardware implementation of the developed algorithm.	59
42	Diagram of the developed OOS protection algorithm in the hardware implementation from the controller software showing the event detection, angle computation and the threshold and operation submodules.	60
43	Measured generator (E_{mach}) angle in respect to equivalent source E_{eq1} , computed angle value and algorithm signals. (a) - generator measured angle value, (b) - computed angle value by the algorithm and LSA value, (c) - algorithm operation and blocking signals in time.	61
44	Measured generator (E_{mach}) angle in respect to equivalent source E_{eq1} , computed angle value and algorithm signals. (a) - generator measured angle value, (b) - computed angle value by the algorithm and LSA value, (c) - algorithm operation and blocking signals in time.	62
45	Fault locations for testing algorithm's security for faults outside of the observed transmission line.	63
46	Reaction to an SLG fault at location F1. (a) shows the instantaneous current values at both measurement locations and the generator rotor angle (E_{mach}) in respect to source angle (E_{eq1}). (b) shows the protection algorithm signals for operation, blocking and event detection and the computed angle value by the algorithm. ① - fault inception, ② - first breaker opening, ③ - second breaker opening and fault clearance, ④ - reclosure of the faulted line.	64
47	Reaction to an TPH fault at location F1. (a) shows the instantaneous current values at both measurement locations and the generator rotor angle (E_{mach}) in respect to source angle (E_{eq1}). (b) shows the protection algorithm signals for operation, blocking and event detection and the computed angle value by the algorithm. ① - fault inception, ② - first breaker opening, ③ - second breaker opening and fault clearance, ④ - reclosure of the faulted line.	66
48	Reaction to an SLG fault at location F2. (a) shows the instantaneous current values at both measurement locations and the generator rotor angle (E_{mach}) in respect to source angle (E_{eq1}). (b) shows the protection algorithm signals for operation, blocking and event detection and the computed angle value by the algorithm. ① - fault inception, ② - first breaker opening, ③ - second breaker opening and fault clearance, ④ - reclosure of the faulted line.	67

49	Reaction to an TPH fault at location F2. (a) shows the instantaneous current values at both measurement locations and the generator rotor angle (E_{mach}) in respect to source angle (E_{eq1}). (b) shows the protection algorithm signals for operation, blocking and event detection and the computed angle value by the algorithm. ① - fault inception, ② - first breaker opening, ③ - second breaker opening and fault clearance, ④ - reclosure of the faulted line.	68
50	Fault location for testing algorithm's security for faults on the observed transmission line.	69
51	Reaction to a SLG fault at location F3. (a) shows the instantaneous current values at both measurement locations and the generator rotor angle (E_{mach}) in respect to source angle (E_{eq1}). (b) shows the protection algorithm signals for operation, blocking and event detection and the computed angle value by the algorithm. ① - fault inception, ② - first breaker opening, ③ - second breaker opening and fault clearance, ④ - reclosure of the faulted line.	70
52	Reaction to a TPH fault at location F3. (a) shows the instantaneous current values at both measurement locations and the generator rotor angle (E_{mach}) in respect to source angle (E_{eq1}). (b) shows the protection algorithm signals for operation, blocking and event detection and the computed angle value by the algorithm. ① - fault inception, ② - first breaker opening, ③ - second breaker opening and fault clearance, ④ - reclosure of the faulted line.	71
53	Simple system equivalent for decoupled out-of-step protection explanation.	74
54	Power-angle curves for the two-machine system and the demonstration of a stable power swing process on a power-angle curve. (a) Power-angle curves for pre-fault, faulted state and post-fault state, with the LSA point denoted as δ_{LSA} . (b) Power system operation after a disturbance; during this operation the angle difference is decelerating until reaching the maximum angular difference of δ_2 , where all the surplus of energy has been dissipated. (c) Power system operation after the surplus of energy after the disturbance has been dissipated and the angular difference is decreasing while system is settling at a stable operation point. (c) system operation in a new equilibrium point noted as δ_n	75
55	Demonstration of an unstable power swing process on a power-angle curve from observing derivative values (a) Power-angle curve illustrating the pre-, faulted- and postfault operations, with the LSA point denoted as δ_{LSA} . (b) Power system operation after a disturbance, during this operation the rate of change in the angle difference is negative, and power derivative remains positive until reaching the maximum active power value at δ_m . (c) Power system operation after passing the maximum power value, during this operation the power derivative is negative and the rate of change in the angle difference is negative. (d) System operation becomes unstable after passing the LSA point, the rate of change of the angle difference becomes positive.	76
56	Principle diagram of the developed discrete angle derivative OOS protection algorithm.	78
57	Simple system for testing the decoupled out-of-step protection algorithm. .	79

58	The decoupled algorithm reaction to a stable power swing in the network. (a) - the measured voltage and active power values, (b) - measured angle difference value between the sources and the signal states of the protection algorithm. BLK - protection blocked, RES - protection restrained, ALW - protection allowed to operate, OP - protection operation. ① - fault inception, ② - Blocking criterion is disabled, ③ - Blocking criterion of the protection reactivates as the voltage returns above the threshold value of 0.89 p.u.	80
59	The decoupled algorithm reaction to a unstable power swing in the network. (a) - the measured voltage values and measured active power values, (b) - measured angle difference value between the sources and the signal states of the protection algorithm. BLK - protection blocked, RES - protection restrained, ALW - protection allowed to operate, OP - protection operation. ① - fault inception, ② - Blocking criterion is disabled, ③ - protection operation command.	81
60	Principle diagram of the developed OOS protection algorithm in the hardware controller software.	82
61	The decoupled algorithm reaction to a stable power swing in the network. (a) - the measured voltage values and measured angle difference between the sources, (b) - computed first and second derivative values as well as the protection signals for the software and hardware implementation of the protection algorithm. SW - software implementation, HW - hardware implementation, BLK - protection blocked, RES - protection restrained, ALW - protection allowed to operate, OP - protection operation. ① - fault inception, ② - fault clearing in the network, ③ - software implementation reblocking, ④ - hardware implementation reblocking.	83
62	The decoupled algorithm reaction to a unstable power swing in the network. (a) - the measured voltage values and measured angle difference between the sources, (b) - computed first and second derivative values as well as the protection signals for the software and hardware implementation of the protection algorithm. SW - software implementation, HW - hardware implementation, BLK - protection blocked, RES - protection restrained, ALW - protection allowed to operate, OP - protection operation. ① - fault inception, ② - fault clearing in the network, ③ - software implementation issues an operation command, ④ - hardware implementation issues and operation command.	85
63	Fault location for testing the algorithm's security for faults outside of the observed transmission line.	86
64	The decoupled algorithm reaction for an SLG fault at location F1. (a) - the measured RMS voltages, voltage threshold for blocking and measured angle difference between E_{mach} and E_{eq1} , (b) - computed first and second derivative values as well as the protection signals for the hardware implementation of the protection algorithm. BLK - protection blocked, RES - protection restrained, ALW - protection allowed to operate, OP - protection operation. ① - fault inception, ② - fault clearing in the network, ③ - protection deblocking, ④ - auto-reclosure of the faulted line.	87

65	The decoupled algorithm reaction for a TPH fault at location F1. (a) - the measured RMS voltages, voltage threshold for blocking and measured angle difference between E_{mach} and E_{eq1} , (b) - computed first and second derivative values as well as the protection signals for the hardware implementation of the protection algorithm. BLK - protection blocked, RES - protection restrained, ALW - protection allowed to operate, OP - protection operation. ① - fault inception, ② - fault clearing in the network, ③ - protection deblocking, ④ - auto-reclosure of the faulted line.	88
66	The decoupled algorithm reaction for disconnection of the observed transmission line. (a) - the measured RMS voltages, voltage threshold for blocking and measured angle difference between E_{mach} and E_{eq1} , (b) - computed first and second derivative values as well as the protection signals for the hardware implementation of the protection algorithm. BLK - protection blocked, RES - protection restrained, ALW - protection allowed to operate, OP - protection operation. ① - line disconnection.	89
67	Diagram of the developed two-area model for testing out-of-step protections. Area 1 is represented by a synchronous generator and a Type 4 wind power plant and Area 2 is modelled as a static source. IED 2 is marked with an asterisk, because the IED in that position was only used by algorithm 3, since it needs two IEDs to function.	92
68	Schematic diagram of the control of the used Type 4 wind turbine.	94
69	Modified IEEE 39 bus network with added type 4 wind farms. Red marks Case A testing location and blue Case B testing location, wind farms are added to buses 21, 15, 25, 16 and 29 [79, 80].....	95
70	Iceland power system, the corresponding corridors of lines connecting two parts of the network are outlined in red and green for the northern and southern ring connections respectively [81].....	96
71	OOS event 1 measured and simulation values. (a) the frequency in the south-west centre of inertia, (b) the frequency of the east centre of inertia and (c) the active power flow in the southern ring connection, where the OOS event takes place. ① - the start of the event with the fault in the north corridor substation, ② - fault clearance, ③ - first pole slip in simulated values, ④ - first pole slip in measured values.....	97
72	OOS event 2 measured and simulation values. (a) the frequency in the south-west centre of inertia, (b) the frequency of the east centre of inertia and (c) the active power flow in the southern corridor, where the OOS event takes place. ① - the start of the event with the loss of load, ② - inter trip on the 220 kV substation at the southern corridor, ③ - north corridor disconnection from overload, ④ - first pole slip in measured values, ⑤ - first pole slip in simulation.	98
73	Experimental setup for OOS protection testing using physical hardware.....	99
74	Measured generator angle in respect to E_{eq} , computed angle value and algorithm signals for different delay settings. (a) - generator measured angle value, (b) - computed angle value by the algorithm and LSA value, (c) - algorithm operation and blocking signals in time. ① - algorithm blocking in the case of 50 ms delay, ② - algorithm blocking in the case of 100 ms delay, ③ - algorithm blocking in the case of 200 ms delay.	101

75	Measured generator angle in respect to E_{eq} , computed angle value and algorithm signals for different delay settings. (a) - generator measured angle value, (b) - computed angle value by the algorithm and LSA value, (c) - algorithm operation and blocking signals in time. ① - algorithm operation in the case of 50 ms delay, ② - algorithm operation in the case of 100 ms delay, ③ - algorithm operation in the case of 200 ms delay.	102
76	Measured voltage values, measured generator angle in respect to E_{eq} and algorithm signals for different delay settings for stable power swing case. (a) - measured voltage values, (b) - generator measured angle value, (c) - algorithm operation and blocking signals in time. ① - algorithm unblocking in the case of 50 ms delay, ② - algorithm unblocking in the case of 100 ms delay, ③ - algorithm unblocking in the case of 200 ms delay, ④ - algorithm reblocking in the case of 50 ms delay, ⑤ - algorithm reblocking in the case of 100 ms delay, ⑥ - algorithm reblocking in the case of 200 ms delay.	103
77	Measured voltage values, measured generator angle in respect to E_{eq} and algorithm signals for different delay settings for unstable power swing case. (a) - measured voltage values, (b) - generator measured angle value, (c) - algorithm operation and blocking signals in time. ① - algorithm unblocking in the case of 50 ms delay, ② - algorithm unblocking in the case of 100 ms delay, ③ - algorithm unblocking in the case of 200 ms delay, ④ - algorithm operation in the case of 50 ms delay, ⑤ - algorithm operation in the case of 100 ms delay, ⑥ - algorithm operation in the case of 200 ms delay.	104
78	OOS protection characteristic with the setting values for the computed example case.	107
79	Comparisons of proposed algorithm performances: (a) Comparison of percentage of OOS conditions detected, (b) Comparison of average operation times. DER - algorithm based on discrete angle derivatives, LSA - algorithm based on PMU-determined impedances.	108
80	Overall results from all testing scenarios. (a) shows overall missed operation percentages and (b) shows average operating times of the test scenarios. Blue column represents simulation Case S, red Case M and orange Case L. Device 1 - Angle-controlled OOS protection, Device 2 - Impedance-based OOS protection and Device 3 - OOS algorithm based on direct voltage comparison.	108
81	Total missed operations in percent and average operating times for Case S. Blue, red and yellow columns represent a grid equivalent with infinite, medium and weak network equivalent respectively. (a) - missed operations, (b) - average operation time.	109
82	Total missed operations in percent and average operating times for Case M. Blue, red and yellow columns represent a grid equivalent with infinite, medium and weak network equivalent respectively. (a) - missed operations, (b) - average operation time.	110
83	Total missed operations in percent and average operating times for Case L. Blue, red and yellow columns represent a grid equivalent with infinite, medium and weak network equivalent respectively. (a) - missed operations, (b) - average operation time.	111

84	OOS detection rates for tested cases in the IEEE 39 Bus System. Red displays the detection rate for Case A and blue for Case B. DER - algorithm based on discrete angle derivatives, LSA - algorithm based on PMU-determined impedances, Device 2 and Device 4 - impedance-based OOS protections. . .	112
85	OOS tripping times of protection devices for Case A. (a) represents the case study with a longer line between two systems and (b) represents a short line between two systems. DER - algorithm based on discrete angle derivatives, LSA - algorithm based on PMU-determined impedances, Device 2 and Device 4 - impedance-based OOS protections.	113
86	OOS tripping times of protection devices for Case B. (a) represents a long line between the machine and the system, (b) represents a short line between the machine and the system. DER - algorithm based on discrete angle derivatives, LSA - algorithm based on PMU-determined impedances, Device 2 and Device 4 - impedance-based OOS protections.	114
87	Developed protection algorithm testing setup with measured data streaming.	117
88	Protection algorithm response to Event 1 data. The dashed line marked as ① shows the start of the OOS event at 1.3 seconds. (a) the voltage at the two measurement locations in the southern corridor and (b) the measured power in the southern corridor during the event, (c) the protection algorithm signals from the controller. BLK - algorithm blocked, RES - algorithm restrained, ALW - algorithm allowed to operate, OP - algorithm operation signal.	118
89	Protection algorithm response to Event 2 data. The dashed line marked as ① shows the start of the OOS event at 2.1 seconds. (a) the voltage at the two measurement locations in the southern corridor and (b) the measured power in the southern corridor during the event, (c) the protection algorithm signals from the controller. BLK - algorithm blocked, RES - algorithm restrained, ALW - algorithm allowed to operate, OP - algorithm operation signal.	119
90	Protection algorithm response to Event 3 data. The dashed line marked as ① shows the start of the OOS event at 0.5 seconds. (a) the voltage at the two measurement locations in the southern corridor and (b) the measured power in the southern corridor during the event, (c) the protection algorithm signals from the controller. BLK - algorithm blocked, RES - algorithm restrained, ALW - algorithm allowed to operate, OP - algorithm operation signal.	120
91	Protection algorithm response to Event 4 data. The dashed line marked as ① shows the start of the OOS event at 1.3 seconds. (a) the voltage at the two measurement locations in the southern corridor and (b) the measured power in the southern corridor during the event, (c) the protection algorithm signals from the controller. BLK - algorithm blocked, RES - algorithm restrained, ALW - algorithm allowed to operate, OP - algorithm operation signal.	121
92	Frequencies and voltages in the east and west parts of the Iceland power system in the case of developed protection and no protection. The dashed line represents the time of developed protection operation. (a) - frequencies of east and west parts of the network, (b) - voltages of PMU1 and PMU2.	122

List of Tables

1	Comparison of commercially used power swing and out-of-step detection methods.	23
2	Comparison of unconventional out-of-step detection methods based on local measurements.	36
3	Comparison of unconventional out-of-step detection methods based on wide-area measurements.	37
4	Used data for the synchronous generator for OOS verification test system in per unit on 1000 MVA base.	54
5	Used data for the synchronous generator IEEE Type 1 type exciter for OOS verification test system.	55
6	Used data for the synchronous generator TGOV1 turbine governor for OOS verification test system in per unit on 1000 MVA base.	55
7	System aspects which are varied for protection testing in the SMIB test model.	93
8	Used data for the synchronous generator for SMIB test cases in per unit on 1000 MVA base.	93
9	Used data for the synchronous generator IEEE ST1 type exciter for SMIB test cases.	93
10	Used data for the synchronous generator IEEE G1 turbine governor for SMIB test cases in per unit on 1000 MVA base.	93
11	Used data for the PMSM generator for SMIB test cases in per unit on 2 MVA base.	93
12	Parameters of the Type 4 wind power plant grid-side converter.	94
13	Communication time delay requirement for synchrophasor applications [82, 85, 86].	100
14	Devices used for HiL testing.	105
15	Settings for the angle-controller out-of-step protection algorithm.	105
16	Settings for the impedance-based out-of-step protection.	107
17	Settings for the impedance-based out-of-step protection for test cases in IEEE39 Bus System.	111
18	Conducted real-time simulations using Iceland's power system model and the simulation results.	116

References

- [1] H. Ritchie, M. Roser, and P. Rosado, "Co2 and greenhouse gas emissions," *Our World in Data*, 2020. <https://ourworldindata.org/co2-and-other-greenhouse-gas-emissions>.
- [2] IEA, "World Energy Outlook 2021," tech. rep., IEA, 2021.
- [3] Eurostat, "Renewable energy statistics," tech. rep., Eurostat, 2021.
- [4] ENTSO-E, "Wide Area Monitoring - Continental Europe," tech. rep., ENTSO-E, 2015.
- [5] "H2020 Migrate." <https://www.h2020-migrate.eu>. Accessed: 13.10.2022.
- [6] ENTSO-E, "Continental Europe Synchronous Area Separation on 08 January 2021 - Final Report," tech. rep., 2021.
- [7] M. Aru, "Erinevate distantkaitsete käitumise uurimine muutuva elektrisüsteemi inerti tingimustes (analysis of different distance relay behaviours in variable power system inertia conditions)," Master's thesis, Tallinn University of Technology, Tallinn, 2018. In Estonian.
- [8] K. Pill, "Elektrisüsteemi asünkroonkäigukaitsete algoritmide analüüs (analysis of different power system out of step detection algorithms)," Master's thesis, Tallinn University of Technology, Tallinn, 2018. In Estonian.
- [9] M. Tealane, "HIL Testing an Adaptive Out-of-Step Protection Algorithm based on Wide-Area Measurements." RTDS User Spotlight 2.0 Episode 4, 2022.
- [10] M. Tealane, "Adaptive out-of-step Protection Based on Wide Area Measurements." Communication based protection seminar. Delft, The Netherlands, 2022.
- [11] N. Fischer, G. Benmouyal, D. Hou, D. Tziouvaras, and J. Byrne-Finley, "Tutorial on power swing blocking and out-of-step tripping," 2015.
- [12] J. Zaborszky and J. Rittenhouse, *Electric Power Transmission: The Power System in the Steady State*. Ronald Press Company, 1954.
- [13] O. Dahl, *Electric Power Circuits, Theory and Applications, V.2: Power System Stability*. 1938.
- [14] J. Machowski, Z. Lubosny, J. W. Bialek, and J. R. Bumby, *Power System Dynamics: Stability and Control*. Wiley, 3rd edition ed., 2020.
- [15] A. Phadke and J. Thorp, *Synchronized Phasor Measurements and Their Applications*. Power Electronics and Power Systems, Springer US, 2008.
- [16] "IEEE/IEC International Standard - Measuring relays and protection equipment - Part 118-1: Synchrophasor for power systems - measurements," *IEC/IEEE 60255-118-1:2018*, pp. 1–78, 2018.
- [17] A. Molina-Cabrera, M. A. Ríos, Y. Besanger, N. Hadjsaid, and O. D. Montoya, "Latencies in power systems: A database-based time-delay compensation for memory controllers," *Electronics*, vol. 10, no. 2, 2021.

- [18] V. Terzija, G. Valverde, D. Cai, P. Regulski, V. Madani, J. Fitch, S. Skok, M. M. Begovic, and A. Phadke, "Wide-area monitoring, protection, and control of future electric power networks," *Proceedings of the IEEE*, vol. 99, no. 1, pp. 80–93, 2011.
- [19] X. Liu, S. Zhang, X. Zeng, L. Yao, Y. Ding, and C. Deng, "Evaluating the network communication delay with wams for multi-energy complementary systems," *CSEE Journal of Power and Energy Systems*, vol. 6, no. 2, pp. 402–409, 2020.
- [20] S. Horowitz and A. Phadke, *Power System Relaying*. John Wiley and Sons, 2014.
- [21] IEEE, "Power swing and out-of-step considerations on transmission lines," tech. rep., IEEE PSRC WG D6, 2006.
- [22] European Commission, "2030 climate & energy framework," tech. rep., European Commission, 2019.
- [23] A. Sauhats, A. Utans, G. Pashnin, and D. Antonovs, "Out-of-step relays testing procedure," *Scientific Journal of Riga Technical University. Power and Electrical Engineering*, vol. 28, pp. 9–14, 01 2011.
- [24] J. Megger and J. M. Gersusa, "Setting and testing of power swing blocking and out of step relays considering transient stability conditions," in *2008 IET 9th International Conference on Developments in Power System Protection (DPSP 2008)*, pp. 150–155, 2008.
- [25] Q. Verzosa, "Realistic testing of power swing blocking and out-of-step tripping functions," in *2013 66th Annual Conference for Protective Relay Engineers*, pp. 420–449, 2013.
- [26] M. Saad, A. Eltom, G. Kobet, and R. Ahmed, "Performance comparison between dual-blinder and phasor-based out-of-step detection functions using hardware-in-the loop simulation," pp. 1–8, 10 2015.
- [27] D. A. Tziouvaras and D. Hou, "Out-of-step protection fundamentals and advancements," in *57th Annual Conference for Protective Relay Engineers, 2004*, pp. 282–307, 2004.
- [28] N. Fischer, G. Benmouyal, and S. Samineni, "Tutorial on the impact of the synchronous generator model on protection studies," 2015.
- [29] IEEE, "Application of out-of-step protection schemes for generators," tech. rep., IEEE PSRC WG J5, 2020.
- [30] J. Holbach, "New out of step blocking algorithm for detecting fast power swing frequencies," pp. 182 – 199, 04 2006.
- [31] C. W. Taylor, J. M. Haner, L. A. Hill, W. A. Mittelstadt, and R. L. Cresap, "A new out-of-step relay with rate of change of apparent resistance augmentation," *IEEE Transactions on Power Apparatus and Systems*, vol. PAS-102, no. 3, pp. 631–639, 1983.
- [32] J. M. Haner, T. D. Laughlin, and C. W. Taylor, "Experience with the r-rdot out-of-step relay," *IEEE Transactions on Power Delivery*, vol. 1, no. 2, pp. 35–39, 1986.
- [33] P. Horton and S. Swain, "Using superimposed principles (delta) in protection techniques in an increasingly challenging power network," in *2017 70th Annual Conference for Protective Relay Engineers (CPRE)*, pp. 1–12, 2017.

- [34] ENTSO-E, "System protection behaviour and settings during system disturbances," tech. rep., ENTSO-E, 2018.
- [35] D. Hou, G. Benmouyal, and D. Tziouvaras, "Zero-setting power-swing blocking protection," *IET Conference Proceedings*, pp. 249–254(5), January 2005.
- [36] Toshiba Corporation, *Line differential protection IED instruction manual*, 2017.
- [37] M. Tealane, J. Kilter, and K. Pill, "Real-time testing of out-of-step protection devices," in *2021 IEEE PES Innovative Smart Grid Technologies Europe (ISGT Europe)*, pp. 1–5, 2021.
- [38] A. Sauhats, A. Svalovs, and I. Svalova, "Development of algorithms for prevention of asynchronous operation in high-voltage networks," vol. 1, p. 6 pp. Vol.1, 07 2003.
- [39] A. Sauhats, A. Utans, D. Antonovs, and A. Svalovs, "Multi-terminal out-of-step protection system," in *2016 IEEE 16th International Conference on Environment and Electrical Engineering (EEEIC)*, pp. 1–6, 2016.
- [40] A. Sauhats, A. Utans, D. Antonovs, and A. Svalovs, "Angle control-based multi-terminal out-of-step protection system," *Energies*, vol. 10, no. 3, 2017.
- [41] A. Sauhats, A. Utans, and E. Biela-Dalidovicha, "Equal area criterion and angle control-based out-of-step protection," in *2017 IEEE 58th International Scientific Conference on Power and Electrical Engineering of Riga Technical University (RTUCON)*, pp. 1–6, 2017.
- [42] S. Paudyal, R. Gokaraju, M. Sachdev, and S. Cheng, "Out-of-step detection using energy equilibrium criterion in time domain," *Electric Power Components and Systems*, vol. 37, pp. 714–739, 06 2009.
- [43] S. Paudyal, G. Ramakrishna, and M. S. Sachdev, "Application of equal area criterion conditions in the time domain for out-of-step protection," *IEEE Transactions on Power Delivery*, vol. 25, no. 2, pp. 600–609, 2010.
- [44] M. Abedini, M. Davarpanah, M. Sanaye-Pasand, S. M. Hashemi, and R. Iravani, "Generator out-of-step prediction based on faster-than-real-time analysis: Concepts and applications," *IEEE Transactions on Power Systems*, vol. 33, no. 4, pp. 4563–4573, 2018.
- [45] K. Sreenivasachar, "Out-of-step detection on transmission lines using apparent impedance differential method," *IEEE Transactions on Power Delivery*, pp. 1–1, 2021.
- [46] M. R. Nasab and H. Yaghobi, "A real-time out-of-step protection strategy based on instantaneous active power deviation," *IEEE Transactions on Power Delivery*, vol. 36, no. 6, pp. 3590–3600, 2021.
- [47] V. Centeno, A. G. Phadke, A. Edris, J. Benton, M. Gaudi, and G. Michel, "An adaptive out-of-step relay [for power system protection]," *IEEE Transactions on Power Delivery*, vol. 12, no. 1, pp. 61–71, 1997.
- [48] H. Zare, H. Yaghobi, and Y. Alinejad-Beromi, "Adaptive concept of controlled islanding in power systems for wide-area out-of-step prediction of synchronous generators based on adaptive tripping index," *IET Generation, Transmission Distribution*, vol. 12, no. 16, pp. 3829–3836, 2018.

- [49] S. Zhang and Y. Zhang, "A novel out-of-step splitting protection based on the wide area information," *IEEE Transactions on Smart Grid*, vol. 8, no. 1, pp. 41–51, 2017.
- [50] P. Regulski, W. Rebizant, M. Kereit, and H.-J. Herrmann, "Pmu-based generator out-of-step protection," *IFAC-PapersOnLine*, vol. 51, pp. 79–84, 01 2018.
- [51] T. D. Duong, S. D'Arco, and A. Holdyk, "A method for predictive out-of-step tripping based on synchrophasors," in *15th International Conference on Developments in Power System Protection (DPSP 2020)*, pp. 1–6, 2020.
- [52] N. G. Chothani, B. R. Bhalja, and U. B. Parikh, "New support vector machine-based digital relaying scheme for discrimination between power swing and fault," *Int Generation Transmission & Distribution*, vol. 8, pp. 17–25, 2014.
- [53] M. R. Aghamohammadi and M. Abedi, "DT based intelligent predictor for out of step condition of generator by using PMU data," *International Journal of Electrical Power & Energy Systems*, vol. 99, pp. 95–106, 2018.
- [54] E. A. Frimpong, P. Y. Okyere, and J. Asumadu, "On-line determination of transient stability status using mlpnn," in *2017 IEEE PES PowerAfrica*, pp. 23–27, 2017.
- [55] D. Fan and V. Centeno, "Adaptive out-of-step protection schemes based on synchrophasors," in *2014 IEEE PES General Meeting | Conference Exposition*, pp. 1–5, 2014.
- [56] K. Shimizu and A. Ishigame, "Novel transient stability assessment using post-disturbance voltage fluctuations," in *2020 International Conference on Smart Grids and Energy Systems (SGES)*, pp. 12–17, 2020.
- [57] J. R. Camarillo-Peñaranda, D. Celeita, M. Gutierrez, M. Toro, and G. Ramos, "An approach for out-of-step protection based on swing center voltage estimation and analytic geometry parameters," *IEEE Transactions on Industry Applications*, vol. 56, no. 3, pp. 2402–2408, 2020.
- [58] M. Tealane, J. Kilter, M. Popov, O. Bagleybter, and D. Klaar, "Online detection of out-of-step condition using PMU-determined system impedances," *IEEE Access*, vol. 10, pp. 14807–14818, 2022.
- [59] Siemens AG, "Siprotec 5 distance protection, line differential protection, and breaker management for 1-pole and 3-pole tripping 7sa87, 7sd87, 7sl87, 7vk87 v9.2 and higher," tech. rep., Siemens AG, 2022.
- [60] "IEEE guide for protective relay applications to transmission lines," *IEEE Std C37.113-2015 (Revision of IEEE Std C37.113-1999)*, pp. 1–141, 2016.
- [61] Y. Xue, T. Van Custem, and M. Ribbens-Pavella, "Extended equal area criterion justifications, generalizations, applications," *IEEE Transactions on Power Systems*, vol. 4, no. 1, pp. 44–52, 1989.
- [62] K. O. H. Pedersen, A. H. Nielsen, and N. K. Poulsen, "Short-circuit impedance measurement," *IEE Proceedings - Generation, Transmission and Distribution*, vol. 150, no. 2, pp. 169–174, 2003.
- [63] Y. Wang, W. Xu, and J. Yong, "An adaptive threshold for robust system impedance estimation," *IEEE Transactions on Power Systems*, vol. 34, no. 5, pp. 3951–3953, 2019.

- [64] M. Leinakse, H. Kiristaja, and J. Kilter, "Identification of intra-day variations of static load characteristics based on measurements in high-voltage transmission network," in *2018 IEEE PES Innovative Smart Grid Technologies Conference Europe (ISGT-Europe)*, pp. 1–6, 2018.
- [65] B. Alinezhad and H. Kazemi Karegar, "On-line thévenin impedance estimation based on pmu data and phase drift correction," *IEEE Transactions on Smart Grid*, vol. 9, no. 2, pp. 1033–1042, 2018.
- [66] GE Digital, "Phasor controller," tech. rep., 2021.
- [67] A. Pai, *Energy Function Analysis for Power System Stability*. Power Electronics and Power Systems, Springer US, 2012.
- [68] A. Manunza, "Out of step condition and torsional stress of synchronous generators (eeug meeting 2007: European emtp-atp conference) – (applications in electrical machines and industry (1))," *EMTP journal*, vol. 13, pp. 89–95, 2008.
- [69] RTDS Technologies, *RSCAD Controls Libarary Manual*, 2021.
- [70] "Communication networks and systems for power utility automation - all parts."
- [71] A. Phadke and J. Thorp, *Synchronized Phasor Measurements and Their Applications*. Springer, 01 2017.
- [72] P. Kundur, *Power system stability and control*. McGraw-Hill, 1994.
- [73] D. R.-V. Mania Pavella, Damien Ernst, *Transient Stability of Power Systems*. Springer, 2000.
- [74] C. Taylor, N. Balu, and D. Maratukulam, *Power System Voltage Stability*. EPRI power system engineering series, McGraw-Hill, 1994.
- [75] S. Savulescu, *Real-Time Stability in Power Systems: Techniques for Early Detection of the Risk of Blackout*. Kluwer international series in engineering and computer science: Power electronics & power systems, Springer, 2006.
- [76] S. Savulescu, *Real-Time Stability Assessment in Modern Power System Control Centers*. IEEE Press Series on Power and Energy Systems, Wiley, 2009.
- [77] J. Das, *Power System Protective Relaying*. CRC Press, 2017.
- [78] RTDS Technologies, *Modelling of permanent magnet generator based wind turbine systems in the RTDS*, 2017.
- [79] M. Tealane, J. Kilter, M. Popov, O. Bagleybter, and D. Klaar, "Online detection of out-of-step condition using pmu-determined system impedances," *IEEE Access*, vol. 10, pp. 14807–14818, 2022.
- [80] M. Tealane, J. Kilter, O. Bagleybter, B. Heimisson, and M. Popov, "Out-of-step protection based on discrete angle derivatives," *IEEE Access*, vol. 10, pp. 78290–78305, 2022.
- [81] "Landsnet's transmission system." <https://landsnet.is/>. Accessed: 30.03.2022.

- [82] H. H. Alhelou, A. Y. Abdelaziz, and P. Siano, *Wide area power systems stability, protection, and security*. Springer, 2020.
- [83] K. Zhu, J. Song, M. Chenine, and L. Nordström, "Analysis of phasor data latency in wide area monitoring and control systems," pp. 1 – 5, 06 2010.
- [84] A. Phadke and J. Thorp, "Communication needs for wide area measurement applications," in *2010 5th International Conference on Critical Infrastructure (CRIS)*, pp. 1–7, 2010.
- [85] D. Mohanta and M. Reddy, *Synchronized Phasor Measurements for Smart Grids*. Energy Engineering, Institution of Engineering and Technology, 2017.
- [86] M. Adamiak, A. Apostolov, M. Begovic, C. Henville, K. Martin, G. Michel, A. Phadke, and J. Thorp, "Wide area protection—technology and infrastructures," *IEEE Transactions on Power Delivery*, vol. 21, no. 2, pp. 601–609, 2006.
- [87] REMI, "Asynchronous run prevention automatic device AGNA," tech. rep., Riga Technical University, 2008.
- [88] Siemens AG, "Siprotec 4 line distance protection 7sa6xx v4.7," tech. rep., Siemens AG, 2011.
- [89] Schneider Electric, "Easergy micom p44y technical manual," tech. rep., Schneider Electric, 2019.
- [90] F. Gonzalez-Longatt, C. Adiyabazar, and E. Vazquez, "Setting and testing of the out-of-step protection at mongolian transmission system," *Energies*, vol. 14, p. 8170, 12 2021.

Acknowledgements

My deepest gratitude goes to my partner Sanja. Without your continuous support, patience and encouragement writing this thesis would not have been possible.

I want to acknowledge my supervisor, Jako Kilter, for his guidance and support during my studies. I also want to thank my colleagues in TalTech who have supported me throughout my studies.

I want to kindly acknowledge Marjan Popov, whom I had the opportunity to work with during my stay in Technical University of Delft. Thank you for all the mentoring, guidance and help. I also want to express my thanks to Remko Koornneef for the assistance and support.

Special thanks to Oleg Bagleybter from GE Grid Automation for the support and assistance as well as Landsnet and Birkir Heimisson for offering me a chance to work with them, and being optimistic about adopting new solutions.

Abstract

Future Power System Out-of-Step Protection Concept Utilizing Synchronized Phasor Measurements

Electrical power systems all around the world are in a state of change, with the objective of decarbonisation and a more sustainable future. This means a significant amount of renewable-based inverter-connected generation integration to existing networks and a consequent decrease of generation using synchronous machines. This transition causes a shift in historical consumption and generation patterns from the traditional centralised power production to a more decentralized form. Consequent change in fundamental structure of the power system raises questions of how the current well-known system protection systems will behave in this new, more decentralised disposition of the network. Advances in power system monitoring with wide-area solutions enable the development of more advanced application and protection algorithms that consider various generation patterns, data availability and adequate measurement availability.

Based on the literature it was not possible to understand in a sufficient manner if the existing protection systems, which are currently installed in networks, will be able to distinguish between stable and unstable power swings with the inclusion of inverter-based renewable generation in the system. This thesis elaborates on this topic in a more detailed manner and provides assessment on the effect of changing grid source impedance, which comes from the change in the mix of generation, to the existing out-of-step (OOS) protection devices. The performance of three commercially available devices using different OOS detection algorithms has been evaluated using real-time simulation and a hardware-in-the-loop (HiL) simulation approach. The results obtained indicate that there are direct shortcomings in the existing protection algorithms, and it is possible that the current algorithms could fail to detect OOS conditions with the inclusion of inverter-based renewable generation in the network, or the instability detection becomes delayed.

To overcome the limitations in the performance of the existing OOS protection devices, two novel algorithms based on synchronised phasor measurements were developed in this research work. The first developed algorithm relies on the real-time source impedance computation using step changes in measured values, and constructing the well-known power-angle characteristic to determine the Last Stable Angle (LSA) value. The second developed algorithm presented in this thesis is based on discrete angle derivatives (DER). This algorithm complements the first by not requiring step changes in the load to occur in the network. Based on the changes of the electrical quantities, i.e., the voltages and currents, the developed algorithm detects unstable system conditions when the critical point of stability has been exceeded. Both developed algorithms are setting-less and can be easily applied on transmission lines where an out-of-step condition is expected.

Extensive HiL testing was conducted to verify the performance of the developed OOS protection algorithms. The algorithms have been subjected to various grid events, e.g., different fault types and damped power swings in the network. It can be concluded that the developed algorithms exhibit secure behaviour in the case of faults and stable swings in the network, and provide up to 20 % higher detection rate of unstable power swings compared to the best commercially available methods today. The LSA algorithm provides, on average, a 16 % increase in operation speed over existing solutions, whereas DER operates 38 % faster. Both developed protection algorithms are easily adaptable to existing wide-area monitoring and protection systems requiring low processing power and a minimum of two measurement locations. The DER protection algorithm has been commissioned and is in operation in the Iceland power system.

Keywords: Hardware-in-the-loop testing, Out-of-step protection, Power system protection, Power system transient stability, Real-time simulations, Renewable power integration, Wide-area protection schemes.

Kokkuvõte

Tuleviku elektrisüsteemi faasimõõtmistel põhinev sünkronismikaotuskaitse kontseptsioon

Tänapäeva elektrisüsteemid on pidevas muutumises tulenevalt valdkonna dekarboniseerimise ja jätkusuutliku tulevikuga seotud eesmärkidest. See tähendab märkimisväärsel hulgal taastuvatel energiaallikatel põhinevate elektrijaamade ühendamist elektrivõrguga. Nende elektrijaamade ühendamisel kasutatakse jõuelektronikal põhinevaid läheneviise, millest tulenevalt väheneb sünkroonmasinatel põhinevate tootmisüksuste hulk. Suures plaanis toimub tsentraliseeritud tootmismudelil üleminek hajutatud energiatootmisele. Põhimõtteline muutus elektrisüsteemi ülesehituses seab kahtluse alla, kuidas toimivad olemasolevad võrgu kaitsesüsteemid. Samal ajal toimuvad ka suured muutused elektrisüsteemi jälgimiseks ja juhtimiseks kasutatavate laiseiresüsteemide raamistikus ja võimalik on luua järjest enam kaasaegsemaid rakendusi ja kaitsealgoritme, mis võtavad arvesse lisaks mõõteandmete piisavusele ka erinevaid tootmisstsenaariume.

Kirjanduse analüüsi põhjal puudub piisav teadmine, kas olemasolevad elektrisüsteemi kaitsed on võimelised tuvastama ning eristama stabiilseid ja mittestabiilseid võimsuste võnkumisi kui elektrivõrku lisandub suurel määral läbi inverterite ühendatud tootmisüksusi. Käesolev doktoritöö käsitleb seda teematikat põhjalikumalt ja teostatud on laiapõhjaline analüüs olemasolevate sünkronismikaotuskaitsete talitlemisest muutuva toiteallika impedantsi tingimustes, mis tuleneb tootmisüksuste koosseisu muutusest. Kasutades reaalarjasimulatsioone testiti kolme kommertskasutuses olevat kaitserieled, mis kasutavad erinevaid algoritme mittestabiilsete võnkumiste tuvastamiseks. Teostatud katsetest järeldub, et olemasolevad kaitselahendused võivad läbi inverterite ühendatud tootmisüksuste lisandumisel mitte toimida või nende toimes võib tekkida liigseid viiteid.

Käesoleva uurimistöö raames arendati välja kaks laiseire faasimõõtmistele põhinevat uuenduslikku algoritmi, mis võimaldavad vältida olemasolevate kaitseadmete toimimise kitsaskohti. Esimene uudsetest lahendustest põhineb elektrisüsteemi impedantsi arvutamisel reaalarjas lähtudes astmelistest muutustest mõõtesignaalis ja mille alusel konstrueeritud dünaamilist stabiilsust iseloomustaval nurk-karakteristikul määratletakse stabiilne talitusvahemik (LSA algoritm). Teine välja töötatud algoritm põhineb elektrilise nurga väärtuse tuletistel (DER algoritm), täiendades seega esimest algoritmi, sest puudub vajadus hüppeliste muutuste toimumiseks võrgus. Mõlemad loodud algoritmid ei vaja otsest asukohapõhist sätestamist ja neid on võimalik koheselt rakendada ülekandeliinidel, kus võib eeldada sünkronismi kaotust.

Arendatud algoritmide talitluskindluse ja usaldusväärsuse tagamiseks on teostatud suuremahulised katsetused rakendades reaalarjasimulatsioone ja tagasisidestatusel põhinevat riistvaralist katsetamist. Lisaks stabiilsetele elektrisüsteemi võnkumistele on algoritmide käitumist katsetatud erinevates võrgusituatsioonides, sh erinevat tüüpi sise- ja välislühised ning elektrisüsteemi stabiilsed võnkeprotsessid. Teostatud katsetustest selgus, et mõlemad käesoleva uurimistöö raames välja töötatud algoritmid on toimekindlad nii võrgulühiste kui stabiilsete võnkumiste korral. Kokkuvõtvalt saab katsetuste tulemustest järeldada, et välja töötatud algoritmid on kuni 20 % efektiivsemad mittestabiilsete võnkumiste avastamisel võrreldes parima kommertskasutuses oleva kaitselahendusega. Samuti saab välja tuua, et LSA algoritm reageerib keskmiselt 16 % ja DER algoritm 38 % kiiremini kui olemasolevad kaitselahendused. Mõlemad välja töötatud algoritmid vajavad vähest arvutusvõimekust ja nende toimimiseks on minimaalselt tarvis kahte faasimõõteseadet. See lähtekoht võimaldab välja töötatud algoritme hõlpsasti kasutusele võtta olemasolevates laiseiresüsteemides. DER kaitsealgoritm on kasutusele võetud Islandi põhivõrgus.

Märksõnad: Elektrisüsteemi dünaamiline stabiilsus, Elektrisüsteemi kaitsmine, Laiseire kaitsesüsteemid, Sünkronismikaotuskaitse, Taastuvenergiaallikate integratsioon, Reaalaajasimulatsioonid, Tagasisidestatunud riistvara testimine.

Appendix 1

I

M. Tealane, J. Kilter, and K. Pill, "Real-time testing of out-of-step protection devices," in *2021 IEEE PES Innovative Smart Grid Technologies Europe (ISGT Europe)*, pp. 1-5, 2021

© 2021 IEEE. Reprinted, with permission

Real-time testing of out-of-step protection devices

Marko Tealane, Jako Kilter

Dept. of Electrical Power Engineering and Mechatronics

Tallinn University of Technology

Tallinn, Estonia

Marko.Tealane@taltech.ee, Jako.Kilter@taltech.ee

Kristen Pill

Energy System Control Centre

Elering AS

Tallinn, Estonia

Kristen.Pill@elering.ee

Abstract—In future power systems the share of power electronic interfaced generation will increase and respective challenges related to power system protection will emerge. In this paper the performance of different out-of-step protection algorithms is assessed using actual relays from the network and real-time digital simulator RTDS. For the performance analysis various grid conditions were considered, e.g. system strength, line lengths and generation mix between renewables and conventional synchronous units. The results indicate that there are performance differences between the algorithms (relays), therefore, analysis considering the specific system characteristics should be made. Information obtained from this analysis is essential input for transmission system operators when planning their system operation and protection for future networks.

Index Terms—out-of-step protection, power system transient stability, real-time simulations

I. INTRODUCTION

Disturbances in the network are an inherent part of power system operation. These disturbances can cause oscillations in synchronous machines - sometimes resulting in unstable power swings, which cause excess heat generation and extra mechanical stress in power system components [1] [2]. Therefore, it is important to detect these type of swings as fast as possible and for this special type of relays are implemented. These out-of-step relays are usually installed on transmission lines and on generators. The algorithms implemented in general have the same principle, but specific settings are determined by grid conditions at the installed relay location.

Most of the out-of-step algorithms implemented in current power systems have been developed considering the availability of synchronous generation. However, in the future, the level of synchronous units will decrease and more power electronic (PE) based renewable generation will be integrated into the system [3]. This change will have an effect on the operation of different type of protection, including out-of-step protection. Currently, there is limited knowledge available in the literature about the performance of the out-of-step algorithm in power systems with significant level of PE based generation.

In [4], [5] and [6] the out-of-step algorithms are tested and their operation proven using only numerical simulations. Some results, including actual devices and real-time simulations, have been presented in [7]. The given tests, however, do not clarify the performance of out-of-step protection algorithms

in situations where the synchronously connected units are substituted by converter connected solutions. The objective of this paper is to provide insight to existing out-of-step protection operation and performance in the case of different PE based renewable production scenarios and grid topologies.

Discussion and analysis of the performance of out-of-step protection algorithms in this paper is based on the real-time performance testing of three actual protection devices using real-time digital simulator (RTDS). This hardware in the loop (HiL) approach enables to directly compare, verify and assess the performance of actual devices. Since the actual implementation of out-of-step detection algorithms in the devices is not revealed by manufacturers, HiL testing is the only way to analyze the actual behavior of these protection devices. In this paper three physical out-of-step detection devices, most commonly utilized in power system, are tested. These three devices use different algorithms for identifying out-of-step conditions. For analyzing various grid conditions, e.g. different line lengths, power generation scenarios, etc. are simulated.

This paper is organized as follows: Section II describes the tested devices and their operating principles, Section III describes the used testing methodology and HiL testing setup, mass testing results are covered in Section IV, and the paper is concluded in Section V.

II. TESTED OUT-OF-STEP DETECTION DEVICES

Multiple approaches have been developed for detecting out-of-step conditions in power systems. The main advantages and disadvantages of the most common methods for out-of-step detection used on transmission lines are thoroughly described in [8] and [9]. The main methods, that are used by commercially available devices, have been developed assuming a single machine infinite bus model [10]. The three devices chosen and tested in this paper all utilize different algorithms for detecting unstable swings in the network. First device tested utilizes a modified swing centre voltage based algorithm, the second device implements an impedance based out-of-step detection and the third algorithm makes use of direct voltage phasor comparison in two line ends to detect an out-of-step condition on the transmission line.

To better understand the operation of these protection devices, the actual working principles of the physical devices must be considered. Therefore these descriptions of the algorithms, provided by the manufacturers, are given for reference.

More detailed overview of the tested algorithms in focus in this paper are presented in the following subsections.

A. Modified swing centre voltage out-of-step detection (algorithm 1)

The first protection device tested is using a modification of swing centre voltage method, that has been described in detail in [10]. The particular algorithm used in testing, is simulating two voltage vectors and monitoring the angle between the monitored vectors. [11] That way, the rotor angle difference between the two equivalent generators on Fig. 1 can be assessed. Voltage vector simulation is performed according to the following equations:

$$\underline{E}_{1\Sigma} = \underline{U} + \underline{I} \cdot \underline{Z}_{\Sigma 1} \quad (1)$$

$$\underline{E}_{2\Sigma} = \underline{U} - \underline{I} \cdot \underline{Z}_{\Sigma 2} \quad (2)$$

$$\phi = \text{atan}\left(\frac{\underline{E}_{1\Sigma}}{\underline{E}_{2\Sigma}}\right) \quad (3)$$

where

\underline{I} - measured phase current;

$\underline{E}_{1\Sigma}, \underline{E}_{2\Sigma}$ - simulated voltage vectors;

ϕ - angle difference between simulated vectors;

\underline{U} - measured phase voltage;

$\underline{Z}_{\Sigma 1}, \underline{Z}_{\Sigma 2}$ - compensating grid impedance settings depending on the power system parameters.

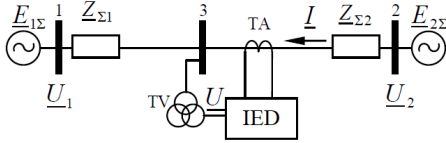


Fig. 1: Equivalent circuit of the power system. [11]

From the two simulated vectors, the protection device fixes vector $\underline{E}_{1\Sigma}$ onto 0 degrees and moves vector $\underline{E}_{2\Sigma}$ in relation to that. An out-of-step condition is detected when the angle between the two simulated voltage vectors exceeds the limit value of 55 degrees [11]. For testing, in the context of this paper, the modified two-area power system with default settings are considered sufficient.

B. Impedance based out-of-step detection (Algorithm 2)

The second tested protection device is using an impedance based out-of-step protection. There are multiple ways to implement impedance-based detection of power swings in distance relays. The impedance based out-of-step detection methods are thoroughly described in [10], [12] and [13]. The second algorithm specifically is utilizing a combination of two characteristic protection scheme in R-X plane, that is shown on Fig. 2a, and continuous impedance tracking, as shown on Fig. 2b. To detect a power swing, the device measures the rate of change of the impedance vector and its continuity.

Two impedance characteristics are built in the device. The outer characteristic is called a power swing detection range.

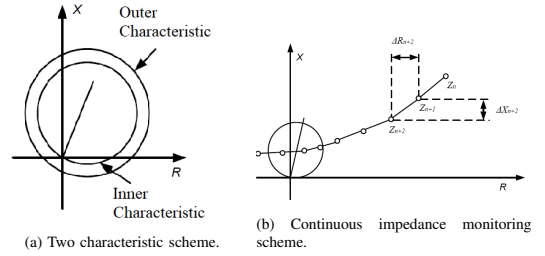


Fig. 2: Different impedance based power swing detection characteristics. (a) Concentric characteristic scheme, (b) Continuous impedance calculation scheme.

Inside the first characteristic, another characteristic called fault detection range, is built using the set largest distance protection set values. In order to detect power swings, protection measures time it takes for impedance locus to cross the power swing detection area between the two characteristics. If the internal timer expires before the impedance locus enters the fault detection zone, a power swing is declared. A more detailed overview of the method is presented in [14].

C. Direct voltage comparison out-of-step detection (Algorithm 3)

The third algorithm is using two IED's for directly comparing the voltage vectors in each end of the transmission line, using telecommunication between the two devices. The principle scheme of the protection is shown on Fig. 3a. Voltage U_A is acquired by IED A, and corresponding voltage U_B is acquired by IED B. Using telecommunication channel between the relays, the voltage data at both terminals are provided to the respective opposite terminals. Voltage phasor, obtained from IED A, is used as a reference and is fixed on x-axis of the protection characteristic. In the case of unstable swings, compared to the reference voltage U_A , the second voltage phasor U_B will appear in second or third quadrant (α -zone or β -zone) of the protection zone, that is shown on Fig. 3b. In order for the protection to issue a tripping command, the voltage vector U_B needs to be stable in each quadrant for at least 1.5 cycles to avoid tripping from transient situations. [15]

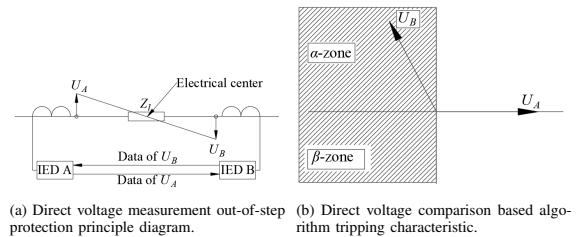


Fig. 3: Principle scheme of voltage comparison algorithm a) - measurement principle; b) Direct voltage comparison based algorithm tripping characteristic. U_A - voltage phasor measured by IED A, U_B - voltage phasor measured by IED B.

III. PROTECTION TESTING METHODOLOGY

Out-of-step tripping algorithms can be generally evaluated with two criteria: a) the amount of time needed to declare out-of-step condition after a fault is cleared, b) the percentage of correct out-of-step detections. In this paper, a test network has been built, to test and evaluate the performance of three devices utilizing the previously described different out-of-step detection algorithms. The description of the built test network and performed testing is described below.

A. Testing methodology and test model

For testing the operation of three out-of-step detection algorithms a real-time digital simulator (RTDS) is used. The principle diagram for the test setup is shown in Fig. 4. The testing is made by utilizing HiL methodology. For testing, the power system is simulated in RTDS, and from RTDS low level analogue values are sent to signal amplifiers, that thereafter amplify the signal to proper level for the IEDs. The tested IEDs provide digital outputs back to the RTDS, where the response from the IEDs is recorded.

The power system model implemented for the testing of protections is a modified two-area power system model based on [16]. The schematic of the model is shown in Fig. 5. For algorithm 1 and 2 only one IED was used at the position IED A, for algorithm 3 both IED A and IED B were used. The model consists of two areas that are interconnected with two transmission lines. Area 1 is modelled as a synchronous system equivalent with variable impedance, while Area 2 is modelled as a load, a synchronous generator and a power electronics (PE) based generation source. The PE based source is modelled as a Type 4 wind power plant, with structure and control algorithms taken from the RTDS standard library [17]. The output power of the Type 4 plant is scaled according to the different generation scenarios. At the same time, with scaling the PE based source, the apparent power of the synchronous generator in Area 2 was decreased from the initial value of 1000 MVA, by the same specific percentage of the RES % level. This is done in order to not just decrease the output of the generation, but also to decrease the total inertia in Area 2. The percentage of RES in Area 2 was varied from 0 to 70% during testing. In order to create an out-of-step condition in the test model, a prolonged three phase fault was applied on the bus in Area 2. After the clearing of the fault, Line 2 is disconnected from the system and an out-of-step condition appears on Line 1.

Testing scenarios were defined by changing the transmission line lengths between Area 1 and Area 2. The simulation cases are defined by the transmission line lengths as follows: Case S represents 10 km long transmission lines, Case M represents 100 km long transmission lines and Case L represents 200 km long transmission lines between the two modelled areas. The line lengths are chosen in order to represent short, medium and long transmission lines according to source impedance ratios. To create different grid conditions, the grid equivalent power in Area 1 and the PE based production share in Area 2 is varied. A total of three short circuit power levels of Area 1

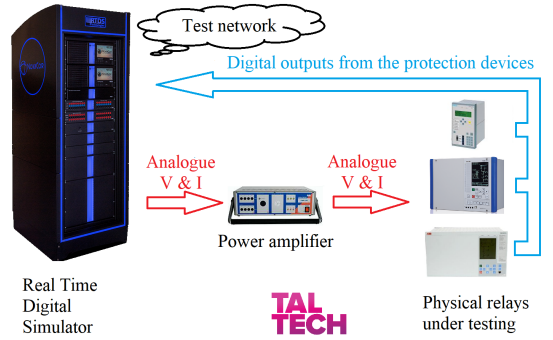


Fig. 4: Principle diagram of the hardware-in-the-loop testing with analogue outputs from the RTDS and digital outputs from the three tested protection IEDs.

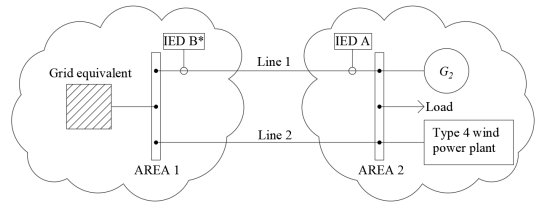


Fig. 5: Diagram of the developed two-area model for testing out-of-step protections. Area 1 is modelled as a static source, Area 2 is represented by a synchronous generator and a Type 4 wind power plant. IED B is marked with an asterisk, because the IED in that position was only used by algorithm 3, since it needs two IEDs to function.

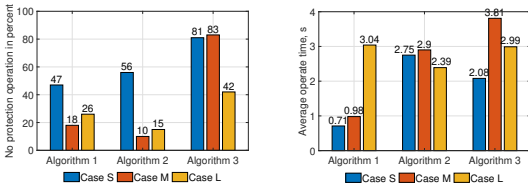
are used – infinite bus, 10 GVA and 5 GVA, which are used in each of the simulation cases.

In addition algorithm 1 (swing centre voltage) and algorithm 2 (impedance) need specific settings in order to function. For algorithm 1, compensating impedance values, that are dependent on the grid, as explained in Section II.A, are needed. Since the testing is performed with variable grid conditions, a total of nine sets of compensating impedance settings are calculated - three for each of the test cases according to the Area 1 grid strength. The settings are calculated as per manufacturer's suggestion shown in the user manual of the device. For calculation of settings the base case of fully synchronous production in Area 2 was considered.

The impedance-based algorithm requires distance protection settings for operation. Therefore, protection settings were calculated using a recommended safety margin of 1.2 times of the particular test case line reactance. The same values were applied as both the reactance and resistance setting of distance protection, because quadrilateral characteristic was used in the device [14]. Higher zone settings were not considered because the bulk power system is not modelled, hence setting higher level zones is not feasible. However, it should be noted that according to theory higher impedance zones should enhance the out-of-step protection performance.

IV. TESTING RESULTS

This section includes results of HiL testing of out-of-step protection relays from three manufacturers. During the tests various scenarios were considered. Results are presented according to short (Case S), medium (Case M) and long line (Case L) test cases. To evaluate protection performance the operation time of the tested devices was recorded. The operation times of the protection are measured from the removal of a three phase fault. When the protection operates, lower operation times are preferred, in order to minimize the risk for damaging equipment and further splitting in the network after system separation. A total of 1500 simulations were performed, and the overall results of all the simulations for missed trips are shown in Fig. 6a, and the average operation times of the protection devices are shown in Fig. 6b. A more detailed discussion and analysis of the results is given in following subsections.

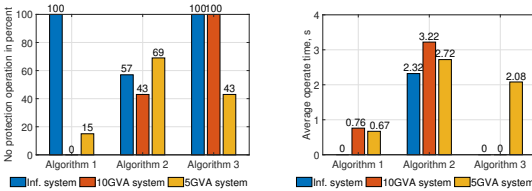


(a) Missed protection operation percent-ages. (b) Average operation times of tested algorithms.

Fig. 6: Overall results from all testing scenarios. (a) shows overall missed operation percentages and (b) shows average operating times of the test scenarios. Blue column represents simulation case S, red case M and grey case L. Test case S – 10 km long transmission lines, test case M – 100 km transmission lines and test case L – 200 km long transmission lines between Area 1 and Area 2.

A. Results for Case S

Total missed operation percentages of protection algorithms and the corresponding operation times for simulation case S are shown in Fig. 7a and Fig. 7b respectively.



(a) Detection rates of tested out-of-step protections. (b) Average operation speeds of tested protections.

Fig. 7: Total missed operations in percent and average operating times for simulation case S. Blue, red and yellow columns represent a grid equivalent with infinite, 10 GVA and 5 GVA short circuit capacity respectively.

Regarding detection rates of Algorithm 1 for simulation Case S, it can be seen that the protection does not detect the out-of-step condition with infinitely strong grid equivalent.

For weaker Area 1 grid equivalent, Algorithm 1 displays best results in detection and speed of detection, as can be observed from Fig. 7a and Fig. 7b respectively. Overall, by observing the two criteria, it can be observed that for shorter transmission lines Algorithm 1 appears to be most suitable, because this algorithm has the best detection rates, as well as fastest detection times.

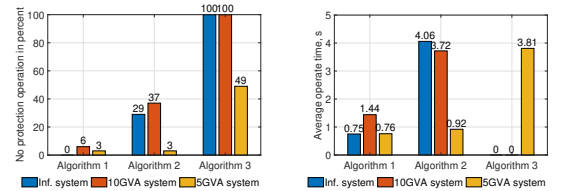
The protection relay using algorithm 2, displays difficulties detecting an out-of-step condition in all receiving system short circuit capacity levels, as shown on Fig. 7a. Overall, this algorithm did not operate for 56% of the tests in simulation case S. It had the best performance with 10 GVA short circuit power in Area 1, when the protection did not operate during 43% of the simulations. Regarding operation time of this algorithm, it can be observed in Fig. 7b, that this algorithm has the slowest operation times in this simulation case.

For the protection devices using algorithm 3, there are significant shortcomings in detecting an out-of-step condition with simulation case S. For the infinite system bus and 10 GVA system bus, the protection did not detect out-of-step conditions in any of the conducted simulations. In the case of 5 GVA system bus, the third algorithm failed to operate in 81% of the simulation cases (Fig. 6a).

B. Results for Case M

Simulation results for case M, shown in Fig. 8a and Fig. 8b, indicate that first algorithm's detection performance is improved compared to case S, however, the operation times have increased. The failed detection rate is decreased from 47% to 18% compared to simulation Case S.

The protection device using algorithm 2, is displaying the best detection performance for simulation Case M, failing to detect an out-of-step condition in case of 10% of the simulations (Fig. 6a). At the same time, this algorithm exhibits significantly slower operation times, as can be seen in Fig. 8b.



(a) Detection rates of tested out-of-step protections. (b) Average operation speeds of tested protections.

Fig. 8: Total missed operations in percent and average operating times for simulation Case M. Blue, red and yellow columns represent a grid equivalent with infinite, 10 GVA and 5 GVA short circuit capacity respectively.

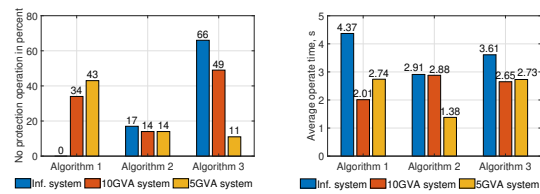
The third algorithm in simulation Case M, shows inferior detection rates compared to the other two algorithms. As with simulation case S, this algorithm does not detect out-of-step conditions with infinite strength and 10 GVA system equivalents. For the weakest system bus used for testing, the protection algorithm fails to detect an out-of-step condition in 49 % of the test cases. In addition, for this simulation case,

the third algorithm displays slowest operating times from all the test cases conducted.

C. Results for Case L

Results for simulation Case L are shown in Fig. 9a and Fig. 9b. It can be observed that none of the tested algorithms present a 100% failure to operate in this simulation case. Regarding operation speed, all tested algorithms show similar results for this simulation case. The device utilizing algorithm 1 shows inferior performance compared to case M, in both detection rates and operation speed.

The performance of the device using algorithm 2 is increased in both cases, when comparing the detection rate and operation speed to simulation case M. For this simulation case, algorithm 2 displays best overall detection rates, with a total missed operation rate of 15%.



(a) Detection rates of tested out-of-step protections. (b) Average operation speeds of tested protections.

Fig. 9: Total missed operations in percent and average operating times for simulation Case L. Blue, red and yellow columns represent a grid equivalent with infinite, 10 GVA and 5 GVA short circuit capacity respectively.

For simulation case L, the device utilizing algorithm 3 presents the best performance metrics when compared to the algorithm's performance with other cases. This indicates that Algorithm 3 is more suitable for detecting out-of-step conditions in weaker systems with longer transmission lines. It can also be observed that for the weakest system equivalent case, algorithm 3 shows the best detection rate from all the algorithms tested. However, regarding operation time, the algorithm presents slower operation than algorithm 2.

V. CONCLUSIONS

In this paper three different out-of-step relays used in power systems were tested and their performance evaluated using HiL testing methodology and a built test network model. For the analysis, the share of PE based generation, system strength and line lengths were varied in the test model, and the performance of tested relays was assessed in different grid conditions. The testing results show that:

- The tested swing centre voltage based out-of-step detection has better performance compared to others for shorter transmission lines.
- The impedance based out-of-step protection device shows better performance for medium and longer transmission lines.

- Direct voltage phasor comparison algorithm is more suitable for longer transmission lines with weaker system configurations.

Based on the testing, it can be concluded that some algorithms are more affected by changes in the grid conditions than others. From simulation results it is seen, that the performance of the algorithms is most influenced by the transmission line length. Besides the transmission line length, the swing centre voltage and impedance based algorithms were more affected by the share of renewable penetration in the grid. The receiving end system strength had least influence on the performance of the relays' performance. For the device utilizing the direct voltage comparison, the receiving system strength had a more significant influence on protection performance than the PE penetration levels. Given the conducted test results, the protection relay or algorithm planned to be used needs to be studied individually. The testing conducted in this paper confirms the need for a deeper analysis before choosing a particular algorithm for future power systems.

REFERENCES

- [1] IEEE, "Power swing and out-of-step considerations on transmission lines," 2006.
- [2] S. Horowitz and A. Phadke, *Power System Relaying*. John Wiley and Sons, 2014.
- [3] European Commission. (2019) 2030 climate & energy framework. [Online]. Available: https://ec.europa.eu/clima/policies/strategies/2030_en
- [4] A. Sauhats, A. Utans, G. Pashnin, and D. Antonovs, "Out-of-step relays testing procedure," *Scientific Journal of Riga Technical University. Power and Electrical Engineering*, vol. 28, pp. 9–14, 01 2011.
- [5] J. Megger and J. M. Gersusa, "Setting and testing of power swing blocking and out of step relays considering transient stability conditions," in *2008 IET 9th International Conference on Developments in Power System Protection (DPSP 2008)*, 2008, pp. 150–155.
- [6] Q. Verzosa, "Realistic testing of power swing blocking and out-of-step tripping functions," in *2013 66th Annual Conference for Protective Relay Engineers*, 2013, pp. 420–449.
- [7] M. Saad, A. Eltom, G. Kobet, and R. Ahmed, "Performance comparison between dual-blinder and phasor-based out-of-step detection functions using hardware-in-the loop simulation," 10 2015, pp. 1–8.
- [8] ENTSO-E, "System protection behaviour and settings during system disturbances," 2018.
- [9] N. Fischer, G. Benmouyal, D. Hou, D. Tziouvaras, and J. Byrne-Finley, "Tutorial on power swing blocking and out-of-step tripping," 2015.
- [10] D. A. Tziouvaras and D. Hou, "Out-of-step protection fundamentals and advancements," in *57th Annual Conference for Protective Relay Engineers, 2004*, 2004, pp. 282–307.
- [11] A. Sauhats, A. Svalovs, and I. Svalova, "Development of algorithms for prevention of asynchronous operation in high-voltage networks," vol. 1, 07 2003, p. 6 pp. Vol.1.
- [12] J. Blumschein, Y. Yelgin, and M. Kereit, "Proper detection and treatment of power swing to reduce the risk of blackouts," in *2008 Third International Conference on Electric Utility Deregulation and Restructuring and Power Technologies*, 2008, pp. 2440–2446.
- [13] J. Holbach, "New out of step blocking algorithm for detecting fast power swing frequencies," 04 2006, pp. 182 – 199.
- [14] Siemens AG, *SIPROTEC 4 Line Distance Protection 7SA6xx V4.7*, 2011.
- [15] Toshiba Corporation, *Line differential protection IED instruction manual*, 2017.
- [16] P. Kundur, *Power System Stability And Control*. McGraw-Hill, 1994.
- [17] RTDS, "Modelling of permanent magnet generator based wind turbine systems in the rtds," 2017.

Appendix 2

II

M. Tealane, J. Kilter, M. Popov, O. Bagleybter, and D. Klaar, "Online detection of out-of-step condition using pmu-determined system impedances," *IEEE Access*, vol. 10, pp. 14807–14818, 2022

Received January 13, 2022, accepted January 29, 2022, date of publication February 4, 2022, date of current version February 10, 2022.

Digital Object Identifier 10.1109/ACCESS.2022.3149103

Online Detection of Out-of-Step Condition Using PMU-Determined System Impedances

MARKO TEALANE¹, (Student Member, IEEE), JAKO KILTER¹, (Senior Member, IEEE),
MARJAN POPOV², (Fellow, IEEE), OLEG BAGLEYBTER³, AND DANNY KLAAR⁴

¹Department of Electrical Power Engineering and Mechatronics, Tallinn University of Technology, 19086 Tallinn, Estonia

²Faculty of EEMCS, Delft University of Technology, 2628 Delft, The Netherlands

³Grid Automation, GE Renewable, Edinburgh EH10 4QE, U.K.

⁴TenneT TSO B.V., 6812 Arnhem, The Netherlands

Corresponding author: Marjan Popov (m.popov@tudelft.nl)

This work was supported in part by the SA Archimedes Foundation Kristjan Jaak Scholarship under Grant 16-3.5/1470; in part by the Esi-Bida and ReSident Project by the Dutch Scientific Council De Nederlandse Organisatie voor Wetenschappelijk Onderzoek (NWO) under Grant 647.003.004; and in part by the Project and the Consortium Consisting of Transmission System Operator (TSO) TenneT, Distribution System Operators (DSOs) Alliander-Quiron, Stedin, Enduris, and General Electric and VSL.

ABSTRACT This paper presents a robust and adaptive out-of-step (OOS) protection algorithm, using wide-area information, that can be applied on tie-lines in observable power systems. The developed algorithm is based upon real-time computation of the system impedance and makes use of the well-known power-angle characteristic. In this way, a setting-less OOS concept in real-time environment is developed, which is applicable for tie-lines in an arbitrary power system. Furthermore, the developed protection algorithm is installed on hardware and is verified by numerous tests. The performance of the new hardware implementation is compared to the traditional impedance-based OOS protection methods. The results confirm that the proposed algorithm detects OOS conditions faster and more reliably than the traditional impedance-based solutions.

INDEX TERMS Out-of-step protection, power system transient stability, tie-lines, real-time HiL testing.

I. INTRODUCTION

Severe faults can cause large deviations of electric power supplied by the generators in electric power systems. Generator prime movers are unable to quickly react to these changes, thus the imbalance between mechanical and electric power causes generator rotor speed variations, which result in power flow fluctuations in the network. Depending on the severity of these disturbances and the applied controls, the generators can either reach a new stable equilibrium point (through the process known as a stable power swing) or lose synchronism with each other and run in an out-of-step (OOS) condition.

This OOS condition should be identified and reacted to as quickly as possible in order to limit the amount of stress on the power system components. For this purpose dedicated OOS detection relays are installed in the power grids. These are usually installed on generators and transmission tie-lines, depending on power grid topology and system dynamics. Commercially, the most widely used method for detecting OOS conditions is based on the impedance measurement

The associate editor coordinating the review of this manuscript and approving it for publication was Sarasij Das.

trajectory in order to distinguish between short circuit faults, recoverable power swings and OOS conditions [1], [2]. By adopting impedance-based method, the minimum measured impedance during the swinging period can be used to determine the electrical swing centre during oscillations. This approach, however, is sensitive to network reconfiguration as well as to load or generation changes, as predetermined settings are needed. These settings should be calculated offline, and because their determination requires extensive system studies, they cannot account for real-time changes in the network. Several other OOS detection methods are also proposed in the literature.

Table 1 presents a brief review of existing approaches in the industry and proposed methods in the literature to consistently detect an OOS condition. The advantages and certain limitations of the methods are also highlighted.

Additionally to the methods listed in the comparative table, some recent work on OOS protection based on local, bay level, measurements include [18], [19] and [20]. These methods, however, can only be applied on generator terminals, since they require direct input from generator measurements.

TABLE 1. Existing OOS protection methods and approaches in literature and industry.

Classification	Method	Advantages	Limitations
Commercially available OOS detection approaches	Impedance based detection [1] [2]	Depending on the implementation, possess ability to differentiate stable and unstable swings	Difficulties in detecting very fast swings, rigorous analysis is required for setting the blinders.
	Angle-controlled OOS protection [3]	More reliable and faster than impedance-based OOS protection	Needs predetermined settings to operate and cannot adapt to system reconfigurations.
	R-Rdot method [4]	Faster detection than impedance based detection	Requires more computing capacity than the impedance based method.
Unconventional OOS detection approaches based on local measurements	Superimposed current detection [5]	Very fast swing detection, ability to detect very fast swings.	Difficulties in detecting very slow swings, no differentiation between a stable and unstable swing
	Power-time ($P-t$) curve based detection [6] [7]	Instability is directly detected from measurements	Can only be applied directly at generator terminals. Not yet implemented in a prototype.
	Faster than real-time OOS detection [8]	Provides extremely fast OOS detection.	Requires very detailed knowledge about generator parameters, can only be applied directly at generator terminals.
Unconventional OOS detection based on wide-area information	Lyapunov function based OOS detection [9]	Method shows excellent results in OOS detection	Not yet implemented in a prototype.
	Direct angle difference measurement based OOS protection [10]	Method does not require any computation of protection settings.	Requires monitoring of all the generator buses in the network.
	Predictive OOS based on synchrophasors [11]	Enhances existing OOS protection, provides more secure and reliable operation compared to existing methods. Has been proven in a prototype installation.	OOS detection speed is not known, is not effective in detecting non-oscillatory unstable swings.
	Swing center voltage estimation and analytic geometry parameters [12]	Provides settingless OOS protection, has been prototyped in a real industrial system.	OOS detection speed is not elaborated.
	Machine learning based approaches [13] [14] [15]	Methods offer fast and accurate OOS condition detection.	The correct performance of the methods require extensive training using detailed model. Not implemented in a prototype.
	Proposed approach	The method adapts to grid condition changes in real-time, is settingless and requires only two measurement location. Provides faster and more reliable OOS detection than conventional approaches, and has been prototyped.	Not yet implemented in a real network installation.
	Fast online coherency OOS detection [16]	The method shows more reliable OOS detection than conventional solutions.	OOS detection speed is not elaborated, not yet implemented in a prototype
Voltage fluctuations based OOS detection [17]	The method shows fast detection of instability.	Not yet implemented in a prototype	

An adaptive OOS relay design and application based on wide-area measurements utilising an equal-area criterion had already been proposed more than 20 years ago [21]. This approach relies on checking the measurement data against pre-stored network, generation and load data as well as breaker and line data and requires complex offline studies to function. In more recent years, a number of effective methods have been developed for detection of OOS conditions based on wide-area information - some of the most notable work includes [22]–[24] and [25]. All these methods, however,

rely on measurements that are located directly at all of the generator terminals, or at the corresponding high-voltage terminals. This limiting factor is often overlooked and therefore makes the developed methods difficult to apply in real power systems due to the lack of coverage of PMUs in a large power system.

This paper proposes a novel approach for OOS detection and tripping based on computing the approximate angle difference between the centres of inertia on either end of a tie-line, thus relying only on two measurement locations in

a wide-area measurement system. The new method makes use of the computed system impedances at the remote ends of the tie-lines, where the algorithm is applied, to represent the whole network behind both ends of the tie-line as a two-machine equivalent system. A theoretical Last Stable Angle (*LSA*) value is found from the previously computed equivalent machine angles, which changes according to loading and grid conditions. After a disturbance takes place, the angle and its change between two equivalent sources is computed and compared to the *LSA* value.

The proposed algorithm is developed and verified in two stages - firstly by using software-in-the-loop simulations and thereafter by using real-time digital simulator to stream PMU data of a test network to a commercially available PhasorController device utilizing hardware-in-the-loop testing. The performance of the hardware implementation of the developed algorithm is firstly compared to the software implementation, and thereafter case studies for performance evaluation are performed in conjunction with two commercially available impedance-based out-of-step protection relays. The case studies performed show, that the developed algorithm operates faster and is more reliable in detecting out-of-step conditions compared to current out-of-step protection solutions.

The rest of the paper is organised as follows: Section II presents the proposed algorithm; Section III describes the methodology for testing the algorithm; Section IV shows case studies performed along with the results, and, finally, the paper ends up with meaningful conclusions being drawn.

II. PROPOSED ALGORITHM

A. EQUIVALENT SYSTEM

The idea behind the developed algorithm is that the bulk system can be simplified by using the assumption made in [26]; a multi-machine system can be separated into two groups around a tie-line. The simplified two-machine - system constructed around the observed tie-line can be reduced to a single machine infinite bus (SMIB) equivalent system with the parameters δ , ω_s , M , P_m and P_e . The reduction process is described in detail in [26]. With the classical representation, the generator dynamics can be represented by the swing equation (1),

$$\frac{M}{\omega_s} \frac{d^2 \delta}{dt^2} = P_m - P_e(\delta) \quad (1)$$

where M - inertia constant of the equivalent machine; ω_s - rotor speed of the generator; δ - internal voltage angle of the generator; P_m - mechanical input power of the generator; P_e - electrical output power of the generator.

The electrical output power of the generator depends on the angle difference between the receiving system voltage phasor and the generator internal voltage phasor, the magnitudes of voltage phasors and the total system impedance between generator and the system. The generator's electrical output

power can be represented by equation (2),

$$P_e(\delta) = \frac{|E_1||E_2|}{x_{tot}} \sin \delta \quad (2)$$

where $|E_1|$, $|E_2|$ - are the equivalent internal voltage magnitudes of the machines; x_{tot} - is total reactance between the two sources, and δ - is angle difference of the equivalent phasors.

By using the power-angle curve, the generator stability can be determined. The stability is directly linked to the internal angle differences of the two equivalent sources. On the power-angle characteristic, two operating points can be fixed by generator preloading and the electrical power curve as shown in Fig. 1a. The operating point located in the first half of the characteristic is a stable operating point. According to the Equal Area Criterion, the maximum angle difference for a recoverable swing cannot be greater than the second operating point, though it may be smaller. Further increase of the angle difference beyond *LSA* will definitively result in an unstable generator operation. Therefore, the *LSA* point is critical to distinguish between a stable and unstable swing. In order to assess this *LSA* point, the impedances of the equivalent sources must be known.

B. EQUIVALENT SYSTEM IMPEDANCE COMPUTATION

The concept of the determination of the system's actual strength or the Thevenin impedance of a power network based on local measurements and small disturbances (such as load changes) was explored in [27]. This method describes the estimation of short-circuit impedance for a particular node in a power system. The Thevenin equivalent of the system Z_{eq} , which is seen at the monitored location, is calculated from the recorded PMU voltage and current measurements. The scheme of impedance computation is illustrated in Fig. 1b, where the measured voltage and current phasors at the bus are denoted by \underline{V} and \underline{I} .

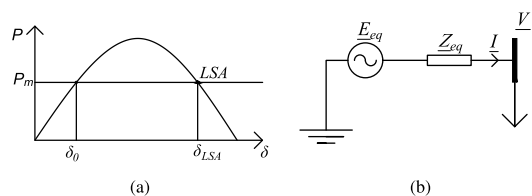


FIGURE 1. (a) Power-angle curve constructed from calculated values, with Last Stable angle point denoted as *LSA*. (b) Equivalent impedance computation scheme illustration.

In order to find the upstream system impedance from the locally measured quantities, two assumptions should be taken into account: 1) the downstream load is volatile; 2) during this variation the system remains constant. Voltage $\underline{V}(t)$ and current $\underline{I}(t)$ are measured and sampled at instants t_1 and t_2 , which correspond to the pre-and post-disturbance values in the measured signals. Hence, the equivalent impedance

Z_{eq} can be found by using the following equation [27]:

$$Z_{eq} = -\frac{V(t_2) - V(t_1)}{I(t_2) - I(t_1)} = -\frac{\Delta V}{\Delta I} \quad (3)$$

The delta value limits to compute the system impedance can be set empirically [27]. Alternatively, in order to improve the accuracy and the noise reduction of the measurements, an adaptive threshold can be used, as proposed in [28]. In this paper, the threshold values for detecting a disturbance are set empirically to 1 % of the primary measurement quantity, so that the impedance computation is not triggered by the ambient noise in the measurements. In addition, the impedance computation is vulnerable to phasor drift due to off-nominal system frequency, in which these can shift the angle during the time pre- and post-disturbance quantity sampling takes place. This problem, however, can be overcome by compensating the phasor drift as suggested in [29]. The sampling of voltage and current components is shown in Fig. 2b and Fig. 2a respectively, which, after sampling, are used to compute Z_{eq} according to Eq. (5).

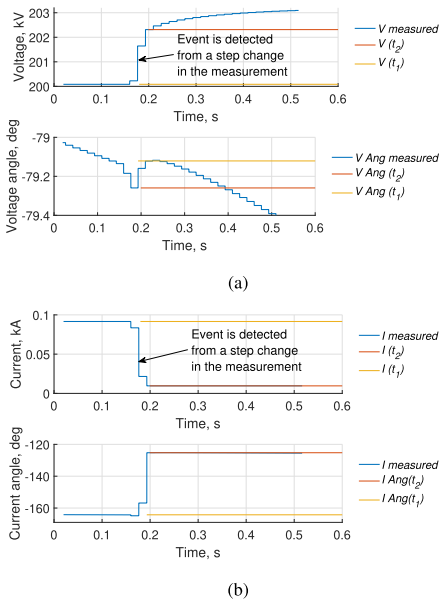


FIGURE 2. Voltage magnitude and angle sampling (a) and current magnitude and angle sampling (b) in the case of a step change. The pre-disturbance samples are denoted by t_1 and post-disturbance values by t_2 .

It can be concluded that the computation of system impedance is only directly applicable in the case of a radial network, since in a meshed network all sources contribute to the actual changes in currents and voltages. Therefore, the total change in current and voltage behind the measured tie-line cannot be observed from one location. The same concept, however, can still be used to determine the system equivalent by making use of the superposition criterion, and utilising two measurement points.

Hence, for the system impedance computation of meshed networks, this method requires current measurement at two feeders in the same substation. An illustration of this is shown in Fig. 3, where one PMU measures bus voltage (V_1), the currents of the tie-line (I_{tl}) and, additionally, a load feeder (L_{r1}), in which a step change in load may occur. In the figure a step change in a load feeder is caused by a reactor, although a capacitor bank, a filter or other volatile load could be used. A second PMU measures the same feeders and parameters at the other end of the tie-line.

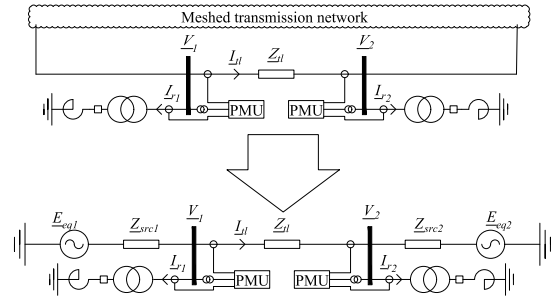


FIGURE 3. Principle scheme for system impedance estimation on meshed networks.

Whenever a step change in the measured current or voltage occurs, e.g. due to switching of the reactor in the load feeder, the system impedance is determined according to (3). Hence, by applying the superposition criterion, the system equivalent impedance Z_{src1} behind the measured tie-line at bus 1 in Fig. 3 can be calculated using the proportional change of current in the measured load feeder and the change of the tie-line current as follows:

The approach proposed in (4) is used as a basis to compute the system impedance behind the tie-line, which is needed to determine the LSA threshold. Protection operation and OOS condition identification are based on that determined concept.

$$Z_{src1} = -\frac{V_1(t_2) - V_1(t_1)}{I_{r1}(t_2) - I_{r1}(t_1)} \cdot \frac{(I_{r1}(t_1) - I_{r1}(t_2))}{(I_{r1}(t_1) - I_{r1}(t_2)) - (I_{tl}(t_1) - I_{tl}(t_2))} = -\frac{\Delta V_1}{\Delta I_{r1}} \frac{\Delta I_{r1}}{\Delta I_{r1} - \Delta I_{tl}} = -\frac{\Delta V_1}{\Delta I_{r1} - \Delta I_{tl}} \quad (4)$$

C. DEVELOPING OUT-OF-STEP PROTECTION CONCEPT

The proposed OOS protection solution is based on the change of computed voltage phasors of the two equivalent sources behind the computed impedances located at the remote ends of the observed tie-lines. The required equivalent system voltage is accordingly computed at both ends of the tie-line as follows:

$$\begin{aligned} E_{eq1} &= Z_{eq1} \cdot I_{tl} + V_1 \\ E_{eq2} &= Z_{eq2} \cdot I_{tl} + V_2 \end{aligned} \quad (5)$$

For the equivalent system depicted in Fig. 3, the angle difference between the two equivalent generator voltages is illustrated in Fig. 4.

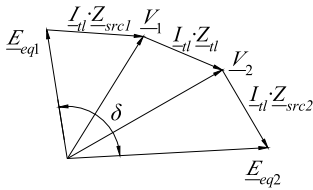


FIGURE 4. Equivalent phasor diagram constructed from computed equivalent system impedances and measured quantities.

In this way, from the angle difference the power-angle curve is then determined, and the LSA point (noted as δ_{LSA} on Fig. 1) is computed. The LSA point is fixed by using the angle difference of the equivalent vectors as $\pi - \delta_0$. This value is continuously recalculated by using the measurement values and the previously obtained equivalent impedances.

During an OOS condition, the angle difference between the two equivalent source voltages increases over the LSA point. The protection will declare an OOS condition when the following conditions are met:

$$\left\{ \begin{array}{ll} \delta > \delta_{LSA} & \text{for two consecutive measurements} \\ \frac{d\delta}{dt} > 0 & \text{for two consecutive measurements} \\ V_1 > 0.5p.u. \\ V_2 > 0.5p.u. \\ \frac{d\delta}{dt} < 20\pi \frac{rad}{s} & \text{for two consecutive measurements} \end{array} \right.$$

The first two criteria indicate that the angle difference exceeded the LSA and is continuing to increase. The last three criteria, are used as a safety feature to block the protection from maloperation when a short-circuit fault occurs.

Voltage thresholds with the value of 0.5 p.u. have been set to verify whether the tie-line is energised and no fault is present on the line. The $\frac{d\delta}{dt}$ threshold acts as an additional fault-detection mechanism, and prevents the protection operation due to oscillations with high frequency. During a fault occurrence there will be a high step change of the computed angle value, which might exceed the LSA for the duration of the fault. Nevertheless, the protection must not operate during a fault. A derivative setting value of $20\pi \frac{rad}{s}$, in this case with a 60 Hz power system, enables the protection to detect power system oscillations with the frequency of up to 10 Hz. These blocking criteria can be adjusted freely if more protection sensitivity or security are required. When any of the blocking criteria of the protection are fulfilled, the OOS algorithm operation will be blocked for 200 ms. If thereafter any of the criteria are still fulfilled, the blocking will be applied until the drop-off of the criterion.

The LSA point is limited to a minimum of 90 degrees, in order to avoid it being set in the first half of the

power-angle characteristic. At the same time, the LSA point is limited to a maximum of 130 degrees. This is important, because the protection should be still operational during low or no load current in the observed tie-line before the LSA value is sampled.

D. HARDWARE IMPLEMENTATION OF THE DEVELOPED ALGORITHM

In order to compare the developed algorithm’s performance to already existing commercial solutions, it was adapted and installed on external hardware using a commercially available Phasor Controller (PhC) [30]. The algorithm is divided into four main parts and the structure of the implemented algorithm on hardware was organised as shown in Fig. 5.

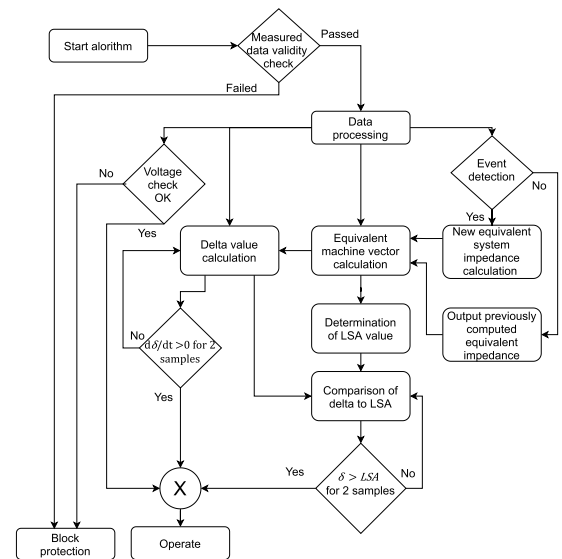


FIGURE 5. Principle diagram of the developed algorithm in industrial controller.

Valid PMU measurement signals must be collected from both measurement points in the network in order for the algorithm to operate. The data validity is checked and handled by the PhC, and the check is performed before the data is going to be processed. If the measured data does not pass the validity check, meaning the data is not time synchronized or is missing, then the protection algorithm is blocked. When the validity check is passed, then the voltage values of the measurement points are checked and compared to the threshold values in order to detect short-circuit faults. If any measurement point has a lower voltage value than the specified threshold, the protection is blocked for the predetermined time, until the voltage has been restored in the network. This is done in order to avoid maloperations during short-circuit faults in the network, when the PMU measurements are affected by fault conditions and do not represent the electromechanical behavior of the grid.

At the same time, the data measurements provide input to the event detection for impedance calculation. Upon detecting a step change in the measurement quantities, the event detection block stores the measured values, which are then used to compute the equivalent impedance needed for the equivalent voltage vector computation as shown in (2). When no event is detected in the measurement data, the event detection block will output the previously computed equivalent impedance values to the vector computation.

By utilizing the measured voltage vectors and currents, the equivalent machine vectors of the centres of inertia are computed according to (5). Using the computed equivalent machine vectors, the *LSA* value is fixed every time a new equivalent impedance value is provided. The *LSA* value is computed using the difference in angular value of the two computed equivalent machine vectors according to power-angle characteristic as $\pi - \delta$. In parallel, the current δ value is being computed continuously and compared against the determined threshold value. When the δ value exceeds the determined *LSA* value for more than two samples, and the derivative of δ has been positive for the past two samples, the protection sends a trip command.

III. TESTING METHODOLOGY AND TEST SETUP

The performance of the algorithm is investigated by applying it in the IEEE 39 bus network model. The network is modified by adding generic grid-following wind farms (W1 - W5) at some buses. The model used for the power plants is described in [31]. In this way, the developed solution can be tested for different grid conditions. The modified test network is shown in Fig. 6. Two different test locations are chosen to show the developed solution’s suitability for arbitrarily chosen tie-lines. The first test location is circled in red and shown as Case A, and the other is circled in blue and is denoted as Case B. Case A is an example to observe power swings between two areas, whilst Case B demonstrates power swings in a single machine system connected to an infinite bus system.

For both locations, two tie-lines were observed in order to see the proposed algorithm’s behaviour for various grid conditions. For Case A, the protection was tested for the lines between buses 14-15 and 16-17. To create an OOS condition, a three phase short circuit is made on bus 16. The fault is cleared by disconnecting one of the transmission lines emanating from bus 16. For Case B, the transmission lines under observation are between buses 26-29 and 28-29. Power swings are created by a three-phase short circuit applied on bus 29. The fault is cleared by disconnecting one of the two tie-lines connected to this bus. This contingency causes power swings along the remaining transmission lines.

In addition, the proposed algorithm is installed on a PhC and tested in parallel with two physical relays. Both relays incorporate an impedance based OOS algorithm and are set up to trip on the way in (TOWI) and trip on the way out (TOWO) of the configured impedance characteristic. The settings of the protection devices are obtained according to

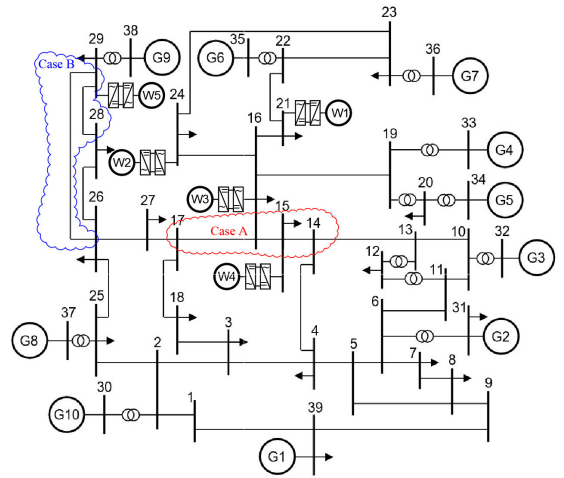


FIGURE 6. Modified IEEE 39 bus network with added type 4 wind farms. Red marks Case A testing location and blue Case B testing location, wind farms are added to buses 21, 15, 25, 16 and 29.

the manufacturer’s guidelines as explained in the user manuals of the relays’; the settings are calculated by using a base case of fully synchronous system [32], [33]. The protective relays, together with the PhC, are tested by applying hardware-in-the-loop (HIL) tests, and the results obtained are compared to the applied concept described in Section II. An illustration of the experimental setup is provided in Fig. 7. The PhC device, where the proposed algorithm is implemented, receives measurement data over the network according to IEEE C37.118 standard. Different data rates would have an effect on the decision time of the algorithm, since the algorithm’s criteria are linked to consecutive measurements. Therefore, the slower the data rate, the slower the decision time. For uniformity throughout the paper, the data rate used for PMU data for all the conducted tests is 60 Hz. The PhC provides feedback about operation and measured values back to the Real-Time Digital Simulator using IEC61850 GOOSE messages. The protection relays, situated on lines 16-17, 15-14, and at the line remote ends near bus 29 for cases A and B respectively, receive analogue signals through signal amplifiers connected to the simulator. Protection relay output signals are provided as digital input signals to the simulator.

In order to test the protections for various grid conditions, the output power of the windfarms is scaled up while simultaneously decreasing the synchronous generation capacity. In Case A, for a specific renewable energy penetration scenario (RES %), all four windfarms (denoted as W1 - W4 on Fig. 6) in the network area provide the specific percentage of the base case synchronous generation output of the four generators (denoted as G4, G5, G6 and G7) in the area. At the same time, the apparent power of these generators is decreased from the initial value of 1000 MVA by the same specific percentage of the RES % level. This is not only to

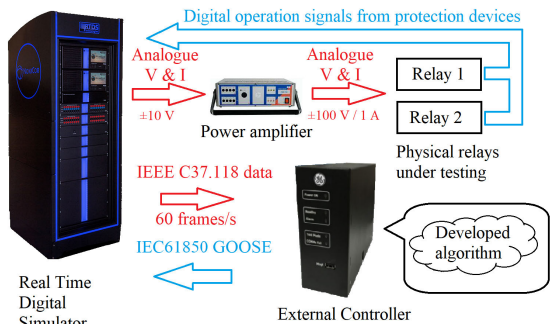


FIGURE 7. Experimental setup for OOS protection testing using physical hardware.

decrease the output of the generation, but also to decrease the system inertia. For Case B, the scaling is performed for one generator (G9) and one windfarm (W5). Besides this, each test case is repeated five times to verify that the algorithm detects OOS conditions.

IV. CASE STUDIES

A. IMPEDANCE COMPUTATION

For testing and verifying the impedance computation part of the developed algorithm, a simple system with variable system impedances on either side of the transmission line, as shown in Fig. 8, was built. One of the impedance buses is chosen to be close to the source, representing a generator bus, whilst the other is located in the middle of the system to represent an arbitrary node in a system. The test system nominal voltage is 345 kV and with a frequency of 60 Hz. To test the accuracy of the system impedance computation, the two system impedances are varied between 5 Ohm and 100 Ohm.

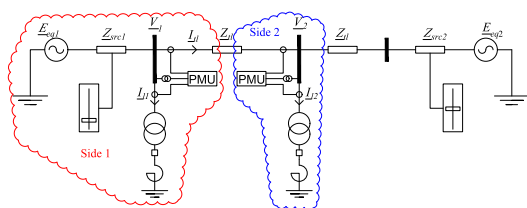


FIGURE 8. Test network for testing impedance computation of the developed algorithm.

In this work, the RTDS library models of the PMUs are used [34]. For side 1 in red in Fig. 8, the average absolute impedance computation error is 0.3% with a standard deviation of 0.55%. Therefore, this impedance computation is considered reliable. For side 2, the average absolute impedance computation error is 4.2% with a standard deviation of 2.15%. The error of the computed impedance depends on system impedances and is shown in Fig. 9. It can be noted that the error increases when the system impedance increases. The impedance behind the measurement point on Side 2 has a

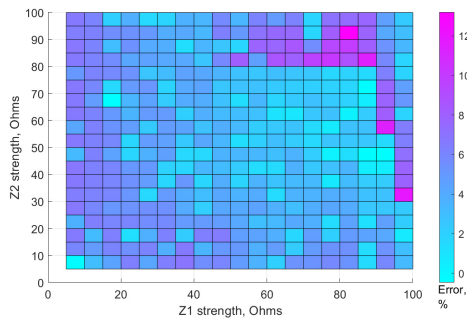


FIGURE 9. Absolute error in the impedance computation on Side 2 of the test network related to the system impedances.

greater influence on the system impedance computation. The maximum error of the impedance computation is computed as 13.2%.

B. TESTING RESULTS FOR THE DEVELOPED ALGORITHM

The lab environment network latency from the RTDS to the industrial controller was measured to be under 1 ms. However, in order to represent a more realistic scenario, a Phasor Data Concentrator (PDC) Wait Time setting of 100 ms was implemented in the PhC, which is representative of real-world PMU applications. Normally, the PDC Wait Time setting means that in order to align the measurement data from different PMUs in the network, the controller will wait for a period of time until the measurements arrive. Thereafter, the processing of the measurements will begin in the logic built inside the device.

In order to verify the security of the developed algorithm, the δ value and generators' reaction for a five-cycle fault on bus 16, followed by the disconnection of line between bus 16 and 17, is shown in Fig. 10. The proposed OOS protection is demonstrated on a transmission line between buses 15 and 14. The upper figure shows the generator angle, and it can be seen that the fault produces a stable swing with stable generator angles. For the lower figure, the computed δ values of the RTDS and hardware implementations are shown. From the δ value plot, it can be observed that the value computed in the PhC is lagging behind the RTDS model application for around 110 ms. This is due to the applied PDC Wait Time setting and processing of the controller logic itself.

Fig. 11 shows the performance of the developed algorithm in RTDS and in the PhC for a six-cycle fault occurring on bus 16. This fault leads to an unstable swing causing generators 4 - 7 to go out-of-step with the rest of the system. This can clearly be seen in the upper figure, where the generator rotor angles are shown. In the lower figure, the computed δ values are shown for both RTDS and hardware implementation of the proposed algorithm. It is observed that due to the unstable swing in the network, the computed δ value exceeds the algorithm's predetermined LSA threshold and keeps increasing. This results in a trip command from the developed algorithm.

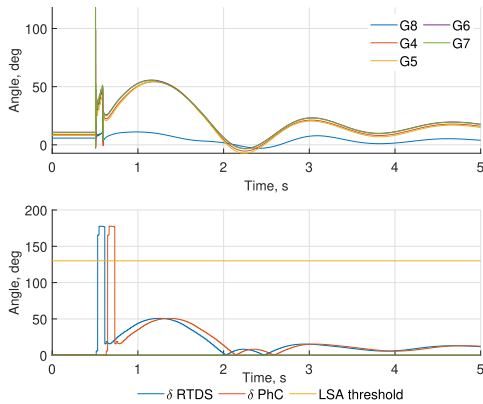


FIGURE 10. Generator angle response and δ value calculation response to a five-cycle long fault at bus 16.

The operation signals are represented by a green dashed line for RTDS implementation of the algorithm, and a magenta dashed line for the physical controller implementation. It can also be noted that the time shift of δ computation between the RTDS and hardware implementation of the algorithm is 110 ms.

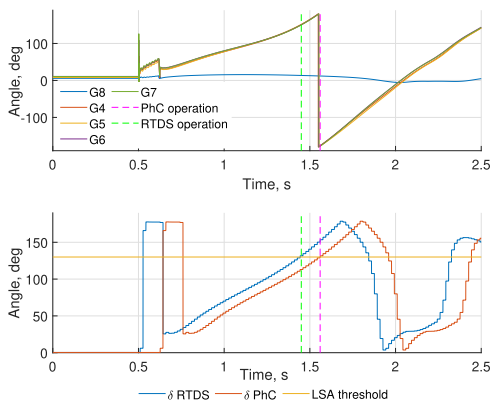


FIGURE 11. Generator angle response and δ value calculation response to a six-cycle long fault at bus 16.

OOS tripping speed and security can generally be evaluated by two criteria: a) the amount of time needed to report OOS condition after a fault is cleared, and b) the percentage of correct OOS detections. Comparisons of these two metrics between the RTDS and the hardware application of the proposed algorithm are shown in Fig. 12a and Fig. 12b respectively.

When looking at the average operation time in Fig. 12a, it can be seen that the hardware implementation shows higher operation times, than the RTDS implementation of the proposed algorithm. For Case A, the RTDS software implementation shows an average operation time of 1.14 s, whilst the controller implementation shows an average operation time of 1.32 s. This means that the controller shows an increase

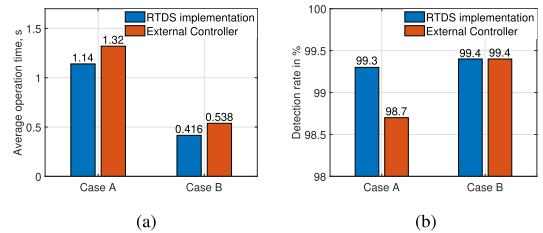


FIGURE 12. Comparisons of proposed algorithm performances: (a) Comparison of average operation times, (b) Comparison of percentage of OOS conditions detected.

of 180 ms in operating time. For Case B, the RTDS implementation shows an average operation time of 0.416 s, and the hardware implementation shows an average operating time of 0.538 s. Therefore the hardware implementation has, on average, 122 ms slower operating time for Case B. This is expected behavior due to the delays implemented in the PhC and logic processing of the developed algorithm in the controller.

In Fig. 12b, the detection rates of all of the OOS conditions for the performed tests of the algorithm are shown. It can be seen that there is a 0.6% difference in the detection rates of RTDS and hardware implementation of the proposed algorithm for the performed tests in Case A. For Case B no difference in detection rates between the hardware and software implementation has been identified. Therefore, based on the performed analysis, it is safe to say that the hardware implementation of the proposed solution is successful and reliable.

C. ALGORITHM RESPONSE FOR GRID EVENTS

The PhC implementation of the developed algorithm has been tested for various grid events. Two specific cases have been chosen and are explained in more detail. For this, the algorithm is installed on the IEEE 39 bus test system's line 14-15 and the algorithm's behavior for two faults is shown - a single-line to ground fault on the protected line and a two-phase fault outside of the protected line.

The algorithm's response for a single-line to ground fault on the protected line 14-15, and the subsequent one pole open condition, is shown in Fig. 13a. In the figure, the signals regarding the algorithm response is displayed on the first graph, and the second graph displays the computed δ value in the algorithm. The actual values during the event in the power system are shown in Fig. 13b, where the instantaneous current values from either end of the protected line can be seen on the first two graphs, and the last graph displays the generator rotor angle values. It can be seen from the instantaneous current values in the figure, that there is a single-phase fault on the transmission line, followed by a single-pole trip, which is thereafter reclosed after 0.4 seconds. From the protection reaction, it can be observed, that in both ends of the protected line the algorithm registers an event, however, following the event no blocking or operation signals are activated, therefore

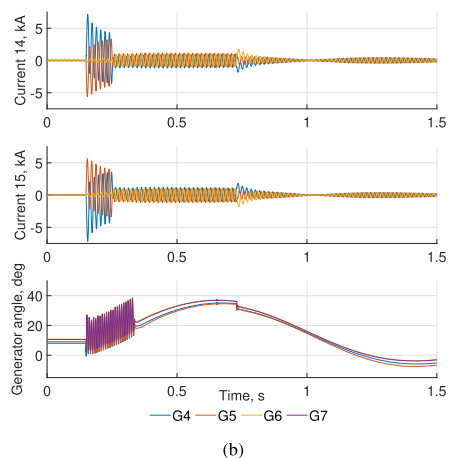
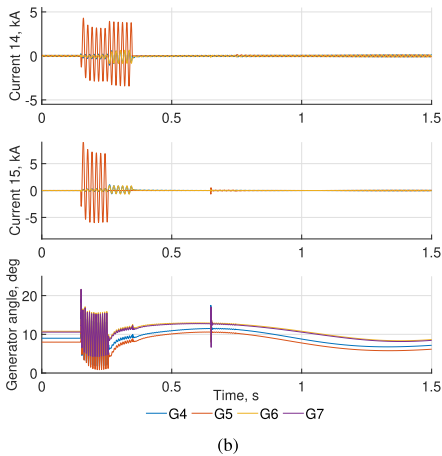
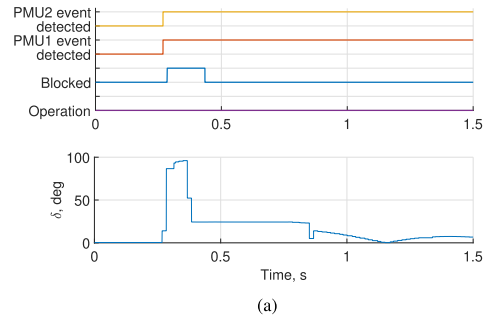
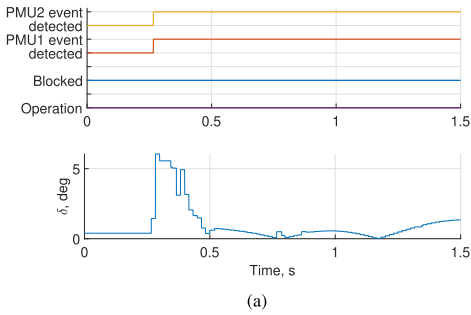


FIGURE 13. Algorithm response and measurements in the case of a single-line to ground fault on the protected line. (a) shows the signals regarding the developed algorithm response and the computed δ value by the algorithm, (b) shows the instantaneous measurements from either end of the transmission line, where the protection has been installed, and the generator rotor angles in the system.

FIGURE 14. Algorithm response and measurements in the case of an external two-phase fault. (a) shows the signals regarding the developed algorithm response and the computed δ value by the algorithm, (b) shows the instantaneous measurements from either end of the transmission line, where the protection has been installed, and the generator rotor angles in the system.

it can be concluded, that the developed algorithm shows stable operation during an internal single-phase fault, and during one pole open condition.

The algorithm’s response to an external two-phase fault is shown in Fig. 14a. In this case, the protection is still installed on transmission line between buses 14-15, and the fault takes place on line 15-16, after which the faulted line is tripped and reclosed 0.4 seconds after tripping. In the figure, the signals related to the algorithm response is displayed on the first graph, and the second graph displays the computed δ value in the power system during the event in the power system are shown in Fig. 14b, where the first two graphs show the instantaneous current values from either end of the protected line, and the last part of the graph displays the generator rotor angle values. Looking at the protection response, it can be seen, that, in a similar manner to a single-phase fault, event is picked up on both ends of the protected line. In this case, however, due to the fault type and location, the computed angular difference has a large jump, that causes the algorithm to be blocked from operation during a fault condition as explained in Section IIc. The computed angle

value stabilizes to a constant value after the fault has been cleared, and the blocking of the protection function drops off. The algorithm does not issue an operation command, therefore it can be concluded, that the developed algorithm shows stable operation during external faults.

D. COMPARISON WITH IMPEDANCE PROTECTION FOR CASE A

The test results of protection operation times for Case A are shown in Fig. 15a and Fig. 15b. The operation times shown in these figures are the times the protection needs to provide a trip command starting from the removal of the fault. The operation time of “0” means that the protection did not provide an OOS tripping command for a duration of five seconds after fault initiation; hence, the simulation was terminated without protection trip for all of the five conducted tests at that RES % scenario. Fig. 15a shows the operation times for a case study on tie-line between buses 14 and 15, which represents a longer line between the two system parts. It can be observed that when increasing RES penetration in one of the areas, the difference between the protection operations is narrowing.

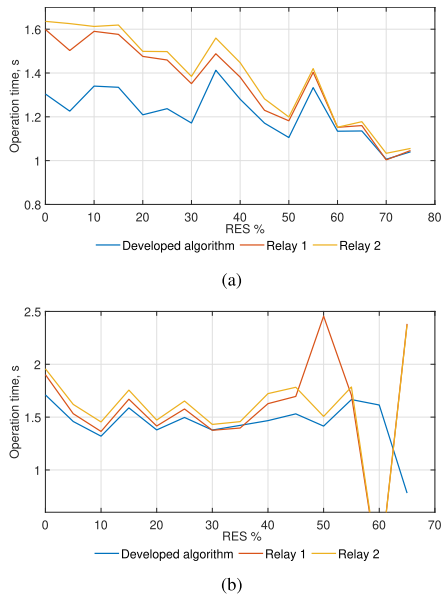


FIGURE 15. OOS tripping times of protection devices for Case A. (a) represents case study with a longer line (Line 14-15) between two systems and (b) represents a short line (Line 16-17) between two systems.

However, for all situations the developed algorithm in hardware implementation performs better, as faster OOS detection times are obtained than from the traditional impedance based protection.

For the shorter line testing results, as shown in Fig. 15b, the new method has faster OOS detection times than the traditional protections for almost all of the observed RES % scenarios. It can also be seen that the tested impedance based relays do not operate at all for RES penetration levels from 55% to 60%. For 65% RES penetration both relays operated only on the second unstable swing, which resulted in the significantly delayed operation.

E. COMPARISON WITH IMPEDANCE PROTECTION FOR CASE B

The combined protection operations for both tested lines for Case B (SMIB) are shown in Fig. 16a and in Fig. 16b. Fig. 16a shows the results of the protection operating times versus the renewable energy penetration when an OOS condition was created on a longer tie-line. The blue line shows the operation times of the developed algorithm’s hardware implementation, whilst the red and yellow lines show the operation times of physical relays. From this figure, it can be seen that the developed solution and Relay 2 have very similar operating times whilst Relay 1 operates around 200 ms slower. It can also be observed that Relay 2 does not detect the OOS condition between 65% and 75% of renewable penetration. In addition, starting from RES penetration of 60%, Relay 1 issues a tripping command not from OOS protection, but rather from the distance protection element, which results

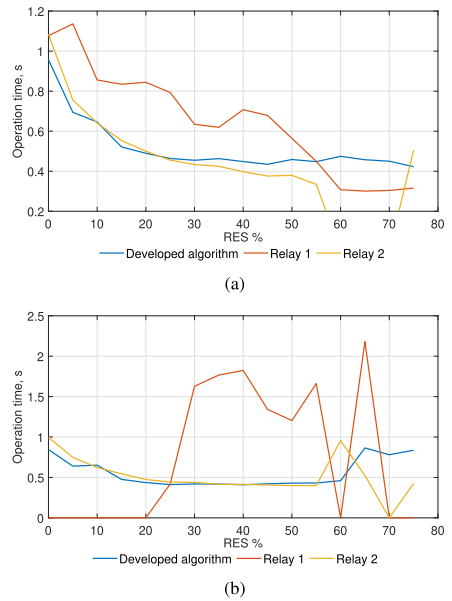


FIGURE 16. OOS tripping times of protection devices for Case B. (a) represents a long line (Line 26-29) between the machine and the system, (b) represents a short line (Line 28-29) between the machine and the system.

in a very short operation time. This is an obvious case of maloperation of the distance protection element, which may be caused by an incorrect configuration of the Power Swing Blocking element.

Fig. 16b shows the protection operating times versus RES % penetration for the case of OOS condition on the shorter tie-line. It can be seen that, as before, the developed solution and Relay 2 have very similar operating times for the tested renewable penetration levels, except for very high penetration scenarios. It should be noted that in this case Relay 1 (shown in red) scores the worst detection rate of the OOS condition, as it only operated consistently for RES penetration between 25 and 50%. The other physical relay did not experience similar difficulties in detecting an OOS condition; only failing to detect OOS at 75% RES penetration level.

V. CONCLUSION

The paper introduces a novel robust and adaptive OOS protection algorithm for tie-lines based on PMU-determined system impedances. The algorithm successfully adapts to system condition changes by utilising on-line network impedance computation, and is based only upon two measurement points in the network. Hence, it is suitable to be applied on arbitrary tie-lines in every power system topology, where OOS conditions can occur. Case studies are carried out in SMIB, and IEEE39 bus test network, which demonstrate the effectiveness of the developed algorithm. A prototype of the algorithm is designed and validated in real-time using RTDS and an external industrial controller. For the HiL testing of the

prototype a PDC Waiting Time, or latency, of 100 ms has been used, to simulate real-world like conditions. The robustness and the efficiency of the developed algorithm are verified and compared against commercial OOS relays by conducting numerous tests for different network conditions including different penetration levels of renewable generation. The conducted research shows advantages over the existing methods, namely:

- For all studied cases, the proposed algorithm provides faster operation (up to 200 ms when implemented on actual hardware) compared to the existing impedance-based OOS methods which are currently used in commercially available relays.
- The proposed algorithm provides more reliable OOS detection than traditional impedance based solutions.
- The algorithm is very lightweight and needs little processing power, which offers possibility to be installed in already existing Phasor Data Concentrators or programmable logic devices.
- The algorithm does not require specific settings, therefore, no extensive offline studies of the power system are needed.

REFERENCES

- [1] D. A. Tziouvaras and D. Hou, "Out-of-step protection fundamentals and advancements," in *Proc. 57th Annu. Conf. Protective Relay Eng.*, 2004, pp. 282–307.
- [2] J. Blumschein, Y. Yelgin, and M. Kereit, "Blackout prevention by power swing detection and out-of-step protection," *J. Power Energy Eng.*, vol. 2, no. 4, pp. 694–703, 2014.
- [3] A. Sauhats, A. Utans, and E. Biela-Dalidovicha, "Equal area criterion and angle control-based out-of-step protection," in *Proc. IEEE 58th Int. Sci. Conf. Power Electr. Eng. Riga Tech. Univ. (RTUCON)*, Oct. 2017, pp. 1–6.
- [4] C. W. Taylor, J. M. Haner, L. A. Hill, W. A. Mittelstadt, and R. L. Cresap, "A new out-of-step relay with rate of change of apparent resistance augmentation," *IEEE Trans. Power App. Syst.*, vol. PAS-102, no. 3, pp. 631–639, Mar. 1983.
- [5] *MiCOM O40 Agile P543/P545 Technical manual Ver92M*, Schneider Electr., Rueil-Malmaison, France, 2021.
- [6] S. Paudyal, R. Gokaraju, M. S. Sachdev, and S. Cheng, "Out-of-step detection using energy equilibrium criterion in time domain," *Electr. Power Compon. Syst.*, vol. 37, no. 7, pp. 714–739, Jun. 2009.
- [7] S. Paudyal, G. Ramakrishna, and M. S. Sachdev, "Application of equal area criterion conditions in the time domain for out-of-step protection," *IEEE Trans. Power Del.*, vol. 25, no. 2, pp. 600–609, Apr. 2010.
- [8] M. Abedini, M. Davarpanah, M. Sanaye-Pasand, S. M. Hashemi, and R. Irvani, "Generator out-of-step prediction based on faster-than-real-time analysis: Concepts and applications," *IEEE Trans. Power Syst.*, vol. 33, no. 4, pp. 4563–4573, Jul. 2018.
- [9] K. Sreenivasachar, "Out-of-step detection on transmission lines using apparent impedance differential method," *IEEE Trans. Power Del.*, early access, Nov. 13, 2021, doi: 10.1109/TPWRD.2021.3125525.
- [10] P. Regulski, W. Rebizant, M. Kereit, and H.-J. Herrmann, "PMU-based generator out-of-step protection," *IFAC-PapersOnLine*, vol. 51, no. 28, pp. 79–84, 2018.
- [11] T. D. Duong, S. D'Arco, and A. Holdyk, "A method for predictive out-of-step tripping based on synchrophasors," in *Proc. 15th Int. Conf. Develop. Power Syst. Protection (DPSP)*, 2020, pp. 1–6.
- [12] J. R. Camarillo-Penaranda, D. Celeita, M. Gutierrez, M. Toro, and G. Ramos, "An approach for out-of-step protection based on swing center voltage estimation and analytic geometry parameters," *IEEE Trans. Ind. Appl.*, vol. 56, no. 3, pp. 2402–2408, May 2020.
- [13] N. G. Chothani, B. R. Bhalja, and U. B. Parikh, "New support vector machine-based digital relaying scheme for discrimination between power swing and fault," *IET Gener. Transmiss. Distrib.*, vol. 8, no. 1, pp. 17–25, Jan. 2014.
- [14] M. R. Aghamohammadi and M. Abedi, "DT based intelligent predictor for out of step condition of generator by using PMU data," *Int. J. Electr. Power Energy Syst.*, vol. 99, pp. 95–106, Jul. 2018. [Online]. Available: <https://www.sciencedirect.com/science/article/pii/S0142061517321397>
- [15] E. A. Frimpong, P. Y. Okyere, and J. Asumadu, "On-line determination of transient stability status using MLPNN," in *Proc. IEEE PES PowerAfrica*, Jun. 2017, pp. 23–27.
- [16] D. Fan and V. Centeno, "Adaptive out-of-step protection schemes based on synchrophasors," in *Proc. IEEE PES Gen. Meeting|Conf. Exposit.*, Jul. 2014, pp. 1–5.
- [17] K. Shimizu and A. Ishigame, "Novel transient stability assessment using post-disturbance voltage fluctuations," in *Proc. Int. Conf. Smart Grids Energy Syst. (SGES)*, Nov. 2020, pp. 12–17.
- [18] M. R. Nasab and H. Yaghobi, "A real-time out-of-step protection strategy based on instantaneous active power deviation," *IEEE Trans. Power Del.*, vol. 36, no. 6, pp. 3590–3600, Dec. 2021.
- [19] J. P. Desai and V. H. Makwana, "Phasor measurement unit incorporated adaptive out-of-step protection of synchronous generator," *J. Modern Power Syst. Clean Energy*, vol. 9, no. 5, pp. 1032–1042, 2021.
- [20] B. Deshmukh, S. Biswal, and D. K. Lal, "Synchronous generator out-of-step protection based on Savitzky-Golay filtering technique," in *Proc. Emerg. Trends Ind. 4.0 (ETI 4.0)*, 2021, pp. 1–3.
- [21] V. Centeno, A. G. Phadke, A. Edris, J. Benton, M. Gaudi, and G. Michel, "An adaptive out-of-step relay [for power system protection]," *IEEE Trans. Power Del.*, vol. 12, no. 1, pp. 61–71, Jan. 1997.
- [22] Y. Cui, R. G. Kavasseri, and S. M. Brahma, "Dynamic state estimation assisted out-of-step detection for generators using angular difference," *IEEE Trans. Power Del.*, vol. 32, no. 3, pp. 1441–1449, Jun. 2017.
- [23] J. R. A. K. Yellajosula, Y. Wei, M. Grebla, S. Paudyal, and B. A. Mork, "Online detection of power swing using approximate stability boundaries," *IEEE Trans. Power Del.*, vol. 35, no. 3, pp. 1220–1229, Jun. 2020.
- [24] S. Zhang and Y. Zhang, "A novel out-of-step splitting protection based on the wide area information," *IEEE Trans. Smart Grid*, vol. 8, no. 1, pp. 41–51, Jan. 2017.
- [25] H. Zare, H. Yaghobi, and Y. Alinejad-Beromi, "Adaptive concept of controlled islanding in power systems for wide-area out-of-step prediction of synchronous generators based on adaptive tripping index," *IET Gener. Transmiss. Distrib.*, vol. 12, no. 16, pp. 3829–3836, Sep. 2018.
- [26] Y. Xue, T. Van Custem, and M. Ribbens-Pavella, "Extended equal area criterion justifications, generalizations, applications," *IEEE Trans. Power Syst.*, vol. 4, no. 1, pp. 44–52, Feb. 1989.
- [27] K. O. H. Pedersen, A. H. Nielsen, and N. K. Poulsen, "Short-circuit impedance measurement," *IEEE Proc.-Gener. Transmiss. Distrib.*, vol. 150, no. 2, pp. 169–174, Mar. 2003.
- [28] Y. Wang, W. Xu, and J. Yong, "An adaptive threshold for robust system impedance estimation," *IEEE Trans. Power Syst.*, vol. 34, no. 5, pp. 3951–3953, Sep. 2019.
- [29] B. Alinezhad and H. Kazemi Karegar, "On-line Thévenin impedance estimation based on PMU data and phase drift correction," *IEEE Trans. Smart Grid*, vol. 9, no. 2, pp. 1033–1042, Mar. 2018.
- [30] GE Digital. (2021). *Phasor Controller*. [Online]. Available: <https://www.ge.com/digital/applications/transmission/phasorcontroller>
- [31] *Modelling of Permanent Magnet Generator Based Wind Turbine Systems in the RTDS*, RTDS Technol., Winnipeg, MB, Canada, 2017.
- [32] *SIPROTEC 4 Line Differential Protection with Distance Protection 7SD5 V4.7*, Siemens AG, Munich, Germany, 2016.
- [33] *Easergy MiCOM P44y Technical Manual*, Schneider Electr., Rueil-Malmaison, France, 2019.
- [34] *RSCAD Controls Library Manual*, RTDS Technol., Winnipeg, MB, Canada, 2021.



MARKO TEALANE (Student Member, IEEE) received the B.Sc. and M.Sc. degrees in electrical power engineering from the Tallinn University of Technology, in 2016 and 2018, respectively, where he is currently pursuing the Ph.D. degree in power engineering. He is currently a Researcher with the Tallinn University of Technology. His research interests include power system protection, power system relaying, and wide-area control.



JAKO KILTER (Senior Member, IEEE) received the B.Sc. and M.Sc. degrees in electrical power engineering from the Tallinn University of Technology, and the Ph.D. degree in electrical power engineering from the Tallinn University of Technology, in 2009. Currently, he is a Professor of power systems and the Head of the Power Systems Research Group, School of Engineering, Tallinn University of Technology; the Chair of the High Voltage Committee, Estonian Centre for Standardisation and Accreditation; and the Co-Chair of CIGRE Estonian National Committee. His research and consultancy work over the years has been split between the areas of power system dynamics, wide-area control and applications, and power quality.



MARJAN POPOV (Fellow, IEEE) received the Ph.D. degree in electrical power engineering from the Delft University of Technology, Delft, in 2002. He is a Chevening Alumnus. In 1997, he was an Academic Visitor with the University of Liverpool, Liverpool, U.K., where he was working with the Arc Research Group on modeling SF₆ circuit breakers. His research interests include future power systems, large-scale power system transients, intelligent protection for future power systems, and wide-area monitoring and protection. He is a member of Cigre and actively participated in WG C4.502 and WG A2/C4.39. In 2010, he received the prestigious Dutch Hidde Nijland Prize for extraordinary research achievements. He was a recipient of the IEEE PES Prize Paper Award and the IEEE Switchgear Committee Award, in 2011. He is an Associate Editor of *International Journal of Electrical Power and Energy Systems* (Elsevier). In 2017, together with the Dutch utilities TenneT, Alliander, and Stedin, he founded the Dutch Power System Protection Centre to promote the research and education in power system protection.



OLEG BAGLEYBTER received the Diploma and Ph.D. degrees in electrical engineering from Irkutsk Technical University, in 1999 and 2006, respectively. He worked as a Protection and Control Engineer for one of the Russian utilities and a Product Manager of transmission protection relays at GE Grid Solutions. He is currently working as a Senior Staff Engineering Manager at GE and is responsible for Advanced Automation Applications Research and Development portfolio within the GE Grid Automation business. His focus is on developing and deploying innovative applications and solutions utilising wide area measurements in transmission and distribution grids.



DANNY KLAAR received the M.Sc. degree in electric power engineering from the Delft University of Technology, in 1983. Currently, he is a System Operation Advisor at TSO TenneT. He is a member of Cigre SC C2 and participates in the JWG C2/C5.06. He is also active in the European TSO Association ENTSO-E in the field of system operations, focusing on innovative operational concepts, international collaboration among TSOs, and the impact of regulation in the view of the energy transition towards a carbon neutral society.

...

Appendix 3

III

M. Tealane, J. Kilter, O. Bagleybter, B. Heimisson, and M. Popov, "Out-of-step protection based on discrete angle derivatives," *IEEE Access*, vol. 10, pp. 78290–78305, 2022

Received 5 July 2022, accepted 19 July 2022, date of publication 25 July 2022, date of current version 29 July 2022.

Digital Object Identifier 10.1109/ACCESS.2022.3193390

RESEARCH ARTICLE

Out-of-Step Protection Based on Discrete Angle Derivatives

MARKO TEALANE^{1,4}, (Student Member, IEEE),
JAKO KILTER¹, (Senior Member, IEEE), OLEG BAGLEYBTER², (Member, IEEE),
BIRKIR HEIMISSON³, AND MARJAN POPOV⁴, (Fellow, IEEE)

¹Department of Electrical Power Engineering and Mechatronics, Tallinn University of Technology, 19086 Tallinn, Estonia

²Grid Automation, GE Renewable Energy, Edinburgh EH10 4QE, U.K.

³Landsnet hf., 112 Reykjavik, Iceland

⁴Delft University of Technology, Faculty of EEMCS, 2628 CD Delft, The Netherlands

Corresponding author: Marjan Popov (m.popov@tudelft.nl)

This work was supported in part by the Nederlandse Organisatie voor Wetenschappelijk Onderzoek (NWO) through the Take-Off Project "Power swing detection and prevention in future networks with high penetration of renewable energy," under Grant 19279.

ABSTRACT This paper presents an out-of-step protection algorithm based on angle derivatives, which makes use of wide-area measurements and can be applied on arbitrary tie-lines in electrical power systems. The developed algorithm uses PMU measurements that are taken at both ends of a transmission line. Based on the changes of the electrical quantities in the power system, the algorithm detects unstable system conditions. Thus, the developed solution is settingless and can be easily applied where an out-of-step condition is expected. The concept is deployed by using an industrial controller and tested by conducting numerous hardware-in-the-loop simulations. Additionally, recorded data from actual out-of-step events in the Icelandic power system are used to validate the developed algorithm. The performance of the implemented method is compared against the traditional impedance-based out-of-step protection methods. The results confirm that the proposed algorithm detects out-of-step conditions more reliably and faster than the traditional impedance-based solutions.

INDEX TERMS Out-of-step protection, power system transient stability, tie-lines, real-time HIL testing.

I. INTRODUCTION

Electric power systems are the backbone of modern society. It is very important that the power system remains operational at all times. The continuous increase of energy demand puts additional stress on the power network, and forces the system to operate closer to the stability limits. In addition, the growing amount of renewable energy sources increases the intermittency of the power generation accordingly, putting additional stress to the power system. Moreover, disturbances like short-circuit faults naturally occur during power system operation. As the system becomes more stressed, a variety of disturbances can propagate into a larger scale event, causing a major imbalance between the mechanical input and the electrical output power of the generators, resulting in a loss

The associate editor coordinating the review of this manuscript and approving it for publication was Sarasij Das ¹.

of synchronism in the power system. This is known as an out-of-step (OOS) condition and it causes additional mechanical and thermal stresses on power system components, which can lead to catastrophic failure of equipment and blackouts in the electrical power system [1]. Therefore, protection systems must be ready to detect and react to this kind of conditions in order to prevent permanent failure of crucial equipment and avoid blackouts.

The conventional OOS protection is realized by impedance relays and is based on the trajectory of the impedance, the rate of change of the impedance and the continuity of the computed impedance value [2]. Impedance-based methods are easy to implement, however, to operate correctly, they need specific settings. Therefore, they are susceptible to challenges because of network reconfigurations, and the computation of settings is time consuming due to required extensive system stability studies.

TABLE 1. Existing OOS protection methods and approaches in literature and industry.

Classification	Method	Advantages	Limitations
Commercially available OOS detection approaches	Impedance-based detection [1] [2]	Depending on the implementation, can differentiate between stable and unstable swings.	Difficulties in detecting very fast swings; rigorous analysis is required to set the blinders; no predictive properties
	Angle-controlled OOS protection [3]	More reliable and faster than impedance-based OOS protection	Needs predetermined settings to operate and cannot adapt to system reconfigurations; no predictive properties.
	R-Rdot method [4]	Faster detection compared to impedance-based detection	Requires protection settings; no predictive properties.
Unconventional OOS detection approaches based on local measurements	Superimposed current detection [5]	Very fast swing detection, ability to detect fast swings.	Difficulties in detecting slow swings, no discrimination between a stable and unstable swing; no predictive properties.
	Detection based on Power-time ($P-t$) curve [6] [7]	Instability is directly detected from measurements.	Can only be applied directly at generator terminals; no predictive properties.
	Faster than real-time OOS detection [8]	Provides extremely fast OOS detection; predicts if a swing will become unstable.	Requires detailed knowledge about generator parameters; can only be applied directly at generator terminals.
Unconventional OOS detection based on wide-area information	Lyapunov function based OOS detection [9]	The method shows excellent results in OOS detection.	Highly dependent on the estimation of swing-center voltage value.
	Direct angle comparison based OOS protection [10]	The method does not require any computation of protection settings.	Requires monitoring of all the generator buses in the network; operates after several out-of-step cycles.
	Predictive OOS based on synchrophasors [11]	Enhances existing OOS protection, provides more secure and reliable operation for oscillatory OOS compared to existing methods; has predictive properties.	OOS detection speed is not known; not effective in detecting non-oscillatory unstable swings.
	Clarke transform based method [12]	Provides settingless OOS protection, has been prototyped in a real industrial system.	OOS detection speed is not elaborated; no predictive properties.
	Machine learning approaches [13] [14] [15]	Methods offer fast and accurate OOS condition detection, can predict OOS conditions.	The correct performance of the methods requires extensive training using detailed models.
	Proposed approach	Method <i>does not</i> require offline studies or predetermined settings. It <i>provides</i> faster and more reliable OOS detection than conventional approaches, and has been fully prototyped.	No predictive properties.
	OOS detection based on PMU-determined impedances [16]	The method is more secure and provides faster OOS detection than conventional solutions.	Requires a step change in the network to determine network impedances for OOS detection; no predictive properties.
Fast online coherency OOS detection [17]	The method shows more reliable OOS detection than conventional solutions.	OOS detection speed is not elaborated; only applicable at generator terminals, requires a threshold setting; no predictive properties.	
Voltage fluctuations based OOS detection [18]	The method shows fast detection of instability.	Requires a high level of observability in the network; no predictive properties.	

Table 1 represents an overview of currently available approaches to detect an OOS condition, based on the prior industrial and academic achievements. The advantages and the limitations of the conventional and notable non-conventional OOS protection methods that have been published so far are highlighted.

In [3], an angle-controlled OOS protection is proposed, in which the whole power system is reduced to a two-terminal

network, and the equivalent generator voltage vectors are compared. This also relies on the predetermined impedance settings of the equivalent networks, and thus is difficult to adapt to real-time system reconfigurations. The solution proposed in [6] utilizes power-time curves at the measured location to determine generator stability by applying the energy equilibrium criterion. The advantage of this approach is that the instability is detected directly from the power-time

($P - t$) curve, and it does not require any network reduction and offline studies. However, this concept can be applied only directly at the generator terminals and not on tie-lines in the network because in a multi-machine network, each generator output needs to be individually monitored. In [8], the authors proposed a method to detect the generator instability by utilizing measurement data during the disturbance. With this method, the simulations are run faster than the measurements in real-time. This solution results in a very fast OOS detection, however, it requires detailed knowledge about the generator parameters, which a network operator might not have access to.

Additionally, there are also approaches that have made use of machine learning techniques to tackle the OOS problem [13]–[15]. These approaches, however, require extensive model simulations for the purposes of training the machine learning algorithms, and therefore do not show major advantages (at present) over the classical impedance-based protections.

Furthermore, a number of effective OOS protection methods based on wide-area information have been published recently in literature. Some of the most notable recent work can be found in [19]–[21] and [22]. All these methods, however, rely on measurements that are located directly at the generator terminals or at the corresponding high-voltage terminals. This limiting factor is often overlooked, while it makes the developed methods difficult to apply in actual power systems due to the lack of coverage of PMUs in a large power system.

Apart from the methods listed in the comparative table, some recent work on OOS protection based on local measurements include [23], [24] and [25]. These methods, however, can only be applied on generator terminals, since they require direct input from generator measurements.

In addition there exist OOS protection algorithms in literature, that make use of state estimation techniques together with local and wide-area information in [26]. The method shows improved results compared to impedance-based generator OOS protection, however, the effectiveness of this method on arbitrary tie-lines in the network has not been investigated.

This paper proposes a new OOS protection algorithm based on angle derivatives, which requires only two PMU measurements to be applied. The developed algorithm is suitable to be used in arbitrary power systems on transmission lines where an OOS condition can be expected. It relies on PMU measurement data from both ends of the transmission line, and is based on the well-known power-angle curve, and the stability phenomena of the power system when an OOS condition takes place. The novel algorithm is implemented and tested using an industrial controller by using real-time hardware-in-the-loop (HiL) simulations. A real-time simulation model of the Icelandic power system (Landsnet) is developed and validated using measured OOS event data. This model, as well as the existing wide-area measurement data from Landsnet, are used for testing the proposed algorithm in various scenarios.

Furthermore, a comparative study using two commercially available impedance-based OOS relays and the newly developed solution is performed in a customized IEEE 39-bus network.

The rest of the paper is organized as follows: Section II presents the proposed algorithm; Section III describes the methodology for the algorithm testing; Section IV details and validates the real-time network model of the Icelandic power system; Section V shows the performed case studies with results, and finally, the paper ends up with conclusions.

II. PROPOSED ALGORITHM

A. THE OUT-OF-STEP PHENOMENON BACKGROUND

The proposed algorithm relies on the widely applied power-angle characteristic of a generator. According to the classical representation, a generator's dynamic behavior is represented by the swing equation [27] (1) as follows,

$$\frac{M}{\omega_s} \frac{d^2 \delta}{dt^2} = P_m - P_e(\delta) \quad (1)$$

where M - the inertia constant of the equivalent machine; ω_s - the rotor speed of the generator; δ - the internal voltage angle of the generator; P_m - the mechanical input power of the generator; P_e - the electrical output power of the generator.

The electrical output of the generator ($P_e(\delta)$) depends on the angular difference of two equivalent voltage phasors that are separated by impedance x_{tot} . This relation forms, what is known as, the power-angle curve of a generator and is expressed by equation (2),

$$P_e(\delta) = \frac{|\bar{E}_1| |\bar{E}_2|}{x_{tot}} \sin \delta \quad (2)$$

where $|\bar{E}_1|$, $|\bar{E}_2|$ - the equivalent internal voltage phasor magnitudes of the sources; x_{tot} - the equivalent reactance between the two sources, and δ - the angle difference of the equivalent phasors.

The resistances of machines and transmission lines are neglected in equation (2), since resistances introduce a damping term in the swing equation. In addition the mechanical input power of the generators is assumed to be constant, as well as the generators are assumed to be constant voltage sources behind a reactance, which neglects the effects of automatic voltage regulation. In this way we consider the worst-case scenario of the power-angle relationship in the network. Furthermore, it should be acknowledged that the due to these reasons the actual power-angle curve may deviate from the idealistic curve, which is used to explain the general phenomenon of transient stability. However, it has to be pointed out, that in the networks used for case studies, the generators are equipped with voltage control and the resistances are considered as well as the losses in the network. With this approach the algorithm is tested in near-realistic conditions.

This power-angle curve can be applied to determine the power transfer across a single transmission line in a meshed

transmission network. A multi-machine system can be separated into two groups of machines, that represent the inertia centers at either end of a transmission line [28]. Note that the equation (2) is applicable also for power flow through an arbitrary transmission line, when the equivalent internal voltage phasors are replaced with the voltage values at the ends of the transmission line in question. Hence, by using the power-angle curve, the dynamic stability around a tie-line can be assessed.

Fig. 1b represents the power-angle characteristics for pre-, faulted- and postfault state of a two-machine equivalent system shown in Fig. 1a. On the power-angle characteristic, two operating points can be determined by using a prefault steady-state power transfer (noted as P_m). The operating point located in the left half of the characteristic is a stable operating point. According to the Equal Area Criterion (EAC) [27], the maximum angle difference of a recoverable swing cannot be greater than the second operating point (called Last Stable Angle - LSA), though it may be smaller. The further increase of the angle difference beyond the LSA point will definitely result in an unstable generator operation. Thus, the LSA point is critical to distinguish between a stable and an unstable swing. The LSA point is located on the postfault curve, which sits lower than the prefault curve due to the transmission impedance increasing upon switching off the faulty element.

When observing the dynamic behavior of a power system, it can be noted that during a fault, the electrical active power is lowered due to the reduced voltage magnitudes. However, the mechanical energy given to the generators by the prime movers remains rather constant. Due to this difference in energy the angular difference between the equivalent voltages begins to increase. After the fault clearing the increased value is indicated as δ_1 , and the surplus of energy obtained during a fault condition is indicated by the shaded area in Fig. 1b.

Thereafter, the electrical output power is higher than the mechanical input power, and the increase of the angular difference keeps increasing. Due to inertia, the angular difference keeps increasing, until the surplus of energy obtained during fault disappears. This means that during that time the first derivative of the angle value will be positive, because the angle difference keeps increasing. However, the second derivative of the angle difference will be negative, since the rate at which the angle is increasing, is lowering. In addition, during this process the electrical power output will also be increasing. Accordingly, the first derivative value of the active power will have a positive value. The angular difference will increase until reaching a maximum value denoted by δ_m . At this point, equality between the obtained and the dissipated energy is reached. This process is illustrated in Fig 1c.

Once the maximum angle value is reached, the angular difference will start to decrease, and the system will move towards a new stable equilibrium point. During this process, the angle change speed and the change in active power will be negative, thus the derivative values are negative. The process is illustrated in Fig. 1d, and is known as a stable power swing. It has to be noted that during a stable power swing

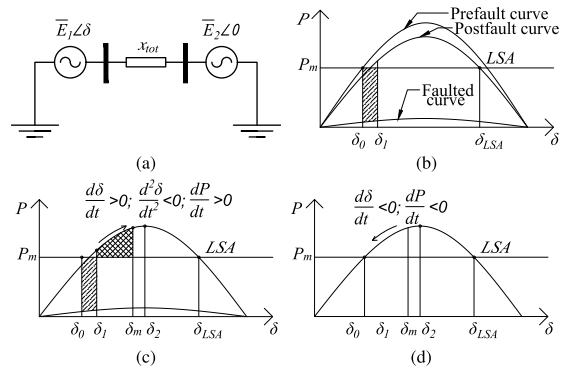


FIGURE 1. Two-machine system and the demonstration of a stable power swing process on a power-angle curve. (a) Two-machine equivalent with a connecting transmission reactance, (b) Power-angle curve illustrating the pre-, faulted- and postfault operations, with the Last Stable Angle point denoted as δ_{LSA} . (c) Power system operation after a disturbance; during this operation the angle difference is decelerating until reaching the maximum angular difference of δ_m , where the surplus of energy has all been dissipated. (d) Power system operation after the surplus of energy after the disturbance has been dissipated and the angular difference is decreasing while system is settling at a stable operation point.

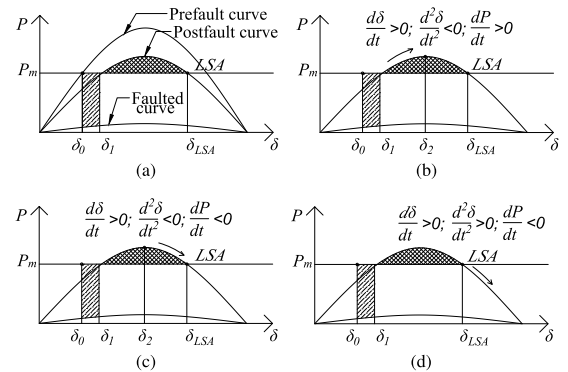


FIGURE 2. Demonstration of an unstable power swing process on a power-angle curve (a) Power-angle curve illustrating the pre-, faulted- and postfault operations, with the Last Stable Angle point denoted as δ_{LSA} . (b) Power system operation after a disturbance, during this operation the angle difference is decelerating, and power derivative remains positive until reaching the maximum active power value at δ_2 . (c) Power system operation after passing the maximum power value, during this operation the power derivative is negative and the angle difference is decelerating until reaching the Last Stable Angle point. (d) System operation becomes unstable after passing the Last Stable Angle point.

the operating point may pass beyond the maximum power point δ_2 , however, it will not cross δ_{LSA} .

The process of an unstable swing is illustrated in Fig. 2, where post-fault impedance is assumed to be higher than in the stable case. For comparison purposes this example of an unstable swing is again started with a fault in the power system. The beginning of the swing process is similar to the stable swing explained before, and is illustrated in Fig. 2a. After the fault clearance the angular difference

is again increasing, and during the start of the process the acceleration and the speed of the angle change have the same signs as those with the stable swing, as illustrated in Fig. 2b. However, in this case, the angular difference continues to increase, passing the point δ_2 in the power-angle curve. The electrical power value begins to lower, and consequently the derivative of power will become negative, as illustrated in Fig. 2c. Subsequently, with the further increase in angular difference, the *LSA* point (denoted by δ_{LSA}) will be passed. When the system has passed this point, the angular difference will start accelerating. This means that the stable operation of the power system is no longer possible and the system will experience an OOS condition. This condition is indicated by the second derivative of the angle value becoming positive, with the first derivative value remaining positive. Simultaneously, the first derivative value of the active power is negative. This situation is illustrated in Fig. 2d. It has been shown that the use of the power-angle characteristic and *EAC* concept applies for assessing complex stability phenomena in large multi-machine systems, in addition to a two-machine equivalent network [29].

It should be noted, however, that in reality the power-angle curve is different than the idealised curve used for the explanation above, i.e. the amplitude value of the power-angle curve is shifted away from the theoretical maximum at 90 degrees. The reason for this is that the voltages are not constant and the losses are not taken into account. The mechanisms and mathematical explanation of the variations in the power-angle curve are discussed in more detail in [30] and [31].

To summarize, the growing angle difference and dropping active power together point to the right half of the power-angle curve, while the change of sign of the angle difference acceleration (second derivative becoming positive) indicates the crossing of the *LSA* point. These three criteria unambiguously identify that the power swing becomes non-recoverable and therefore can be used as a basis for the proposed OOS protection algorithm.

B. DEVELOPED OUT-OF-STEP PROTECTION ALGORITHM

The developed protection algorithm uses the measurements provided by the PMUs on both ends of a transmission line. This allows for the computation of angular difference derivative values, in addition to the monitoring of the voltage, current and power values.

It must be noted that due to the discrete nature of PMU measurements the continuous derivatives mentioned in Section II should be substituted with finite differences, i.e. we are supposed to replace $\frac{d\delta}{dt}$ with $\frac{\Delta\delta}{\Delta t}$. Nevertheless, for the purpose of simplicity we will continue to use the same terminology as above, bearing in mind that all the derivatives will be estimated using sampled discrete measurements and finite differences.

According to the explanation given above for an OOS condition, shown in Fig. 2d, the criteria for the protection

operation are as follows:

$$\begin{cases} \frac{d\delta}{dt} > 0 & \text{for two consecutive measurements} \\ \frac{d^2\delta}{dt^2} > 0 & \text{for three consecutive measurements} \end{cases}$$

These conditions might be also fulfilled during normal operation, while the operating point is situated in the stable operation area of the power-angle curve. In order to stop the OOS protection algorithm from operation during normal conditions, blocking and restraining criteria have been defined. The criteria for *blocking* the protection function during normal grid conditions are as follows:

$$\begin{cases} \text{Measured voltage above } 0.89 \text{ p.u.} \\ \text{Measured voltage below } 0.2 \text{ p.u.} \end{cases}$$

The first criterion is used to ensure protection is blocked when the network operates in nominal condition. The second criterion is used to check if there is a fault present on the protected line. The values proposed above should be considered as indicative, the exact thresholds may be adjusted based on the local deployment conditions. If either of those conditions are fulfilled, the protection will not operate.

In order to *restrain* the protection from operation while the system is experiencing a stable power swing, the following criteria are used:

$$\begin{cases} \frac{dP}{dt} > 0 & \text{for two consecutive measurements} \\ \frac{dV}{dt} > 0 & \text{for two consecutive measurements} \end{cases}$$

The first criterion restrains the protection from operating whilst the operation point is located in the first half of the power-angle curve, where, during the angular difference increase, the active power transfer also increases. The second criterion restrains the protection algorithm from operation when the system is in the process of leaving the swinging condition, and the voltages increase. The objective of using these criterion is to allow the protection to only operate when the system is moving towards instability after passing the theoretical maximum power transfer point on the power-angle curve.

It has to be noted that the algorithm requires multiple consecutive measurements to fulfill the presented criteria in order to operate, in order to avoid the algorithm from operating from a singular measurement result which may be caused by noise. Therefore, the operation time of the algorithm is also dependent on the sampling rate used for the input data streams.

The algorithm is divided into three main segments and its structure is shown in Fig. 3. The first segment, circled in red in Fig. 3, is responsible for checking the data validity and blocking the protection based on voltage measurements. The second segment, circled in green, computes and assesses the active power and voltage derivative values and restrains the protection operation if necessary. Finally, the

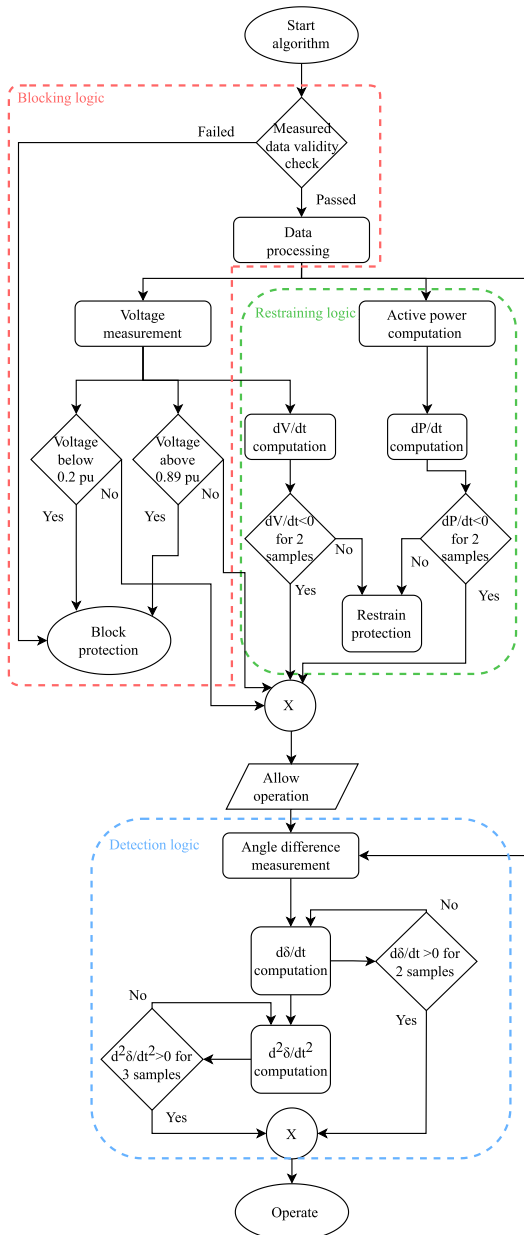


FIGURE 3. Principle diagram of the developed OOS protection algorithm.

third segment, denoted in blue, computes the first and second derivatives of the angle difference, and is responsible for OOS detection and protection operation command. The main advantages of the developed algorithm compared to existing solutions are, that it requires no offline studies or simulations and requires little processing power, therefore it is easily adoptable on already existing hardware.

III. TESTING METHODOLOGY AND TEST SETUP

In this section, the implementation of the developed algorithm is explained together with the simulation platform and the IEEE 39 bus model used as a testing network. The algorithm is tested using HiL simulations by feeding PMU measurement data into a dedicated phasor-based controller. Simultaneously, analogue voltage and current waveform signals are provided to the impedance-based OOS protection devices in order to compare the performance of the new method and existing solutions.

A. IMPLEMENTATION OF THE DEVELOPED ALGORITHM FOR HiL TESTING

The algorithm is developed and deployed on an external programmable controller device [32]. This phasor-based controller is capable of receiving multiple PMU data inputs and executing complex custom-built algorithms in a fast, deterministic manner.

The data validity check shown at the start of the algorithm in Fig. 3 is handled by the controller hardware. If the measured data does not pass the validity check, meaning that the data is not time-synchronized or PMU frames are missing, the protection algorithm is blocked. When the validity check is passed, the measurement values are allowed to be supplied to the protection algorithm described in Section II.

The controller, where the proposed algorithm is implemented, receives measurement data from real-time simulations over an Ethernet network according to IEEE C37.118 standard. The data rate used affects the decision time of the algorithm, since the algorithm's criteria are linked to consecutive measurements. Therefore, the slower the data rate, the slower the decision time. For uniformity throughout the paper, the PMU data rate used for the tests conducted with IEEE 39 bus networks was 60 fps (frames per second). The data rate for tests with the Icelandic simulated network, as well as recorded OOS events from Iceland, was 50 fps. The controller provides feedback signals and calculated values back to the Real-Time Digital Simulator using IEC 61850 GOOSE messages. PDC (Phasor Data Concentrator) Wait Time [33] of 100 ms was implemented in the controller in order to consider the representative latency of the data collection using PMUs from different geographic locations. The processing cycle time of the controller was configured at 16.667 ms and 20 ms for the IEEE 39 bus network and Icelandic system tests respectively.

The proposed algorithm installed on the controller is tested in parallel with two physical relays using HiL test setup. The illustration of the setup is shown in Fig. 4. The information marked by red represents the input values to the hardware: analogue voltage and current signals for the impedance-based OOS protection relays, and IEEE C37.118 PMU data for the phasor-based controller. The information marked in green shows operation signals in the form of digital inputs from the relays and IEC 61850 data for the controller. The particular test scenarios and the test network model are explained further in the next sections.

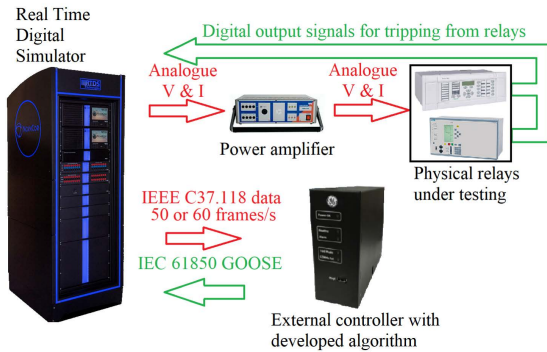


FIGURE 4. Experimental setup for HiL OOS protection testing using hardware.

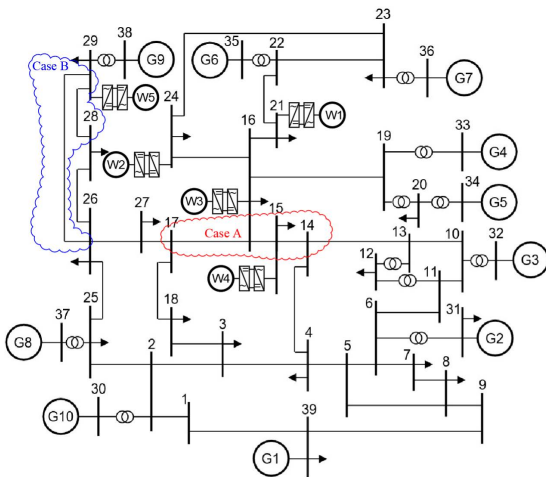


FIGURE 5. Modified IEEE 39 bus network with added type 4 wind farms. Red marks Case A testing location and blue Case B testing location, wind farms W1-W5 are added to buses 21, 15, 25, 16 and 29, respectively.

B. MODIFIED IEEE 39 BUS TEST SYSTEM AND TEST CASES

In order to test the performance of the algorithm in a multi-machine network, the IEEE 39 bus network model was used. The model is modified by adding generic grid-following wind farms (W1 - W5) at some buses, using an existing wind power plant model in the simulation software [34]. In this way, the developed solution can be tested for different grid and generation mix conditions. The modified test network is shown in Fig. 5. Two different test locations are chosen to investigate different power swing conditions in the network and test the protection devices for various scenarios. The first test location is circled in red and shown as Case A, whilst the second denoted in blue is Case B. The former location demonstrates the power swing scenario occurring between two larger parts of the network, while the latter location represents a case of a single machine connected to an infinite bus system.

Both locations cover two tie-lines each in order to see the proposed algorithm’s behavior for different tie-line lengths. For Case A, the protection was tested for the lines between buses 14-15 and 16-17. To create an OOS condition in the power system, a three-phase short circuit is applied on bus 16. The fault is cleared by disconnecting one of the transmission lines emanating from bus 16, and thereafter power swings take place on the remaining tie-line between the two parts of the network. For Case B, the transmission lines under observation are those between buses 26-29 and 28-29. Power swings are created by applying a three-phase short circuit on bus 29. The fault is cleared by disconnecting one of the two tie-lines connected to this bus, leading to power swings along the remaining transmission lines.

For the studied Case A, the impedance-based protection relays are situated on bus 15 for line 14-15 and on bus 16 for line 16-17. For Case B, the impedance-based protection relays are at bus 29 of the transmission lines for both tested lines. The PMUs that stream measurement data to the phasor-based controller are situated on both ends of the transmission lines in all of the tested cases.

Both of the tested relays incorporate an impedance-based OOS algorithm, and are set to trip on the way in (TOWI) and on the way out (TOWO) of the configured impedance characteristic. The settings of the protection devices are obtained according to the manufacturer guidelines as explained in the user manuals of the relays; the settings were calculated using a base case of fully synchronous system [35], [36].

In order to test the OOS protections for various grid conditions, the output power of the wind power plants is scaled up while simultaneously decreasing the synchronous generation capacity. For Case A, for a specific renewable penetration scenario (RES %), all four wind power plants (denoted as W1-W4 in Fig. 5) in the network area provide the specific percentage of the base case synchronous generation output of the four generators (denoted as G4, G5, G6 and G7) in the area. At the same time, the apparent power of these generators is decreased from the initial value of 1000 MVA by the same specific percentage of the RES % level. This is done in order to also decrease the total inertia of the generators together with their output power. For Case B, one generator (G9) and one windfarm (W5) are scaled accordingly. Additionally, at each RES % case the simulation is repeated five times to evaluate the consistency of the tested OOS protection devices. This results in a total number of 300 real-time simulations for the case studies using IEEE 39 bus test network.

C. CONCEPT VERIFICATION

In this subsection, the developed algorithm’s response to a stable and unstable swing for Case A location in the IEEE 39 bus network is shown.

The case of a stable power swing is shown in Fig. 6. The swing is initiated by a five-cycle long fault in the system occurring at 0.15 seconds (shown by Ⓛ), after which the system goes through a stable swing. Fig. 6a shows the signals associated with the developed algorithm in the controller,

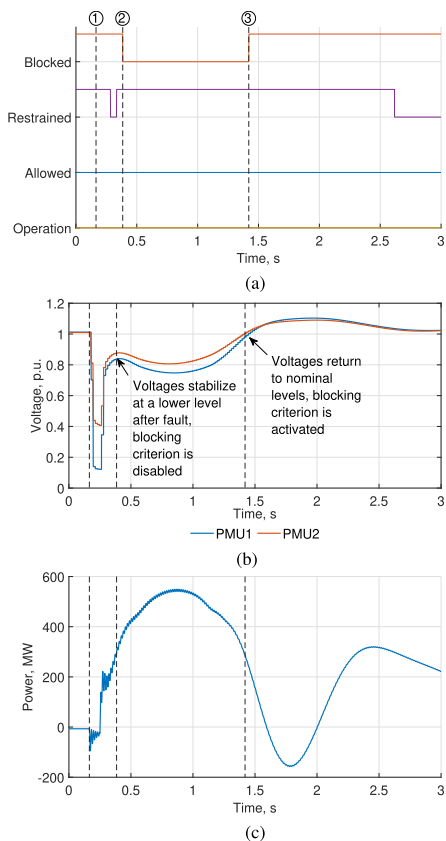


FIGURE 6. Protection algorithm response signals, voltages at both ends of the transmission line and active power through the line during a stable power swing in the network. (a) protection algorithm signals in the external controller, (b) the voltage magnitudes at both ends of the protected transmission line and (c) the active power through the protected line.

as described in Section II of this paper. Figs. 6b and 6c illustrate the streamed measurement values of the voltage and the active power through the transmission line from the real-time simulation. It can be observed that after the short-circuit condition has ended, the blocking criteria for the protection function are disabled (specified by ②). However, the restraining criteria are inactive only for a very short duration, right after the fault has been cleared, and thereafter become active, because the power transferred through the transmission line is increasing, thus the derivative value is positive. In addition, once the power starts decreasing, the voltage value starts increasing. Due to this behavior, the restraint criterion remains active and the protection provides no operation command during a stable swing. After some time the voltage values return to nominal operation level and the blocking criterion is activated, as indicated by ③.

The reaction of the algorithm to an unstable power swing is shown in Fig. 7. The swing is initiated by a six-cycle fault in the system occurring at 0.15 seconds (shown by ①),

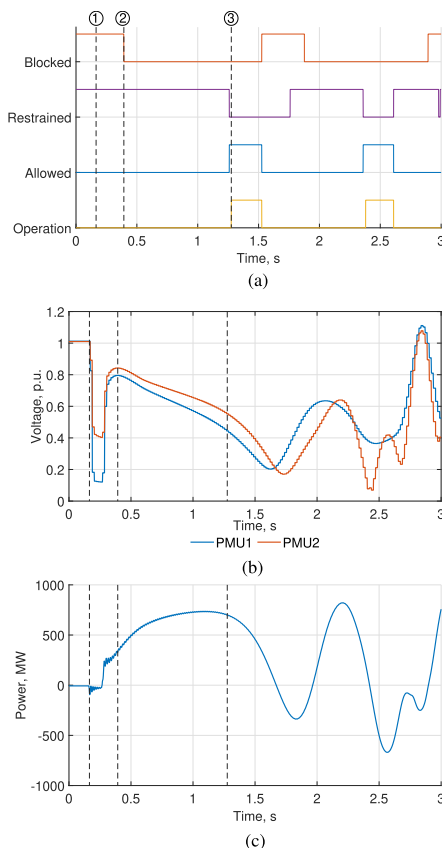


FIGURE 7. Protection algorithm response signals, voltages at both ends of the transmission line and active power through the line during an unstable power swing and subsequent OOS condition. (a) protection algorithm signals in the external controller, (b) the voltage magnitudes at both ends of the protected transmission line and (c) the active power through the protected line.

after which the system experiences an unstable swing. Fig. 7a shows the developed algorithm signals in the controller, whilst Figs. 7b and 7c show the measured quantities from the simulation. From the response of the protection, it can be observed that after the short-circuit fault the blocking criterion is disabled, as shown by ②. This is because the voltage value is out of bounds of the blocking criterion. However, the restraint criterion is active, since the measured active power transfer through the transmission line is increasing. In the meantime, it can be seen that the voltage value is decreasing, and, accordingly, the derivative of the voltage value is negative. Once the active power starts decreasing, the restraining criterion deactivates. This means that both the blocking and the restraining criteria are not active; therefore the protection will issue an operating command as soon as the first and second derivatives of the angular difference are both positive for two and three consecutive cycles respectively. The protection detects the unstable condition, which is seen

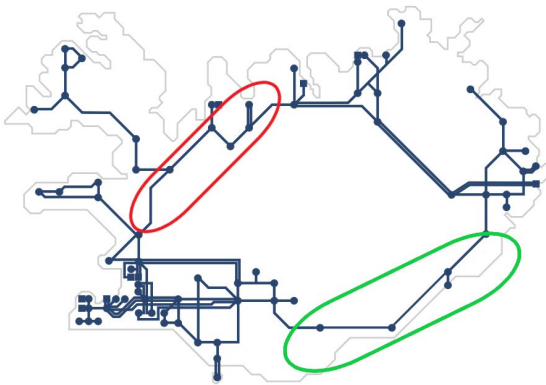


FIGURE 8. Icelandic power system, the corresponding corridors of lines connecting two parts of the network are outlined in red and green for the northern and southern ring connections respectively. [37].

by the operation signal activation at instance ③. Hence it can be concluded that the developed protection algorithm is able to distinguish between unstable and stable swings in the network, and is able to issue tripping commands when there is an unstable power swing developing on the protected line.

IV. ICELANDIC POWER SYSTEM MODEL VERIFICATION FOR REAL-TIME SIMULATIONS

To display the developed algorithm’s robustness for the application in arbitrary power systems, the Icelandic power system has been used for additional simulations. In order to perform real-time simulations to test the OOS protection, the Icelandic power system was modelled in RTDS environment. Fig. 8 shows the Icelandic power system, which has two centers of inertia, situated in southwest and in the eastern part of the island. The two main centers of inertia are connected with links, known as the northern ring connection (north corridor), circled with red, and the southern ring connection (south corridor), circled with green. In addition, the southern ring connection uses series compensation by utilizing a series capacitor that can be switched on or off. On these two ring connections power swings are expected, and the developed protection algorithm is expected to be installed.

The Icelandic grid uses a wide-area monitoring system with a number of PMUs installed in the network. The wide-area monitoring system has recorded several system-level events including OOS conditions, which are used to compare the developed network model behavior to the actual system behavior. The network model in RTDS environment was developed based on the PSS/E[®] network model provided by Landsnet.

Two recorded OOS events were used to validate the created model in RTDS. The first OOS event was initiated by a busbar flashover in one of the substations located in the northern ring connection, which led to the loss of the substation and disconnection of the northern transmission corridor, resulting

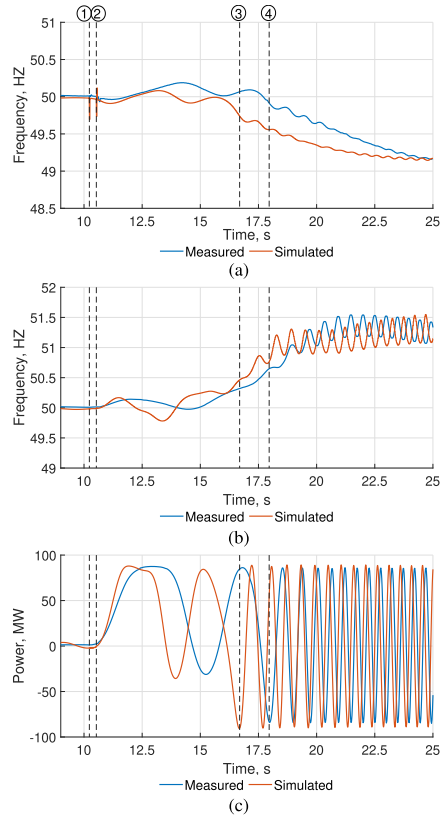


FIGURE 9. OOS event 1 measured and simulation values. (a) the frequency in the south-west center of inertia, (b) the frequency of the east center of inertia and (c) the active power flow in the southern ring connection, where the OOS event takes place. ① - the start of the event with the fault in the north corridor substation, ② - fault clearance, ③ - first pole slip in simulated values, ④ - first pole slip in measured values.

in an OOS condition in the southern ring. The second event was initiated by a sudden loss of load in the south-western inertia center. This contingency caused system split, where some generators in the south west system were connected to the rest of eastern network only through the southern ring connection, and led to an OOS condition in the southern corridor of the network.

The comparison of the measured values and the simulated results for the first OOS event is shown in Fig. 9. The frequencies of the south-western inertia center and the northern inertia center are shown in Figs. 9a and 9b, whereas the active power flow in the southern corridor during the event is shown in Fig. 9c. The specific events of interest are marked throughout the subfigures, where ① marks the start of the sequence of events with a flashover at the substation in the northern corridor, at 10.2 seconds. After 300 ms (marked as ②), the fault is cleared by tripping the remote ends of the lines from the faulted busbar, leading to the disconnection of the northern transmission corridor. Thereafter, the active

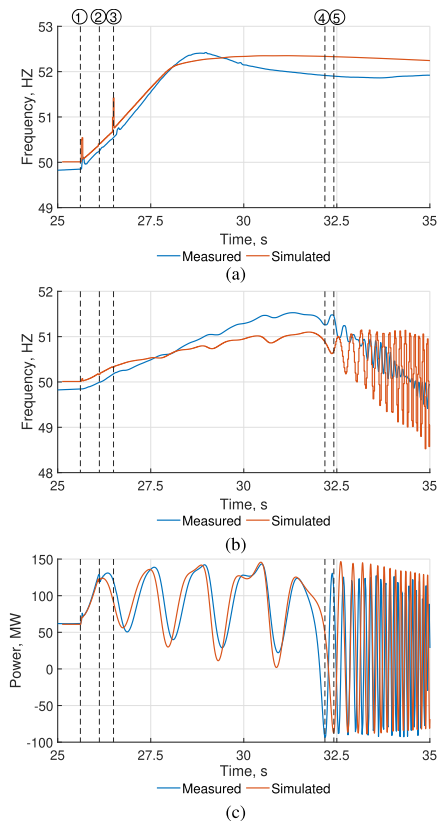


FIGURE 10. OOS event 2 measured and simulation values. (a) the frequency in the south-west center of inertia, (b) the frequency of the east center of inertia and (c) the active power flow in the southern corridor, where the OOS event takes place. ① - the start of the event with the loss of load, ② - inter trip on the 220 kV substation at the southern corridor, ③ - north corridor disconnection from overload, ④ - first pole slip in measured values, ⑤ - first pole slip in simulation.

power is transferred through the southern corridor, and the system goes through a stable swing, after which it fails to maintain stability. The northern and southern parts of the network experience the first pole slip at ③ and ④ for the measured and simulated results respectively.

It can be observed that the simulated and measured data show a slight deviation, however, the general behavior of the simulated network and the measurement data is similar. For both cases, after the initial event occurs, the system goes through a stable swing. The simulated results show greater swing frequency than the measured one. This is likely caused by a difference in generator dispatch during the event, as well as by the effects of the user-defined governor models.

The comparison of the measured values and simulated results for the second OOS event is shown in Fig. 10. The frequencies of the south-western inertia center and the northern inertia center are shown in Fig. 10a and Fig. 10b, respectively, whereas the active power flow in the southern corridor during

the event is shown in Fig. 10c. The specific events of interest are marked throughout the subfigures, where ① denotes the start of the sequence of events with a large loss of load in the network at 25.6 seconds. The loss of load is followed by an inter-trip from the overload protection of the southern corridor marked as ②. Due to disconnection in the 220 kV substation nearest to the southern link, only two generators remain connected to the network through the southern corridor. At ③, the northern corridor link is disconnected by the overload protection, effectively separating the two inertia centers of the network. As a result, the two generators left on the southern corridor pass through three stable power swings, which are increasing in magnitude, and experience a pole slip at ④ and ⑤ for the measured values and simulation results, respectively.

From the comparison of the measured and simulated values it can be observed that the simulated results are well aligned with the actual measured values for this event. The frequency in the south-western inertia center follows closely the measured values, and in the northern part there is a slight difference in the gradient of the frequency increase, which may be caused by a difference in production units during the actual event and the simulation, together with the effect of non-standard governors used in the Icelandic power system. As for the power flow in the southern corridor, the simulated values closely match the measured values. Based on these results, it can be concluded that the model follows the real-life characteristics of the Icelandic power system and can be used to investigate OOS protection algorithm in the future.

V. CASE STUDIES

This section presents the test results of the developed protection algorithm using real-time simulations with the IEEE 39 bus test network and the recorded data from OOS events in the Icelandic power system, as well as the simulations with the developed Icelandic power network model. While there are numerous other methods developed for OOS protection, as shown in Section I, the aim of the conducted case studies is to compare the performance of the developed solution to currently available impedance-based protection devices.

A. COMPARATIVE RESULTS FROM IEEE 39 BUS NETWORK SIMULATIONS

In this subsection, the results of the comparative analyses of the developed algorithm and the currently available impedance-based OOS protection relays are shown. The overall detection rate of the OOS conditions for both of the test cases, and the tested algorithms, is shown in Fig. 11.

Regarding Case A, it can be seen that Relays 1 and 2 fail to operate in 6.7 % and 3.6 % of all the performed tests respectively. In contrast the new algorithm operates in 100 % of all the tests. However, when looking at a single machine going OOS with the rest of the system (Case B), the conventional relays show significantly lower detection rates compared to the developed algorithm. The failure rate is 23 % and 22.2 % for Relay 1 and Relay 2, respectively. At the same time, the

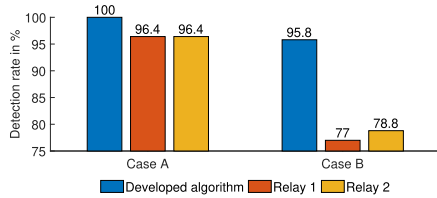


FIGURE 11. OOS condition detection rates for developed algorithm and tested relays in percentage across the simulated cases A and B.

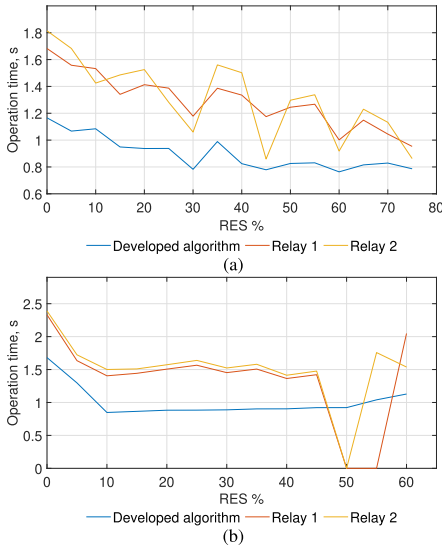


FIGURE 12. OOS protection operating times of protection devices for Case A. (a) represents a case study on the transmission line between buses 14-15 and (b) represents a case study on the transmission line between buses 16-17.

developed algorithm successfully operates in 95.8 % of the Case B tests, giving the failure rate of 4.2 %.

1) COMPARISON OF RESULTS IN CASE A

The operating time comparison between the two tested impedance-based relays and the developed OOS algorithm is shown in Fig. 12. The operating times show how long it takes the protection device to provide a trip command after the short-circuit fault has been cleared. The value of '0' means that the protection device did not provide any tripping command within five seconds after the OOS condition, at which point the simulation is terminated. Fig. 12a shows the operating times when the protection is installed on the transmission line between buses 14-15, and Fig. 12b shows the operating times when the protection is used on the transmission line between buses 16-17.

From this figure it can be observed that the developed algorithm shows significantly lower operating times on both of the installed transmission lines. The developed algorithm, on average, is 490 ms and 540 ms faster compared to Relay 1

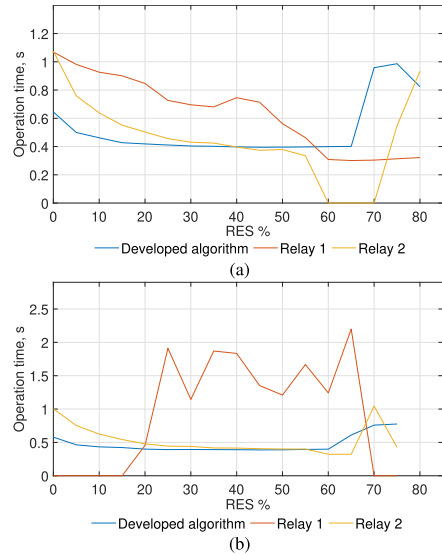


FIGURE 13. OOS protection operating times of protection devices for Case B. (a) represents a case study on the transmission line between buses 26-28 and (b) represents a case study on the transmission line between buses 28-29.

and Relay 2 respectively. For the transmission line between buses 16-17 both of the impedance-based protection relays failed to operate in the 55 % RES scenario and Relay 1 also failed to operate in the 60 % RES scenario, however, the developed algorithm successfully operated.

2) COMPARISON OF RESULTS IN CASE B

The protection operating time comparison for Case B is shown in Fig. 13. Overall, the developed algorithm has the same operating time in this simulation case compared to Relay 2. Compared to Relay 1, the developed algorithm operates 300 ms faster. Fig. 13a shows the operating times of the case study on the transmission line between buses 26-29, and Fig. 13b shows the protection operation times for the case study performed between buses 28-29. It can be observed that compared to simulation Case A the protection operation times are closer together for this case. The developed protection algorithm displays very similar operating times to Relay 2, whilst Relay 1 shows slower operating times for the majority of conducted tests. For the cases performed on the transmission line between buses 26-28, it should be noted that Relay 1 issued a trip command from the distance protection function instead of the OOS protection function. This applies to tests conducted with 60 % and above RES % scenarios. Additionally, it can be seen that Relay 2 does not operate for some of the RES % scenarios, whilst the other two tested devices do.

Regarding the case study performed on the transmission line between buses 28-29, it can be seen that in this case Relay 1 fails to operate on lower RES % as well as higher.

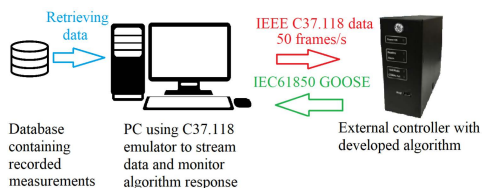


FIGURE 14. Developed protection algorithm testing setup with measured data streaming.

In addition, the operating time is higher compared to the other two tested approaches, because in this case study the protection operates on the second swing.

B. PROTECTION TESTING RESULTS USING OUT-OF-STEP EVENT RECORDINGS

The developed OOS protection algorithm has been also tested using event recordings from the Icelandic power system. To test the algorithm, the recorded historical PMU data has been streamed from a personal computer (PC) using a C37.118 emulator. The data was streamed to the phasor-based controller, where the developed algorithm is installed. The experimental setup for this case is shown in Fig. 14. The response of the algorithm has been recorded for a total of four OOS events that have been studied. The developed solution showed good results, providing successful operation for all of the recorded OOS events. The OOS event recordings used for the algorithm testing are described as follows:

- Event 1 and event 2 are nearly identical; both events were initiated by a flashover at a substation in the northern corridor of the power system, followed by its disconnection; the increased power flow through the southern corridor triggered an OOS event in the power system.
- Event 3 was initiated by an energization of a transmission line in the eastern part of the system, which caused undamped oscillations between the two centers of inertia, however, the OOS condition did not occur on the protected line.
- Event 4 was initiated by a large loss of load in the south-western part of the network. After this contingency, overload protection operated on the northern part of the ring connection, and an inter-trip separated the two generators in the southern corridor, which, after a few oscillations, resulted in an OOS condition on the southern ring connection.

Figs. 15 and 16 show the developed protection algorithm response, the voltage variations at the two measurement locations on the southern link and the measured power for Event 1 and Event 2, respectively. For both events the power system first goes through a stable swing and afterwards becomes unstable, resulting in an OOS situation. The dashed line denoted by ① shows the start of the event. From the protection signals shown in Figs. 15a and 16a for Event 1 and Event 2 respectively, it can be observed that during the first

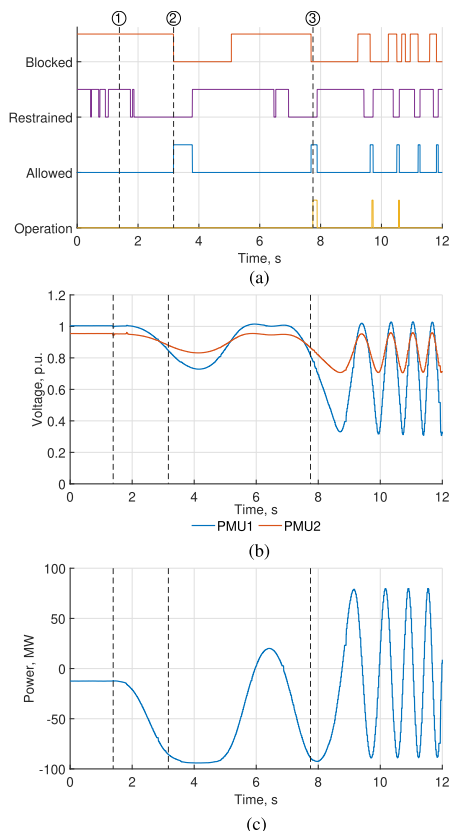


FIGURE 15. Protection algorithm response to Event 1 data. The dashed line marked as ① shows the start of the OOS event at 1.3 seconds. (a) the protection algorithm signals from the controller, (b) the voltage at the two measurement locations in the southern corridor and (c) the measured power in the southern corridor during the event.

stable swing the protection algorithm performs correctly. During this process the algorithm gets deblocked, indicated by ②, due to the occurred voltage dips in the system, and subsequently the restraint criteria are also lifted. The protection, however, does not give a trip signal, because the swing is stable. The second power swing becomes unstable for both events due to the large oscillations in voltages and power. For the unstable swings, the developed protection operates correctly, which can be seen from the operation signal traces indicated by ③. Since there is no specific OOS protection currently active in the Icelandic system, the recorded event continues to evolve into OOS oscillations with increasing frequency, until a distance protection operates somewhere in the network. As shown in Figs. 15 and 16, this situation could have been resolved more rapidly using the proposed OOS solution.

Fig. 17 shows the developed protection algorithm response, the measured voltages at the two ends of the southern corridor, and the corridor power for OOS Event 3. From this

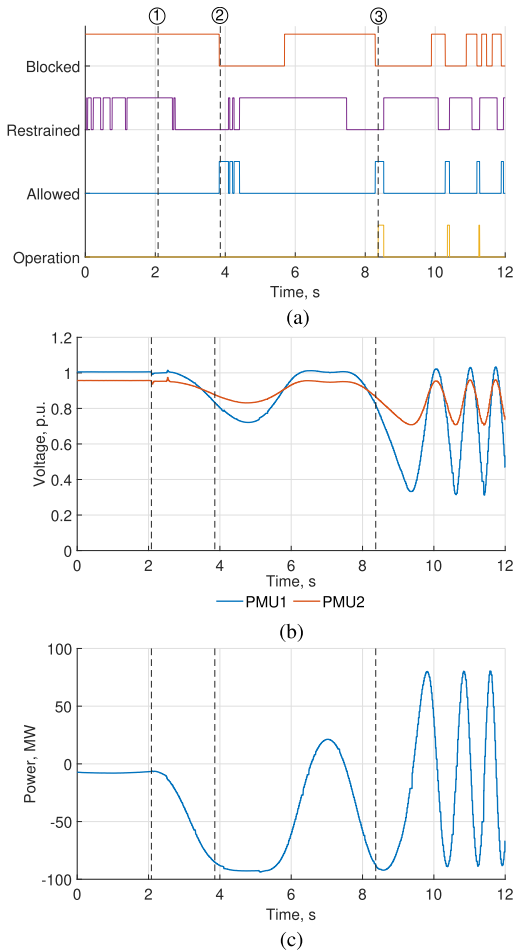


FIGURE 16. Protection algorithm response to Event 2 data. The dashed line marked as ① shows the start of the OOS event at 2.1 seconds. (a) the protection algorithm signals from the controller, (b) the voltage at the two measurement locations in the southern corridor and (c) the measured power in the southern corridor during the event.

figure it can be observed that after the line energization at 0.5 seconds, marked by ①, the system starts to oscillate. The oscillations are undamped and increasing in magnitude for both voltages and measured power, as can be seen in Figs. 17b and 17c. From the protection signal response shown in Fig. 17a, it can be seen that the protection algorithm is deblocked during the power swings, first of which is denoted by ②. As the OOS condition does not show on the protected line, the protection is stable and does not provide any operation command. The condition is cleared by a distance protection operation elsewhere in the network, indicated by ③ at 34 seconds. Therefore, it can be concluded that the developed protection algorithm is stable when the OOS condition is not localized to the protected tie-line.

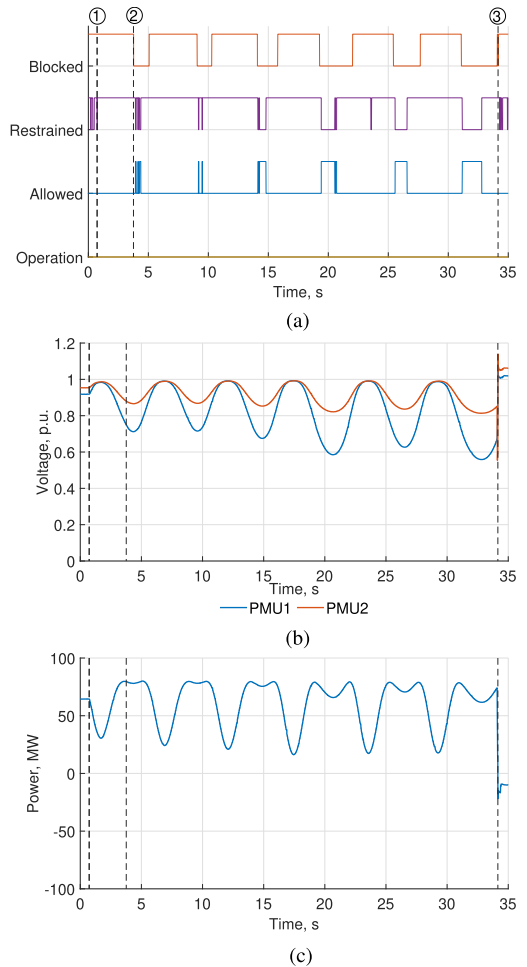


FIGURE 17. Protection algorithm response to Event 3 data. The dashed line marked as ① shows the start of the OOS event at 0.5 seconds. (a) the protection algorithm signals from the controller, (b) the voltage at the two measurement locations in the southern corridor and (c) the measured power in the southern corridor during the event.

Fig. 18 shows the developed algorithm response, measured voltages at the two locations in the southern link and the power flow for OOS Event 4. The dashed line marked in the figure shows the start of the event with the loss of load at 1.3 seconds, indicated by ①. Following the initial loss of load, it can be seen that the power transfer through the corridor, shown in Fig. 18c, starts increasing. At the same time, the voltages, shown in Fig. 18b, decrease, which leads to disabling the blocking criterion of the algorithm, as can be seen from the protection signals shown in Fig. 18a. At the time of 1.8 seconds a jump in power transfer occurs, marked by ②. This signifies the northern corridor disconnection due to overload. Thereafter, the southern ring connection experiences four stable swings, with progressively increasing

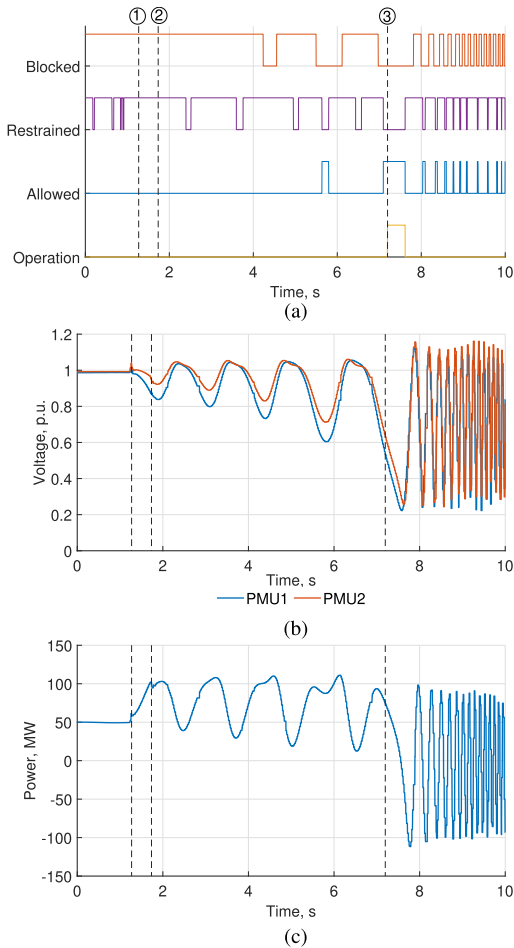


FIGURE 18. Protection algorithm response to Event 2 data. The dashed line marked as ① shows the start of the OOS event at 1.3 seconds. (a) the protection algorithm signals from the controller, (b) the voltage at the two measurement locations in the southern corridor and (c) the measured power in the southern corridor during the event.

magnitude, during which the protection does not operate. After the fourth swing, the system runs into instability, and the protection operates (marked as ③) due to the OOS conditions being fulfilled.

C. PROTECTION TESTING RESULTS FROM ICELANDIC POWER SYSTEM SIMULATIONS

Using the previously verified Icelandic power system model, which was developed in Section IV for real-time simulation, a number of tests were carried out. The simulations were conducted using Event 1 and Event 4 pre-fault conditions as the base case. Different grid conditions were used to test the developed protection algorithm. This was done by switching the series capacitor on the southern link in and out of operation, as well as disconnecting lines in the system. The simulations consisted of symmetrical and asymmetrical faults

performed on different transmission lines in the network including single-pole reclose. From the numerous simulation results, it can be concluded that:

- The algorithm is stable when the power system experiences damped oscillations.
- The algorithm does not operate during single pole tripping and reclosing process.
- The algorithm provides operation for cases when an OOS event occurs for both the southern ring connection and the northern ring connection.

Based on the conducted tests, it can be concluded that the algorithm offers high security and dependability for OOS protection in the power network.

VI. CONCLUSION

In this paper a new OOS protection algorithm based on discrete angle derivatives has been presented, which is tested and implemented on hardware. The testing of the developed algorithm is done by using real-time simulations that build on the well-studied IEEE 39 bus power network. The performance of the developed algorithm is compared to the conventional impedance-based OOS protection relays. Furthermore, the algorithm is tested using the developed and validated real-time simulations model of the Icelandic transmission network, as well as using recorded data from several OOS events that occurred in the Icelandic power system. The algorithm shows reliable and fast operation for various states of the grid in the case of OOS events, and high security during stable power swings. The developed algorithm is fully measurement-based and settingless. Therefore, it is suitable to be applied on arbitrary locations in power systems, where OOS conditions are expected to occur. The results of the simulations and numerous tests show that:

- The developed algorithm performs better in terms of operating time compared to present commercially available impedance-based protection devices.
- Based on the case studies, the algorithm has higher reliability than the impedance-based protection algorithms.
- In addition to numerical real-time simulations, the algorithm has been also tested on actual recordings of OOS events, which proves its stability and dependability for real installations.

Finally, the concept has been tested and implemented in practice by Landsnet in their WACS scheme.

ACKNOWLEDGMENT

The financial support provided by the Dutch Scientific Council NWO is highly appreciated. The first author thanks Delft University of Technology for providing the opportunity to conduct this research work at TU Delft. The cooperation and support provided by Landsnet hf. and GE Renewable Energy is highly acknowledged.

REFERENCES

- [1] J. Blumschein, Y. Yelgin, and M. Kereit, "Blackout prevention by power swing detection and out-of-step protection," *J. Power Energy Eng.*, vol. 2, no. 4, pp. 694–703, 2014.

- [2] D. A. Tziouvaras and D. Hou, "Out-of-step protection fundamentals and advancements," in *Proc. 57th Annu. Conf. Protective Relay Eng.*, 2004, pp. 282–307.
- [3] A. Sauhats, A. Utans, and E. Biela-Dalidovicha, "Equal area criterion and angle control-based out-of-step protection," in *Proc. IEEE 58th Int. Scientific Conf. Power Electr. Eng. Riga Tech. Univ. (RTUCON)*, Oct. 2017, pp. 1–6.
- [4] C. W. Taylor, J. M. Haner, L. A. Hill, W. A. Mittelstadt, and R. L. Cresap, "A new out-of-step relay with rate of change of apparent resistance augmentation," *IEEE Trans. Power App. Syst.*, vol. PAS-102, no. 3, pp. 631–639, Mar. 1983.
- [5] *MiCOM O40 Agile P543/P545 Technical Manual Ver92M*, Schneider Electric, Rueil-Malmaison, France, 2021.
- [6] S. Paudyal, R. Gokaraju, M. S. Sachdev, and S. Cheng, "Out-of-step detection using energy equilibrium criterion in time domain," *Electr. Power Compon. Syst.*, vol. 37, no. 7, pp. 714–739, Jun. 2009.
- [7] S. Paudyal, G. Ramakrishna, and M. S. Sachdev, "Application of equal area criterion conditions in the time domain for out-of-step protection," *IEEE Trans. Power Del.*, vol. 25, no. 2, pp. 600–609, Apr. 2010.
- [8] M. Abedini, M. Davarpanah, M. Sanaye-Pasand, S. M. Hashemi, and R. Irvani, "Generator out-of-step prediction based on faster-than-real-time analysis: Concepts and applications," *IEEE Trans. Power Syst.*, vol. 33, no. 4, pp. 4563–4573, Jul. 2018.
- [9] K. Sreenivasachar, "Out-of-step detection on transmission lines using apparent impedance differential method," *IEEE Trans. Power Del.*, early access, Nov. 8, 2021, doi: [10.1109/TPWRD.2021.3125525](https://doi.org/10.1109/TPWRD.2021.3125525).
- [10] P. Regulski, W. Rebizant, M. Kereit, and H.-J. Herrmann, "PMU-based generator out-of-step protection," *IFAC-PapersOnLine*, vol. 51, no. 28, pp. 79–84, 2018.
- [11] T. D. Duong, S. D'Arco, and A. Holdyk, "A method for predictive out-of-step tripping based on synchrophasors," in *Proc. 15th Int. Conf. Develop. Power Syst. Protection (DPSP)*, 2020, pp. 1–6.
- [12] J. R. Camarillo-Penaranda, D. Celeita, M. Gutierrez, M. Toro, and G. Ramos, "An approach for out-of-step protection based on swing center voltage estimation and analytic geometry parameters," *IEEE Trans. Ind. Appl.*, vol. 56, no. 3, pp. 2402–2408, May 2020.
- [13] N. G. Chothani, B. R. Bhalja, and U. B. Parikh, "New support vector machine-based digital relaying scheme for discrimination between power swing and fault," *IET Gener., Transmiss. Distrib.*, vol. 8, no. 1, pp. 17–25, Jan. 2014.
- [14] M. R. Aghamohammadi and M. Abedi, "DT based intelligent predictor for out of step condition of generator by using PMU data," *Int. J. Electr. Power Energy Syst.*, vol. 99, pp. 95–106, Jul. 2018. [Online]. Available: <https://www.sciencedirect.com/science/article/pii/S0142061517321397>
- [15] E. A. Frimpong, P. Y. Okyere, and J. Asumadu, "On-line determination of transient stability status using MLPNN," in *Proc. IEEE PES PowerAfrica*, Jun. 2017, pp. 23–27.
- [16] M. Tealane, J. Kilter, M. Popov, O. Bagleybter, and D. Klaar, "Online detection of out-of-step condition using PMU-determined system impedances," *IEEE Access*, vol. 10, pp. 14807–14818, 2022.
- [17] D. Fan and V. Centeno, "Adaptive out-of-step protection schemes based on synchrophasors," in *Proc. IEEE PES Gen. Meeting | Conf. Expo.*, Jul. 2014, pp. 1–5.
- [18] K. Shimizu and A. Ishigame, "Novel transient stability assessment using post-disturbance voltage fluctuations," in *Proc. Int. Conf. Smart Grids Energy Syst. (SGES)*, Nov. 2020, pp. 12–17.
- [19] Y. Cui, R. G. Kavasseri, and S. M. Brahma, "Dynamic state estimation assisted out-of-step detection for generators using angular difference," *IEEE Trans. Power Del.*, vol. 32, no. 3, pp. 1441–1449, Jun. 2017.
- [20] J. R. A. K. Yellajosula, Y. Wei, M. Grebla, S. Paudyal, and B. A. Mork, "Online detection of power swing using approximate stability boundaries," *IEEE Trans. Power Del.*, vol. 35, no. 3, pp. 1220–1229, Jun. 2020.
- [21] S. Zhang and Y. Zhang, "A novel out-of-step splitting protection based on the wide area information," *IEEE Trans. Smart Grid*, vol. 8, no. 1, pp. 41–51, Jan. 2017.
- [22] H. Zare, H. Yaghobi, and Y. Alinejad-Beromi, "Adaptive concept of controlled islanding in power systems for wide-area out-of-step prediction of synchronous generators based on adaptive tripping index," *IET Gener., Transmiss. Distrib.*, vol. 12, no. 16, pp. 3829–3836, Sep. 2018.
- [23] M. R. Nasab and H. Yaghobi, "A real-time out-of-step protection strategy based on instantaneous active power deviation," *IEEE Trans. Power Del.*, vol. 36, no. 6, pp. 3590–3600, Dec. 2021.
- [24] J. P. Desai and V. H. Makwana, "Phasor measurement unit incorporated adaptive out-of-step protection of synchronous generator," *J. Modern Power Syst. Clean Energy*, vol. 9, no. 5, pp. 1032–1042, 2021.
- [25] B. Deshmukh, S. Biswal, and D. K. Lal, "Synchronous generator out-of-step protection based on Savitzky–Golay filtering technique," in *Proc. Emerg. Trends Ind. 4.0 (ETI)*, May 2021, pp. 1–3.
- [26] E. Farantatos, R. Huang, G. J. Kokkinides, and A. P. Meliopoulos, "A predictive generator out-of-step protection and transient stability monitoring scheme enabled by a distributed dynamic state estimator," *IEEE Trans. Power Del.*, vol. 31, no. 4, pp. 1826–1835, Aug. 2016.
- [27] P. Kundur, *Power System Stability and Control*. New York, NY, USA: McGraw-Hill, 1994.
- [28] Y. Xue, T. Van Custem, and M. Ribbens-Pavella, "Extended equal area criterion justifications, generalizations, applications," *IEEE Trans. Power Syst.*, vol. 4, no. 1, pp. 44–52, Feb. 1989.
- [29] M. Pavella, E. Damien, and D. Ruiz-Vega, *Transient Stability of Power Systems*. Cham, Switzerland: Springer, 2000.
- [30] M. Meldorf and J. Kilter, *Elektrisisisteemi Stabiilsus*. Tallinna, Estonia: Tehnikaülikooli Kirjastus, 2011.
- [31] J. Machowski, Z. Lubosny, J. W. Bialek, and J. R. Bumby, *Power System Dynamics: Stability and Control*, 3rd ed. Hoboken, NJ, USA: Wiley, 2020.
- [32] GE Digital. (2021). *Phasor Controller*. [Online]. Available: <https://www.ge.com/digital/applications/transmission/phasorcontroller>
- [33] *IEEE Standard for Phasor Data Concentrators for Power Systems*, Standard C37.247, 2019.
- [34] *Modelling of Permanent Magnet Generator Based Wind Turbine Systems in the RTDS*, RTDS Technologies, Winnipeg, MB, Canada, 2017.
- [35] *SIPROTEC 4 Line Differential Protection with Distance Protection 7SD5 V4.7*, Siemens AG, Munich, Germany, 2016.
- [36] *Easergy MiCOM P44y Technical Manual*, Schneider Electric, Rueil-Malmaison, France, 2019.
- [37] LandsNet. *LandsNet's Transmission System*. Accessed: Mar. 30, 2022. [Online]. Available: <https://landsnet.is/>



MARKO TEALANE (Student Member, IEEE) received the B.Sc. and M.Sc. degrees in electrical power engineering from the Tallinn University of Technology, in 2014 and 2016, respectively, where he is currently pursuing the Ph.D. degree in electrical power engineering. From 2019 to 2020, he was an Academic Visitor with the Delft University of Technology, where he was working on out-of-step protection in the Intelligent Electrical Power Grids Group. In the past, he worked as a Protection Engineer at the Estonian Transmission System Operator. He is currently on sabbatical leave, and works at TU Delft. His research interests include power system protection, power system relaying, and wide-area control.



JAKO KILTER (Senior Member, IEEE) received the B.Sc. and M.Sc. degrees in electrical power engineering from the Tallinn University of Technology, and the Ph.D. degree in electrical power engineering from the Tallinn University of Technology, in 2009. He is currently a Professor in power systems and the Head of the Power Systems Research Group, School of Engineering, Tallinn University of Technology, the Chairperson of the High Voltage Committee with the Estonian Centre for Standardization and Accreditation, and the Co-Chair of CIGRE Estonian National Committee. His research and consultancy work over the years has been split between the areas of power system dynamics, wide-area control and applications, and power quality.



OLEG BAGLEYBTER (Member, IEEE) received the Diploma degree in electrical engineering and the Ph.D. degree from Irkutsk Technical University, in 1999 and 2006, respectively. He is currently working as a Senior Staff Engineering Manager at GE. He is responsible for advanced automation applications research and development portfolio within the GE Grid Automation Business. His focus is on developing and deploying innovative applications and solutions utilizing wide area measurements in transmission and distribution grids. He has worked in the past as a Protection and Control Engineer for a power utility in Siberia and a Product Manager for transmission protection relays for GE Grid Solutions.



BIRKIR HEIMISSON received the B.Sc. degree in electrical engineering from the University of Iceland, in 2011, and the M.Sc. degree in electric power engineering from Chalmers University, in 2014. He joined Landsnet (TSO of Iceland) as a System Operator, in 2014. Together with system operation, he led the smart-grid development with focus on wide-area-measurements and control. Additionally, he was the work-package leader for Landsnet in EU Horizon 2020 MIGRATE Project.

In 2019, he moved to research and development, where he focuses on digital substation implementation based on IEC 61850 and smart-grid development.



MARJAN POPOV (Fellow, IEEE) received the Ph.D. degree in electrical power engineering from the Delft University of Technology, Delft, in 2002. He is currently a Chevening Alumnus. In 1997, he was an Academic Visitor with the University of Liverpool, Liverpool, U.K., working in the Arc Research Group on modeling SF6 circuit breakers. His research interests include future power systems, large-scale power system transients, intelligent protection for future power systems, and wide-area monitoring and protection. He is a member of Cigre and actively participated in WG C4.502 and WG A2/C4.39. In 2010, he received the prestigious Dutch Hidde Nijland Prize for extraordinary research achievements. He was a recipient of the IEEE PES Prize Paper Award and IEEE Switchgear Committee Award in 2011 and an Associate Editor for Elsevier's International Journal of Electrical Power and Energy Systems. In 2017, together with the Dutch utilities TenneT, Alliander, and Stedin, he founded the Dutch Power System Protection Centre to promote the research and education in power system protection.

...

Curriculum Vitae

1. Personal data

Name	Marko Tealane
Date and place of birth	7 May 1992 Tallinn, Estonia
E-mail	marko.tealane@taltech.ee

2. Education

2017–...	Tallinn University of Technology, School of Engineering, Electrical Power Engineering and Mechatronics, PhD studies
2014–2016	Tallinn University of Technology, Faculty of Electrical Power Engineering, Electrical Power Engineering, MSc <i>cum laude</i>
2011–2014	Tallinn University of Technology, Faculty of Electrical Power Engineering, Electrical Power Engineering, BSc

3. Professional employment

2022– ...	Elering AS, Condition Assessment Specialist
2022–2022	Tallinn University of Technology, Expert
2018–2022	Tallinn University of Technology, Early Stage Researcher
2015–2018	Elering AS, Dynamic State Analyst

4. Honours and awards

- 2020, Elering's Energy Scholarship
- 2019, Kristjan Jaak scholarship for study periods abroad (The Netherlands)

5. Defended theses

- 2016, Low frequency power oscillations in a power system and consideration of the phenomena in relay protection, MSc, supervisor Jako Kilter, Tallinn University of Technology, Faculty of Power Engineering
- 2014, The possibility of integrating a nuclear power station in Estonia , supervisor Heiki Tammoja, Tallinn University of Technology, Faculty of Power Engineering

6. Supervised dissertations

- Fred Antsu, Master's Degree, 2023, (sup) Marko Tealane; Jako Kilter, Releekaitse ja automaatika süsteemide testimise analüüs IEC61850 põhistes alajaamades (Analysis of Protection and Automation Systems Testing in IEC61850 Substations), Tallinn University of Technology School of Engineering, Department of Electrical Power Engineering and Mechatronics
- Ija Ivanova, Master's Degree, 2023, (sup) Marko Tealane; Jako Kilter, Vanade alajaamade kaughallatavateks muutmise võimalused Silpower 6/0,4 kV alajaamade näitel (The remote control implementation possibilities for old substations on the example of Silpower 6/0,4 kV substations), Tallinn University of Technology School of Engineering, Department of Electrical Power Engineering and Mechatronics

- Andi Ingalt, Master's Degree, 2022, (sup) Marko Tealane, Toitepinge mõju alajaama sekundaarseadmete toimele (The effect of supply voltage on substation secondary equipment), Tallinn University of Technology School of Engineering, Department of Electrical Power Engineering and Mechatronics
- Leino Schnur, Master's Degree, 2022, (sup) Marko Tealane; Jako Kilter, Alalisvooluühenduste mõju vahelduvvooluvõrgu distantskaitsele (Impact of HVDC connections to AC grid distance protection), Tallinn University of Technology School of Engineering, Department of Electrical Power Engineering and Mechatronics
- Ott Pukk, Master's Degree, 2022, (sup) Karl Kull; Marko Tealane, Eesti elektroenergeetika jalajälje, CO₂, arvestuspidamise analüüs (Analysis of Estonian power sector carbon footprint accounting), Tallinn University of Technology School of Engineering, Department of Electrical Power Engineering and Mechatronics
- Henry Kapp, Master's Degree, 2021, (sup) Marko Tealane, Maaühenduskaitsese koordineerimine resonantsmaandatud võrgus (Coordination of Earth-Fault Protection in Resonance Grounded Networks), Tallinn University of Technology School of Engineering, Department of Electrical Power Engineering and Mechatronics
- Hans-Konrad Klaos, Master's Degree, 2021, (sup) Marko Tealane, Tehisintellekti ja IEC 61850 põhine diferentsiaalkaitse: ülekandevõrgu releekaitse kontseptsioon (Artificial intelligence and IEC 61850 based differential protection: A concept for relay protection in transmission network), Tallinn University of Technology School of Engineering, Department of Electrical Power Engineering and Mechatronics
- Anton Veikman, Master's Degree, 2019, (sup) Jako Kilter; Marko Tealane, Sünkroongeneraatori kaitsete uuendamine VKG Energia elektrijaama generaatori G3 näitel (Modernization of Synchronous Generator Protection: an Example Based on Generator G3 of VKG Energia Power Plant), Tallinn University of Technology School of Engineering, Department of Electrical Power Engineering and Mechatronics
- Eerik Ennemuist, Master's Degree, 2019, (sup) Marko Tealane, Releekaitse ja automaatika laboritööde väljatöötamine (The Development of Relay Protection and Automation Laboratory Exercises), Tallinn University of Technology School of Engineering, Department of Electrical Power Engineering and Mechatronics
- Siim Laidvee, Master's Degree, 2018, (sup) Jako Kilter; Marko Tealane, Distantskaitsete testimine Omicroni ja RTDS simulaatoriga (Testing of Distance Protections with Omicron and RTDS), Tallinn University of Technology School of Engineering, Department of Electrical Power Engineering and Mechatronics
- Kristen Pill, Master's Degree, 2018, (sup) Jako Kilter; Marko Tealane, Elektrisüsteemi asünkroonkäigukaitsete algoritmide analüüs (Analysis of different Power System Out of Step detection algorithms), Tallinn University of Technology School of Engineering, Department of Electrical Power Engineering and Mechatronics
- Mart Aru, Master's Degree, 2018, (sup) Jako Kilter; Marko Tealane, Erinevate distantskaitsete käitumise uurimine muutuva elektrisüsteemi inertsi tingimustes (Analysis of different distance relay behaviours in variable power system inertia conditions), Tallinn University of Technology School of Engineering, Department of Electrical Power Engineering and Mechatronics

7. Scientific work

Papers

1. M. Tealane, J. Kilter, O. Bagleybter, B. Heimisson, and M. Popov, "Out-of-step protection based on discrete angle derivatives," *IEEE Access*, vol. 10, pp. 78290–78305, 2022
2. M. Tealane, J. Kilter, M. Popov, O. Bagleybter, and D. Klaar, "Online detection of out-of-step condition using pmu-determined system impedances," *IEEE Access*, vol. 10, pp. 14807–14818, 2022
3. M. Tealane, J. Kilter, and K. Pill, "Real-time testing of out-of-step protection devices," in *2021 IEEE PES Innovative Smart Grid Technologies Europe (ISGT Europe)*, pp. 1–5, 2021
4. Rajkumar, V. S.; Tealane, M.; Stefanov, A.; Palensky, P., Cyber Attacks on Protective Relays in Digital Substations and Impact Analysis, not contained in this thesis, *2020 8th Workshop on Modeling and Simulation of Cyber-Physical Energy Systems*, IEEE, 2020
5. Rajkumar, V. S.; Tealane, M.; Stefanov, A.; Presekal, A.; Palensky, P., Cyber Attacks on Power System Automation and Protection and Impact Analysis, not contained in this thesis, *2020 IEEE PES Innovative Smart Grid Technologies Europe (ISGT-Europe)*, IEEE, 2020
6. Kiitam, I.; Saarna, M.; Taklaja, P.; Tealane, M.; Palu, I., Electrical and Mechanical Properties of Service-aged Medium Voltage Porcelain Support Insulators, not contained in this thesis, *2020 6th IEEE International Energy Conference (ENERGYCon)*, IEEE, 2020
7. Dubey, R.; Popov, M.; Chavez, J.; Terzija, V.; Azizi, S.; Sun, M.; López, S.; Pindado, L.; Andrino, R.; López, D.; Guibout, C.; Watare, A.; Kilter, J.; Reinson, A.; Tealane, M.; Martínez, E.; Villén, M. T.; Borroy, S.; Grasset, H., not contained in this thesis, Low Latency Stockwell Transform Based Secured Distance Protection Scheme for Power Network Connected with High Renewable Penetration, *Protection, Automation and Control (PAC) World Conference 2018*, Omicron, 2018
8. Chavez, J.; Popov, M.; Dubey, R.; López, D.; López, S.; Pindado, L.; Andrino, R.; Terzija, V.; Azizi, S.; Sun, M.; Grasset, H.; Martínez, E.; Villén, M. T.; Borroy, S.; Guibout, C.; Watare, A.; Kilter, J.; Reinson, A.; Tealane, M., Exposing available distance relay operations near high wind penetration, not contained in this thesis, *Protection, Automation and Control (PAC) World Conference 2018*, Omicron, 2018
9. Martínez, E.; Villén, M. T.; Borroy, S.; Grasset, H.; Popov, M.; Dubey, R.; Chavez, J.; Terzija, V.; Azizi, S.; Sun, M.; López, S.; Pindado, L.; Andrino, R.; López, D.; Guibout, C.; Watare, A.; Kilter, J.; Reinson, A.; Tealane, M., Empirical Analysis of Potential Improvements for High Voltage Protective Algorithms, not contained in this thesis, *Protection, Automation and Control (PAC) World Conference 2018*, Omicron, 2018
10. Martínez, E.; Villén, M. T.; Borroy, S.; Grasset, H.; Popov, M.; Dubey, R.; Chavez, J., Terzija, V., Azizi, S.; Sun, M.; López, S.; Pindado, L.; Andrino, R.; López, D.; Guibout, C., Watare, A.; Kilter, J.; Reinson, A.; Tealane, M., Effects of Type-4 Wind Turbine on Present Protection Relaying Algorithms, not contained in this thesis, *Protection, Automation and Control (PAC) World Conference 2018*, Omicron, 2018

Conference presentations

1. M. Tealane, J. Kilter and K. Pill. *Real-time testing of out-of-step protection devices*, IEEE PES ISGT Europe, Oct 2021
2. M. Tealane. *HIL Testing an Adaptive Out-of-Step Protection Algorithm based on Wide-Area Measurements*, RTDS User Spotlight 2.0, May 2022
3. M. Tealane. *Adaptive Out-of-Step Protection based on Wide Area Measurements, Communication Based Protection*, 2 June 2022, Delft, The Netherlands

Elulookirjeldus

1. Isikuandmed

Nimi	Marko Tealane
Sünniaeg ja -koht	07.05.1992, Tallinn, Eesti
E-mail	marko.tealane@taltech.ee

2. Haridus

2017–...	Tallinna Tehnikaülikool, Inseneriteaduskond, Elektroenergeetika ja mehhatroonika, doktoriõpe
2014–2016	Tallinna Tehnikaülikool, Energeetika teaduskond, Elektroenergeetika, MSc <i>cum laude</i>
2011–2014	Tallinna Tehnikaülikool, Energeetika teaduskond, Elektroenergeetika, BSc

3. Teenistuskäik

2022– ...	Elering AS, Seadmete seisundi hindamise spetsialist
2022–2022	Tallinna Tehnikaülikool, Releekaitse ja automaatika ekspert
2018–2022	Tallinna Tehnikaülikool, Doktorant-nooremteadur
2015–2018	Elering AS, Siirdetalitluse analüütik

4. Autasud

- 2020, Eleringi Energeetikastipendium
- 2019, Kristjan Jaagu välisõpingute stipendium (Madalmaade Kuningriik)

5. Kaitstud lõputööd

- 2016, Elektrisüsteemi madalsageduslik võimsuse võnkumine ja sellega arvestamine releekaitstes, MSc, juhendaja Jako Kilter, Tallinna Tehnikaülikool, Elektroenergeetika Instituut
- 2014, Tuumajaama integreerimise võimalus Eestisse, BSc, juhendaja Heiki Tammoja, Tallinna Tehnikaülikool, Elektroenergeetika Instituut

6. Juhendatud väitekirjad

- Fred Antsu, magistrikraad, 2023, (juh) Marko Tealane; Jako Kilter, Releekaitse ja automaatika süsteemide testimise analüüs IEC61850 põhistes alajaamades, Tallinna Tehnikaülikool, Inseneriteaduskond, Elektroenergeetika ja mehhatroonika instituut
- Ija Ivanova, magistrikraad, 2023, (juh) Marko Tealane; Jako Kilter, Vanade alajaamade kaughallatavateks muutmise võimalused Silpower 6/0,4 kV alajaamade näitel, Tallinna Tehnikaülikool, Inseneriteaduskond, Elektroenergeetika ja mehhatroonika instituut
- Andi Ingalt, magistrikraad, 2022, (juh) Marko Tealane, Toitepinge mõju alajaama sekundaarseadmete toimele, Tallinna Tehnikaülikool, Inseneriteaduskond, Elektroenergeetika ja mehhatroonika instituut

- Leino Schnur, magistrakraad, 2022, (juh) Marko Tealane; Jako Kilter, Alalisvooluühenduste mõju vahelduvvooluvõrgu distantskaitsele, Tallinna Tehnikaülikool, Inseneriteaduskond, Elektroenergeetika ja mehhatroonika instituut
- Ott Pukk, magistrakraad, 2022, (juh) Karl Kull; Marko Tealane, Eesti elektroenergeetika jalajälje, CO₂, arvestuspidamise analüüs, Tallinna Tehnikaülikool, Inseneriteaduskond, Elektroenergeetika ja mehhatroonika instituut
- Henry Kapp, magistrakraad, 2021, (juh) Marko Tealane, Maaühenduskaitsede koordineerimine resonantsmaandatud võrgus, Tallinna Tehnikaülikool, Inseneriteaduskond, Elektroenergeetika ja mehhatroonika instituut
- Hans-Konrad Klaos, magistrakraad, 2021, (juh) Marko Tealane, Tehisintellekti ja IEC 61850 põhine diferentsiaalkaitse: ülekandevõrgu releekaitse kontseptsioon, Tallinna Tehnikaülikool, Inseneriteaduskond, Elektroenergeetika ja mehhatroonika instituut
- Anton Veikman, magistrakraad, 2019, (juh) Jako Kilter; Marko Tealane, Sünkroongeneraatori kaitsete uuendamine VKG Energia elektriijaama generaatori G3 näitel, Tallinna Tehnikaülikool, Inseneriteaduskond, Elektroenergeetika ja mehhatroonika instituut
- Eerik Ennemuist, magistrakraad, 2019, (juh) Marko Tealane, Releekaitse ja automaatika laboritööde väljatöötamine, Tallinna Tehnikaülikool, Inseneriteaduskond, Elektroenergeetika ja mehhatroonika instituut
- Siim Laidvee, magistrakraad, 2018, (juh) Jako Kilter; Marko Tealane, Distantskaitsete testimine Omicroni ja RTDS simulaatoriga, Tallinna Tehnikaülikool, Inseneriteaduskond, Elektroenergeetika ja mehhatroonika instituut
- Kristen Pill, magistrakraad, 2018, (juh) Jako Kilter; Marko Tealane, Elektrisüsteemi asünkroonkäigukaitsete algoritmide analüüs, Tallinna Tehnikaülikool, Inseneriteaduskond, Elektroenergeetika ja mehhatroonika instituut
- Mart Aru, magistrakraad, 2018, (juh) Jako Kilter; Marko Tealane, Erinevate distantskaitsete käitumise uurimine muutuva elektrisüsteemi inertsitingimustes, Tallinna Tehnikaülikool, Inseneriteaduskond, Elektroenergeetika ja mehhatroonika instituut

7. Teadustegevus

Teadusartiklite, konverentsiteeside ja konverentsiettekannete loetelu on toodud ingliskeelse elulookirjelduse juures.

ISSN 2585-6901 (PDF)
ISBN 978-9949-83-957-5 (PDF)